THE UNIVERSITY
of EDINBURGH

Investigating behaviour of concrete at elevated temperatures

THE UNIVERSITY *of* EDINBURGH

Zhujun Zhang

University of Edinburgh

This dissertation is submitted for the degree of

Doctor of Philosophy

May 2019

I would like to dedicate this thesis to my loving parents ...

Declaration

I declare that this thesis has been composed solely by myself and that it has not been submitted, in whole or in part, in any previous application for a degree. Except where states otherwise by reference or acknowledgment, the work presented is entirely my own.

Zhujun Zhang

May 2019

Acknowledgements

Particular thanks to my supervisor, Professor Pankaj Pankaj, for his guidance and support over four years. Thanks for your suggestions and patience.

Thanks to Professor Asif Usmani for giving me the chance to study in University of Edinburgh and being my supervisor at the beginning of my PhD study.

Thanks to Professor Luke Bisby and Professor Tim Stratford for their help and suggestions to my experiments.

I am appreciate of the help in the lab from my colleagues, Mr Michal Krajcovic, Dr Zafiris Triantafyllidis, and Dr Jamie Maclean. I am also grateful to technicians, Mr Jim Hutcheson and Mr Mark Partington, for technical supports. Thanks to Dr Holly Warren, for making and curing concrete specimens used in this research.

I would like to thank all people in John Muir for lighting these four years. I am grateful to join one of the most brilliant fire group in the world.

Thanks to my friends, who listened my compliant and comforted me when I was depressing.

Lastly, thanks to my parents. Thanks for all support and encouragement during my years of study. I want to share my accomplishment with you.

Abstract

Concrete is one of the most widely used construction materials in the world and it provides superior fire resistance in comparison to other construction materials such as timber and steel. However, the outer walls of high-rise concrete buildings are often covered by foam insulation material and rooms are full of other flammable materials; these have resulted in damage and destruction of concrete structures due to fires in the past. Concrete behaviour at elevated temperatures changes drastically from that at ambient temperature and comprises of several complex thermomechanical responses. The primary aim of this study is to understand how concrete behaves under load and temperature.

This study includes experimental work and computer simulation. The study evaluates mechanical behaviour of concrete due to heating and loading. Two series of tests are conducted: those in which heated samples are subjected to loading, load holding, unloading and recovery; and those in which loaded samples are subjected to heating, maintenance of constant temperature, unloading and recovery. Different strain components, free thermal strain, instantaneous stress-related strain, time-dependent creep strain and load induced thermal strain are evaluated and analysed. The experimental work uses digital image correlation to evaluate strains. By analysing the photos taken during the experiment, the value of strain is evaluated. The method of post-processing photos is found to be a simple and inexpensive way to evaluate strains at elevated temperatures.

This study evaluates the transient temperature distribution under different heating rates and heating time. As the material with a low thermal conductivity, the thermal gradients increase within concrete at larger heating rates. The differential expansion with the thermal gradients can result in damage to concrete. The heat transfer analysis is conducted to find the most efficient and reasonable heating rates for experiments in order to prevent damage due to differential thermal expansion. Also, the heat transfer analysis shows the chamber

temperature needs to be maintained constant for 2 hrs to achieve uniform temperature in the concrete for the size of samples considered.

This study develops a method to simulate time-dependent creep using viscoelasticity with Prony series; this provides a simple way to model time-dependent creep. The parameters are evaluated through curve fitting in MATLAB. Then, the parameters are used in finite element analysis for defining viscoelastic material in ABAQUS. The simulation results fit the experimental data well.

This study examines the components of load induced thermal strain (LITS). As one of the largest strain components at elevated temperatures, LITS is usually treated as plastic strain and irrecoverable during the first heating. The experiments show that LITS is only partly irrecoverable.

Lay summary

Concrete is one of the most widely used construction materials in the world and it provides superior fire resistance in comparison to other construction materials such as timber and steel. However, the outer walls of high-rise concrete buildings are often covered by foam insulation material and rooms are full of other flammable materials; these have resulted in damage and destruction of concrete structures due to fires in the past. The load carrying capacity of concrete decreases at elevated temperatures. It is, therefore, very important to understand how concrete behaves in fire.

In recent years, a number of experiments have been conducted to investigate material behaviour of concrete at elevated temperatures. However, its behaviour at elevated temperatures is still not properly understood. This study considers experimental tests and computer simulations in which concrete specimens are subjected to heating and loading to different temperatures and loads. Two series of tests are conducted to understand how concrete behaves: loading then heating and heating then loading. Different strain components are evaluated via the experimental work and some of this behaviour is numerically simulated.

The study shows that high rates of heating creates large temperature variations within concrete which result in differential thermal expansions which, in turn, can damage concrete. Novel experimental protocol was designed to evaluate the behaviour of the thermomechnical behaviour of concrete at elevated temperatures. Experimental studies show that thermal expansion of concrete is lower than that suggested by the European standard. It is well recognised that concrete deforms with time under sustained loads even at ambient temperatures. This study shows that this time-dependent creep is substantial at elevated temperatures and develops a simple yet novel approach to include this in simulations. The study successfully separates out different components of deformation response that arise when loaded concrete is heated and shows that significant proportion of it is recoverable upon unloading.

Contents

List of Figures

List of Tables

List of nomenclatures and abbreviations

Abbreviation

HTL heating-then-loading

LITS load induced thermal strain

LTH loading-then-heating

RH relative humidity

Nomenclature

α thermal coefficient

β coefficient for load induced thermal strain

β_0 constant for time-dependent creep strain

η viscoelasticity

η_{pr} number of Prony terms

λ_c conductivity

ν Poisson's ratio

Φ transient creep function

$\rho(\theta)$ density at temperature θ

ρ_i relaxation time

σ initial compressive stress

σ_θ stress at temperature θ

τ_j retardation time

θ temperature

ε strain

$\varepsilon_{c,\theta}$ failure compressive strain at temperature θ

ε_{cr} time-dependent creep strain

$\varepsilon_{el,\theta}$ instantaneous stress-related strain at temperature θ

ε_{el} instantaneous stress-related strain at ambient temperature

ε_{th} free thermal strain

ε_{tot} total strain

ε_{tr} transient creep strain

A area

$C_p(\theta)$ specific heat at temperature θ

D_g instantaneous elastic compliance

D_j transient retardation strength

E instantaneous elastic modulus at ambient temperature

E_c instantaneous elastic modulus at temperature θ

E_e equilibrium modulus

E_i relaxation strength

f_c compressive strength at ambient temperature

f_t tensile strength at ambient temperature

$f_{c,\theta}$ compressive strength at temperature θ

$f_{t,\theta}$ tensile strength at temperature θ

k thermal conductivity

k_1 constant for time-dependent creep strain

$k_{c,\theta}$ compressive strength coefficient

p dimensionless constant

q rate of heat flow

t time

t_r reference heating time

w moisture content

x length variable

1 Introduction

1.1 Introduction

Concrete has been one of the most widely used materials in the world as it provides superior fire resistance and bears large compressive loads. However, the outer walls of high-rise concrete buildings are often covered by foam insulation material and rooms are full of other flammable materials. In 2010, a 28-story concrete building in Shanghai was destroyed by fire due to the ignition of polyurethane foam insulation installed on the outer wall. In 2017, the Grenfell Tower with 24 storeys was ruined by fire started from a fridge-freezer. The load capacity of concrete decreases at elevated temperatures. It is, therefore, very important to understand how concrete behaves in fire.

The mechanical properties, thermal properties, and deformation properties of concrete are affected by many influencing factors, such as its composition and its curing conditions. In the past decades, a number of experimental programmes have been conducted to explore the material properties of concrete at elevated temperatures. Also, different models have been developed and applied in the relevant simulations. However, the behaviour of concrete at elevated temperatures is still not adequately understood.

During the fire, the concrete expands with increasing temperature theoretically. However, this expansion may be restrained by the load applied by the structure. When concrete temperature increases under sustained load and complex strain components are developed. Also, the considerable thermal gradients arise during heating due to the low conductivity of concrete. All these factors have an effect on the mechanical behaviour of concrete.

Time-dependent creep, as a mechanical response arises all the time under sustained load; it is usually neglected due to the small value at ambient temperatures. However, the time-dependent creep is not negligible at high temperatures. Inclusion of this in simulation is often not considered.

In recent years, researchers have started to pay attention to load induced thermal strain component which is one of largest strain during heating. However, the load induced thermal strain is described as plastic and irrecoverable during the first heating. There is no agreement whether the load induced thermal strain is totally irrecoverable or partly irrecoverable and what all it constitutes.

1.2 Aim of the research

There are a number of aims for the study:

- To evaluate the variations in mechanical behaviour due to heating and loading. By conducting two types of tests: those in which heated samples are subjected to loading, load holding, unloading and recovery; and those in which loaded samples are subjected to heating, maintenance of constant temperature, unloading and recovery. Identify and separate different components of deformation response.

- To develop a method for simulating time-dependent creep, which is significant component at elevated temperatures, and to develop and validate a method to simulate

time-dependent creep strain at different temperatures and different load levels.

- To examine the components of load induced thermal strain. As large strain components are known to arise when concrete is heated under sustained load. In particular it is unclear weather the strain is totally irrecoverable and partly irrecoverable.

- To evaluate the most efficient heating rate for similar experiments. As the material with a low thermal conductivity, the thermal gradients increase within concrete at larger heating rates. The differential expansion with the thermal gradients can result in damage to concrete. Undertake heat transfer analysis to evaluate the most efficient heating rate.

1.3 Layout of the thesis

Chapter 1 - Introduction

This chapter includes the background of the research, aims of the research, and layout of the thesis.

Chapter 2 - Literature review

This chapter reviews thermal properties, mechanical properties and deformation properties of concrete at elevated temperatures from previous experimental observations and constitutive models. Different strain components, including free thermal strain, instantaneous stress-related strain, time-dependent creep and load induced thermal strain, are discussed. The previous experimental methods and influencing factor are discussed to develop the experiments in this study.

Chapter 3 - Finite element simulation of heat transfer in concrete

This chapter conducts finite element simulations to evaluate the transient temperature distributions under different heating rates. The details of the simulations and consequent effects of heating rates are presented and discussed. The most effective heating rate evaluated by simulation is used in the following experiments. The sensitivity analysis is conducted to evaluate the sensitivity of the thermal coefficient and the elastic modulus on the temperatures and thermo-mechanical response of concrete.

Chapter 4 - The experimental protocols

This chapter presents two series of tests to explore the material behaviour of concrete at elevated temperatures: those in which heated samples are subjected to loading, load holding, unloading and recovery; and those in which load samples are subjected to heating, maintenance of constant temperature, unloading and recovery. The digital image correlation is introduced and employed for measuring strain data during tests.

Chapter 5 - Heating-then-loading experiment results and simulations

This chapter presents the experimental data of compressive strength tests, stress-strain relations at elevated temperatures, and heating-then-loading (HTL) tests. The HTL tests comprise of free thermal strain, instantaneous stress-related strain, and time-dependent creep, which are significant components in LITS. Also, the temperature data is compared with heat transfer analysis to modify thermal properties. Viscoelasticity is introduced to simulate time-dependent creep. The Prony series is developed and used via MATLAB and ABAQUS to simulate creep strain and compared with experimental data.

Chapter 6 - Loading-then-heating experiment results and analysis

This chapter presents the experimental data and analysis of loading-then-heating tests. Different strain components, including transient strain, creep strain, and stress-related strain due to the change of the instantaneous elastic modulus at high temperatures, are compared and

discussed. Different LITS components are evaluated and discussed. Also, the experimental data are compared with different constitutive models.

Chapter 7 - Validation of Prony series

This chapter explores the strength and limitations of the viscoelastic model using the Prony series. Simulations of time-dependent creep are compared to previously developed models and experimental data.

Chapter 8 - Conclusions and further work

This chapter summarizes the conclusions of this study and suggests ideas for future research.

2

Literature review

2.1 Introduction

As one of the most popular building materials, concrete has different properties at elevated temperatures. In this chapter, thermal properties, mechanical properties, and deformation properties of concrete at elevated temperatures are discussed based on previous experimental observations and constitutive models.

Different strain components, including free thermal strain, instantaneous stress-related strain, time-dependent creep and load induced thermal strain are discussed. Of particular interest is load induced thermal strain, which is known to be the largest component of the total strain at elevated temperatures.

2.2 Concrete thermal properties at elevated temperatures

Thermal properties of concrete have received much attention in the past decades [4, 15, 16]. The thermal properties at elevated temperatures are important in the evaluation of temperature distributions in concrete during heating (discussed in the following chapter). In the following, thermal conductivity, specific heat and density of concrete at elevated temperatures are discussed.

2.2.1 Conductivity

In recent years, many researchers have conducted experiments to evaluate values of thermal conductivity. Heat conduction happens when there is a temperature difference within a body. The energy is transferred from a high-temperature region to a low temperature region [17]. Thermal conductivity demonstrates the heat conduction capability [18]. It is represented as the ratio of rate of heat flow to temperature gradient [17]

$$k = -\frac{q/A}{\partial\theta/\partial x} \tag{2.1}$$

where k is the thermal conductivity, q is the rate of heat flow, A is the area, θ is the temperature, and x is the length variable. This equation is applied for the heat flow in one direction.

The commonly used experimental methods for thermal conductivity evaluation are the steady state method and the transient method [19]. The steady state method employs constant heat transfer. The temperature is not dependent on time. It is usually used for homogeneous materials and takes more time. For the transient method, the temperature is not constant and dependent on time. It is commonly chosen for heterogeneous materials with moisture [20]. Therefore, the transient method is more suitable for moist concrete [21]. In the experiment study conducted by Kim [22], the mostly significant factors affecting thermal conductivity were age, water content, temperature, amount of cement, types of admixtures, fine aggregate fraction, and aggregate volume fraction.

There is a good agreement that thermal conductivity of concrete decreases gradually with temperature [2, 23]. The majority of research states that the thermal conductivity of concrete at 500 °C is around 50 % of that at ambient temperature [24]. Figure 2.1 shows the variations of thermal conductivity of normal strength concrete with temperatures. The values were compiled by Khaliq [1] based on experimental data [1, 4, 5, 23, 25–27] and different standards [2, 3].

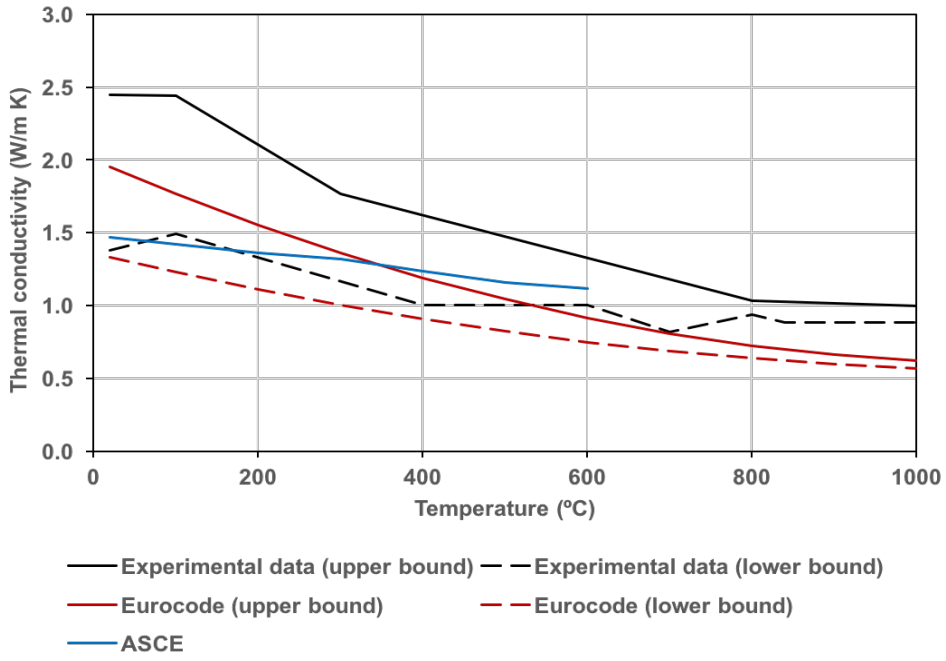

Fig. 2.1 Comparison of thermal conductivity of concrete at elevated temperatures [1–3]

2.2.2 Specific heat

The specific heat is the amount of heat per unit mass required to raise the temperature by one degree Celsius. Khaliq [1] also compiled values of specific heat with temperature based on experimental data [1, 5, 23, 25–28] and different standards [2, 3]. Figure 2.2 shows the variations of volumetric specific heat of normal strength concrete with temperatures.

It has been reported that the specific heat is influenced by various physical and chemical transformations at elevated temperatures [26]. The vaporization of free water affects the specific heat at around 100 °C. Eurocode 2 [2] captures the effect of moisture content (Fig. 2.2). Without consideration of moisture content, the value of specific heat remains almost constant from the ambient temperature to 400 °C. There is a fluctuation between 400 °C to 600 °C due to the dissociation of $Ca(OH)_2$ into CaO and H_2O [26]. There is a considerable increase above 600 °C because of the quartz transformation of some aggregates [26]. The specific heat decreases to an almost constant value after 800 °C.

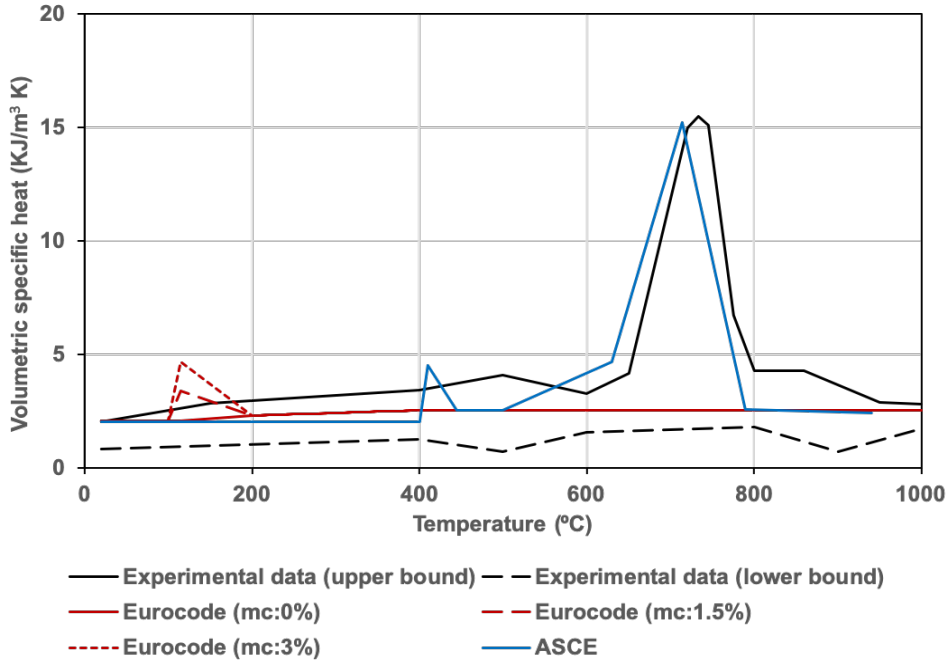

Fig. 2.2 Comparison of volumetric specific heat of concrete at elevated temperatures (mc: moisture content) [1–3]

Schneider [12] summarized influencing factors for specific heat. For the temperature below 200 °C, the specific heat is reported to be highly dependent on moisture content. The type of aggregate had significant influence on the specific heat for temperature above 600 °C, but little influence when the temperature over 800 °C.

2.2.3 Density

The density of concrete is known to decrease with heating temperature due to reduction of moisture [2]. Figure 2.3 shows the variations of density of as a function of temperature for different aggregates based on experimental data [1, 4–6] and Eurocode [2]. The reduction of density is not very obvious under 600 °C for both siliceous and carbonate aggregate concretes. It has been suggested that for the siliceous aggregate concrete, the density remains stable above 600 °C [1, 4–6]. However, the density of the carbonate aggregate concrete

has a considerable decrease above 600 °C [1, 4–6]. This considerable reduction is due to dissociation of dolomite in carbonate aggregate at 600 °C [29].

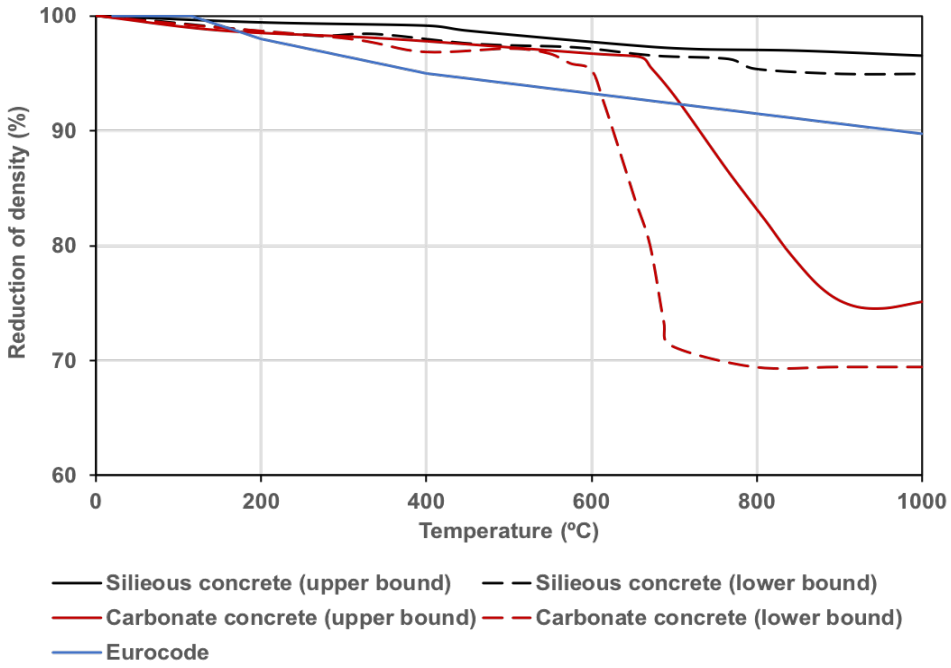

Fig. 2.3 Comparison of density of concrete at elevated temperatures [1, 4, 2, 5, 6]

2.3 Mechanical properties of concrete at elevated temperatures

The mechanical properties odd concrete at elevated temperatures, including compressive strength, instantaneous elastic modulus, stress-strain relations and tensile strength, are considered in the following sections. All the above mentioned properties have a significant reduction at high temperatures.

2.3.1 Compressive strength

Many investigations have been undertaken to evaluate the relationship between the compressive strength and heating temperatures [30, 31]. The compressive strength of concrete

decreases with temperatures [2]. Khaliq [1] summarized the values of compressive strength from 20 °C to 800 °C based on experimental data. Figure 2.4 shows a comparison of compressive strength with different aggregates at elevated temperatures [1] and different standards [2, 3]. The compressive coefficient is the ratio of compressive strength at elevated temperatures and compressive strength at ambient temperature. From these studies, it is apparent that the compressive strength has a considerable decrease above 400 °C.

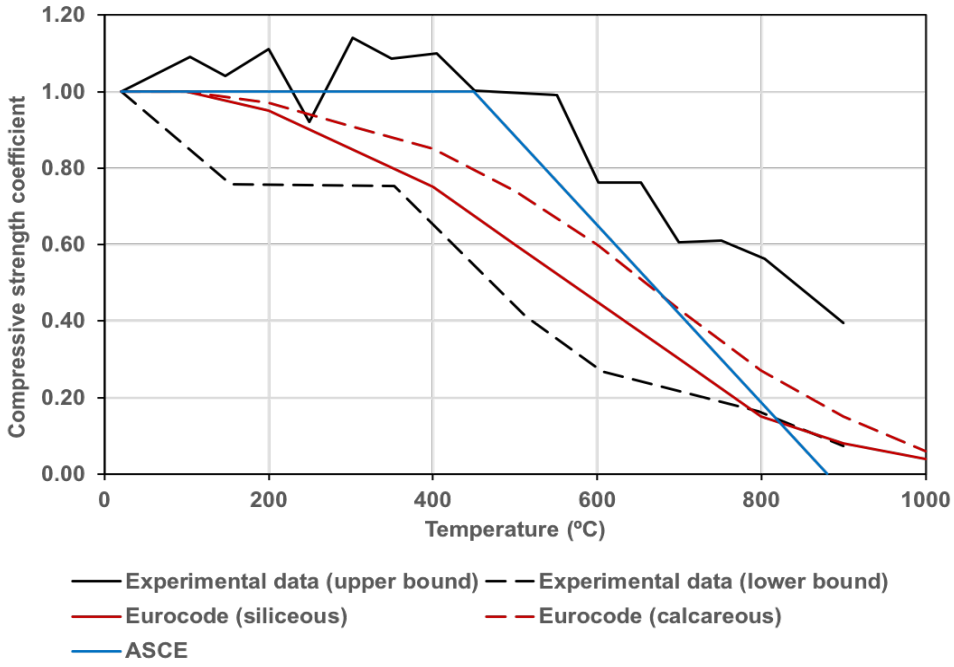

Fig. 2.4 Comparison of compressive strength of concrete with different aggregates at elevated temperatures [1–3]

Schneider [12] summarized influencing factors for the compressive strength of concrete at elevated temperatures as listed in Table 2.1. Several influencing factors are known to have significant effects on the compressive strength of concrete at high temperatures, including types of aggregates, aggregate/cement ratio, and sustained stresses during the heating process. One of the main factors is the type of aggregate. As shown in Fig. 2.4, the decrease in compressive strength of the concrete of calcareous aggregates with temperature is relatively smaller than that for the concrete of siliceous aggregates. Also, the aggregate/cement ratio influences the compressive strength at elevated temperatures significantly. The lean mixes

have a relatively smaller decrease compared to richer mixes [30]. In addition, the concrete specimens under a low constant stress during the heating periods have a smaller reduction in compressive strength compared to the specimens without stresses [30].

Table 2.1 Order of influencing factors of concrete compressive strength at elevated temperatures [12]

Order	Influence factor
First order	Types of aggregate Aggregate/cement ratio Sustained stresses during the heating process
Second order	Maximum size of aggregate
Negligible order	Original compressive strength Water/cement ratio Rate of heating Rate of loading Type of cement Age (exceeding three months)

Many empirical equations based on experimental data have been developed to evaluate the compressive strength of concrete at elevated temperatures. Hertz [32] developed an equation that includes the effect of types of aggregate and initial compressive strength; where the compressive strength is given by

$$f_{c,\theta} = f_c[\frac{1}{1+\frac{\theta}{\theta_1}+(\frac{\theta}{\theta_2})^2+(\frac{\theta}{\theta_8})^8+(\frac{\theta}{\theta_{64}})^{64}}] \tag{2.2}$$

where $f_{c,\theta}$ and f_c are the compressive strength at temperature θ and the compressive strength at ambient temperature. The compressive strength curve for the concrete of siliceous aggregates is described by parameters (θ_1, θ_2, θ_8, θ_{64}) = (15000, 800, 570, 100000). For light weight aggregate, the curve is given by parameters (θ_1, θ_2, θ_8, θ_{64}) = (100000, 1100, 800, 940). For other aggregates, the curve is defined by parameters (θ_1, θ_2, θ_8, θ_{64}) = (100000, 1080, 690, 1000).

2.3.2 Instantaneous elastic modulus

The temperature has a significant influence on instantaneous elastic modulus. Results in the literature indicate that instantaneous modulus decreases with temperatures [2, 33, 34]. Schneider [34] summarized typical reduction of instantaneous elastic modulus at elevated temperatures for different aggregates. Also, Khaliq [1] compiled the values of instantaneous elastic modulus with temperature based on experimental data. The type of aggregate is one of the main influencing factors for the instantaneous elastic modulus at significantly higher temperatures as shown in Fig. 2.5. The instantaneous elastic modulus of quartzite concrete has the largest loss with increasing temperatures. Besides the type of aggregates, experiments [32, 34] indicate other significant influencing factors, such as sustained stresses during the heating process.

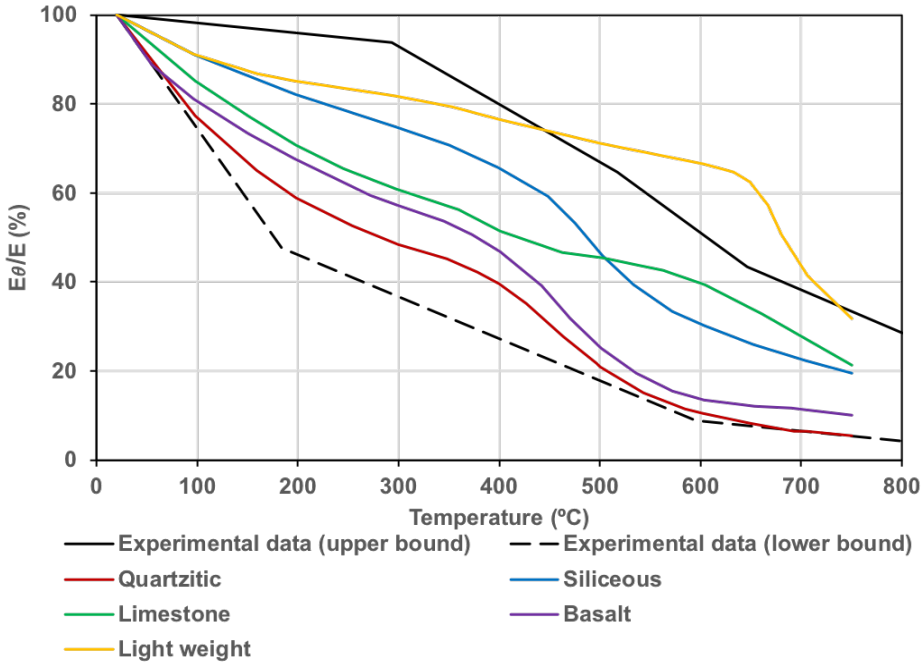

Fig. 2.5 Comparison of instantaneous elastic modulus of concrete with different aggregates at elevated temperatures

Anderberg and Thelanderson [10] developed an equation to describe the curve of instantaneous elastic modulus at elevated temperatures. According to them, the instantaneous elastic

modulus at temperature θ, is given by

$$E_\theta = 2\frac{f_{c,\theta}}{\varepsilon_{c,\theta}} \tag{2.3}$$

where the $f_{c,\theta}$ and $\varepsilon_{c,\theta}$ represent compressive strength and failure compressive strain at temperature θ, respectively. Schneider [35] further considered the effect of the type of aggregates and developed the following equations.
For normal weight concrete:

$$E_\theta = (-0.001552\theta + 1.03104)g'E \qquad for\ 20^\circ C \leq \theta \leq 600^\circ C \tag{2.4}$$

$$E_\theta = (-0.00025\theta + 0.25)g'E \qquad for\ 600^\circ C < \theta \leq 1000^\circ C \tag{2.5}$$

For lightweight concrete:

$$E_\theta = (-0.00102\theta + 1.0204)g'E \qquad for\ 20^\circ C \leq \theta \leq 1000^\circ C \tag{2.6}$$

with

$$g' = 1 + \frac{\sigma}{f_c}\frac{\theta - 20}{100} \tag{2.7}$$

where E is the instantaneous elastic modulus at ambient temperature, σ is the initial compressive stress, and f_c is the compressive strength at ambient temperature, respectively. Although the specific equation of instantaneous elastic modulus is not given in Eurocode [2], the equation can be obtained by differentiating the stress-strain relation Equation 2.9

$$E_\theta = \frac{3f_{c,\theta}}{2\varepsilon_{c,\theta}} \tag{2.8}$$

2.3.3 Stress-strain relations

The mechanical behaviour of concrete is usually represented by stress-strain relations. Eurocode [2] provides an equation to describe stress-strain curves of concrete at elevated temperatures as

$$\sigma_\theta = \frac{3\varepsilon f_{c,\theta}}{\varepsilon_{c,\theta}[2+(\frac{\varepsilon}{\varepsilon_{c,\theta}})^3]} \tag{2.9}$$

where ε is strain and σ_θ is the corresponding stress at elevated temperatures. Figure 2.6 illustrates stress-strain relations of concrete at elevated temperatures based on Eurocode 2 [2]. The slopes of the stress-strain relations decrease with temperatures due to the reduction of compressive strength at elevated temperatures and softening of concrete.

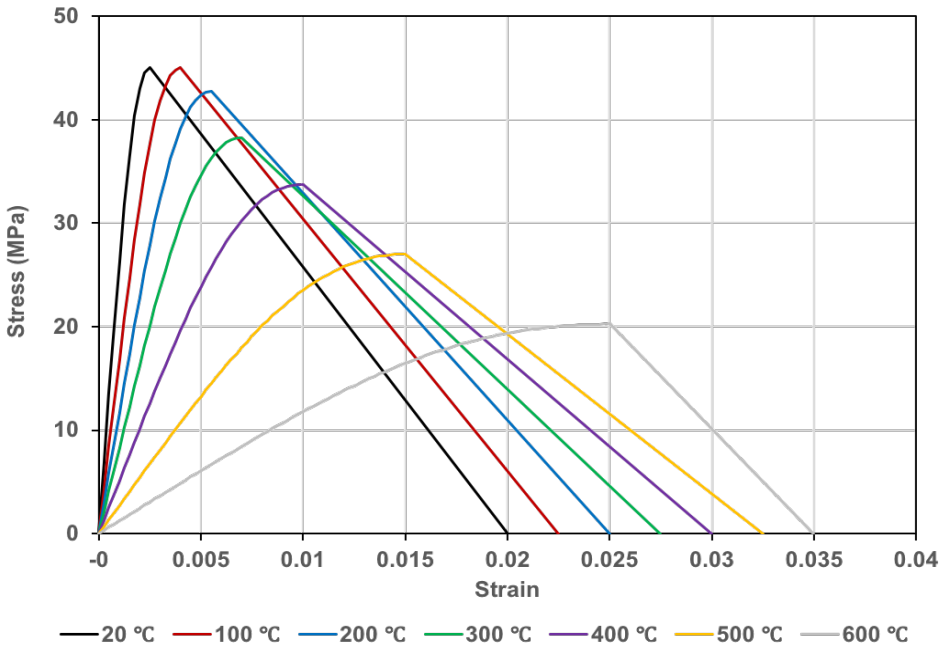

Fig. 2.6 Stress-strain relations of concrete at elevated temperatures [2]

The influencing factors for stress-strain factors at elevated temperatures are summarized in Table 2.2. As discussed earlier, the aggregate/cement ratio and the type of aggregates have significant influences on the compressive strength and instantaneous elastic modulus

of concrete at elevated temperatures. Also, they have influences on the initial slope of the stress-strain curve. The rich mixes have been reported to have lower initial slopes than the lean mixes [30]. Concrete made with softer aggregates has a gradual decrease in the initial slope with temperatures than the concrete made with hard aggregates [10, 36]. Besides, the ultimate strain decreased with sustained stresses [12].

Table 2.2 Order of influencing factors for stress-strain relations at elevated temperatures [12]

Order	Influence factor
First order	Aggregate/cement ratio Types of aggregate Sustained stresses during the heating process
Second order	Types of cement Curing conditions
Negligible order	Original compressive strength Water/cement ratio

2.3.4 Tensile strength

There are limited number studies on tensile strength of concrete at elevated temperatures. Generally, the tensile strength of concrete varies from 7% to 11% of the compressive strength at ambient temperature [37]. Although the tensile strength is much lower than the compressive strength, the tensile properties at elevated temperatures are an important consideration due to cracking of concrete. The low tensile stress is the main reason of cracking and results in the structural damage in tension [38].

The reduction of tensile strength at elevated temperatures based on Eurocode 2 [2] is given by

$$f_{t,\theta} = f_t \qquad for\ 20^\circ C \leq \theta \leq 100^\circ C \tag{2.10}$$

$$f_{t,\theta} = [1-(\theta-100)/500]f_t \qquad for\ 100^\circ C < \theta \leq 600^\circ C \tag{2.11}$$

where $f_{t,\theta}$ and f_t are the tensile strength at temperature θ and the tensile strength at am-

bient temperature, respectively. Bažant [7] developed a constitutive model based on the experimental data from Anderberg [10] in which the tensile strength is given by

$$f_{t,\theta} = (-0.000526\theta + 1.01052) f_t \qquad for\ 20^{\circ}C \leq \theta \leq 400^{\circ}C \tag{2.12}$$

$$f_{t,\theta} = (-0.0025\theta + 1.8) f_t \qquad for\ 400^{\circ}C < \theta \leq 600^{\circ}C \tag{2.13}$$

$$f_{t,\theta} = (-0.0005\theta + 0.6) f_t \qquad for\ 600^{\circ}C < \theta \leq 1000^{\circ}C \tag{2.14}$$

Figure 2.7 shows a comparison of tensile strength model between Eurocode 2 [2] and the model developed by Bažant [7]. The tensile strength coefficient is the ratio of the tensile strength at elevated temperatures to the tensile strength at ambient temperature. The tensile strength decreases with increasing temperatures. The model developed by Bažant was based on experimental data. As can be seen from Fig. 2.7, the concrete loses 20% of its tensile strength at 400 °C. Then, the tensile strength has a considerable decrease from 400 °C to 600 °C due to thermal damage [39] and loses 70% of its initial tensile strength at 600 °C.

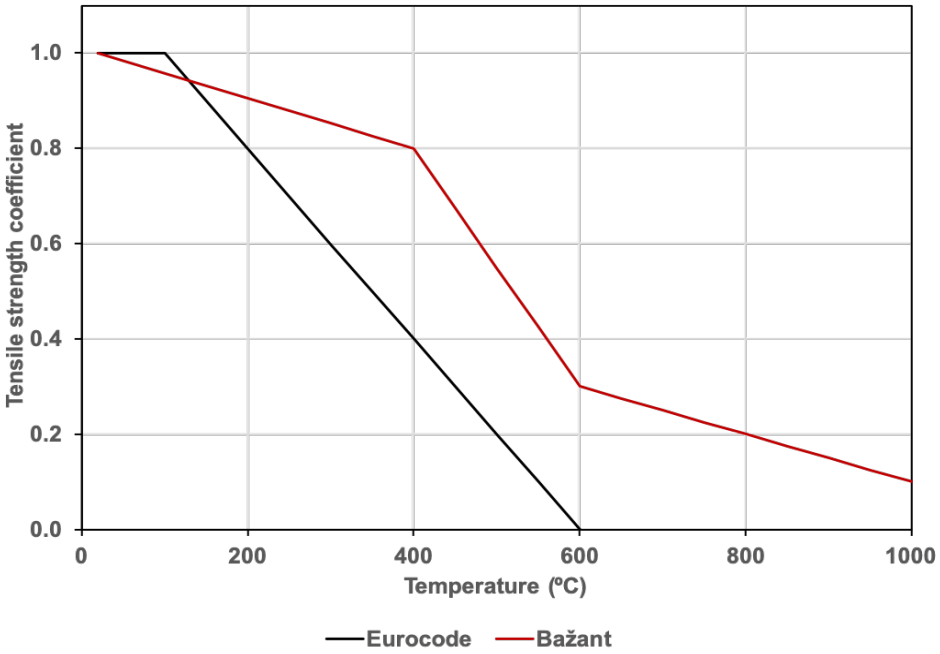

Fig. 2.7 Comparison of tensile strength of concrete at elevated temperatures [2, 7]

2.4 Concrete deformation properties

Concrete under load at elevated temperatures has different strain components: free thermal strain, instantaneous stress-related strain, time-dependent strain, and load induced thermal strain. All these strain components are influenced by temperature. The variations of these components with temperatures is discussed in the following.

2.4.1 Free thermal strain

Concrete expands with increasing temperatures. The free thermal strain is measured under transient heating without any restraints. Khaliq [1] summarized ranges of the free thermal strain from 20 °C to 1000 °C based on experimental data. Figure 2.8 shows a comparison of free thermal strain of concrete at elevated temperatures based on experimental data [28, 40] and different standards [2, 3]. It can be seen that the free thermal strain increases nonlinearly with temperatures. At temperatures exceeding 700 - 800 °C, free thermal strain becomes almost constant as per Eurocode but continues to increase as per ASCE [2, 3].

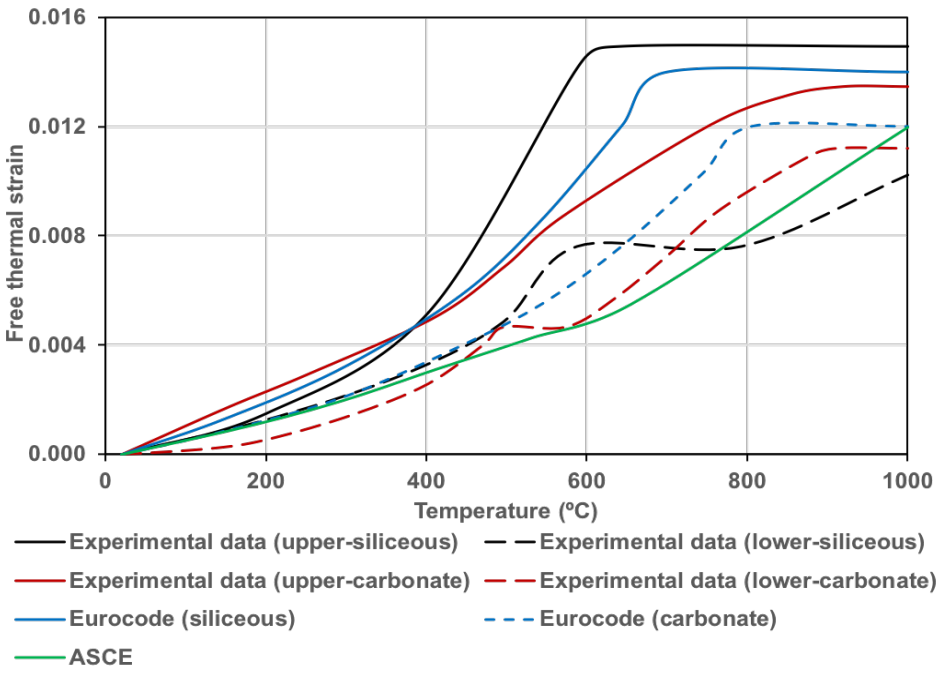

Fig. 2.8 Comparison of free thermal strain of concrete at elevated temperatures [1–3]

It has been suggested that the most significant influencing factor of free thermal strain at elevated temperatures is the type of aggregates [2]. As can be seen from Fig. 2.8, Eurocode [2] provides different values based on the type of aggregates. The concrete made with siliceous aggregate has a higher free thermal strain compared to the concrete with carbonate aggregate. On the contrary, ASCE [3] only has one equation for siliceous and carbonate aggregate concrete. Generally, the value of free thermal strain includes shrinkage. The shrinkage during heating is unavoidable with unsealed specimens [41]. It is difficult to separate free thermal strain and shrinkage during transient heating [41]. However, the shrinkage is very small compared to the thermal expansion. The influence of shrinkage is not considered separately in this study.

2.4.2 Time-dependent creep

The creep discussed in this study is short-term creep of concrete at elevated temperatures. It is often called basic creep [42]. Basic creep is measured when the specimen is loaded at constant temperatures. The experimental work has shown that the creep increases rapidly with increasing temperatures [10, 13]. Figure 2.9 shows basic creep curves of calcareous aggregate concrete evaluated by Gillen [8]. The specimens were heated to 204 °C, 427 °C, and 649 °, respectively. Then, the specimens were loaded to different load levels at each temperature for five hours, including the ambient temperature. It can be seen from Fig. 2.9 that the rate of basic creep is not constant and decreases with time [8]. The creep at 649 °C is around forty times greater than the creep at the ambient temperature, and is approximately twice as long as that at 427 °C. Also, the creep increases with load levels.

Figure 2.10 shows a comparison of basic creep of concrete with different aggregates [8]. From the result of the experiment, it can be seen that the creep curves for siliceous aggregate concrete are similar to those of calcareous concrete for the two lower temperatures considered. At 427 °C, siliceous aggregate concrete has a much larger basic creep than calcareous aggregate concrete.

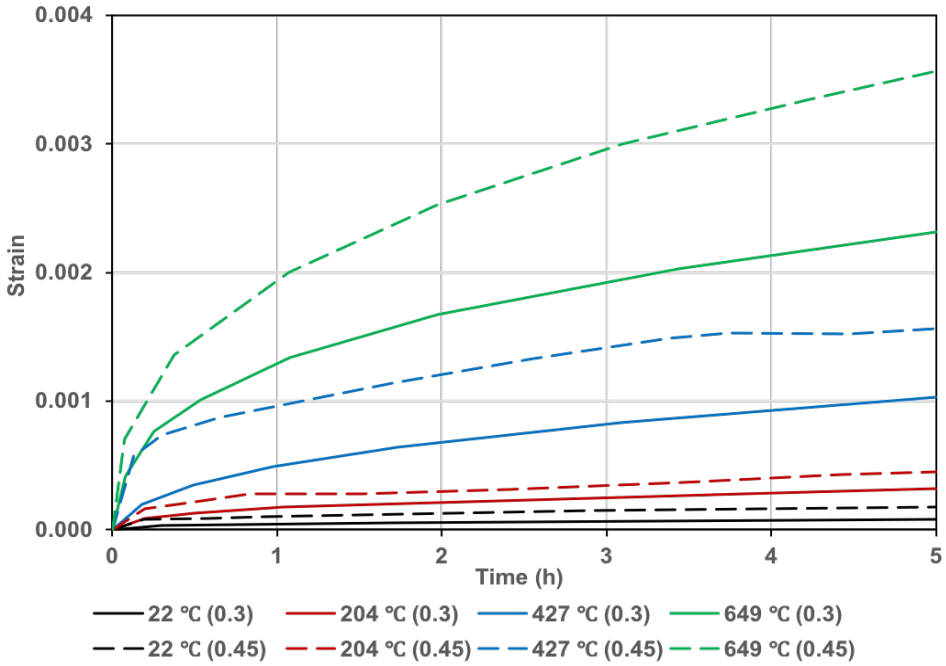

Fig. 2.9 Creep curves of calcareous aggregate concrete under different load levels at elevated temperatures [8]

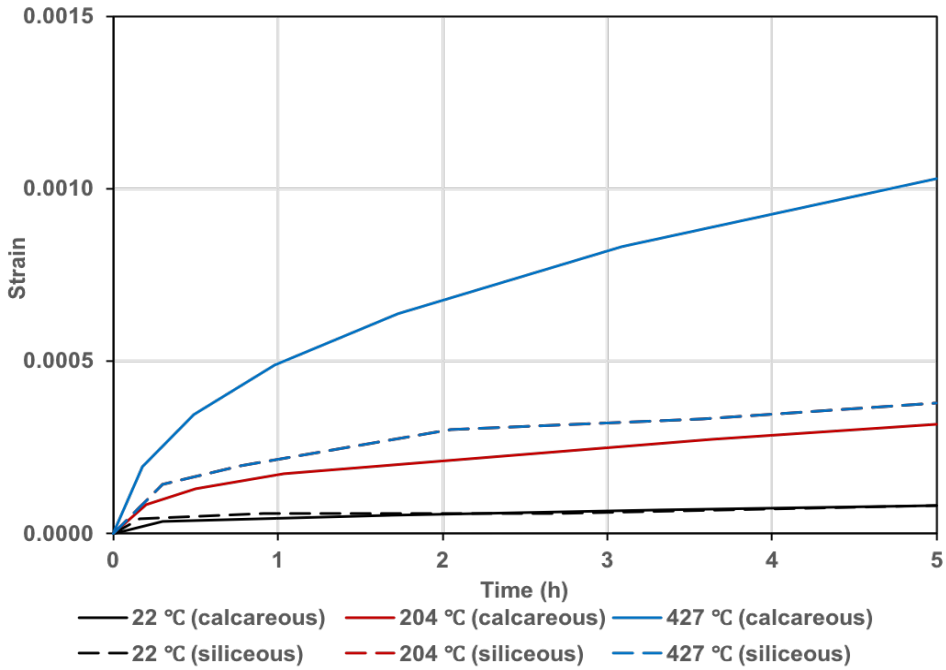

Fig. 2.10 Creep curves of concrete with different aggregates at elevated temperatures [8]

Anderberg [10] developed an equation to represent the basic creep at the constant temperature and the constant load based on experimental data:

$$\varepsilon_{cr} = \beta_0 \frac{\sigma}{f_{c,\theta}} (\frac{t}{t_r})^p e^{k_1(\theta-20)} \tag{2.15}$$

where ε_{cr} is the time-dependent creep strain, t is the time, p is the dimensionless constant, and t_r is the reference time. β_0 and k_1 are constants, evaluated from experimental data. The equation is used to represent the basic creep curve at any temperature and load level. The simulation of the time-dependent creep is discussed in Chapter 5.

2.4.3 Load induced thermal strain

It has been observed that the strain in the preloaded concrete specimen during the first heating cycle is higher compared to the specimen without a preload [7, 10, 13, 12]. The extra strain is referred as Load Induced Thermal Strain (LITS) in research [11, 43–46]. It is also mentioned as the transient strain in some studies [12, 39].

It appears that LITS was first mentioned by Pickett in 1942 [47]. It was defined as the difference between the thermal strain of an unloaded concrete specimen and the strain measured under load for the same type of specimen after subtracting the initial stress-related strain [43]. Due to its large magnitude in comparison to mechanical, creep and shrinkage strains, LITS can dominate the deformation response of concrete structures at elevated temperatures [48].

There has been considerable research on LITS in the past decades [9, 48]. It has been shown that LITS only occurs irrecoverably during the first re-heating of concrete under load. There is no LITS during cooling and the following heating cycles [13]. LITS contains several components. The concrete expands at elevated temperatures. During heating, the expansion may be restrained partially or totally in the loaded direction [9]. Besides, stresses exist due to the temperature gradient of the specimen during heating [48]. The instantaneous elastic modulus decreases at elevated temperatures [2]. From the aspect of material, the temperature

has a significant effect on the moisture content and chemical composition of the cement paste. It results in the micro-cracking in the aggregate and cement paste [12]. All factors contribute to the LITS in concrete.

Giacomo [9] used figures to illustrate definition of LITS. Figure 2.11 shows the strain components developed under different combinations of load. For simplification, only longitudinal strains were considered. During the heating process, the free thermal strain ε_{th} is measured in the unloaded specimen and the shrinkage strain is neglected (or included in the free thermal strain response) as discussed in the previous section (Fig. 2.11 (a)). In the other case, the specimen is loaded at the ambient temperature and the instantaneous stress-related strain ε_{el} is measured immediately after loading (Fig. 2.11 (b)). Then, the specimen is heated under the constant load. The specific strain components developed during the heating process are shown in Fig. 2.11 (c). The extra strain, excluding the effects of the free thermal strain and the instantaneous elastic strain, is considered as LITS. According to the description, LITS is given by

$$LITS = \varepsilon_{tot} - \varepsilon_{th} - \varepsilon_{el} \tag{2.16}$$

where ε_{tot} is the total strain. Although different names of components are used, LITS is calculated using the equation above by many researchers [10, 46, 48].

There is a conflict in the definition mentioned above. From Fig. 2.11, there is elastic strain due to the reduction of the instantaneous elastic modulus at elevated temperatures included in LITS. However, LITS was considered as plastic strain and therefore irrecoverable during the initial heating [13, 43, 49, 50] under load. Some researchers [51–53] suggest exclusion of elastic strain at elevated temperatures. Figure 2.12 shows the modified strain components under different combinations of load. The specimen is loaded at certain temperature and the instantaneous stress-related strain at elevated temperatures, $\varepsilon_{el,\theta}$, is measured immediately after loading. LITS is represented as

$$LITS = \varepsilon_{tot} - \varepsilon_{th} - \varepsilon_{el,\theta} \tag{2.17}$$

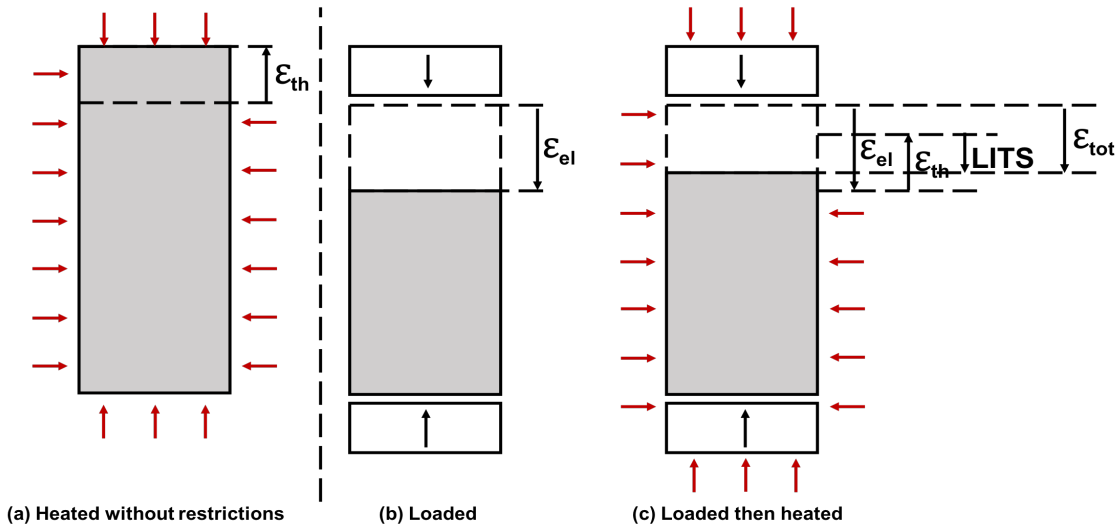

Fig. 2.11 The strain components developed under different combinations of load [9]

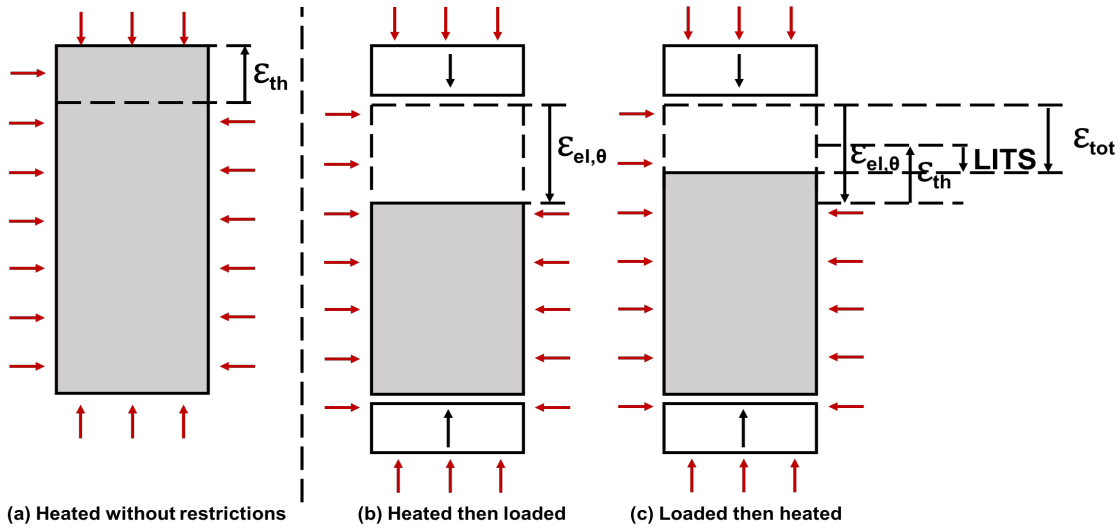

Fig. 2.12 The strain components developed under different combinations of load, considering the reduction of instantaneous elastic modulus at elevated temperatures [9]

2.5 LITS experiment

2.5.1 LITS components

For designing the experiment to measure the value of LITS, it is important to understand the components of LITS. Figure 2.11 illustrates the definition of LITS. According to the definition, LITS includes the increment of instantaneous stress-related strain due to the reduction of instantaneous elastic modulus at elevated temperatures, the time-dependent creep, and the transient creep during transient heating. LITS is represented as

$$LITS = \Delta\varepsilon_{el,\theta} + \varepsilon_{cr} + \varepsilon_{tr} \tag{2.18}$$

where $\Delta\varepsilon_{el,\theta}$ is the increment of the instantaneous stress-related strain, ε_{cr} is the time-dependent creep, and ε_{tr} is the transient creep.

The reduction of the instantaneous elastic modulus at elevated temperatures and the time-dependent creep has been discussed in the previous sections. Figure 2.13 illustrates different

LITS components varied with temperatures evaluated by Anderberg [10] at 35% load level. Figure 2.14 shows the proportion of different LITS components at 600 °C evaluated from Fig. 2.13. Generally, the transient creep is the largest component of LITS [13, 48]. It has been reported to occur only during the first heating on the concrete and it is irrecoverable [10, 48, 54]. During transient heating, the transient creep is assumed to be temperature-dependent [13]. As shown in Fig. 2.14, the proportion of time-dependent creep and increment of stress-related strain are 9% and 15% which are not negligible in the analysis of different LITS components.

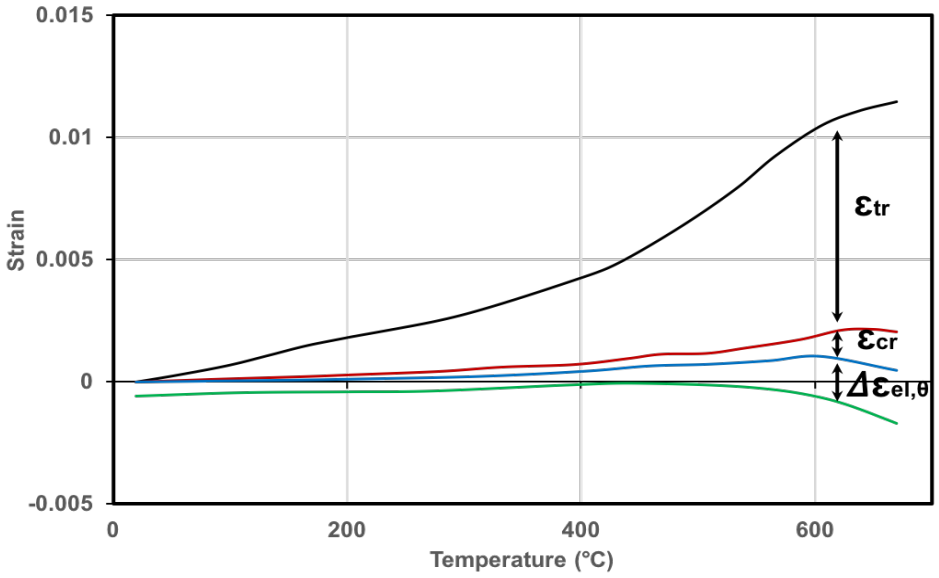

Fig. 2.13 Different LITS components against temperatures under 35% load level [10]

2.5.2 Experimental procedures

It is impossible to design tests to measure LITS directly. However, LITS can be evaluated based on measuring different strain components of concrete at elevated temperatures. Generally, two types of tests are used to explore LITS effect during heating.

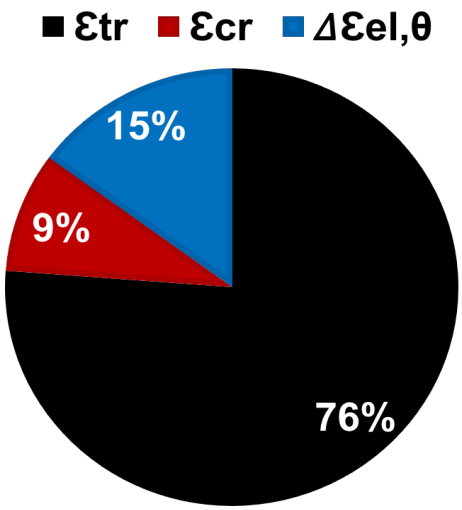

Fig. 2.14 Proportions of different LITS components under 35% load level at 600 °C [10]

The steady state test [55] is used to evaluate the free thermal strain, the instantaneous stress-related strain, and the time-dependent creep. The specimen is heated uniformly to a certain temperature. Then, a specific load is applied and kept constant for hours. It has to be noticed that the temperature gradient exists during the transient heating. The temperature is suggested to be kept constant for one hour to achieve a uniform temperature field within the specimen [56].

The free thermal strain is evaluated during heating without load. When the specimen is loaded until failure, the stress-strain relations of concrete at elevated temperature are obtained. The parameters measured include the compressive strength, the ultimate strain and the instantaneous elastic modulus at elevated temperatures. When the specimen is loaded at a specific load level, the instantaneous stress-related strain is measured immediately. Also, the time-dependent creep curve is evaluated under constant load.

The transient test [57] is used to evaluate instantaneous stress-related strain at ambient temperature and LITS based on the definition discussed in the previous section. The specimen is loaded to a certain load level and the instantaneous stress-related strain is measured

at ambient temperature. Then, the specimen is heated to the reference temperature under constant load. The total strain is loaded to evaluate LITS with the other strain components.

2.5.3 Influencing factors

Numerous experimental investigations have been conducted to study the influence of different factors on LITS. Khoury [13] and Schneider [12] summarized the influence factors of LITS, shown in Table 2.3.

Table 2.3 Order of influencing factors for LITS at elevated temperatures [12, 13]

Order	Influence factor
First order	Temperature Load level Aggregate content by volume (0 - 75 %) Sealing
Second order	Rate of heating Aggregate content by volume (65 - 75 %) Moisture content (65 - 85 % RH) Type pf cement blend (up to 450 °C) Type of aggregate (up to 450 °C) Type of curing
Negligible order	Age

Temperature

Temperature is the most significant influencing factor in LITS. Generally, LITS increases nonlinearly with temperatures based on experimental data [13, 10]. Figure 2.15 shows the common master LITS curves. The curves were evaluated by Khoury [13] and were only valid for temperatures under 450 °C. It is found that there is a kink in the LITS curves at around 150 °C as shown in Fig. 2.15 due to the chemical response of cement paste and drying creep due to moisture loss [11]. Then, the increment of LITS slowed down immediately after 150 °C and started to increase gradually above 200 °C [11]. For temperatures over 450 °C, the master LITS curve no longer fitted the experimental result. At high temperatures, the

magnitude of LITS increased considerably [11]. The model based on the master LITS curve is discussed in the next section.

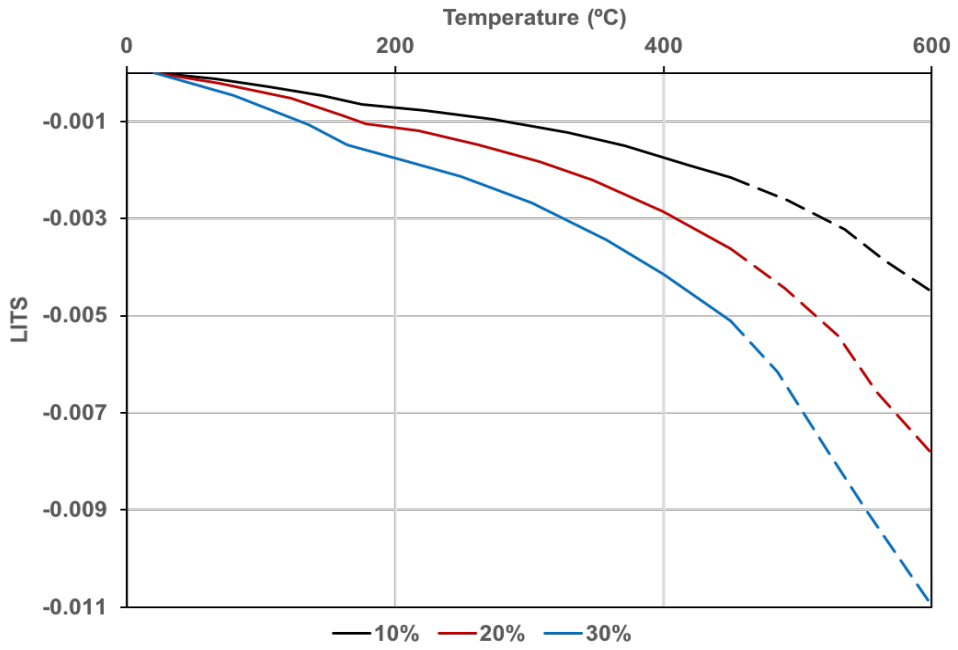

Fig. 2.15 LITS master curves for different load levels during the first heating at the heating rate of 1 °C/min [11]

Load level

The load level is the ratio of the applied stress to the compressive strength at ambient temperature. Experimental results have shown that LITS increases linearly with temperatures under 30 % load level [10, 11, 58, 59]. Figure 2.16 shows the reported influence of load level on master LITS curves with different initial conditions and heating rates [11]. It is interesting to note that the curve is more linear at slower heating rate and for pre-dried specimens [11].

Aggregate

The type of concrete has a relatively small influence on LITS under 450 °C [11]. The LITS curve shown in Fig. 2.15 was evaluated by Khoury [11] regardless of the type of aggregate.

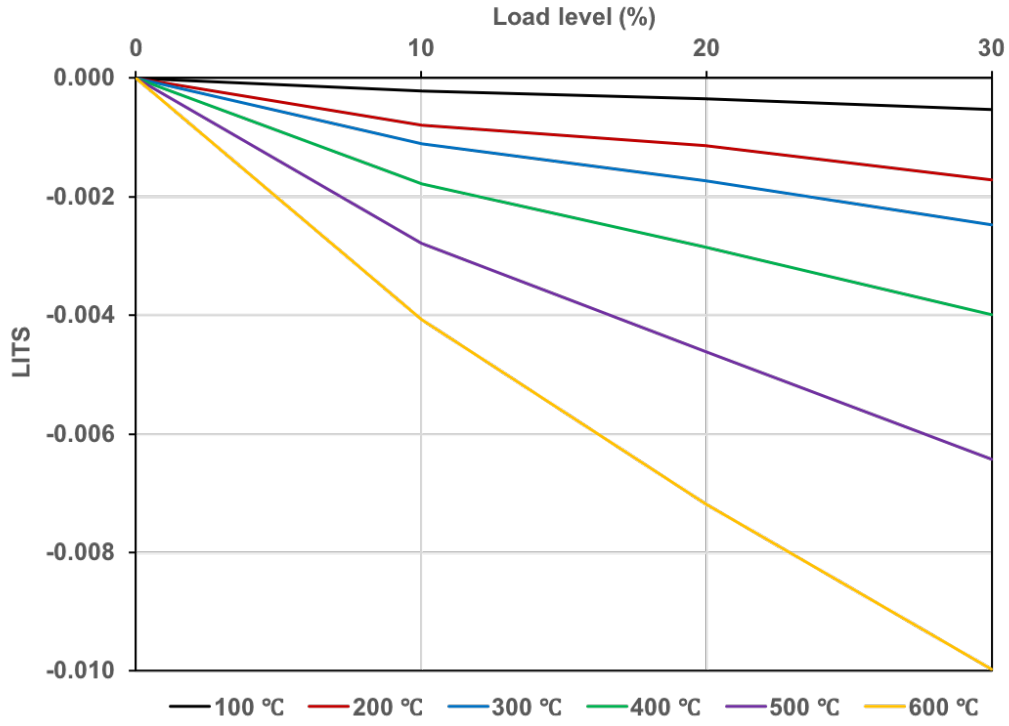

(a) Initially moist, 1 °C/min

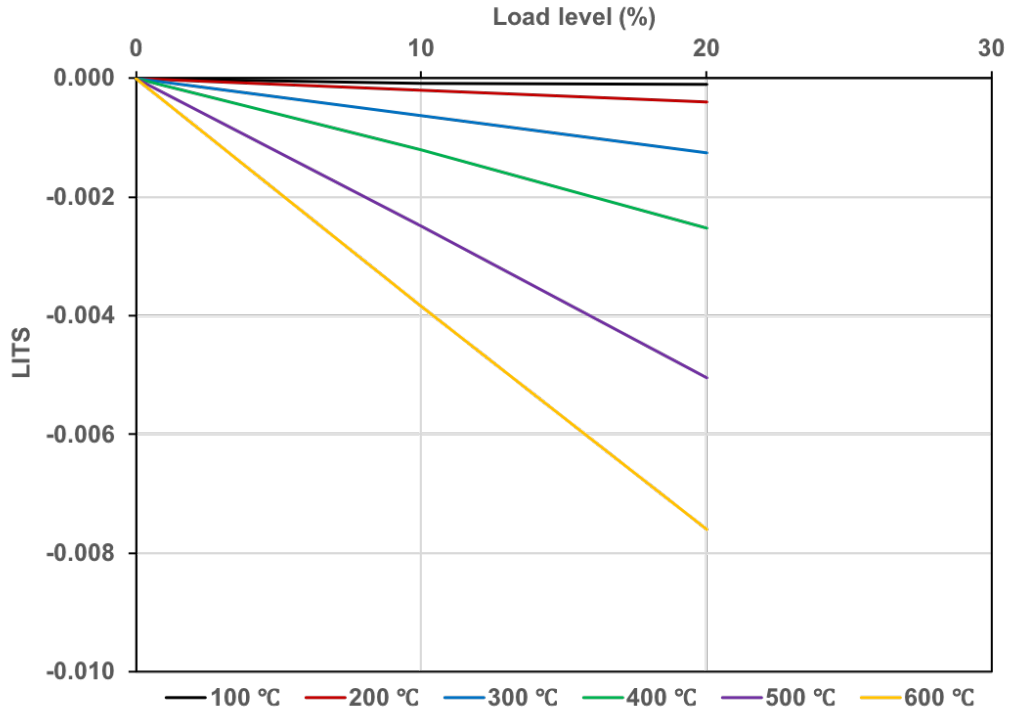

(b) Oven-dry, 0.2 °C/min

Fig. 2.16 Influence of load level on master LITS curves with different initial conditions and heating rates [11]

However, the LITS is strongly influenced by aggregate content [59, 60, 13]. The LITS decreases with harder aggregate due to the reduction of thermal expansion [12, 13, 46].

Heating rate

As shown in Fig. 2.16, the LITS is slightly higher with lower heating rates [11]. Some experiments [61, 62] showed that the heating rate between 2 °C/min and 5 °C/min was not significant for the magnitude of LITS. Some experiments [59, 10, 63] expanded the range wider, 0.2 °C/min to 5 °C/min. For higher heating rates, there is a significant influence on free thermal strain. A heat transfer analysis is conducted in Chapter 3 to evaluate an efficient heating rate.

2.6 LITS simulation

2.6.1 Anderberg and Thelandersson

Anderberg and Thelandersson [10] developed an equation for the transient strain of concrete at elevated temperatures. Different to LITS mentioned earlier, the equation of the transient strain excluded the basic creep. It is included as the transient creep below. The transient creep ε_{tr} is given by

$$\varepsilon_{tr} = k_2 \frac{\sigma}{f_c} \varepsilon_{th} \tag{2.19}$$

where k_2 is a constant between 1.8 to 2.35 based on experimental data, σ/f_c is the load level, and ε_{th} is the free thermal strain. The equation shows a linear relation between the load level and the free thermal strain. Figure 2.17 shows the relationships between the transient creep, load levels, and the free thermal strain for different load levels [10].

The authors [10] indicated that the experimental results were not described accurately by the equation beyond 550 °C. Based on the experiments performed by Schneider [64], the linear relation existed up to 500 °C.

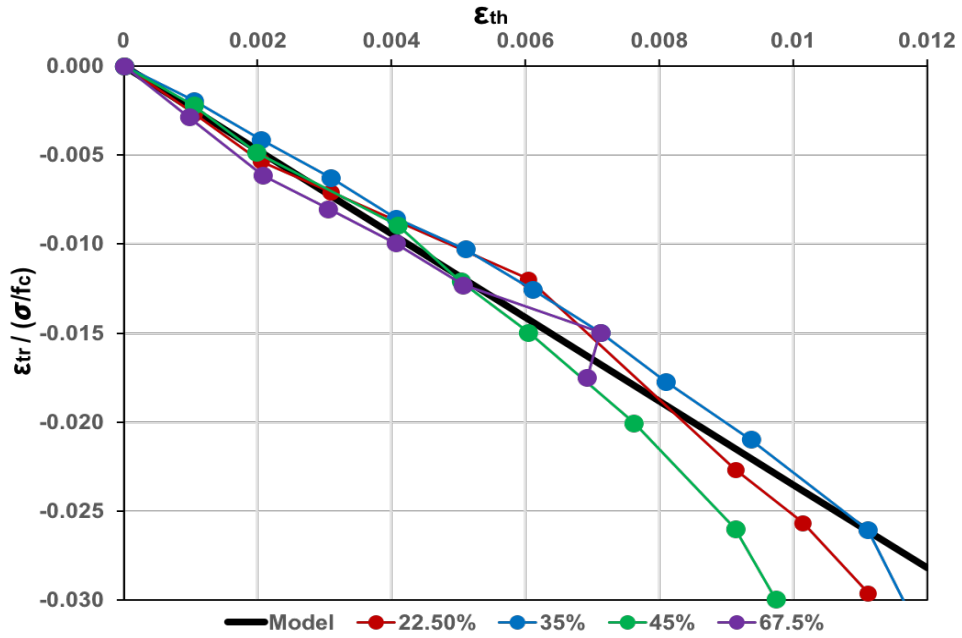

Fig. 2.17 Transient creep versus free thermal strain for quartizite concrete at different load levels [10]

2.6.2 Nielsen

By assuming that transient strain had a linear relation with the temperature instead of the free thermal strain, Nielsen [65] modified Anderberg's model. LITS was given by

$$LITS = \beta \frac{\sigma}{f_c}(\theta - 20) \tag{2.20}$$

where β is the coefficient based on experimental data. For tests below 400 °C, β is assumed to be constant to simplify the model. For the test at higher temperatures, β varied with temperatures to fit experimental data due to LITS increasing more rapidly beyond 450 °C.

2.6.3 Terro

Terro [66] developed the LITS model based on the master LITS curves shown in Fig. 2.15. Based on the discussion of influencing factors, the master LITS curve was found to be

independent from the type of aggregate up to 450 °C. Also, LITS was considered as a linear function of load level up to around 60% load level. LITS was given by

$$LITS(\theta, \sigma/f_c) = LITS(\theta, 0.3) * (0.032 + 3.226\frac{\sigma}{f_c})\frac{V_A}{0.65} \tag{2.21}$$

where $LITS(\theta, 0.3)$ is the value of LITS under the 30% load level at the corresponding temperature θ, and V_A is the volume fraction of aggregates. The equation is valid for temperatures up to 450 °C and load levels up to 30%. $LITS(\theta, 0.3)$ is given by

$$LITS(\theta, 0.3) = A_0 + A_1\theta + A_2\theta^2 + A_3\theta^3 + A_4\theta^4 \tag{2.22}$$

where LITS(θ,0.3) is calculated by parameters (A_0, A_1, A_2, A_3, A_4) = (-43.87, 2.73, 6.35x10^{-2}, -2.19x10^{-4}, 2.77x10^{-7}) [66].

However, the LITS curve of Thames gravel concrete was found to depart from the master LITS curve above 400 °C. The LITS(θ,0.3) is given by

$$LITS(\theta, 0.3) = B_0 + B_1\theta + B_2\theta^2 + B_3\theta^3 + B_4\theta^4 + B_5\theta^5 \tag{2.23}$$

where (B_0, B_1, B_2, B_3, B_4, B_5) = (-1.626x10^{-3}, 5.803x10^{-5}, 6.364x10^{-7}, 3.611x10^{-9}, 9.28x10^{-12}, 8.806x10^{-15}) [66].

2.6.4 Schneider

Schneider [12] evaluated the transient creep with a compliance function. The transient strain is given by [33]

$$\varepsilon_{tr} = \frac{\Phi}{g_1}\frac{f_{c,\theta}}{E_\theta} \tag{2.24}$$

where Φ is the transient creep function, $f_{c,\theta}$ is the compressive strength, and E_θ is the

instantaneous elastic modulus at elevated temperatures, respectively. Φ and g_1 are given by

$$\Phi = g_1[C_1 tanh\gamma_w(\theta - 20) + C_2 tanh\gamma_0(\theta - T_g) + C_3] + \frac{\sigma}{f_c}\frac{\theta - 20}{100} \tag{2.25}$$

$$g_1 = 1 + \frac{\sigma}{f_c}\frac{\theta - 20}{100} \tag{2.26}$$

$$\gamma_w = (0.3w + 2.2) \times 10^{-3} \tag{2.27}$$

where w is the moisture content. The equation of transient creep strain is valid below 30% load level. For quartzite concrete, the Φ is calculated using parameters (C_1, C_2, C_3, γ_0, T_g) = (2.6, 1.4, 1.4, 7.5x10^{-3}, 700). For limestone concrete, the Φ is calculated based on parameters (C_1, C_2, C_3, γ_0, T_g) = (2.6, 2.4, 2.4, 7.5x10^{-3}, 650). For lightweight concrete, the Φ is calculated with parameters (C_1, C_2, C_3, γ_0, T_g) = (2.6, 3, 3, 7.5x10^{-3}, 600).

2.7 Summary

In this chapter, the thermal properties and mechanical properties of concrete at elevated temperatures were discussed.

Based on the experimental data, different strain components under different conditions were discussed and compared. There has been considerable research on LITS. However, only limited data on time-dependent creep and transient creep is available.

3

Finite element simulation of heat transfer in concrete

3.1 Introduction

As one of the primary aims of this thesis is to evaluate the mechanical behaviour of concrete at elevated temperatures, it is essential that concrete samples used in experiments are not damaged in the process of heating due to large thermal gradients. A number of previous studies have considered different heating rates [10, 59, 61–63]. In this study, the rate of heating is not a variable as the research focus is not on the influence of different heating rates. Low heating rates are not efficient as they take a long time to raise the temperature of the sample to the required level and high heating rates cause dangerous self-stresses due to differential thermal expansion. To calculate temperature distributions inside specimens during heating and to choose the most efficient heating rate, the heat transfer simulations were undertaken before the experimentation.

To evaluate the transient temperature distribution under different heating rates and heating times, a finite element simulation was conducted using ABAQUS (Dassault Systemes, France). The following sections consider the details of the simulations and consequent

effect of heating rates. The primary purpose of the simulation is to find the most efficient and reasonable heating rate for LITS experiments. In addition, the sensitivity analysis was undertaken to evaluate the sensitivity of the thermal coefficient and the elastic modulus on the temperatures and thermo-mechanical response of concrete.

3.2 Geometry and boundary conditions

As for the planned experiments, the specimens for simulation were concrete cylinders with a diameter of 100 mm and a height of 200 mm. These dimensions are recommended by a European standard [67]. Only half of the cylinder was analysed as the cylinder is axial-symmetric about the y-axis (Fig. 3.1(a)). The element used in the analysis was a four-node axial-symmetric element. The mesh (Fig. 3.1(b)) had 100 elements in total - 10 along the longitudinal direction and 10 in the radial direction. The boundary conditions comprised of rollers at the bottom of the axisymmetric model (Fig. 3.1(b)). Temperature was applied to the surface of the specimen denoted by red arrows in Fig. 3.1(b). The blue and red dots in the mesh are representative points at the concrete central line and the concrete surface respectively; response of these points will be considered later in this Chapter. The temperature gradient between the concrete central line and the concrete surface is calculated along the red dashed line.

The concrete cylinder is heated in the oven from the ambient temperature to 600 °C. The ambient temperature is assumed to 20 °C. The heating rates selected were 1°C/min, 2°C/min, 5°C/min, and 10°C/min. Radiative heat transfer between chamber and the specimen surface occurs when a temperature difference exists. Also, the heat transfer by conduction causes temperature gradient between the concrete central line and the concrete surface.

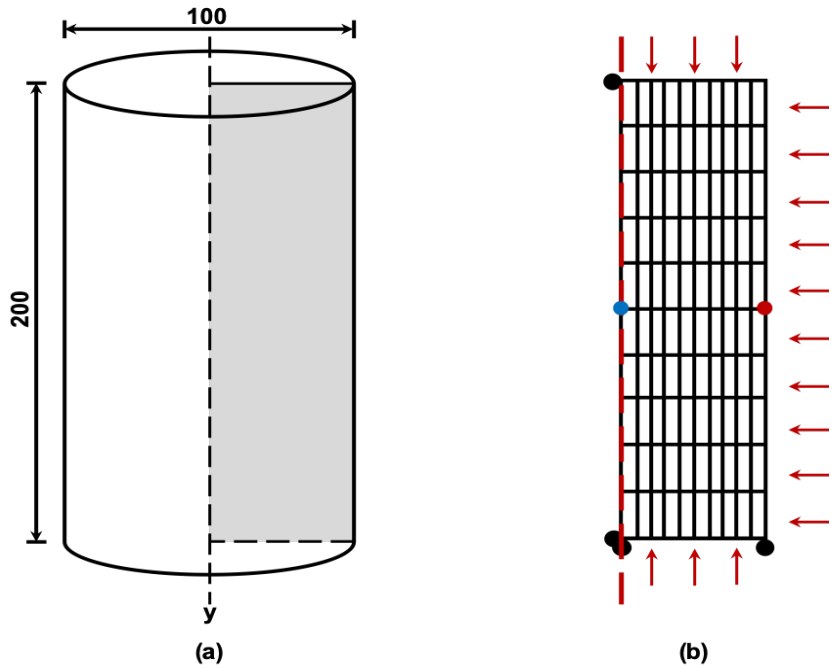

Fig. 3.1 (a) The specimen considered and (b) the finite element mesh and boundary conditions. (Dimensions are in mm)

3.3 Concrete thermal properties

The concrete contains coarse aggregates, sand, cement paste, and water. Each of them has different thermal properties at elevated temperatures. Therefore, thermal properties of concrete are very complex. Many studies have been carried out and most relevant thermal parameters have been investigated. In this simulation, the values provided in Eurocode 2 [2] on conductivity, specific heat, and density of concrete at elevated temperatures were used.

3.3.1 Conductivity

Thermal conductivity of concrete is influenced by type of aggregates. Eurocode 2 [2] gives the lower and upper limit values of the thermal conductivity, respectively
Lower limit:

$$\lambda_c = 1.36 - 0.136(\theta/100) + 0.0057(\theta/100)^2 \quad W/mK \quad for\ 20^\circ C \leq \theta \leq 1200^\circ C \tag{3.1}$$

Upper limit:

$$\lambda_c = 2 - 0.2451(\theta/100) + 0.0107(\theta/100)^2 \quad W/mK \quad for\, 20°C \leq \theta \leq 1200°C \tag{3.2}$$

where λ_c and θ are the conductivity and temperature of normal weight concrete, respectively. The variations of conductivity values at elevated temperatures are plotted and shown in Fig. 3.2. Anderberg [10] compared concrete temperatures based on the above empirical equations and lab measurements. The measured temperatures were found to be lower than calculations. Therefore, the lower limit of conductivity is used in the simulation for this study.

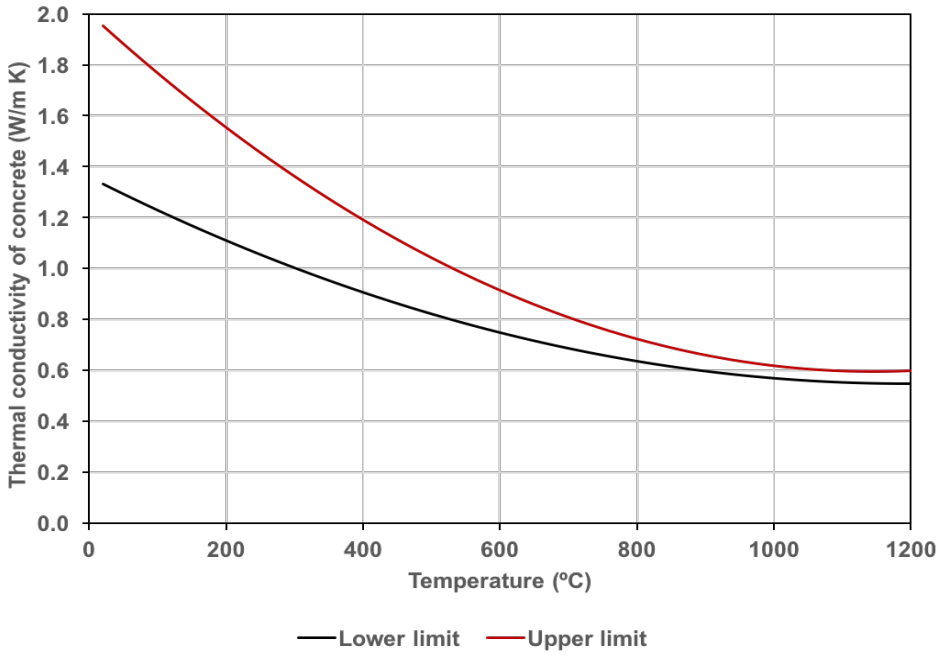

Fig. 3.2 Temperature dependent thermal conductivity of concrete based on Eurocode 2 [2]

3.3.2 Specific heat

The specific heat relates to the heat energy per unit mass required to raise the temperature by one degree Celsius. Eurocode 2 [2] gives the specific heat values of dry concrete as

$$C_p(\theta) = 900 \quad J/kgK \qquad for\ 20^\circ C \leq \theta \leq 100^\circ C \tag{3.3}$$

$$C_p(\theta) = 900 + (\theta - 100) \quad J/kgK \qquad for\ 100^\circ C < \theta \leq 200^\circ C \tag{3.4}$$

$$C_p(\theta) = 1000 + (\theta - 200)/2 \quad J/kgK \qquad for\ 200^\circ C < \theta \leq 400^\circ C \tag{3.5}$$

$$C_p(\theta) = 1100 \quad J/kgK \qquad for\ 400^\circ C < \theta \leq 1200^\circ C \tag{3.6}$$

where $C_p(\theta)$ is the specific heat of dry concrete at temperature θ . The temperature dependent specific heats for different moisture contents are plotted and shown in Fig. 3.3. The Eurocode 2 [2] suggests that the specific heat is influenced by moisture content for $\theta < 200$ °C. There is a bi-linear relationship between 115 °C and 200 °C which is shown in Fig. 3.3. Considering the humid climate in Scotland, the moisture content of concrete was assumed to be 3% in the simulation.

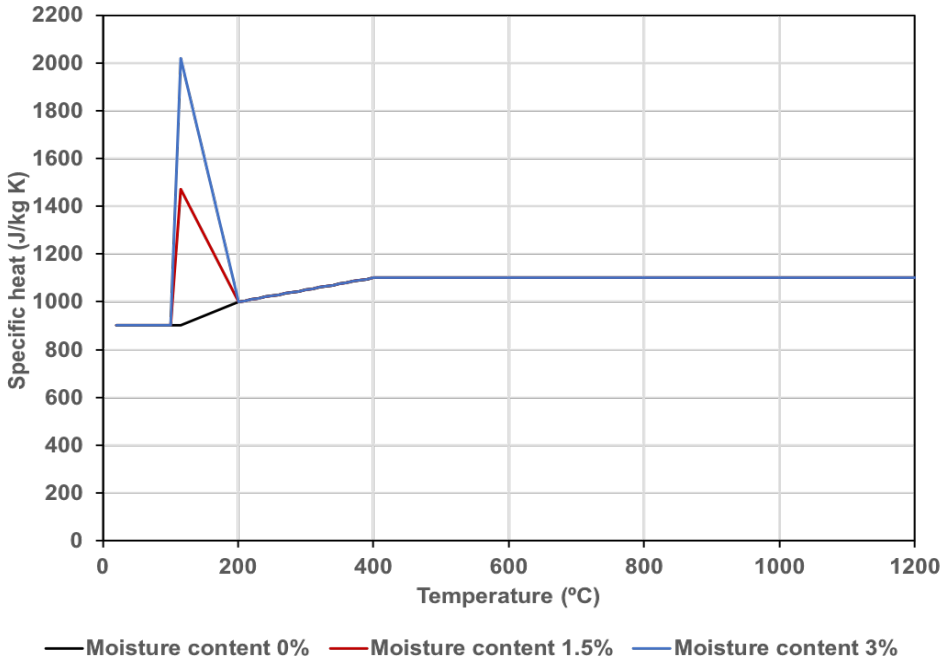

Fig. 3.3 Temperature and moisture content dependent specific heats of concrete based on Eurocode 2 [2]

3.3.3 Density

The density of concrete was assumed to be 2400 kg/m^3 at the ambient temperature. The density of concrete at elevated temperatures is reduced with water loss. Eurocode 2 [2] gives the variation of density with temperatures:

$$\rho(\theta) = \rho(20^\circ C) \qquad for\ 20^\circ C \leq \theta \leq 115^\circ C \tag{3.7}$$

$$\rho(\theta) = \rho(20^\circ C)(1 - 0.02(\theta - 115)/85) \qquad for\ 115^\circ C < \theta \leq 200^\circ C \tag{3.8}$$

$$\rho(\theta) = \rho(20^\circ C)(0.98 - 0.03(\theta - 200)/200) \qquad for\ 200^\circ C < \theta \leq 400^\circ C \tag{3.9}$$

$$\rho(\theta) = \rho(20^\circ C)(0.95 - 0.07(\theta - 400)/800) \qquad for\ 400^\circ C < \theta \leq 1200^\circ C \tag{3.10}$$

where $\rho(\theta)$ is the density of concrete at temperature θ. The reduction of density with temperatures is shown in Fig. 3.4.

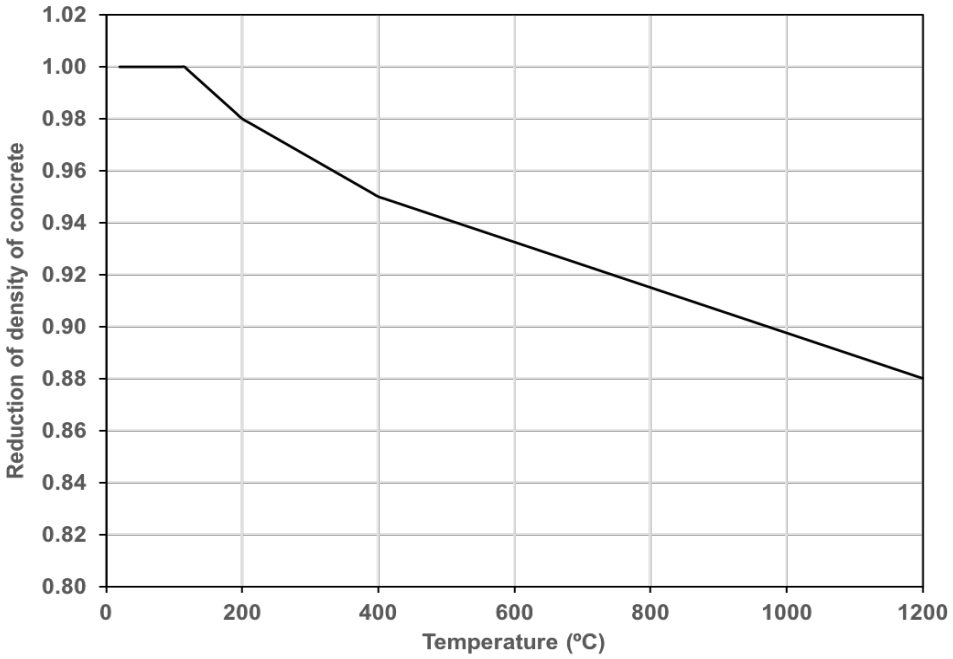

Fig. 3.4 Reduction of density of concrete at elevated temperatures based on Eurocode 2 [2]

3.3.4 Other parameters

Other parameters also needed for the heat transfer analysis are convection factor and emissivity. The convection factor was assumed to be 25 W/m^2K. The emissivity related to the concrete surface was taken as 0.7. These values are suggested by Eurocode 2 [2].

3.4 Mechanical properties of concrete

3.4.1 Compressive behaviour

It has been suggested that the peak compressive strength of concrete decreases linearly as its temperature increases beyond 100 °C [2]. The failure compressive strain also increases with temperature up to 600 °C after which it becomes constant. The compressive strength at the ambient temperature was based on 51 MPa in the simulation based on experimental work conducted by Smith [14]. The reduction of compressive strength of concrete at elevated temperatures is given by the compressive strength coefficient as

$$f_{c,\theta} = k_{c,\theta} f_c \tag{3.11}$$

where f_c and $f_{c,\theta}$ are the compressive strengths at the ambient temperature and temperature θ, respectively, and $k_{c,\theta}$ is the compressive strength coefficient at temperature θ. The value of compressive strength coefficient is suggested by Eurocode 2 [2] as shown in Fig. 3.5.

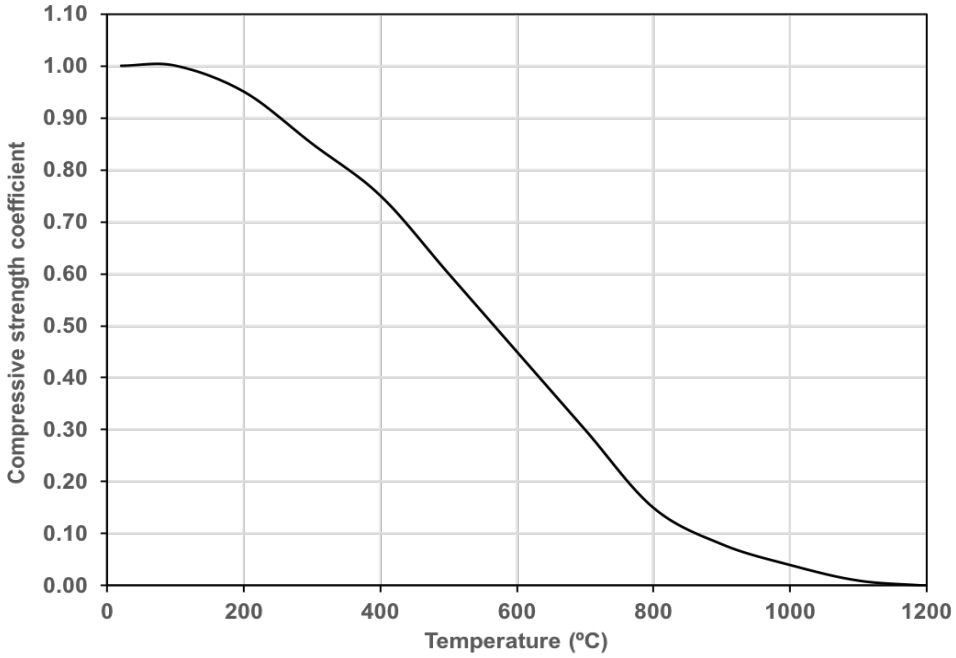

Fig. 3.5 Compressive strength coefficient of concrete at elevated temperatures based on Eurocode 2 [2]

The elastic modulus at elevated temperatures is given by

$$E_\theta = \frac{3f_{c,\theta}}{2\varepsilon_{c,\theta}} \tag{3.12}$$

where E_θ and $\varepsilon_{c,\theta}$ are the elastic modulus and failure compressive strain at elevated temperatures, respectively.

3.4.2 Thermal expansion

Concrete expands as temperature rises. Eurocode 2 [2] gives the thermal strain of siliceous concrete from 20 °C to 1200 °C:

$$\varepsilon_{th} = -1.8\times10^{-4} + 9\times10^{-6}\theta + 2.3\times10^{-11}\theta^3 \qquad for\ 20^\circ C \le \theta \le 700^\circ C \tag{3.13}$$

$$\varepsilon_{th} = 14\times10^{-3} \qquad for\ 700^\circ C < \theta \le 1200^\circ C \tag{3.14}$$

where ε_{th} is the thermal strain at elevated temperatures. Youssef and Maftah [33] derived a linear function of the thermal expansion, which is

$$\varepsilon_{th} = \alpha \times (\theta - 20) \quad for\ \theta > 20^{\circ}C \tag{3.15}$$

where α is the thermal coefficient. This thermal coefficient was evaluated from experiments in subsequent chapters and used in the simulation.

3.4.3 Elasticity relations for axial symmetry

In the simulation, the concrete was considered to be an isotropic material with identical elastic properties at all directions. Coordinates for axial-symmetric model are r (radial), θ (circumferential), and z (axial). Nothing varies at circumferential direction, and therefore elasticity relations are mathematically two-dimensional. The stress-strain relations with isotropic and thermal loading are [68]

$$\begin{Bmatrix} \sigma_r \\ \sigma_\theta \\ \sigma_z \\ \tau_{zr} \end{Bmatrix} = \begin{bmatrix} 1 & f & f & 0 \\ f & 1 & f & 0 \\ f & f & 1 & 0 \\ 0 & 0 & 0 & g_2 \end{bmatrix} \left(\begin{Bmatrix} \varepsilon_r \\ \varepsilon_\theta \\ \varepsilon_z \\ \gamma_{zr} \end{Bmatrix} - \begin{Bmatrix} \alpha T \\ \alpha T \\ \alpha T \\ \alpha T \end{Bmatrix} \right) \tag{3.16}$$

where $f = \frac{\nu}{1-\nu}$, $g_2 = \frac{1-2\nu}{2(1-\nu)}$, and $T = \theta - 20$. T is the temperature change, α is the thermal coefficient, and ν is Poisson's ratio. σ_r, σ_θ, σ_z and τ_{zr} are radial stress, circumferential stress, axial stress and shear stress, respectively. ε_r, ε_θ, ε_z and ε_{zr} are radial strain, circumferential strain, axial strain and shear strain, respectively.

3.5 Analysis and discussion

3.5.1 Heat transfer analysis

The heat transfer analysis is conducted with thermal properties discussed above. The variations and changes of concrete temperature were computed. The simulation includes heat exchange between the concrete surface and chamber. The temperature of the concrete surface increases through convection and radiation. Within the concrete cylinder depth and radius, the temperature of the concrete central line increases due to conduction.

Figure 3.6 shows contours of temperature distributions when the chamber temperature reaches 600 °C with different heating rates. Figure 3.7 shows the temperature differences between the concrete central line and the concrete surface against chamber temperatures for different heating rates. We observe from Fig. 3.6 that the temperature range with the heating rate of 10 °C/min exceeds 300 °C when the chamber temperature reaches 600 °C. Also, Figure 3.7 shows that the temperature difference between the concrete central line and the concrete surface reaches the peak when the chamber temperature reaches the maximum temperature. The maximum temperature differences when the chamber temperature is 600 °C are 30 °C, 60 °C, 150 °C, and 240 °C for heating rates of 1, 2, 5, 10 °C/min, respectively. It is interesting to note that initially 10 °C/min heating rate line is below 1 °C/min line (Fig. 3.7). It is because the abscissa is chamber temperature. The time lag is short for heating rate of 10 °C/min when the chamber temperature reaches 50 °C.

The specimen expands with increasing temperatures. When a temperature gradient exists, the thermal expansion varied. Regions with smaller expansion towards the central line of the specimen restrict the expansion of regions closer to the surface and regions with larger expansion induce mechanical strains in regions not expanding as much. These interactions result in stresses even without the application of any mechanical forces. When the rate of heating is set high (e.g. 10 °C/min), the considerable temperature difference results in significant differential thermal expansion within the specimen, which may cause

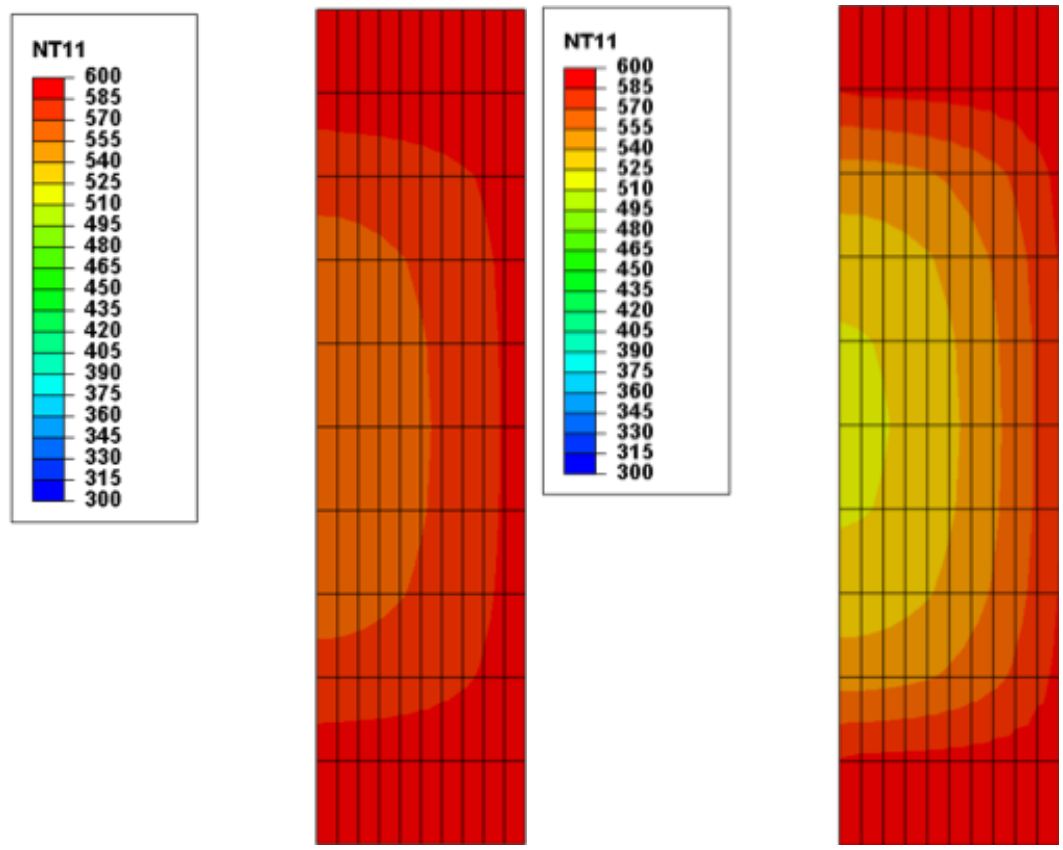

(a) 1 °C/min (b) 2 °C/min

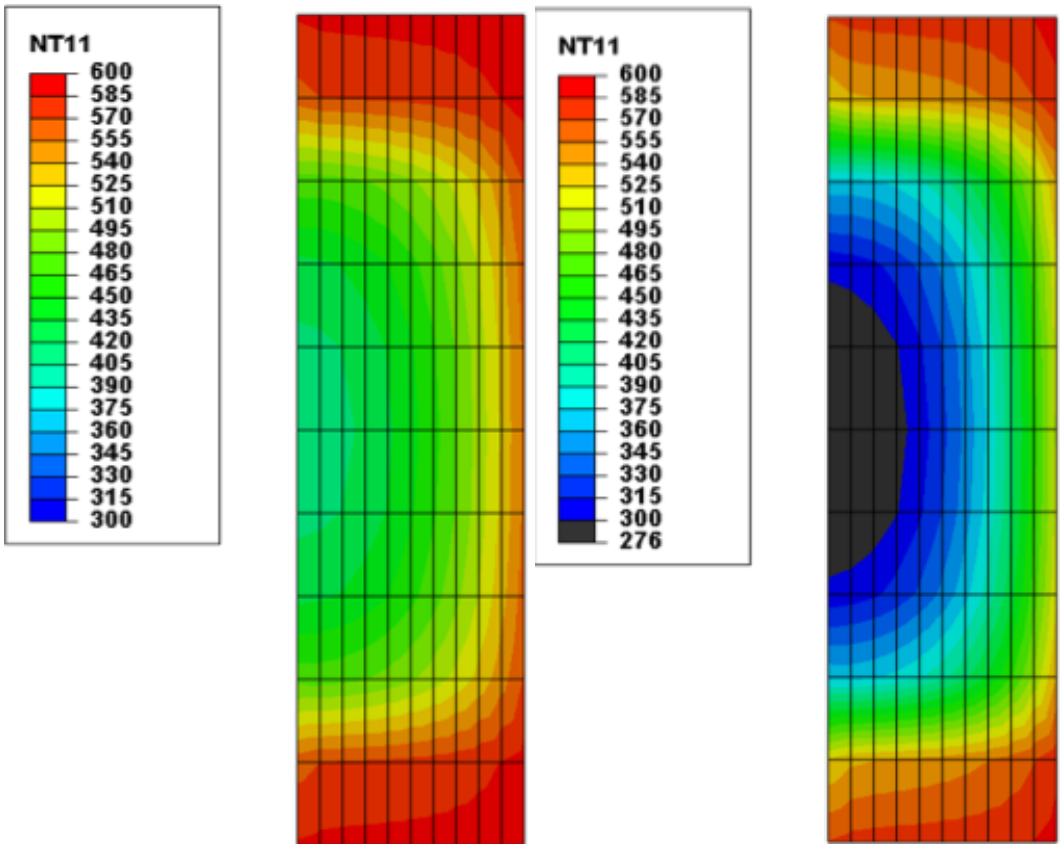

(c) 5 °C/min (d) 10 °C/min

Fig. 3.6 Contours of temperature distributions with different heating rates when the chamber temperature reaches 600 °C

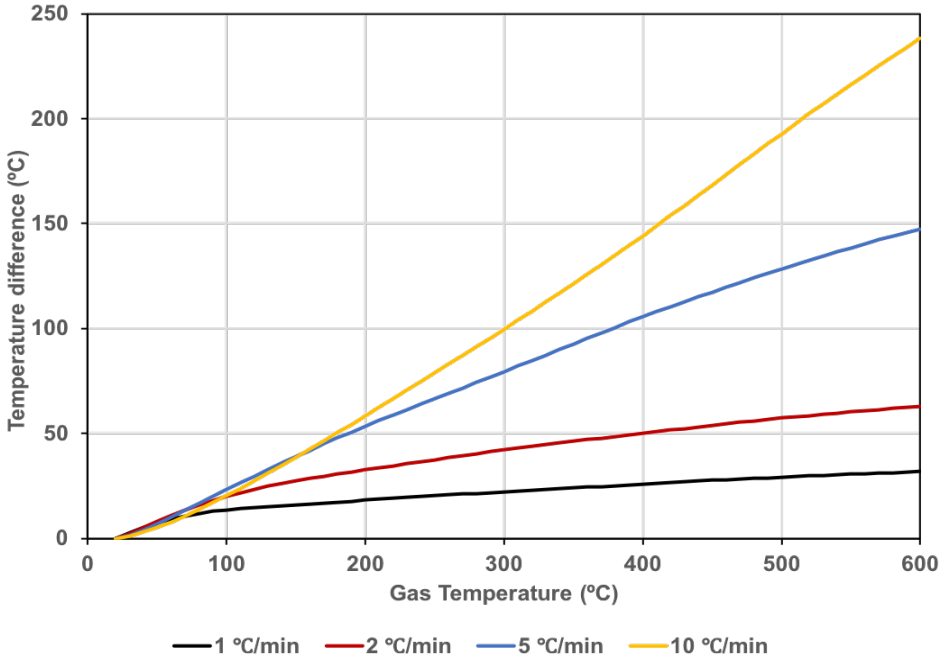

Fig. 3.7 Temperature differences between the concrete central line and the concrete surface against chamber temperatures with different heating rates

damage. On the other hand when the heating rate is low, the required temperature will be achieved after a long time. For example, at the heating rate of 1 °C/min, the heating time required is 10 hrs without including any subsequent constant heating which may be required to ensure uniform temperature in the specimen. The simulations conducted help in the selection of a heating rate which takes less time without causing large stresses due to differential thermal expansion. Therefore, thermomechanical analysis was undertaken for heating rates of 2 and 5 °C/min. Also, thermomechanical analysis with the heating rate of 10 °C/min was conducted to confirm that the heating rate is likely to be too high for the specimen.

RILEM [56] suggests that the chamber temperature should be maintained for 1 hour to reduce the temperature gradient within the specimen. Figures 3.8 and 3.9 show temperature distributions for different maintaining times. Figure 3.10 shows the chamber temperature, the concrete central line temperature, and the concrete surface temperature against time with different heating rates. As can be seen from Figs. 3.8 - 3.10, the concrete surface temperature

reaches the chamber temperature with 1 hour maintaining time. However, the temperature differences between the concrete central line and the concrete surface remains around 20 to 30 °C. The simulation shows that the temperature within the specimen becomes uniform after 2 hrs of constant temperature heating. In the test, the specimen rests at the test temperature for 2 hrs to achieve uniform temperature in concrete.

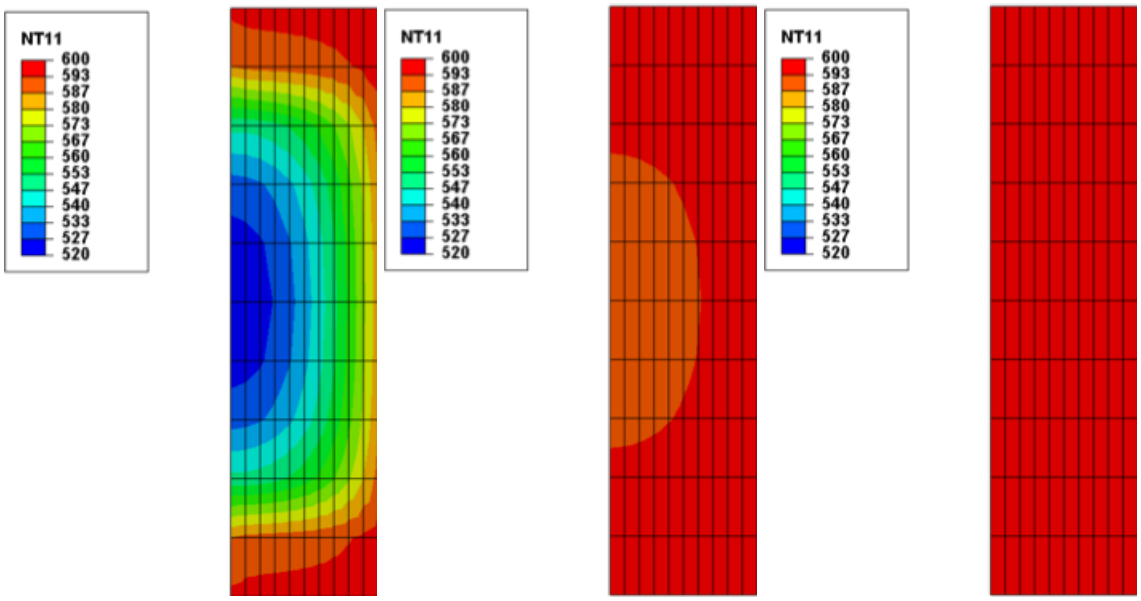

(a) (b) (c)

Fig. 3.8 Temperature distributions of the specimen after the chamber temperature reaches 600 °C with the heating rate of 2 °C/min. (a) Without further heating; (b) after 1 hour of heating; and (c) after 2 hrs of heating

After the experiments discussed in the following chapters, the concrete surface temperature recorded by the thermocouples will be used as the boundary condition in the simulation. Thus a more accurate temperature profile will be employed.

3.5.2 Mechanical analysis

The mechanical analysis includes the thermal expansion and elastic behaviour of concrete. In this chapter, post-elastic behaviour of concrete was not considered in the simulation. During

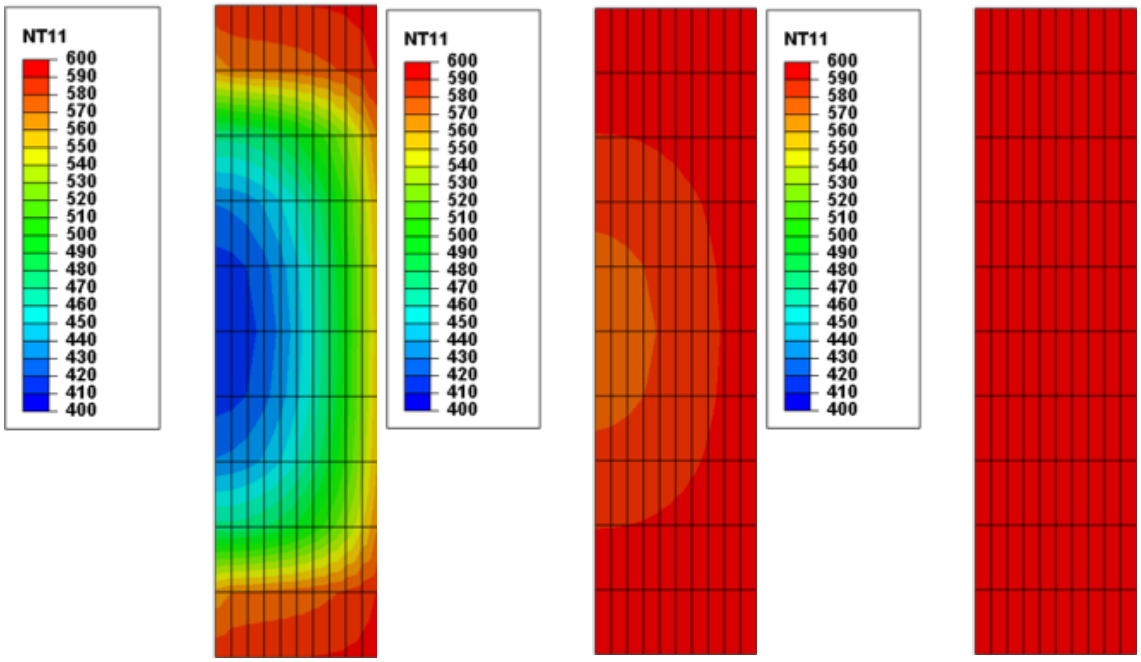

(a) (b) (c)

Fig. 3.9 Temperature distributions of the specimen after the chamber temperature reaches 600 °C with the heating rate of 5 °C/min. (a) Without further heating; (b) after 1 hour of heating; and (c) after 2 hrs of heating

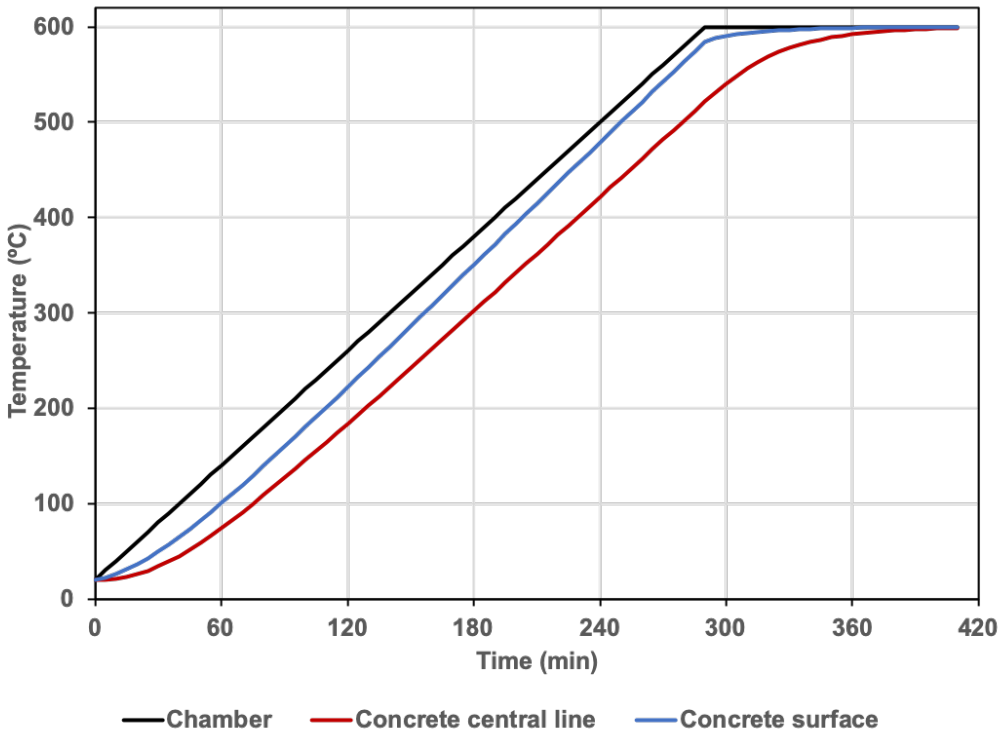

(a) 2 °C/min

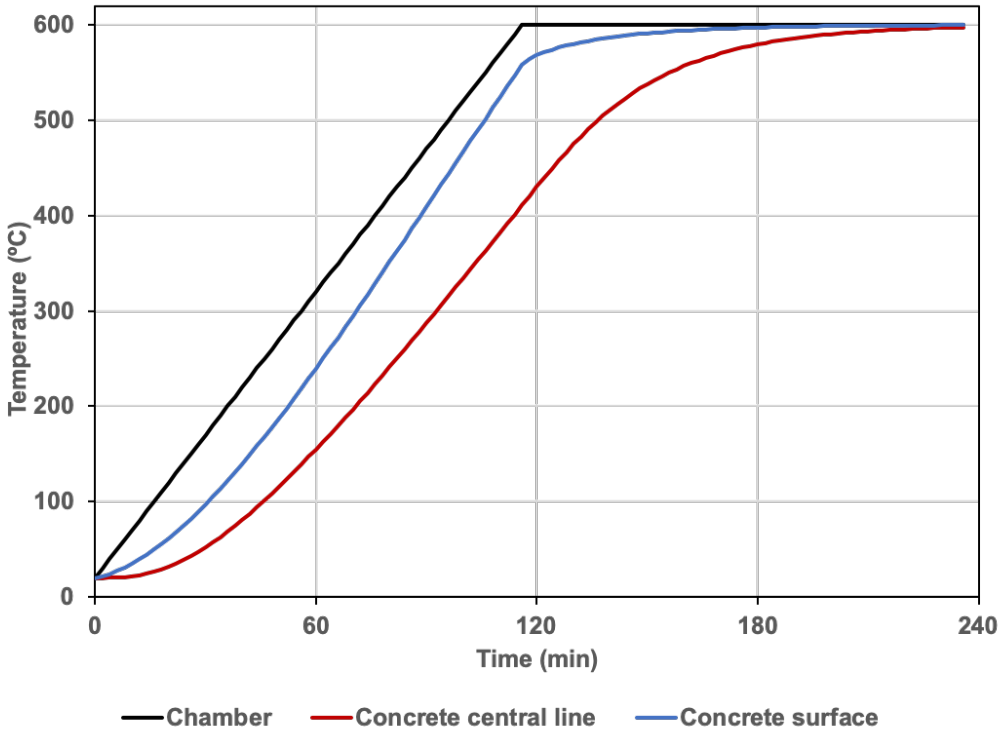

(b) 5 °C/min

Fig. 3.10 Concrete central line temperatures and concrete surface temperatures against time for different heating rates, compared with chamber temperatures

the heating process, the concrete expands with increase in temperature. However, as stated earlier, since the concrete temperature is not uniform during heating, stresses are generated due to different thermal expansions.

Figure 3.11 shows the vertical stresses at the middle cross-section (radially from the central line to the outer surface) for the heating rate of 10 °C/min at different chamber temperatures. The concrete surface has a higher temperature and a larger expansion. The concrete central line has a lower temperature and a smaller expansion. The expansion of concrete surface is restrained and is dominated by compressive stress. The concrete central line expands with increasing temperatures and is dominated by tensile stress. The highest tensile stress caused by temperature gradient reaches to 20 MPa. Generally, the tensile strength of concrete is around 10% of compressive strength at ambient temperature (5.1 MPa) [37]. The self-stresses may cause the damage of the specimen without extra loading.

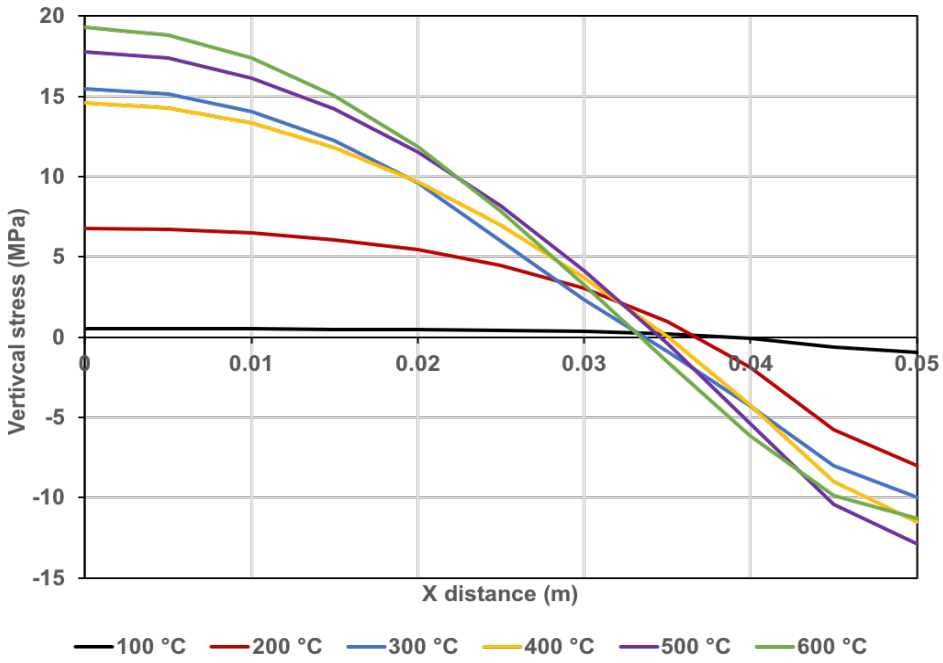

Fig. 3.11 The vertical stresses along the radius (from central line to surface) for the heating rate of 10 °C/min at different chamber temperatures

To choose a more appropriate heating rate, the thermomechanical analysis at heating rates of 2 °C/min and 5 °C/min were considered. Figures 3.12 and 3.13 show stresses along the radius at different chamber temperatures. The vertical stresses caused by the temperature gradients are expected higher than radial stresses. The maximum tensile stress reaches to 10 MPa at the heating rate of 5 °C/min. The considerable tensile stress will result in damage during heating. For reducing the influence of temperature gradient during heating, the heating rate of 2 °C/min is chosen in the experiment.

3.5.3 Parameter sensitivity analysis

The elastic modulus and thermal coefficient play important roles in thermomechanical analysis. In the simulation, the elastic modulus and thermal coefficient are known to be non-linear with temperatures. To explore the temperature influence of these two parameters, a parameter sensitivity analysis was conducted. Once again, post-elastic behaviour was not considered in this analysis.

The sensitivity analysis is based on the planned LITS experiment (to be considered later). The procedure of LITS experiment is shown in Fig. 3.14. The concrete cylinder is first loaded axially to a reference load level (the ratio of compressive stress to compressive strength at ambient temperature), and then heated to the prescribed temperature in the oven at the heating rate of 2 °C/min. The temperature is kept constant for 2 hrs before unloading. In the parametric analysis , the load level is set to 20% and the temperature is set to 600 °C.

To evaluate the influence of elastic modulus and thermal coefficient, different variations were considered: non-linear elastic modulus based on Eq. 3.12 and nonlinear thermal coefficient varying with temperature based on Eqs. 3.14 to 3.15 (Case 1); non-linear elastic modulus and constant thermal coefficient (based on the ambient value) (Case 2); constant elastic modulus (based on the ambient value) and non-linear thermal coefficient varying with temperature (Case 3); constant elastic modulus and linear constant thermal coefficient (Case 4). The stress-strain curves are displayed in Fig. 3.15. The E and α represent elastic modulus and

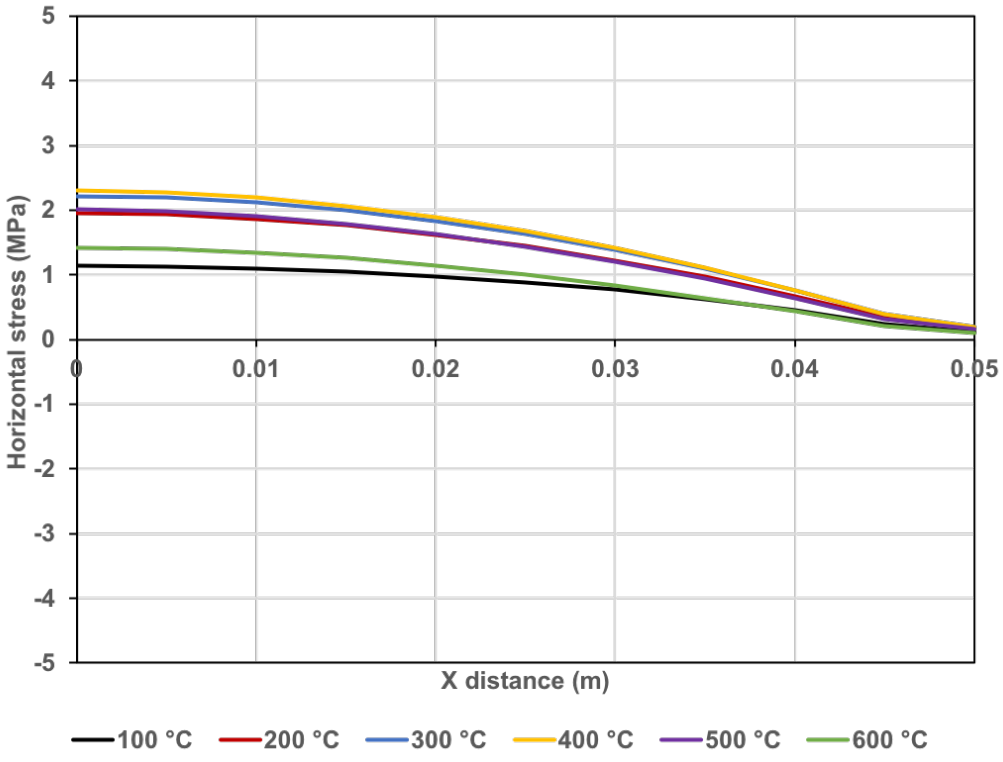

(a) Horizontal stresses

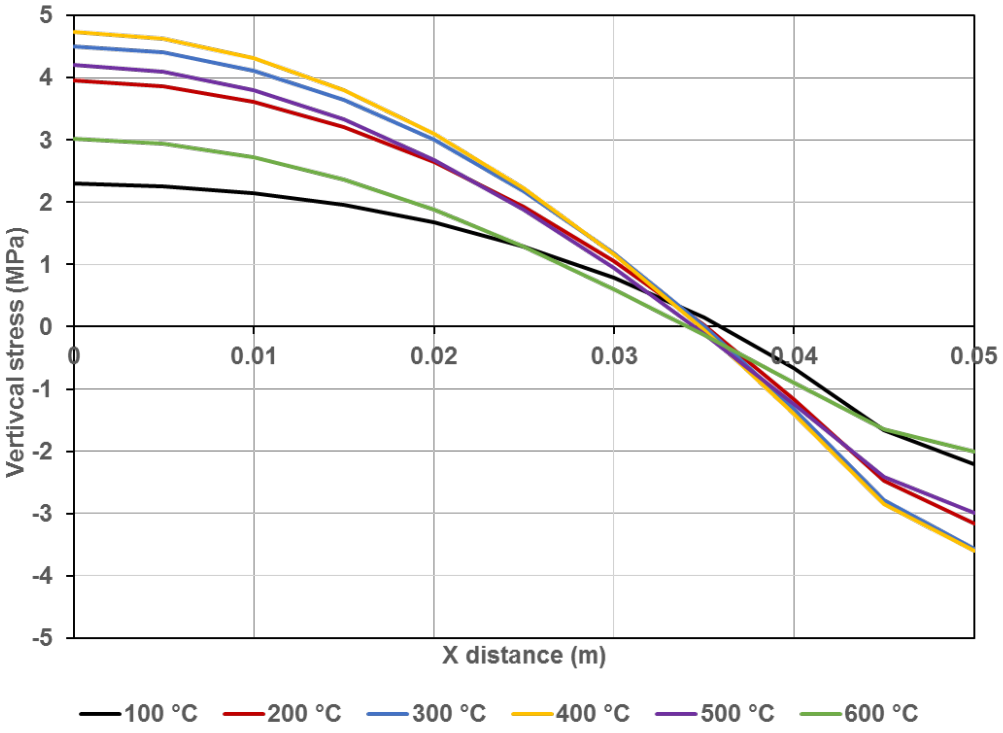

(b) Vertical stresses

Fig. 3.12 The stresses along the radius (from central line to surface) for the heating rate of 2 °C/min at different chamber temperatures

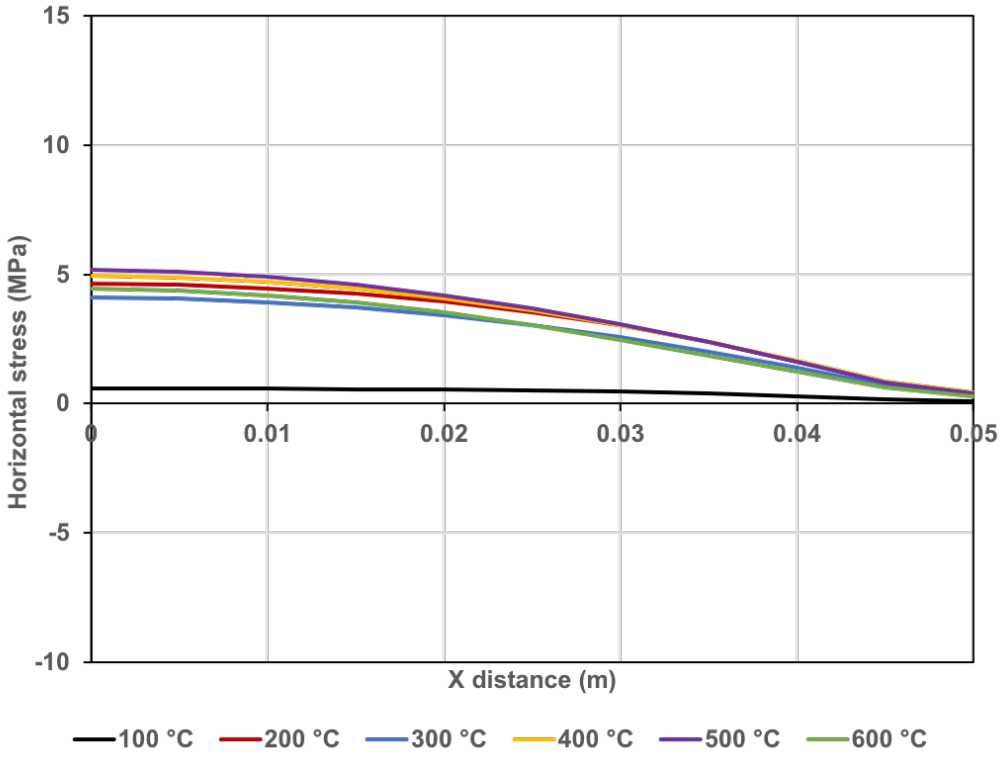

(a) Horizontal stresses

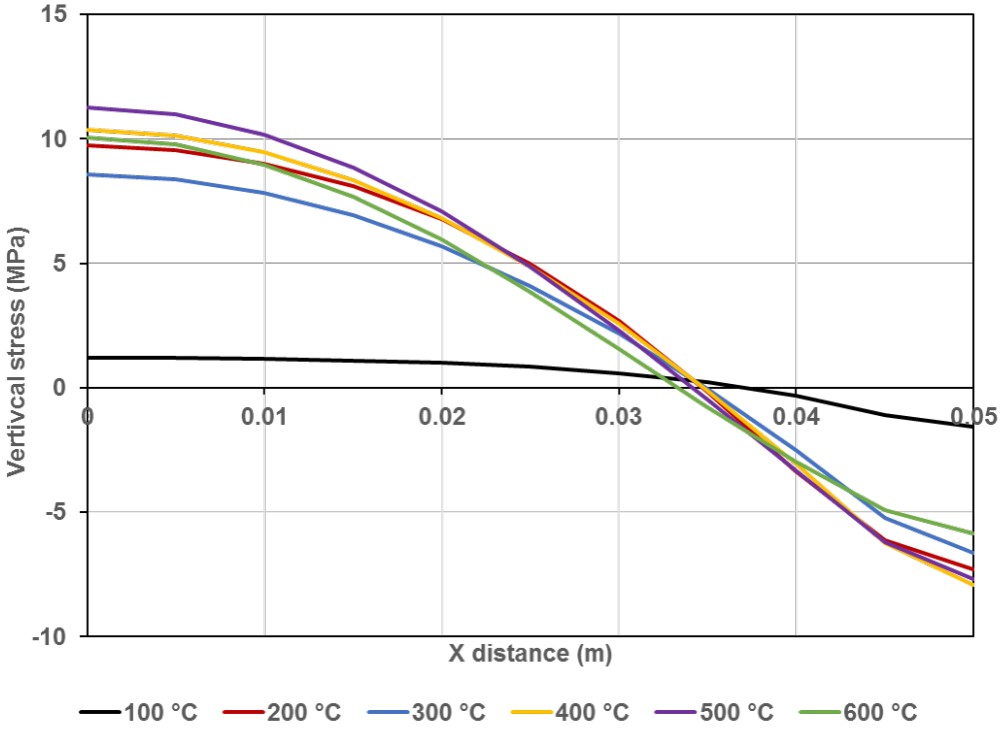

(b) Vertical stresses

Fig. 3.13 The stresses along the radius (from central line to surface) for the heating rate of 5 °C/min at different chamber temperatures

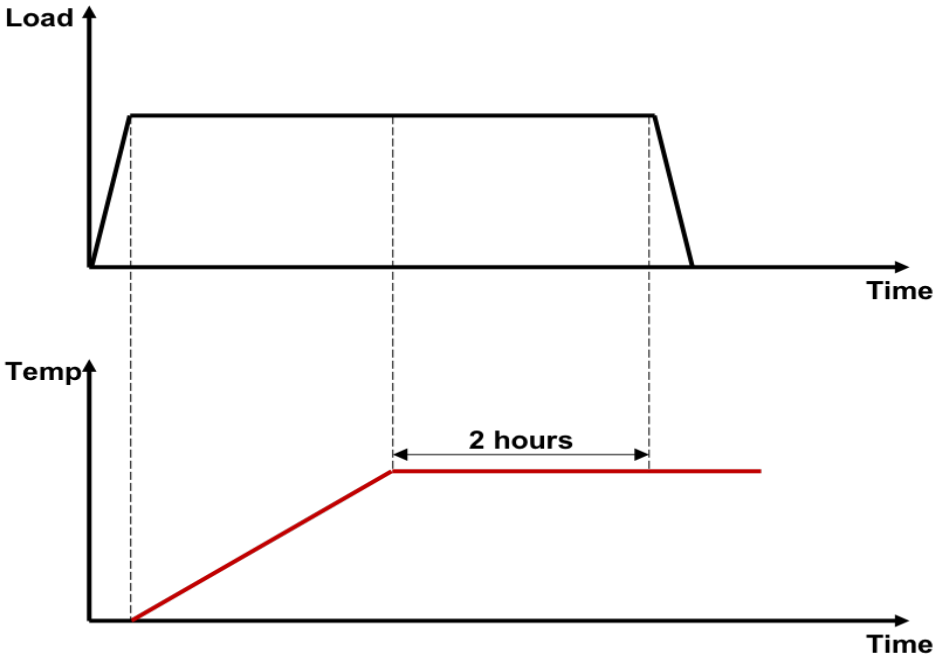

Fig. 3.14 The procedure of LITS experiment

thermal coefficient, respectively.

From Fig. 3.15, it can be seen that the stress-strain curve becomes smooth when the thermal coefficient is non-varying with temperatures. The temperature difference is not remarkable when the heating rate is 2 °C/min. The stress and strain caused by temperature gradient is not obvious due to the similar thermal expansion. That is the reason why the curve becomes smooth when the thermal coefficient is constant at elevated temperatures. Comparing Case 1 and Case 3, the stress-strain curves are quite different whether the elastic modulus is linear at elevated temperatures.

According to the discussion above, the elastic modulus is quite sensitive to temperatures. The result shows considerable difference whether the elastic modulus is non-linear and temperature dependent at elevated temperatures. However, the change of thermal coefficient almost does not affect the results.

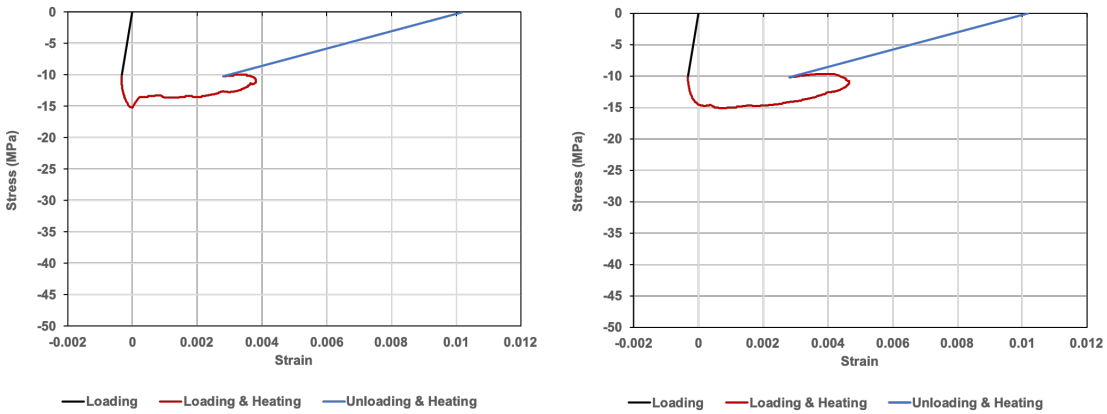

(a) Nonlinear E and nonlinear α (Case 1)

(b) Nonlinear E and constant α (Case 2)

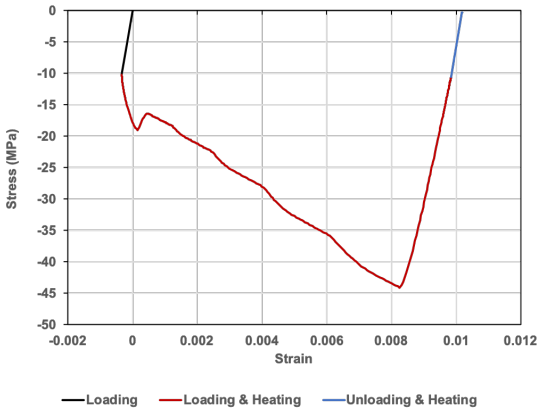

(c) Constant E and nonlinear α (Case 3)

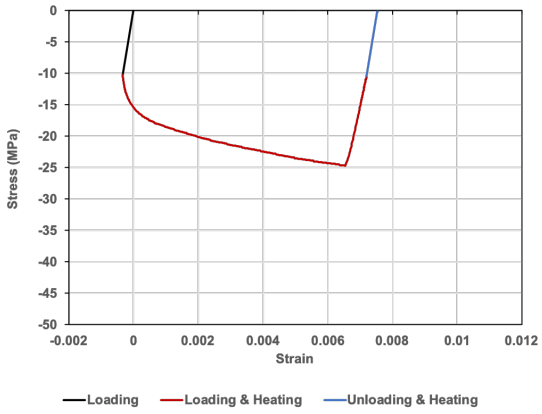

(d) Constant E and constant α (Case 4)

Fig. 3.15 Stress-strain curves with different parameters at the heating rate of 2 °C/min

3.6 Summary

This chapter considered heat transfer and thermomechanical response of the specimens proposed to be tested. The purpose of the analysis was to find the most efficient and reasonable heating rates for the experiment. Four heating rates, 1 °C/min, 2 °C/min, 5 °C/min, 10 °C/min are discussed in the heat transfer analysis. The temperature variation for the heating rate of 10 °C/min exceeds 300 °C when the predicted temperature is 600 °C. Also, the heating process with the heating rate of 1 °C/min takes over 10 hrs which is not efficient. Thermomechanical analysis is conducted for heating rates of 2 °C/min and 5 °C/min. In these analyse, stresses caused by temperature gradients during the heating process are evaluated. Through the heat transfer and mechanical analysis, the heating rate is set to 2 °C/min for the experiments. This heating rate avoids dangerous stresses due to temperature gradient while taking less time in comparison to the heating rate of 1 °C/min. The study also shows that the chamber temperature needs to be maintained constant for 2 hrs to achieve uniform temperature in the concrete.

The sensitivity analysis is conducted with respect to elastic modulus and thermal coefficient values. According to the simulation results, the elastic modulus is sensitive to temperatures. To the contrary, the thermal coefficient is not sensitive to the predicted temperatures. In the following simulation of time-dependent creep, the effect of thermal coefficient is neglected.

4

The experimental protocols

4.1 Introduction

As discussed in Chapter 2, differentiating and quantifying reversible, irreversible and creep components of strain due to heating and loading is complex. The purpose of the study is to separate different components - both reversible and irreversible components. In this chapter, two series of tests are developed to explore LITS effect: those in which heated samples are subjected to loading, load holding, unloading and recovery; and those in which loaded samples are subjected to heating, maintenance of constant temperature, unloading and recovery. Prior to LITS experiments, tests to evaluate stress-strain relationships at elevated temperatures and strength at ambient temperature are considered.

4.2 Specimen design

As mentioned in the previous chapter, cylindrical specimens with a diameter of 100 mm and height of 200 mm were used (Fig. 4.1). The dimensions were as recommended by a European Standard [67]. Sixteen combinations of different load levels (the ratio of stress to compressive strength at the ambient temperature) and temperatures for tests were considered. Details of load and temperature combinations applied are discussed later in this chapter. Each test was repeated once for reliability. Consequently thirty-two specimens were used for

LITS tests. Further three specimens were used for the compressive strength tests at the ambient temperature and six specimens to evaluate stress-strain relations at elevated temperatures.

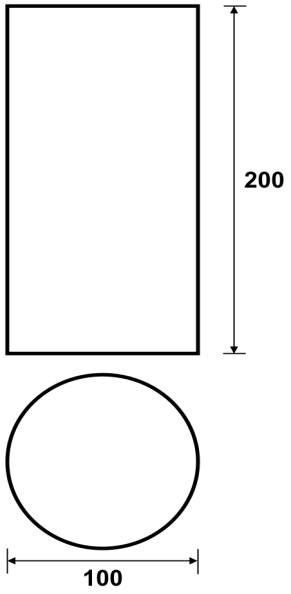

Fig. 4.1 Dimensions of the cylindrical specimen

All cylinders used were cast in the plastic moulds by Smith [14]. The ready-mix concrete was supplied by the local ready-mix supplier. The concrete was made of siliceous aggregates with a maximum aggregate size of 10 mm. The main mix proportions are shown in Table 4.1. All specimens were water cured for one week and then cured in a low humidity environment for seven weeks. These specimens were stored for 5 years after curing.

Table 4.1 Concrete mix proportions [14]

Constituent	**weight units**
Cement	1
Water	0.41
Sand	3.39
Aggregate	4.18

Specimens were capped with plaster to achieve flat of concrete surfaces before the test.

The plaster cap reduces the error in measured strain due to possible toe effect. The bottom surface of the specimen was capped on glass. The water and plaster are mixed in a ratio of 1:2. A gradienter was used to make sure that the cylinder was placed vertically. In addition, the top surface was capped in the Instron machine (to be discussed). The plaster was placed on the top of the cylinder. The bottom platen of the Instron frame was moved upwards to ensure that platen surfaces were perpendicular to the axis of concrete cylinder. The capped cylinder was placed on a smooth surface.

4.3 Apparatus

4.3.1 Instron frame and oven

Tests are carried out using the Instron 600LX Frame and Instron CP103790 Environmental Chamber (Instron, UK). The frame applies uniaxial compressive load up to 600 KN and the oven applies temperatures up to 600 °C. During the test, the concrete cylinder was placed vertically between the two platens at the centre of the oven. The diameter of the platen is 105 mm. The top platen is fixed. The upward pressure head applies distributed load to the concrete cylinder. A mesh guard is set around the cylindrical specimen to protect the oven in case the sample has a sudden brittle failure. Figure 4.2 shows full detailed test setup.

The frame and the oven are controlled separately. The loading program is controlled by the software, Bluehill 3 (Instron,UK). The specimen was loaded at an initial displacement rate of 0.5 mm/min. Then, the load program was changed to load control after the reference load level was reached.

The oven is controlled by the oven controller. The temperature time curve and the heating rate are set by the controller. There is one thermocouple in the oven to measure the real-time chamber temperature through the oven controller. The specimen is heated at a heating rate of 2 °C/min. The temperature of the oven was kept constant for 2 hrs to achieve uniform temperature inside the specimen after the initial heating.

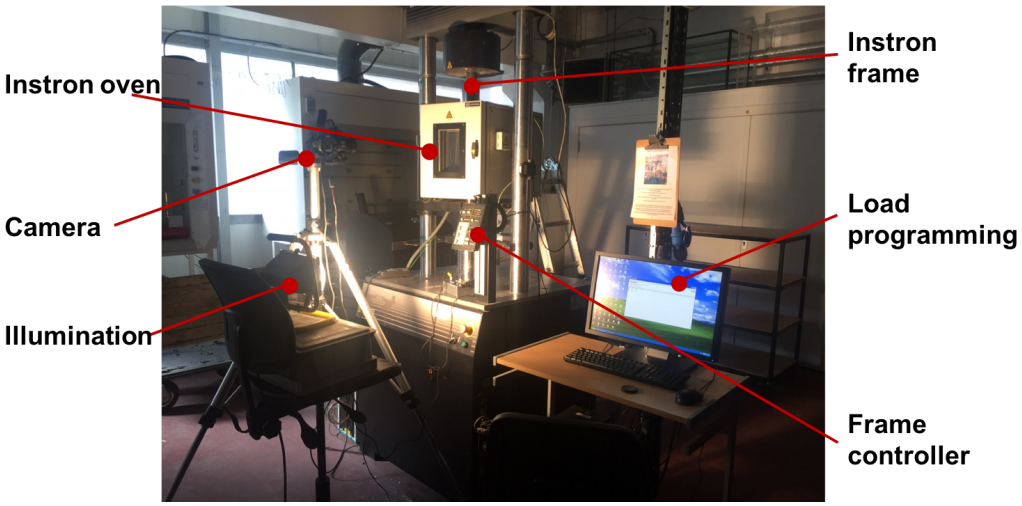

(a) Frame setup

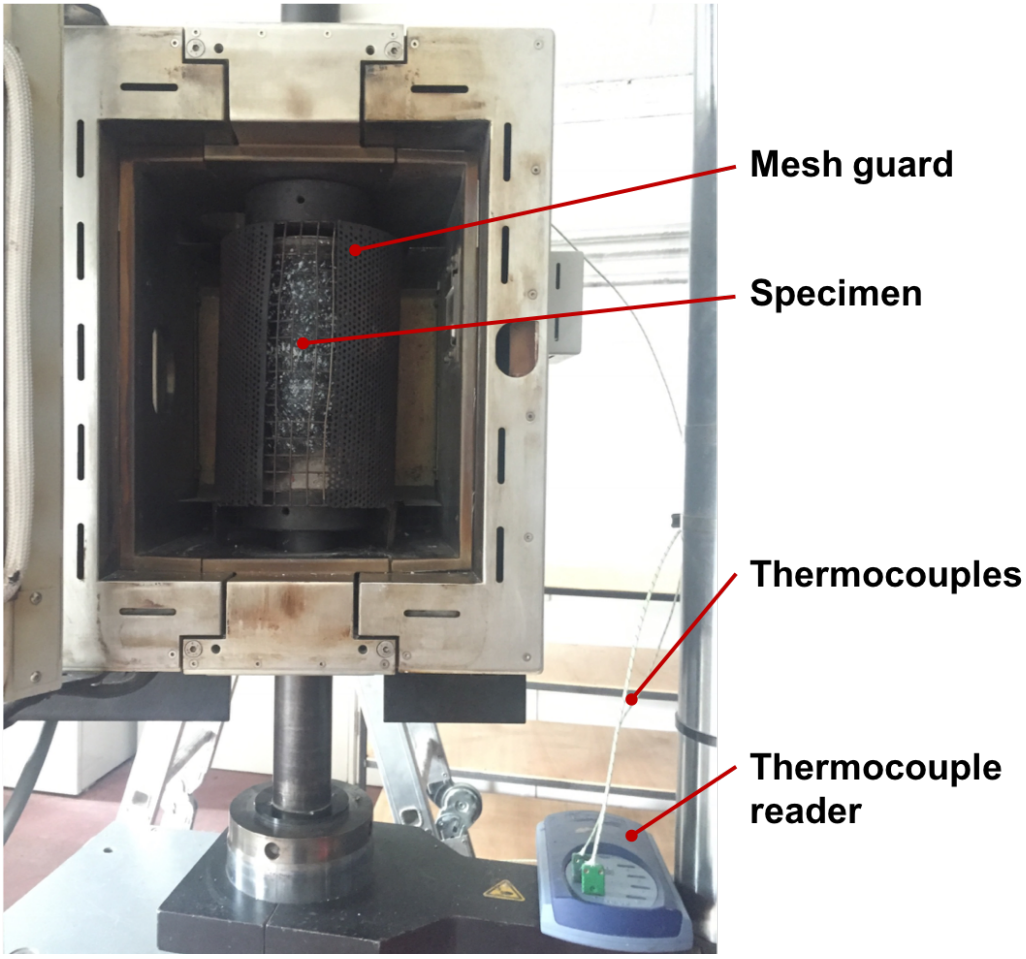

(b) Specimen setup

Fig. 4.2 LITS test setup

4.3.2 Thermocouples

The temperature data was recorded by using thermocouples through the thermocouple reader. To record external temperatures of the concrete, two thermocouples were attached to the surface of the concrete specimen at 50 mm from the top surface and bottom surface respectively with a sealant. The sealant was high temperature resistant up to 1250 °C. An extra thermocouple was inserted in the oven to record chamber temperatures. The position of thermocouples are shown in Fig. 4.3.

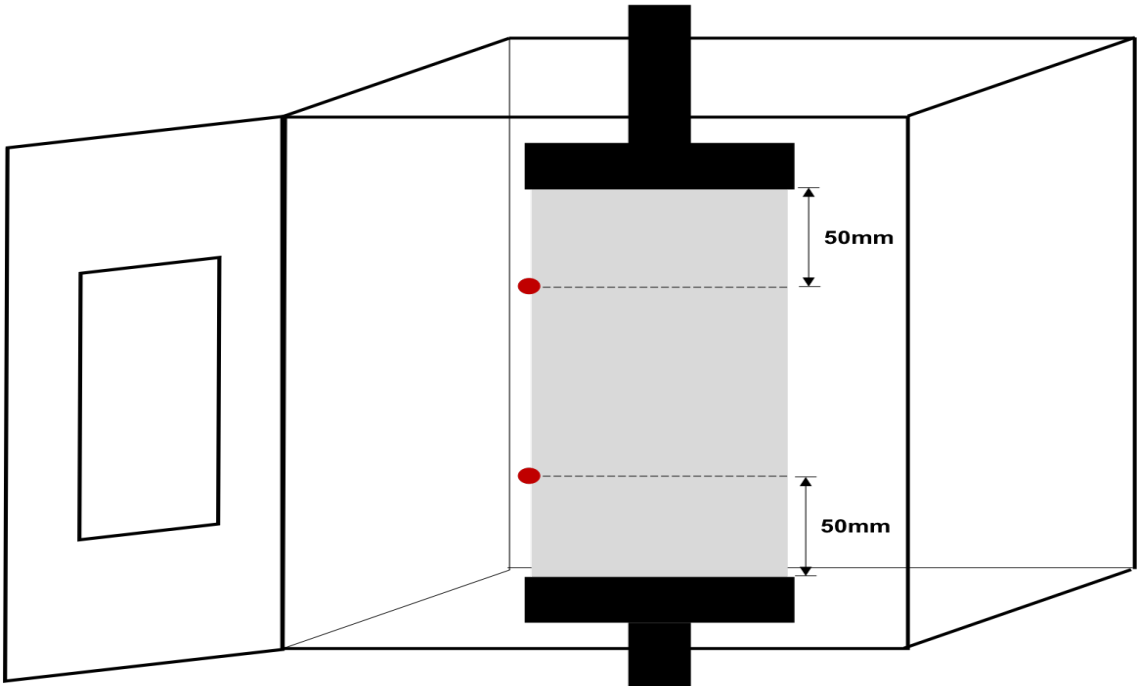

Fig. 4.3 Locations of thermocouples

4.3.3 Camera

Canon 650D camera was used to take high quality photos of the specimen during tests. Regular time intervals were set with a timer. Photos were taken every 5 seconds during the loading process and every 30 seconds during the heating process. The photo is captured through the window of the oven. A slender hole was cut on the mesh guard for capturing the images. To avoid the reflection of the window, external illumination was employed.

4.4 Strain measurement - DIC

The dimension of the specimen was set in the Instron load program before the test. The strain was measured by the displacement of crosshead and the height of cylinder. It is an inadequate approach for measuring strain. Also, during some of the heating processes, the top platen was not in contact with the specimen. Therefore, in such cases free thermal strain cannot be recorded by Instron. Moreover, the machine records the deformation of the entire specimen including error due to flatness.

4.4.1 Strain measurement

Digital Image Correlation (DIC) was used to measure strain distributions that arise during the test. DIC is widely used for surface displacement analysis [69, 70]. As discussed in the previous section, photos are taken by the camera during the test. These photos for each test are post-processed using GeoPIV-RG (University of Western Australia, Australia and Queen's University, Canada). It is an image analysis module for MATLAB (MathWorks, U.S.A.).

The DIC methodology has been described by Stranier [71]. Initially, a region of interest is defined on the first image. The analysis is conducted within the region. Then, the subsets are defined within the region of interest. Through analysing the movements of subsets, the output gives subsets coordinates on each photo.

The coordinates of subsets in the first image are shown in Fig. 4.4. To track the axial strain on the nth image in subsequent images, the following equation is used

$$\varepsilon = \frac{(y_{bn} - y_{tn}) - (y_{b1} - y_{t1})}{y_{b1} - y_{t1}} \tag{4.1}$$

where y_{bn} and y_{tn} are y coordinates of the corresponding bottom patches and top patches on the nth image.

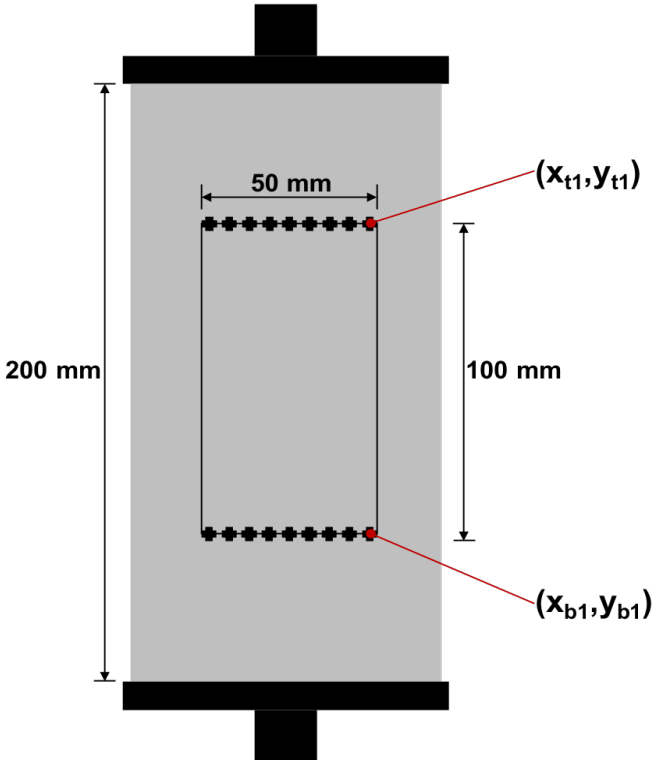

Fig. 4.4 Locations of subsets

The surface of the specimen needs a unique pattern to select subsets and track coordinates within the region of interest. To create the texture on the specimens surface, high temperature resistant paint was used in the test. Black paint was used as the background colour, while the white paint was used to make the speckle pattern on the background. This pattern can be observed in Fig. 4.2.

4.4.2 Sources of errors

To remove the curvature influence of cylinder and to obtain more accurate virtual strain, Bisby and Take [72] have examined patch locations by measuring hoop and axial strains on circular FPR confined concrete cylinders. Figure 4.4 illustrates locations of subsets in this analysis.

The reflection on the glass of the oven is a major source of error. During the test, the light from the lab and people in the lab may result in loss of accuracy. For reducing the reflection, an external illumination was set. Also, the camera should was set perpendicular to the oven.

4.5 Test procedures

One set of tests was undertaken to obtain uniaxial stress-strain behaviour at elevated temperature. A further two series of tests were designed to explore the LITS effects: Loading Then Heating (LTH) test and Heating Then Loading (HTL) test. In these test series, the main parameters varied were load levels and temperatures.

4.5.1 Stress-strain relations at elevated temperatures

The purpose of this test was to obtain stress-strain curves at elevated temperatures. The main parameter in this series of tests was the temperature. The specimens were loaded to failure at elevated temperatures. Prior to the conduct of this test, compression tests were conducted at the ambient temperature. These test were repeated twice as recommended of the European

Standard [73].

In the test at elevated temperatures, the specimens were first heated to three prescribed temperatures: 200 °C, 400 °C and 600 °C. The heating rate employed was 2 °C/min based on the heat transfer analysis in Chapter 3. Once the required temperature was achieved, the specimen was then heated constantly for a period of 2 hrs to achieve the chemo-physical uniformity in the material in accordance with the simulation result. The test at each temperature was repeated once for reliability. The loading and heating process are shown in Fig. 4.5.

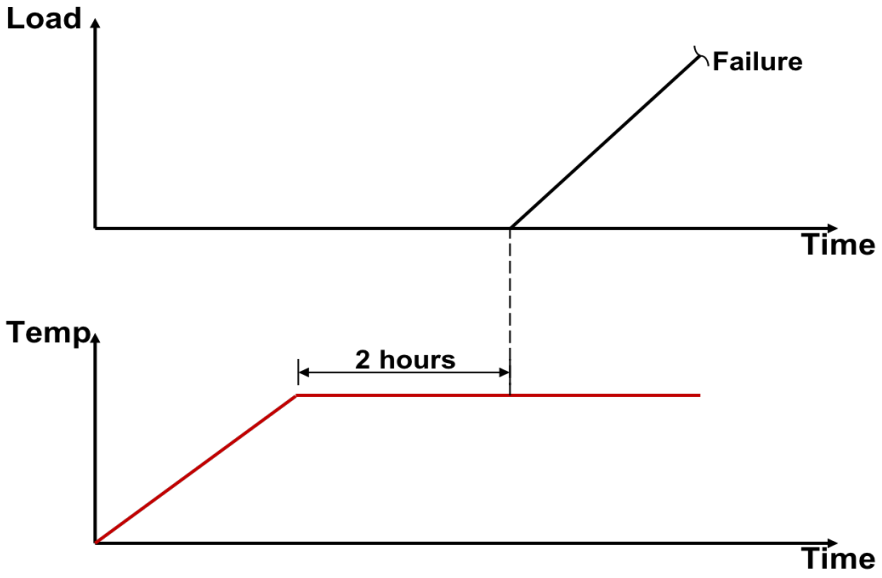

Fig. 4.5 The loading and heating process of stress-strain relations tests

4.5.2 Loading-then-heating tests

The LTH test was used to obtain LITS data. The main parameters in this series of tests were load levels and temperatures. Three load levels, 20%, 30% and 45%, and three temperatures, 200 °C, 400 °C and 600 °C, were applied. However, the combination of 600 °C at the load level of 45% was excluded as there was considerable reduction of compressive strength at 600 °C and there was a concern that the specimen may fail at this combination and damage the equipment. Each combination of parameters is performed twice. Thus, a total of 16 LTH

tests were conducted.

In the LTH tests, load was applied at a displacement rate of 0.5 mm/min until the prescribed load level was reached. Then, the test machine was changed to load control to maintain constant load during the test. The temperature was applied under certain stabilized load. After 2 hrs of heating at a constant temperature, the samples were unloaded at the same displacement rate to evaluate their elastic recovery. The test procedure is shown in Fig. 4.6.

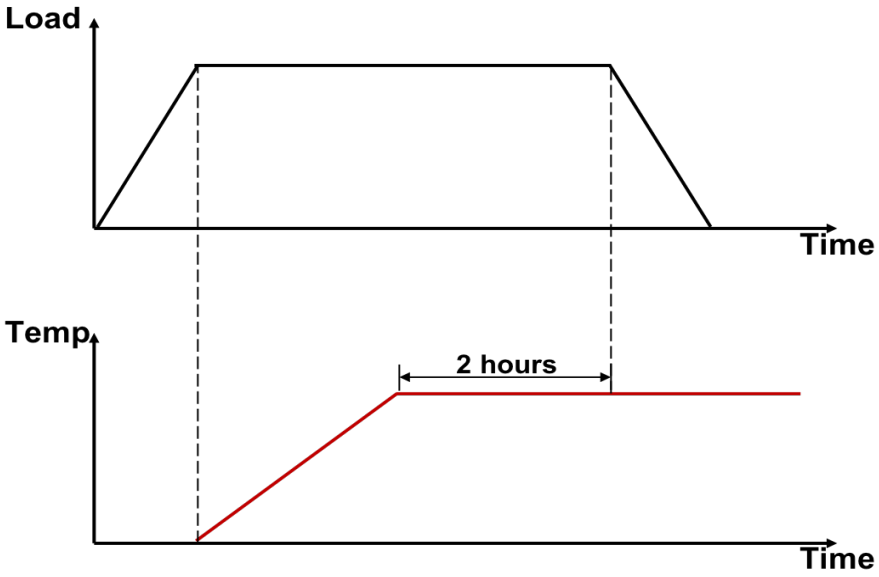

Fig. 4.6 The loading and heating processes of LTH tests

4.5.3 Heating-then-loading tests

The HTL test were designed to compare results with LTH tests. Once again, three load levels, 20%, 30% and 45%, and three temperatures, 200 °C, 400 °C and 600 °C, were applied. Also, in these tests, the combination of highest load level of 45% and temperature of 600 °C was not included. The HTL test also contained time-dependent creep tests at stabilized temperature.

The specimens were subjected to temperature treatment to start with. The load was then

applied with the displacement rate of 0.5 mm/min until the prescribed load level was reached. Constant load was then sustained for 2 hrs and then the samples were unloaded. The loading and heating processes are shown in Fig. 4.7.

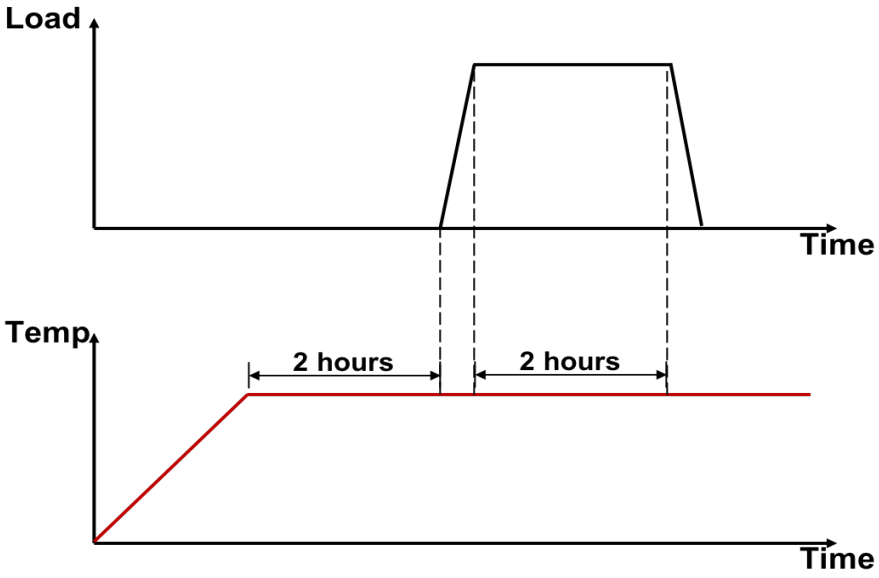

Fig. 4.7 The loading and heating processes of HTL tests

4.6 Summary

The cylindrical specimens were cast and cured in accordance with the European Standard. Before the experiment, the specimen was capped with plaster. Two thermocouples were installed on the surface of the specimen with high temperature resistant sealant. Also, a texture was painted on the specimen surface with high temperature resistant paints.

All the experiments were conducted using Instron frame and oven. They were controlled by the computer and the oven controller, respectively. An extra thermocouple was inserted in the oven to record chamber temperature during the experiment.

The digital image correlation was used to measure strain data during the experiment. The

camera was set to take photos during the experiment at different time intervals. Also, an external illumination was set to reduce the influence of reflection. The method of post-processing photos is discussed along with possible sources of errors.

Several tests and procedures are described in the chapter. The compressive strength tests and stress strain relations tests were designed based on the European Standard. Loading then heating tests and heating then loading tests were designed to evaluate strain components under different load levels and temperatures.

5

Heating-then-loading (HTL) experimental results and simulation

5.1 Introduction

This chapter presents the experimental data of compressive strength tests, stress-strain relations at elevated temperatures, and heating then loading (HTL) tests. The design of experiments was discussed in Chapter 4. The HTL tests comprise of free thermal strain, instantaneous stress-related strain, and time-dependent creep, which are significant components in LITS. Also, the temperature data is compared with heat transfer analysis to modify thermal properties.

5.2 Temperatures

As mentioned in Chapter 4, the concrete surface temperatures were measured at two locations on the surface of specimens during the tests. Also, the chamber temperature was measured by employing an independent thermocouple inserted in the oven. Before the experiment, the heat transfer analysis was conducted as discussed in Chapter 3. In this section, the experimental

results were compared with the simulation results. Differences between experimental data and heat transfer simulation results are discussed.

5.2.1 Chamber temperatures

The chamber temperature of each test was monitored by the thermocouple and recorded through PicoLog (Pico Technology, UK). During heating, the heating programme was set to increase chamber temperature from the ambient temperature to the reference temperature (200 °C, 400 °C, 600 °C) at the heating rate of 2 °C/min. In the tests, ambient temperatures varied from 16 °C to 23 °C. In the heat transfer analysis, the ambient temperature was set to 20 °C. Figure 5.1 shows experimental data of chamber temperatures compared to the simulation results. The solid lines and the dashed lines represent the experimental results and the simulation results, respectively. The chamber temperature from the experimental data at each temperature is the mean value from six tests.

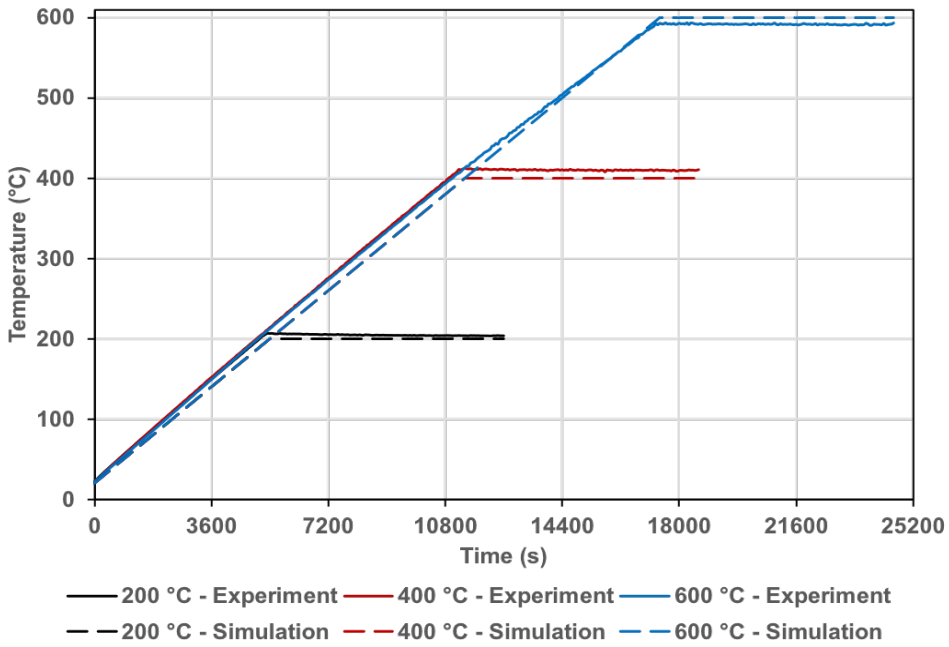

Fig. 5.1 Comparison of chamber temperatures between experimental data and simulation results

In general, the chamber temperatures during tests were as expected and compared well with the simulation results. The slopes of temperature-time curves show that the actual heating rate was slightly higher than 2 °C/min. For reference temperatures of 200 °C and 400 °C, the final chamber temperatures were slightly higher than settings. In the tests in which the reference temperature was 600 °C, the chamber temperatures rose up to 590 °C. Although the oven was rated to apply temperatures up to 600 °C, it was found to go up to 590 °C in reality.

5.2.2 Concrete surface temperatures

As discussed in Chapter 4, two thermocouples were attached to each specimen with the high temperature resistant sealant. Averaged temperatures data at each position when the reference temperature is 200 °C is shown in Fig. 5.2.

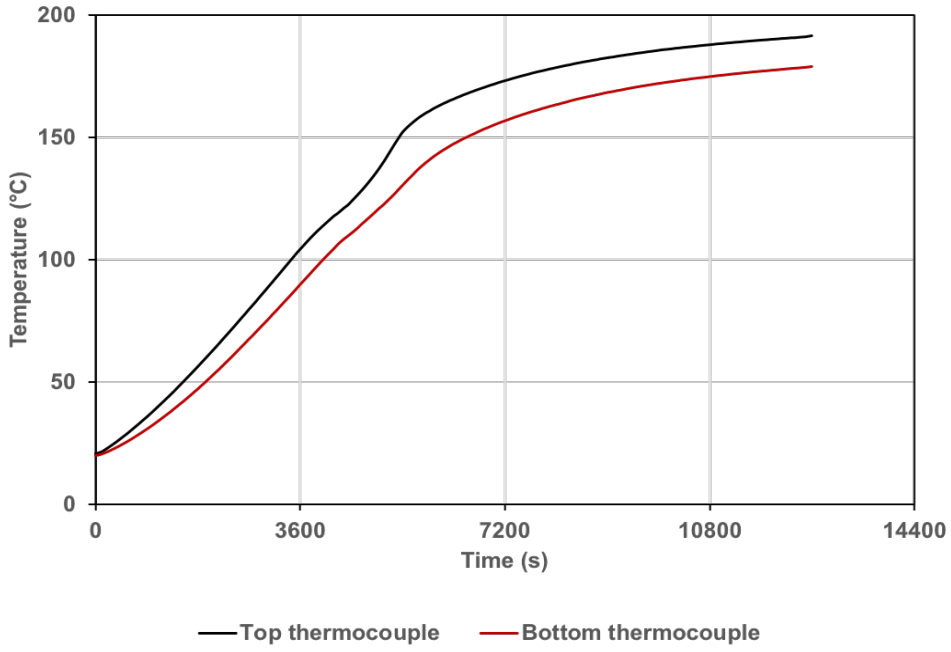

Fig. 5.2 Comparison of averaged concrete surface temperatures at different positions

It can be seen from Fig. 5.2 that the temperature in the oven is not uniform. The con-

crete surface temperatures were consistently higher at the higher position. The measured chamber temperature was higher than the settings. The difference in the concrete surface temperatures at different positions was around 10 °C.

The averaged concrete surface temperatures for different heating tests is shown in Fig. 5.3. The solid lines and the dashed lines represent experimental data and simulation results, respectively. Although the chamber temperatures are slightly higher than those predicted by the simulation, the concrete surface temperatures are slightly lower than simulation results. The thermocouples need to be fixed with sealant as a tape cannot stick to the concrete surface at high temperatures. The thickness of the sealant is a possible reason for slightly lower concrete surface temperatures. In the tests in which reference temperatures are 200 °C and 600 °C, the differences between measured temperatures and simulation results are around 10 °C. In the tests in which reference temperature is 400 °C, the concrete surface reaches to the expected temperature. The comparison shows that thermal properties used for heat transfer analysis were appropriate.

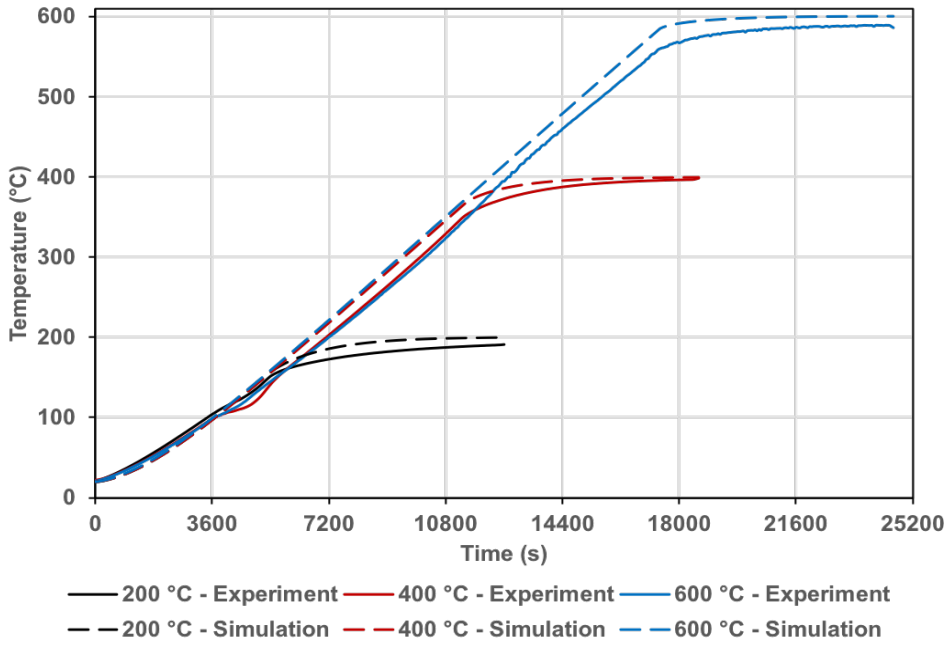

Fig. 5.3 Comparison of averaged concrete surface temperatures between experimental data and simulation results

5.3 Stress-strain relations at elevated temperatures

Three compressive strength tests were done at the ambient temperature. The average concrete compressive strength was found to be 45.5 MPa. The mean stress-strain curves at different temperatures are shown in Fig. 5.4. All specimens were loaded at each temperature until failure. To ensure that creep deformations did not occur, the load was applied at a relatively fast rate of 0.5 mm/min. The descending branch of the stress-strain curves was not measured as the specimen was crushed at the ultimate stress. Figures 5.4 and 5.5 show that the ultimate stress decreases and the ultimate strain increases with temperatures, which is consistent with Eurocode 2 [2]. Four parameters characterise the stress-strain curve. They are ultimate stress, compressive strength coefficient, ultimate strain, and elastic modulus.

Figure 5.5 and 5.6 show the ultimate stress and the compressive strength coefficient as a function of temperature. As discussed in Chapter 3, the reduction of compressive strength

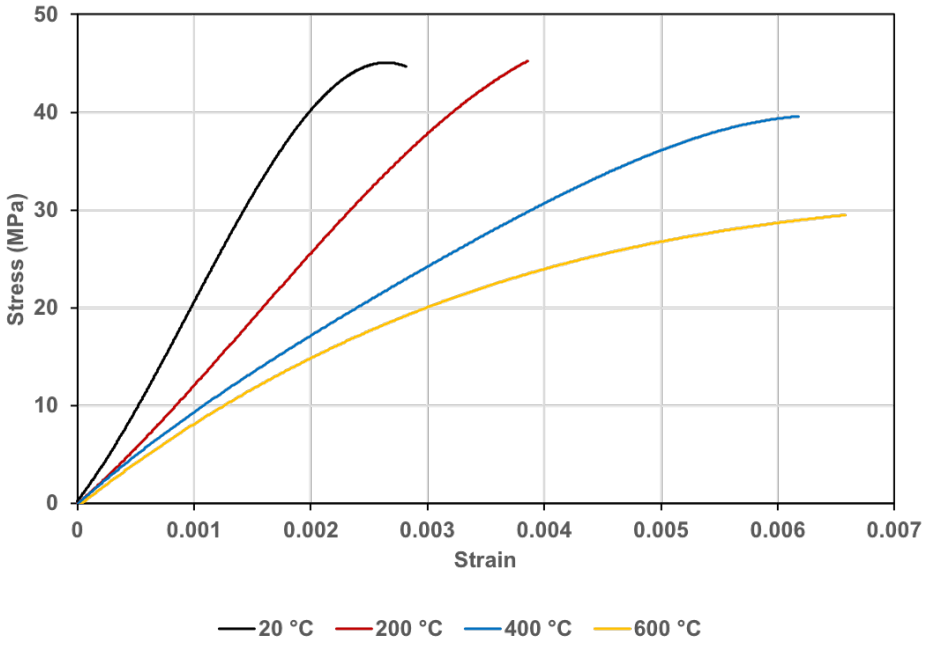

Fig. 5.4 Stress-strain relations at elevated temperatures

of concrete at elevated temperatures is given by the compressive strength coefficient. The coefficient is the ratio of the compressive strength at elevated temperatures to the compressive strength at the ambient temperature. The temperature has almost no influence on the compressive strength for temperatures under 200 °C. The compressive strength decreases rapidly above 400 °C. The specimens had been stored in a dry environment for five years before the tests. The ultimate stress at the higher temperature is higher than expected, possibly due to increased age-related strengthening in a dry environment.

The ultimate strain at each temperature is shown in Fig 5.7. The ultimate strain increased with temperatures. The value of elastic modulus at each temperature is shown in Fig. 5.8. The elastic modulus is evaluated from the stress-strain curves. It is calculated from the slope of the stress-strain curves from the start of the loading to 30% of the ultimate stress at each temperature. The elastic modulus decreases rapidly from the ambient temperature to 200 °C. This data is used to validate mechanical parameters in the simulation.

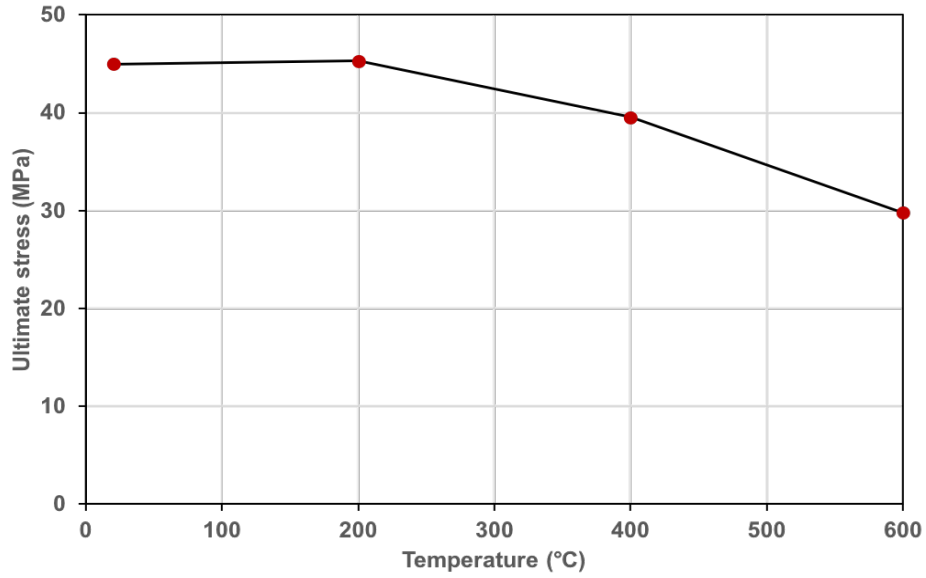

Fig. 5.5 The ultimate stress at different temperatures

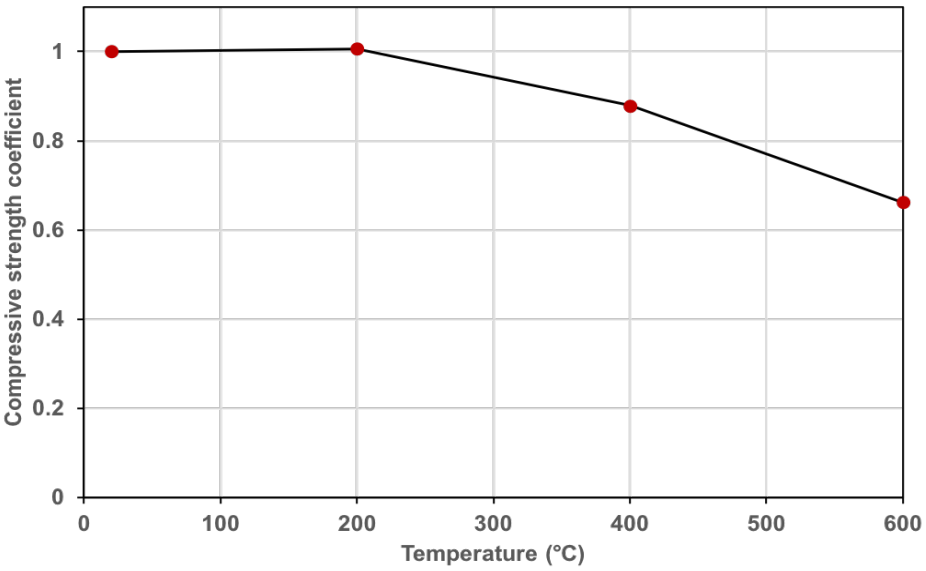

Fig. 5.6 The compressive strength coefficient at different temperatures

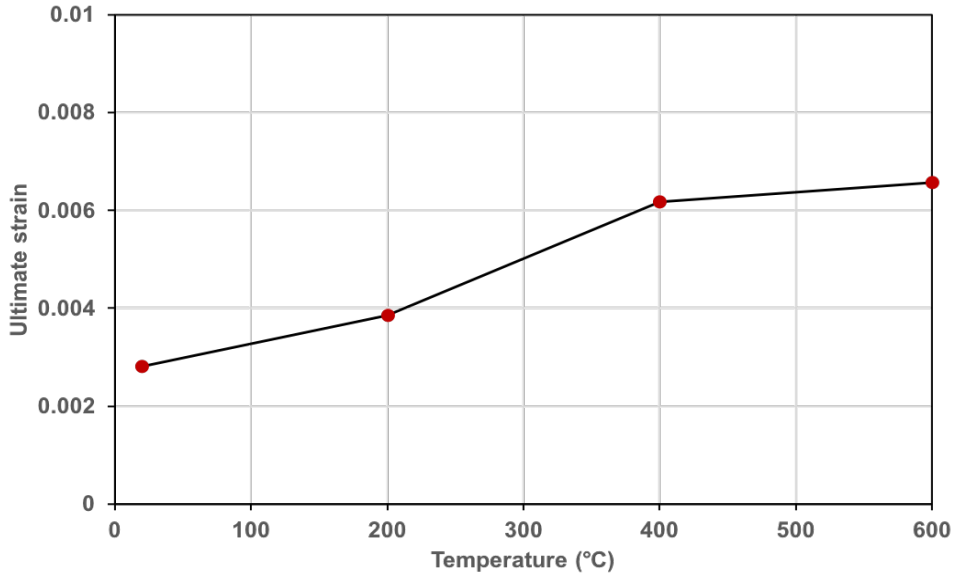

Fig. 5.7 The ultimate strain at different temperatures

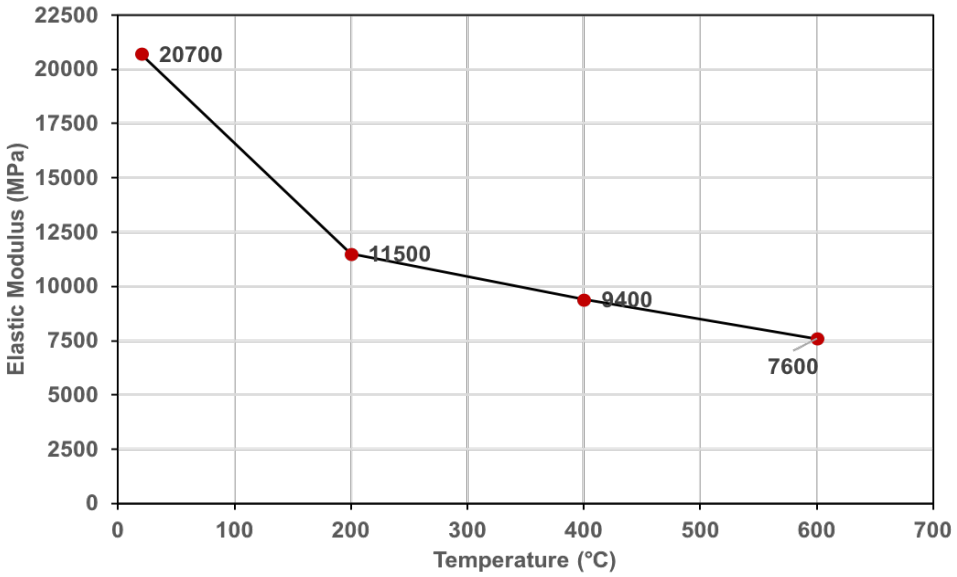

Fig. 5.8 The elastic modulus at different temperatures

5.4 Heating-then-loading (HTL) tests

The HTL test procedure was described in Chapter 4. Each specimen was heated to the reference temperature at a heating rate of 2 °C/min. Then the temperature was kept as constant for 2 hrs to achieve uniform temperatures in the concrete specimen. The specimen was loaded to the reference load level and the constant load was maintained for another 2 hrs. The load was removed at the end of the test. A typical strain against time curve is shown in Fig. 5.9. There is free thermal strain during the heating process. The instantaneous elastic strain is measured when the load is applied. Then, there is a time-dependent creep under constant load and temperature. The free thermal strain and the other strain components are discussed separately.

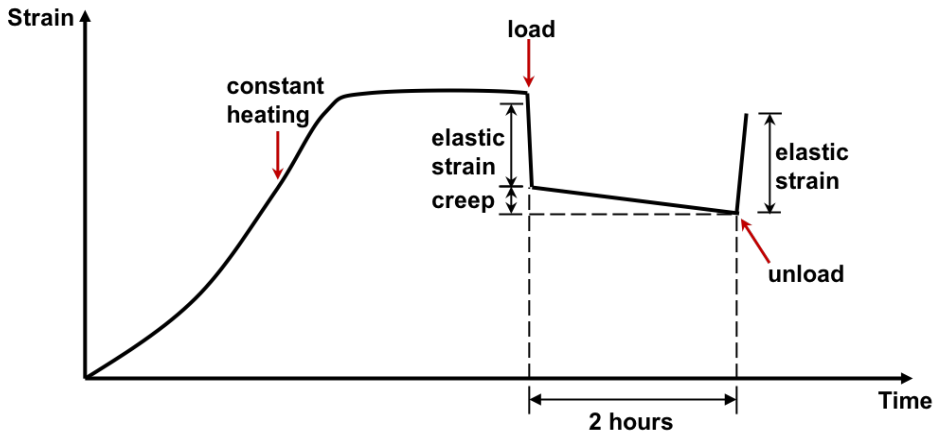

Fig. 5.9 The typical strain against time curve in HTL test

5.4.1 Free thermal strain at elevated temperatures

During the heating process, the specimen was placed in the oven without any restraint. Six specimens were heated from the ambient temperature to 200 °C and 400 °C and four specimens were heated to 600 °C. The free thermal strain was monitored during the test process without load. Free thermal strains at each temperature are shown in Figs. 5.10 - 5.12. It can be seen that thermal strains increase nonlinearly with time. A comparison of Figs. 5.10 - 5.12 also shows that they increase with temperatures. The thermal strain curves for different

samples match up reasonably well, though there were some which were a bit more off than the others (e.g. the yellow line at 400 °C). The yellow line at 400 °C was neglected in the calculation of the average thermal strains.

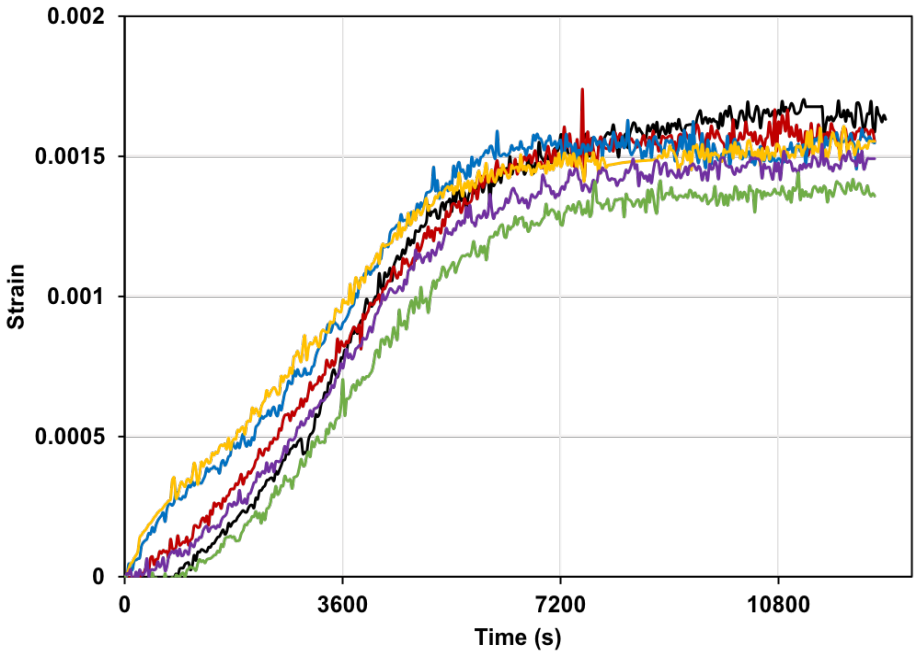

Fig. 5.10 Free thermal strain against time at 200 °C

The averaged free thermal strain at each temperature is shown in Fig. 5.13 along with the simulation results based on Eurocode 2 [2] parameters. It can be see that the time-dependent curves have distinct change in slope at around 1.5 hrs for all temperatures (Figs. 5.10 - 5.12). Additionally, there is a change in slope between 3 hrs and 4 hrs for 400 °C and between 3 hrs and 5 hrs for 600 °C. By comparing the experimental data with simulation results, the Eurocode 2 [2] parameters result in higher prediction of thermal expansion. However, it is interesting to note that the shape of curves is very similar. Free thermal strain is known to be affected by aggregate type and moisture content. In the series of tests conducted, all specimens were from the same batch and had the same aggregate properties. It is likely that the thermal expansion suggested by Eurocode 2 [2] is based on different

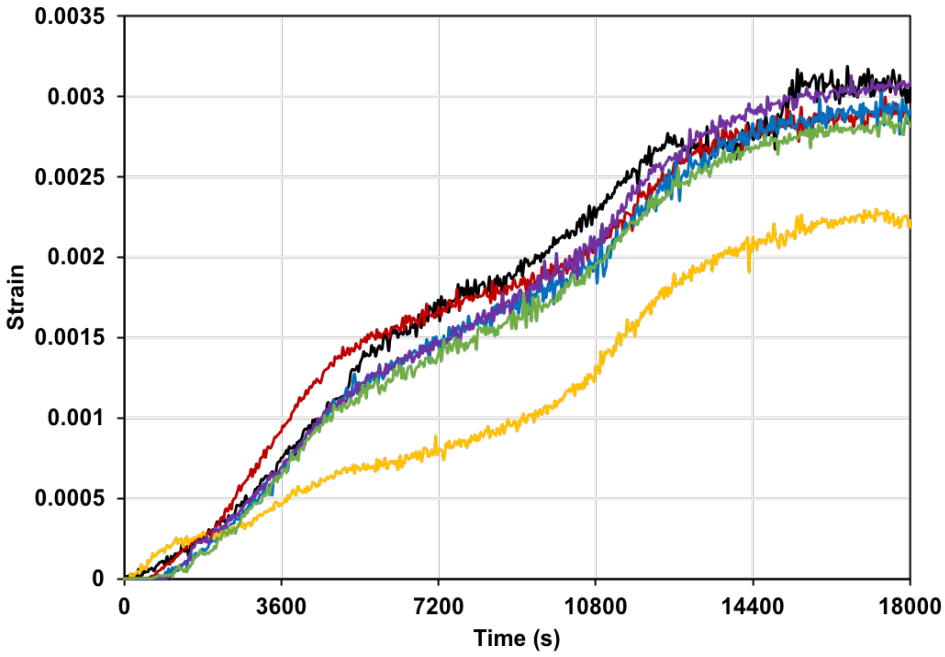

Fig. 5.11 Free thermal strain against time at 400 °C

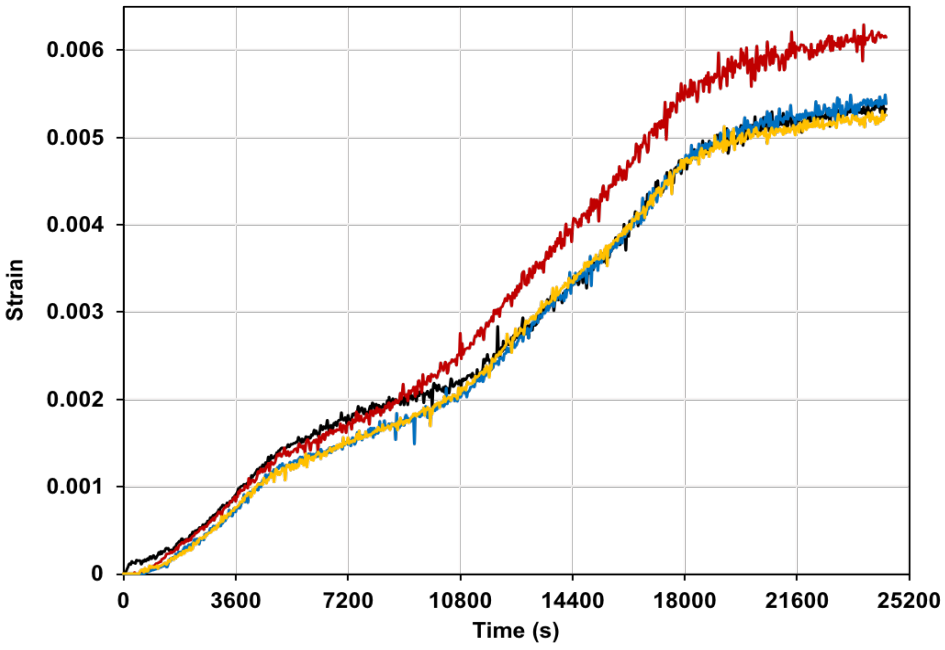

Fig. 5.12 Free thermal strain against time at 600 °C

types of aggregate. In the simulations that follow in this study, thermal coefficients based on experimental data were used.

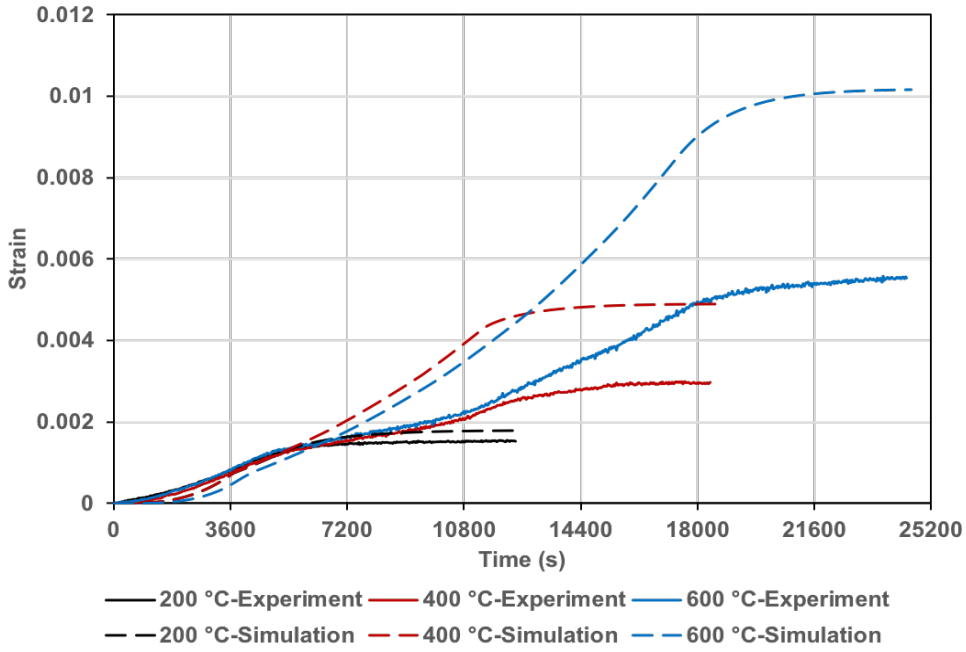

Fig. 5.13 Free thermal strain at elevated temperatures compared with Eurocode 2 [2]

5.4.2 Instantaneous stress-related strain and time-dependent creep at elevated temperatures

Each specimen was loaded under constant temperature. The load was sustained for 2 hrs before unloading. There are eight combinations of different temperatures and load levels as discussed. Each case is repeated once for reliability.

Figures 5.14 - 5.16 illustrate total strain against time after initial heating. The instantaneous stress-related strain matched with elastic modulus at each corresponding temperature. The specimens deformed slowly with time under constant temperature and at sustained constant load level. This deformation is called creep. It can be seen that creep varies with load level and temperature, and increases with time. When the applied load is released, an

instantaneous stress-related strain recovery occurs. It is likely that this will be followed by further reduction in strain (termed at relaxation at zero stress in this case). However, measurements during the relaxation period were not included in the study. Only instantaneous unloading strain was measured.

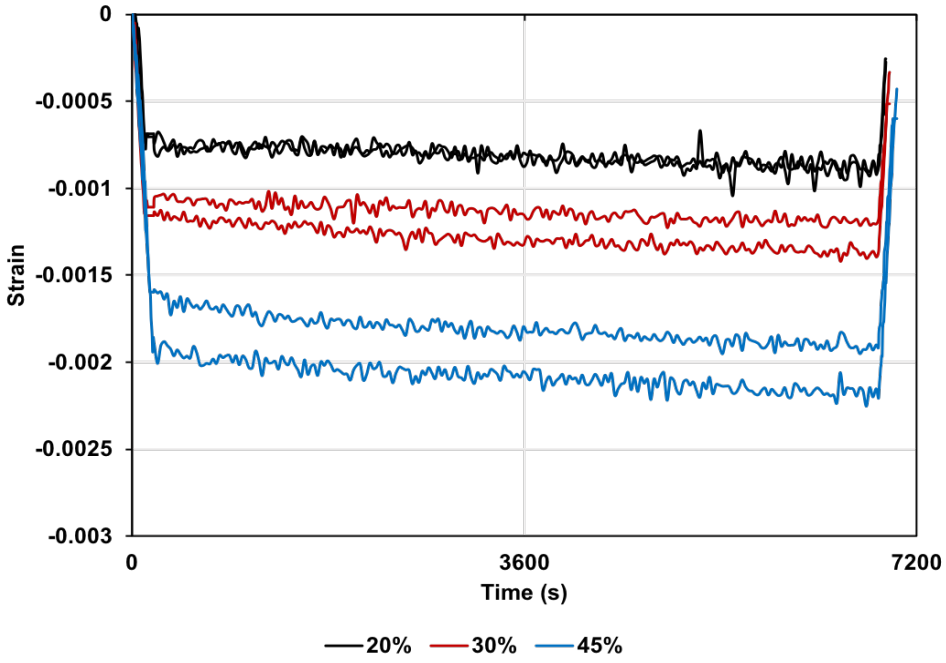

Fig. 5.14 The total strain of heating-then-loading tests at 200 °C without initial heating

The measured mean strain responses for different load levels and temperatures are shown in Fig. 5.17: instantaneous stress-related strain during loading (ε_l), total creep strain after 2 hrs constant heating (ε_{cre}), and instantaneous unloading strain (ε_{ul}). As expected, all strain responses were found to increase with load levels and temperatures. The instantaneous unloading strain is lower than the instantaneous loading strain. Perhaps some of the loading strain is irrecoverable.

Figures 5.18 and 5.19 compare 2-hr creep under different load levels and temperatures. As mentioned above, the value of creep after 2 hrs of load maintenance increases with load levels and temperatures. Figure 5.18 shows that the creep increase rapidly from 200 °C to

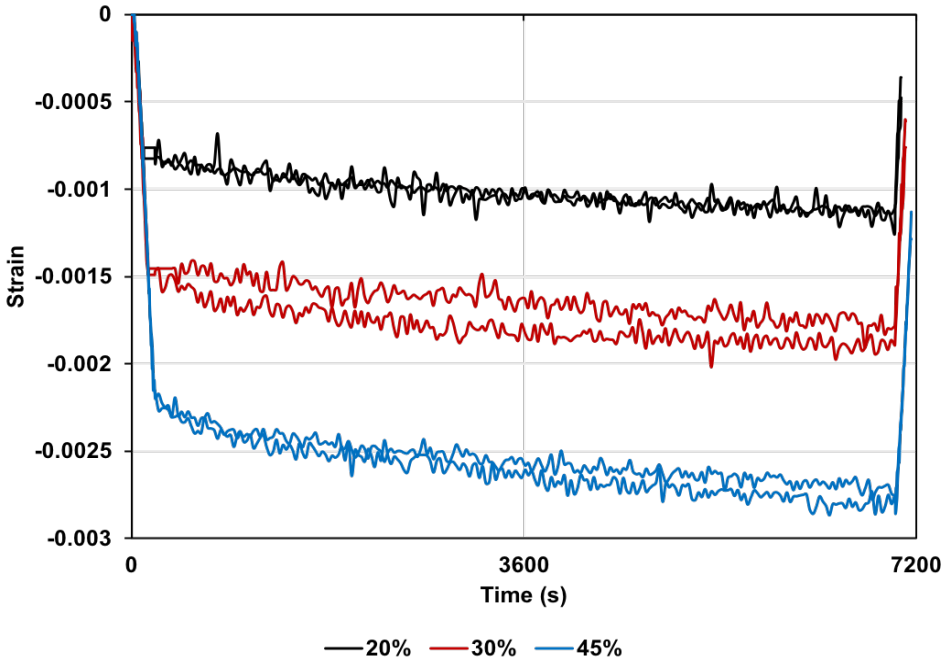

Fig. 5.15 The total strain of heating-then-loading tests at 400 °C without initial heating

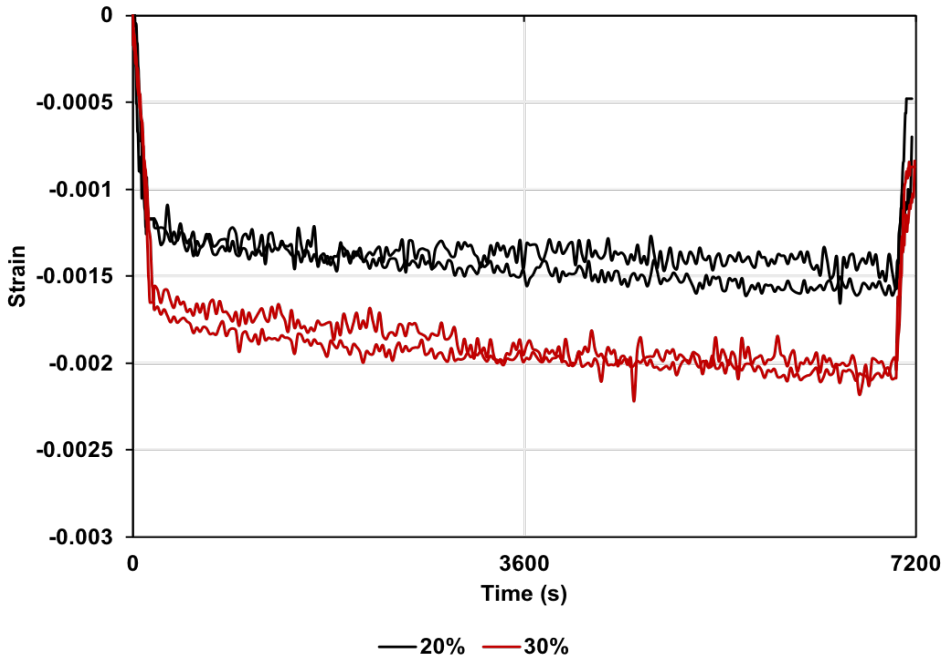

Fig. 5.16 The total strain of heating-then-loading tests at 600 °C without initial heating

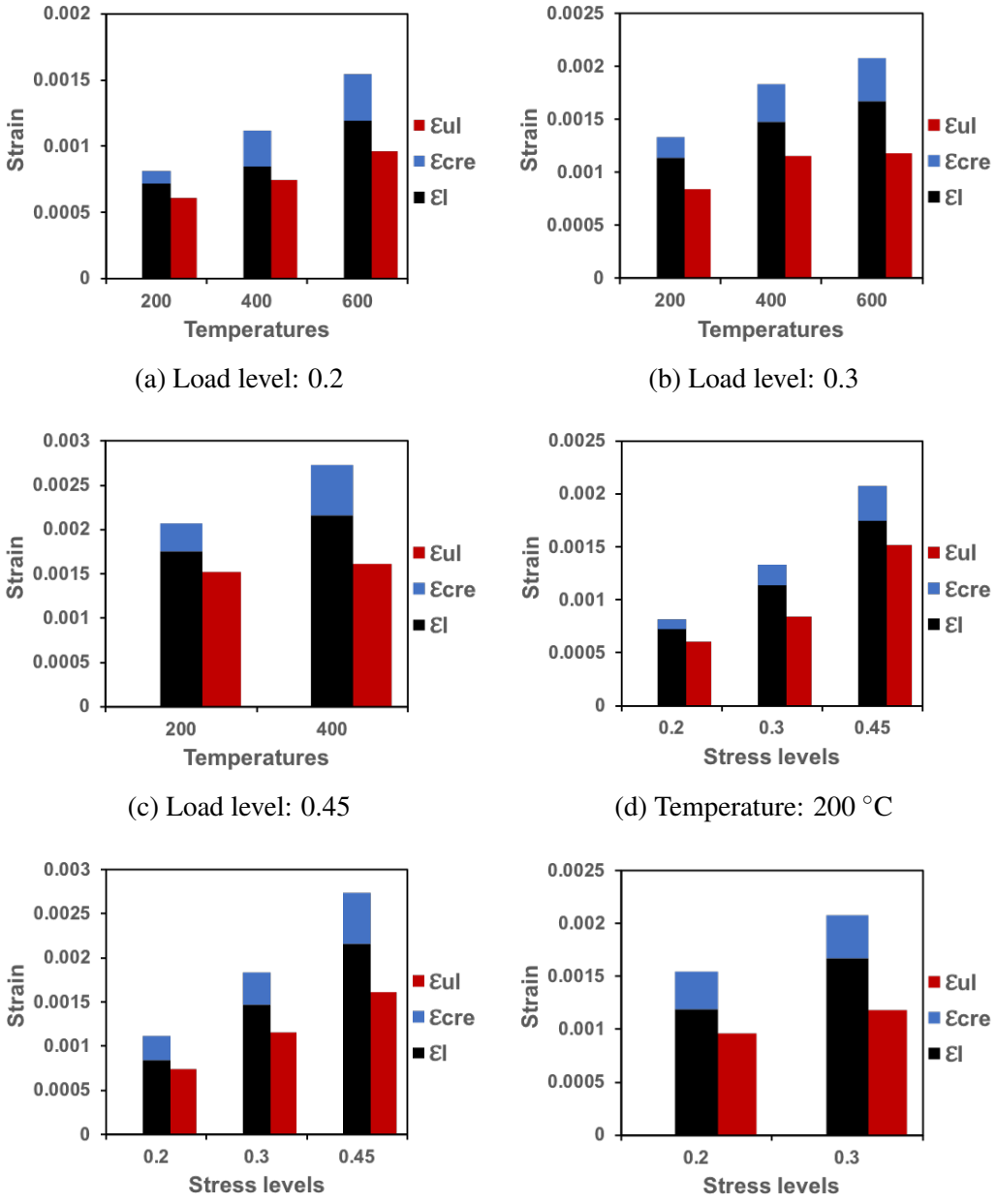

(a) Load level: 0.2

(b) Load level: 0.3

(c) Load level: 0.45

(d) Temperature: 200 °C

(e) Temperature: 400 °C

(f) Temperature: 600 °C

Fig. 5.17 Measured mean strain responses of HTL tests for different load levels and temperatures after initial heating

400 °C. The rate of increase decreases above 400 °C. It can be observed from Fig. 5.19 that the creep increases almost linearly with increasing load levels.

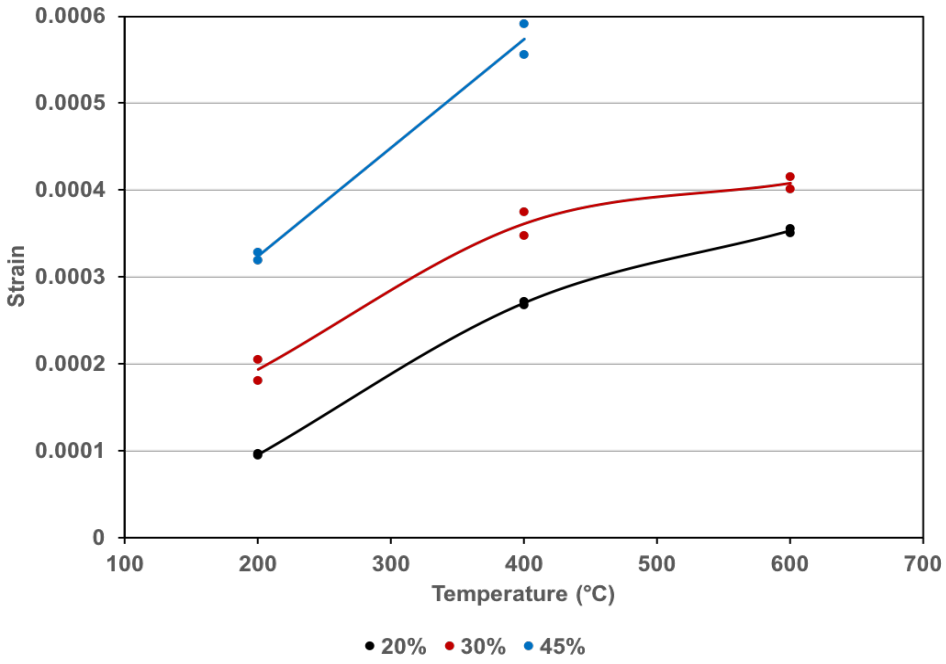

Fig. 5.18 The 2-hr creep under different load levels

Figure 5.20 shows the mean ratios of different strain components under different load levels and temperatures. The ratio of $\varepsilon_{ul}/\varepsilon_l$ remains around 80%. Majority of instantaneous stress-related strain is recovered immediately when the specimen is unloaded. The unloading strain will increase after sufficient time. However, the relaxation period is not considered in this research. The ratios of $\varepsilon_{ul}/\varepsilon_l$ at 30% and 45% load levels increase from 200 °C to 400 °C and decrease from 400 °C to 600 °C. With higher heating temperatures, the concrete will yield and plastic deformation will occur. In the tests, the displacement rate applied to the specimen is designed to reduce the plastic deformation. It should be noticed that the instantaneous stress-related strain contains elastic plastic strain in this research.

The ratio of $\varepsilon_{cre}/\varepsilon_l$ shows that the 2-hr creep is around 20% of the instantaneous load-

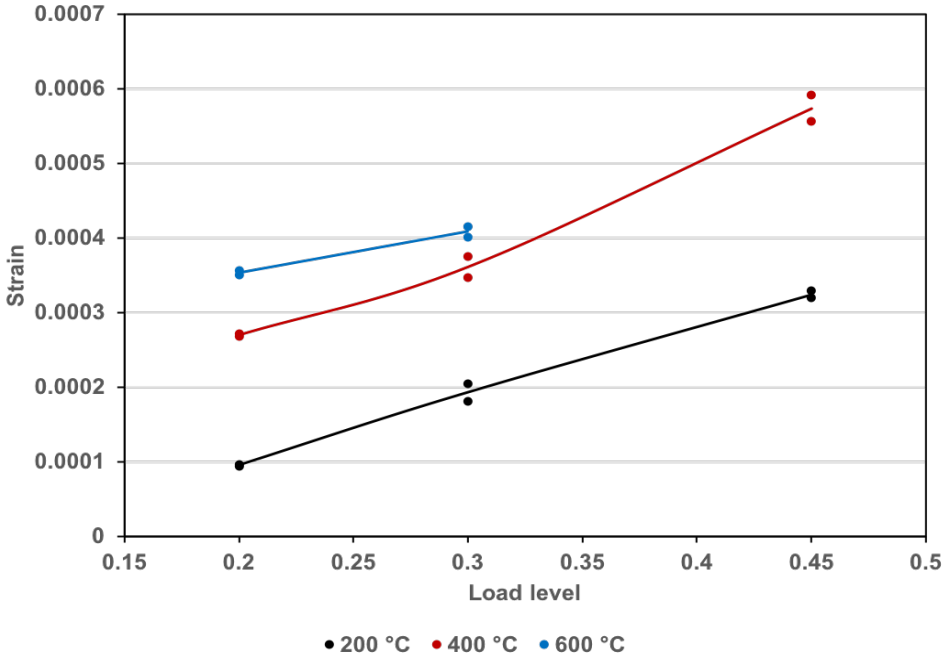

Fig. 5.19 The 2-hr creep under different temperatures

ing strain. It is first found to change with load levels and then remain constant when the load level is higher than 0.3.

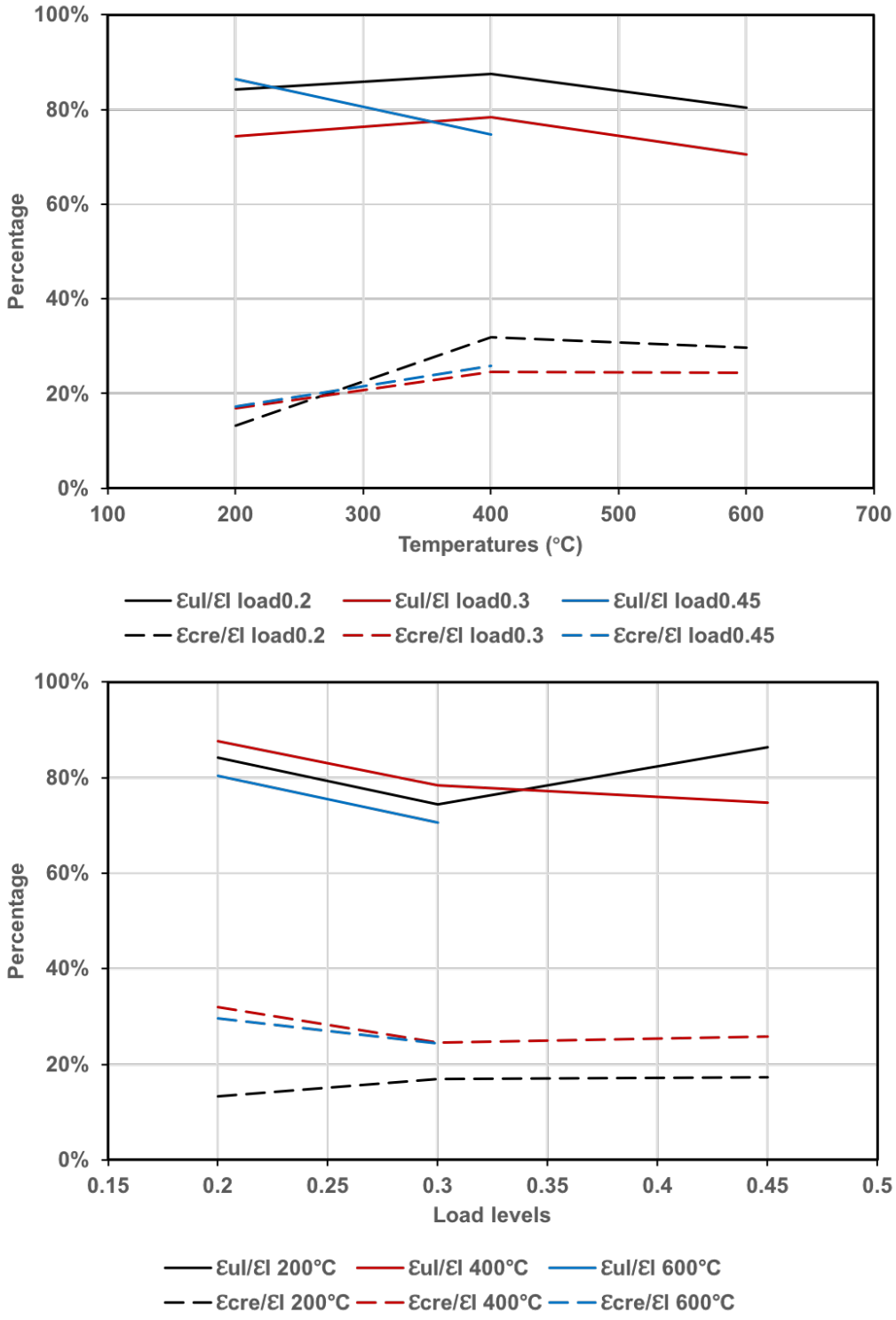

Fig. 5.20 Mean ratios of different strain components under different load levels and temperatures

5.5 Free thermal strain simulations

As discussed earlier, the thermal strain between experimental data and simulation (based on Eurocode 2 [2] parameters) are considerably different. Therefore, the thermal coefficient at each temperature was calculated based on the experimental data. Simulations with constant and variable (non-linear) thermal coefficients are considered.

5.5.1 Thermal coefficient

The free thermal strain data is available from HTL tests. The free thermal strain becomes constant after 2 hrs of heating at a constant temperature. The mean value of free thermal strain at each temperature is shown in Fig. 5.13. The mean thermal strain at the end of heating varies from 0.0015 to 0.0055 at elevated temperatures. As discussed before, the thermal coefficient is given by

$$\varepsilon_{th} = \alpha(\theta - 20) \quad for \theta > 20^{\circ}C \tag{5.1}$$

where ε_{th} and α are the free thermal strain and the thermal coefficient, respectively. From the above equation, the thermal coefficient varies from 7.7x10^{-6} to 9.5x10^{-6}.

5.5.2 Simulation results

Thermal expansion behaviour of concrete at elevated temperatures can be categorised as constant or variable. The study considered both constant and variable (non-linear temperature dependent) thermal coefficients for simulations. The constant thermal coefficient was evaluated from Eq. 5.1 by using the experimental thermal strain at peak temperature applied to the specimen. The variable thermal coefficient was evaluated from experimental thermal strains at 200 °C, 400 °C and 600 °C and assumed to vary linearly between these temperatures. Figure 5.21 shows that the difference between constant and variable thermal coefficients used in simulations. Although, the simulations of constant thermal expansion and variable thermal expansion reach the same value of thermal strain at the end of the heating process

(as the value used at the peak temperature in each case is the same), the free thermal strain variations with time are dissimilar for the two types of simulations.

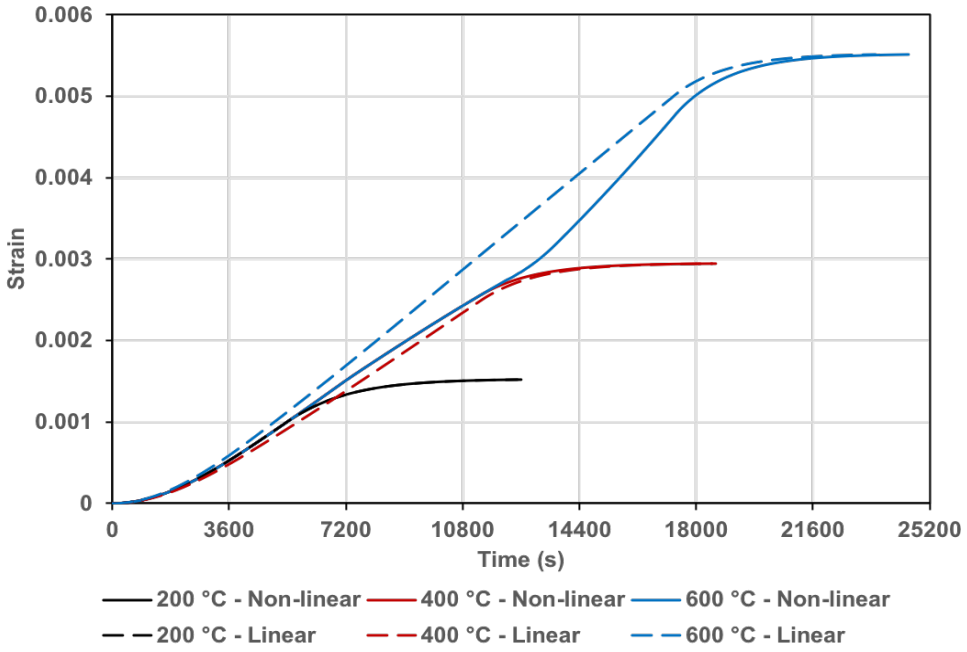

Fig. 5.21 Comparison of free thermal strains with constant and variable thermal coefficients at elevated temperatures

Figure 5.22 compares the free thermal strains at elevated temperatures obtained from experimental data and from simulation results with variable and constant thermal coefficients. It can be observed that both simulations achieve same free thermal strain at the end of the heating process as expected. The variable thermal expansion simulations give good agreement with the measured values even though the values used are only at three distinct temperatures. However, the difference between simulations with the constant and variable thermal coefficients is not significant. The constant thermal coefficient can be used in the simulation for convenience. This is further discussed later.

During the simulation of the heating process, there are two alternative outputs in ABAQUS. One is the TS (Total Strain) and the other one is THE (Thermal Strain). Figure 5.23 shows

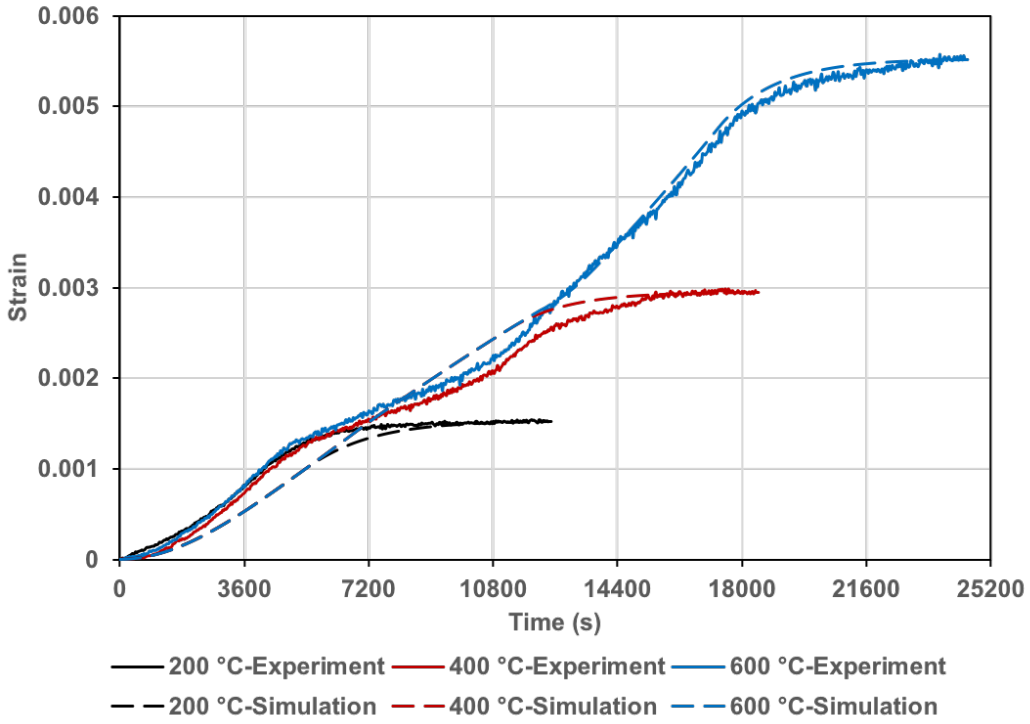

(a) Variable thermal coefficient

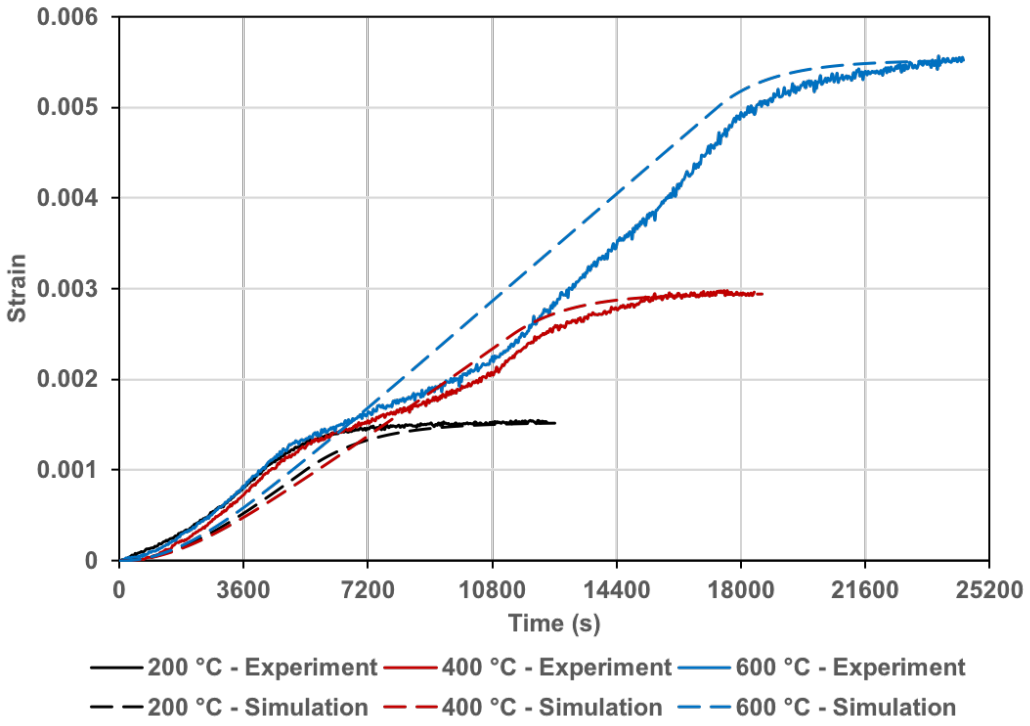

(b) Constant thermal coefficient

Fig. 5.22 Comparisons of free thermal strain between experimental data and simulation results with linear and non-linear thermal coefficients at elevated temperatures

a comparison of these two different outputs. There is a slight difference between the two variables. The main factor that causes the difference is temperature gradient within the specimen during heating. As discussed in the previous chapter, the temperature gradient causes mechanical strains during heating and these strains are included in the total strain. However, the difference is not significant at the heating rate of 2 °C/min.

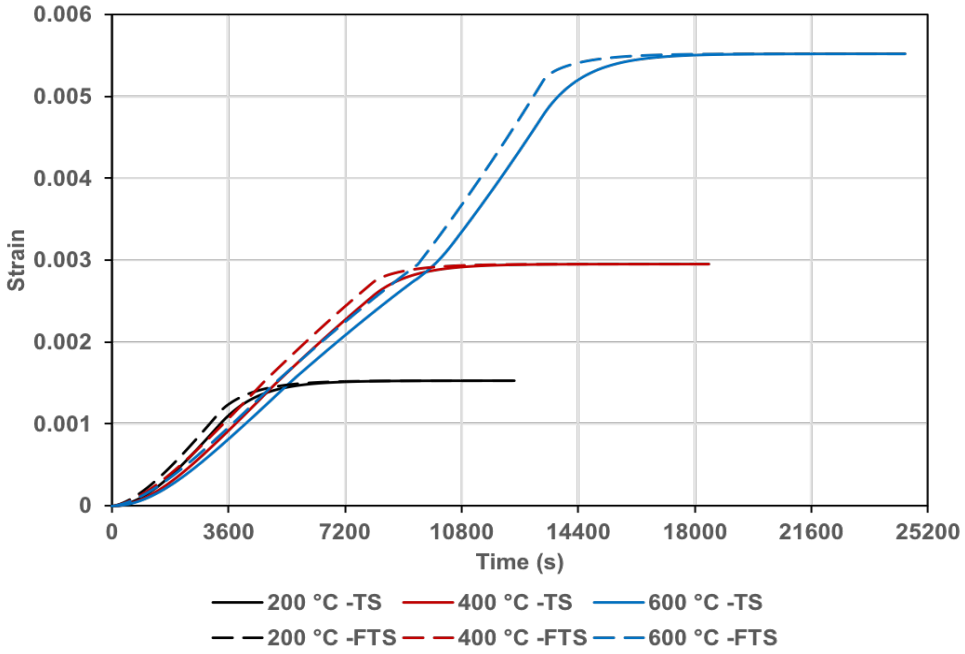

Fig. 5.23 Comparison between TS and THE output variables from ABAQUS

Eurocode 2 [2] suggests that the thermal coefficient increases with temperatures. However, the experimental data (Fig. 5.22) illustrates that the thermal coefficient decreases at 400 °C. Generally, the free thermal strain is influenced by moisture content and thermal gradient. The heat transfer analysis and mechanical analysis were conducted to evaluate temperature distribution, vertical stress and vertical strain. The specimen was heated to 600 °C at a heating rate of 2 °C/min. Only elastic effect was considered. The elastic modulus and thermal coefficient at different temperatures were evaluated from stress strain relation tests and HTL tests, respectively. Three time points based on experimental data were considered for examining detailed information: 6000 seconds, 11000 seconds and 15000 seconds. Over

the period from 6000 seconds to 11000 seconds, the free thermal strain increased slowly. After heating for 11000 seconds, the free thermal strain had a considerable increase. The third time point (15000 seconds) was picked on the steep slope.

Figures 5.24 - 5.26 illustrates distributions of temperature, vertical stress and vertical strain at the middle cross-section (radially from the central line to the outer surface) at different time points. As can be seen from Fig. 5.24, the temperatures within the specimen were around 150 °C to 180 °C. At these temperatures, water loss is likely to reach its peak. Consequently, increase in free thermal strain slows down at this time point. The vertical stresses remained similar from 6000 seconds to 11000 seconds indicating that stresses due variable thermal expansion in this temperature range are not affected. Then, the vertical stresses had a considerable increase after 11000 seconds. It is interesting to notice that the concrete surface which has higher temperatures is dominated by the compressive stresses and the concrete central line which has lower temperatures is dominated by tensile stresses.

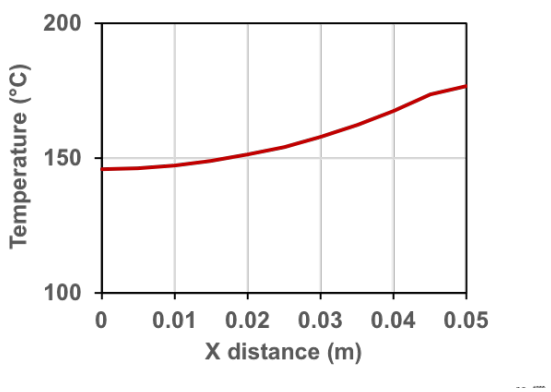

(a) Temperature distribution

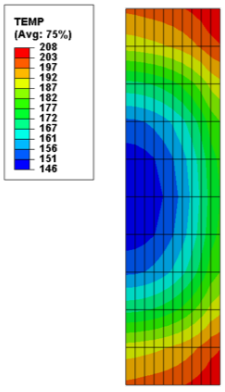

(b) Temperature contour

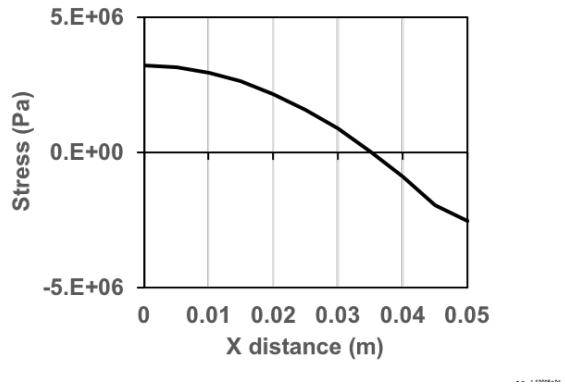

(c) Vertical stress

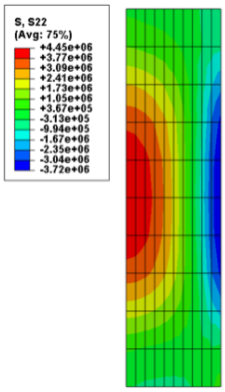

(d) Vertical stress contour

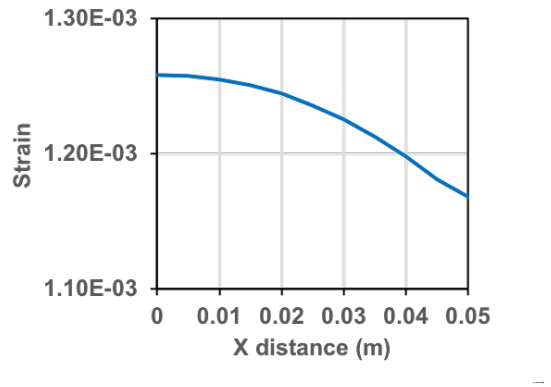

(e) Vertical strain

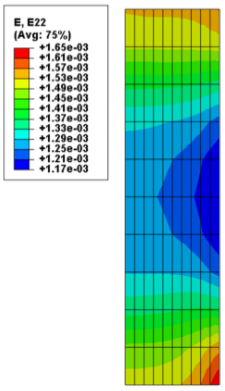

(f) Vertical strain contour

Fig. 5.24 The temperature distribution, vertical stress and vertical strain along the axis and contour plots after heating 6000 seconds

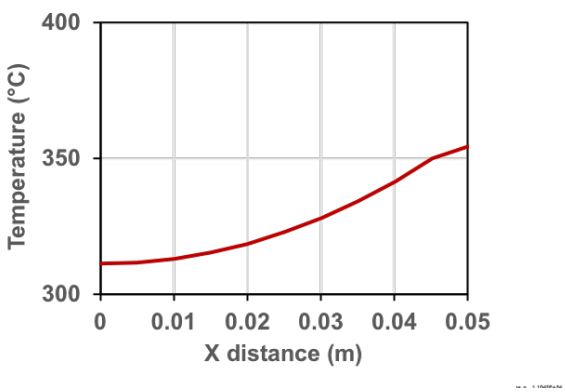

(a) Temperature distribution

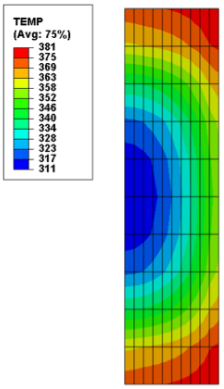

(b) Temperature contour

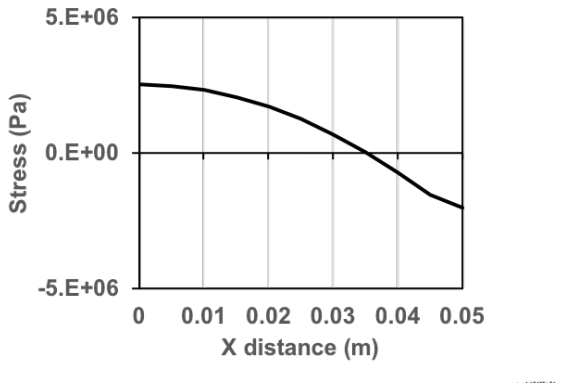

(c) Vertical stress

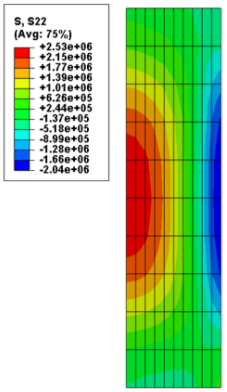

(d) Vertical stress contour

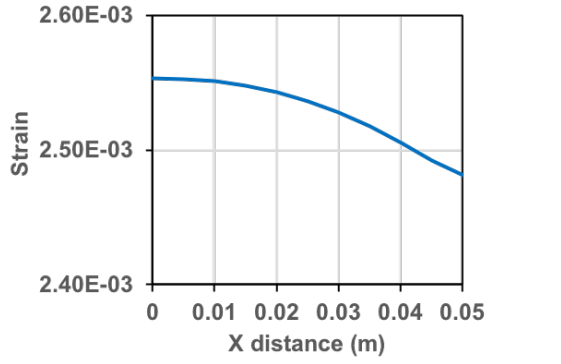

(e) Vertical strain

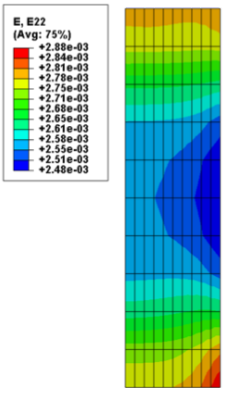

(f) Vertical strain contour

Fig. 5.25 The temperature distribution, vertical stress and vertical strain along the axis and contour plots after heating 11000 seconds

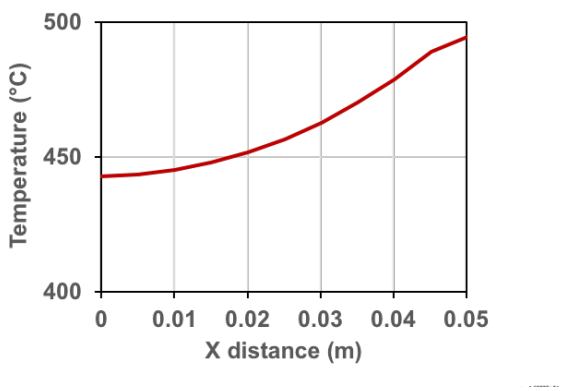

(a) Temperature distribution

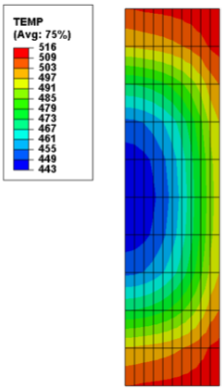

(b) Temperature contour

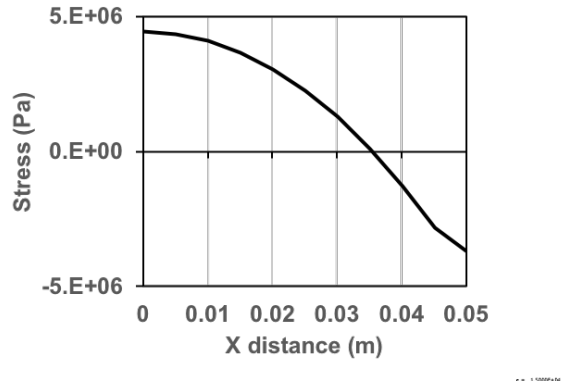

(c) Vertical stress

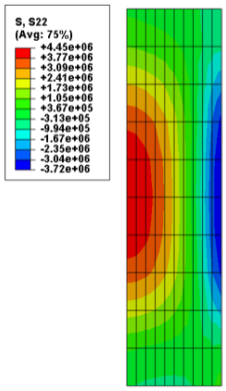

(d) Vertical stress contour

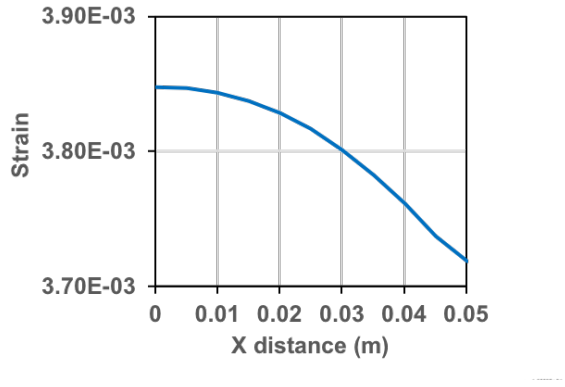

(e) Vertical strain

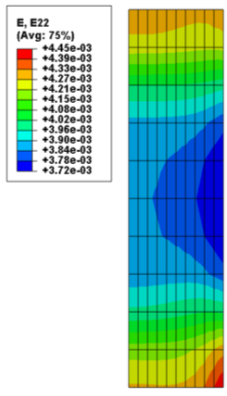

(f) Vertical strain contour

Fig. 5.26 The temperature distribution, vertical stress and vertical strain along the axis and contour plots after heating 15000 seconds

5.6 Creep under sustained load simulations

5.6.1 Viscoelastic model

The concrete deforms continuously when it is subjected to a constant load. In the HTL tests, the instantaneous elastic strain is predicted by the instantaneous elastic modulus at elevated temperatures. The concrete deforms slowly with time when the load is constant. The strain curves in the HTL tests show that the deformation caused by constant load is time dependent. This time dependent material behaviour is usually modelled using concepts of viscoelasticity or viscoplasticity. If it is assumed that all strain can be recovered upon unloading then viscoelasticity is the simplest way to model the time dependent creep.

Kelvin-Voigt model

One approach to model viscoelasticity is via the Kelvin-Voigt model, which includes a spring and a dashpot, as shown in Fig. 5.27. The spring represents solid-like properties and the dashpot represents liquid-like properties. For the spring, stress is linearly proportional to strain. For the dashpot, the stress is proportional to the strain rate. The stress-strain relation is given by

$$\sigma(t) = E\varepsilon(t) + \eta\frac{d\varepsilon(t)}{dt} \tag{5.2}$$

where $\sigma(t)$ and $\varepsilon(t)$ are time-dependent stress and strain, respectively. E and η are elastic modulus and viscosity, respectively.

To evaluate creep due to sudden application of a step stress σ_0, the boundary conditions are

$$\sigma = 0, \varepsilon = 0 \qquad for\, t = 0 \tag{5.3}$$

$$\sigma = \sigma_0 \qquad for\, t > 0 \tag{5.4}$$

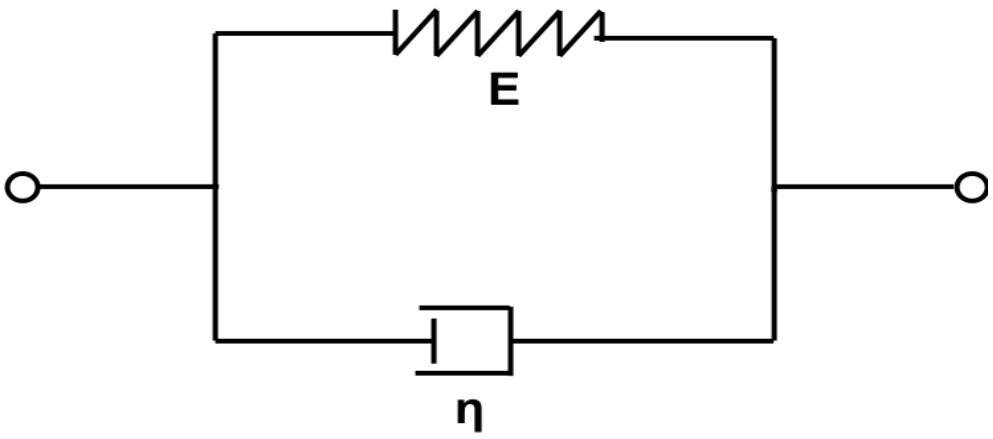

Fig. 5.27 Schematic diagram of Kelvin-Voigt model

Substituting $\sigma = \sigma_0$ and dividing by η in Eq. 5.2 gives

$$\frac{\sigma_0}{\eta} = \frac{E}{\eta}\varepsilon + \frac{d\varepsilon}{dt} \tag{5.5}$$

By solving the ordinary differential equation, the strain in Kelvin-Voigt model is obtained as

$$\varepsilon(t) = \frac{\sigma_0}{E}(1 - e^{-t/\tau}) \quad with \quad \tau = \eta/E \tag{5.6}$$

where τ is referred to the retardation time.

The creep compliance is represented as the ratio of strain to stress at time t. It is a characteristic of creep under temperatures and load levels. The compliance function is expressed as

$$\begin{aligned} D(t) &= \frac{\varepsilon(t)}{\sigma} \\ &= \frac{1}{E(t)} \end{aligned} \tag{5.7}$$

where D(t) is the creep compliance. In the linear elasticity, the creep compliance is independent of load levels. Substituting Eq. 5.7 in Eq. 5.6 gives

$$\varepsilon(t) = D(t)\sigma_0 \tag{5.8}$$

As stated earlier, the Kelvin-Voigt model is based on two parameters, E and η, whose values can be evaluated from experimental data by curve fitting.

Maxwell model

Another model used in viscoelastic simulation is the Maxwell model, shown in Fig. 5.28. The spring and the dashpot are connected in series.

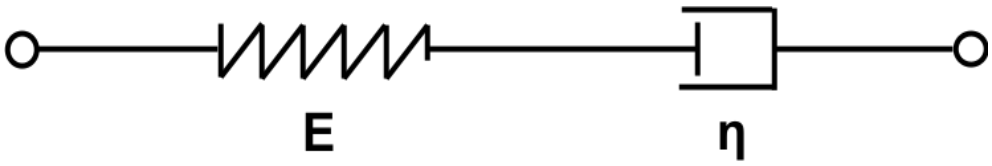

Fig. 5.28 Schematic diagram of Maxwell model

The stress-strain relation is given by

$$\frac{d\varepsilon(t)}{dt} = \frac{1}{E}\frac{d\sigma(t)}{dt} + \frac{\sigma(t)}{\eta} \tag{5.9}$$

For stress relaxation, the strain applied is constant as ε_0. The stress is calculated by integration

$$\sigma(t) = \varepsilon_0 E e^{-t/\rho} \tag{5.10}$$

where ρ is the relaxation time.

Superposition principle

The superposition principle states that responses to different load levels can be superimposed. However, it is not valid for all conditions. For the concrete, the superposition principle is only valid for the load levels below 40% - 50% of uniaxial strength. The damage law must be applied at higher load levels.

The Boltzmann superposition principle provides the response of a material to varying loading history. Consider Fig. 5.29 (a) in which the applied stress changes at times t_1, t_2 ... ,each resulting in individual strains as shown in Fig. 5.29 (b). Using Eq. 5.8 and Boltzmann superposition principle the total strain response is given by

$$\begin{aligned}\varepsilon(t) &= D(t-t_1')\sigma_1 + D(t-t_2')(\sigma_2-\sigma_1) + ... + D(t-t_i')(\sigma_i-\sigma_{i-1}) \\ &= \int_0^t D(t-t')d\sigma(t')\end{aligned} \tag{5.11}$$

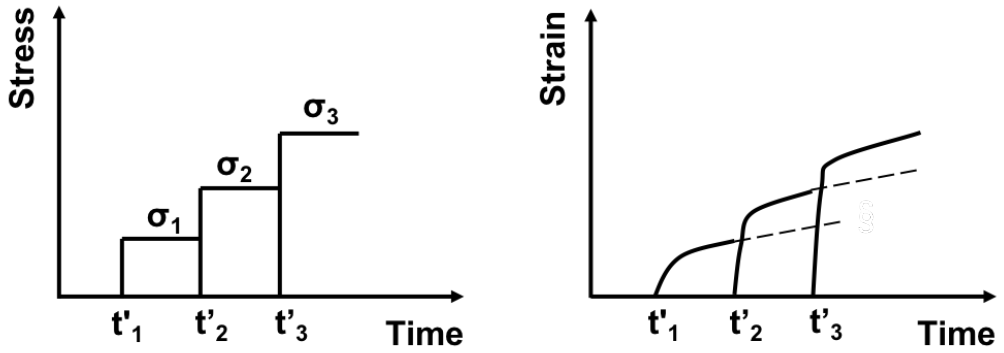

(a) Applied stress curves (b) Strain curves

Fig. 5.29 The creep curve by Boltzmann superposition principle

Prony series

The Kelvin-Voigt chain in Fig. 5.30 is significant in modelling the time dependent creep. To achieve more accurate creep curve, the Kelvin-Voigt chain comprises of η_{pr} Kelvin-Voigt models and an initial elastic element E_g.

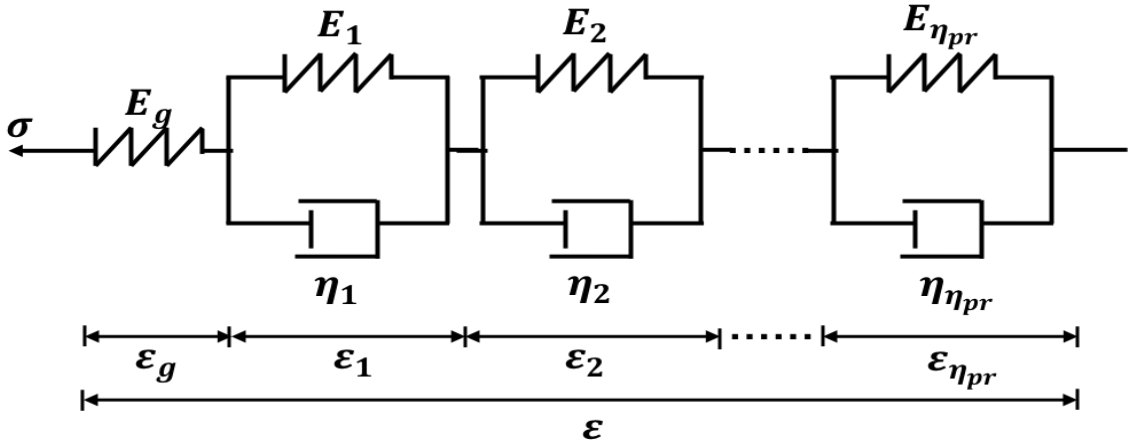

Fig. 5.30 The Kelvin-Voigt chain

In the Kelvin-Voigt chain, the total strain is the sum of strains in each unit and each unit has the same stress, i.e.

$$\sigma = \sigma_g = \sigma_1 = \sigma_2 = ... = \sigma_{\eta_{pr}} \tag{5.12}$$

$$\varepsilon = \varepsilon_g + \varepsilon_1 + \varepsilon_2 + ... + \varepsilon_{\eta_{pr}} \tag{5.13}$$

Therefore, strain at any time t due to the application of a constant stress σ_0 is given by

$$\begin{aligned} \varepsilon(t) &= \varepsilon_g + \varepsilon_1 + \varepsilon_2 + ... + \varepsilon_{\eta_{pr}} \\ &= \sigma_0 D_g(1 - e^{-t/0}) + \sigma_0 D_1(1 - e^{-t/\tau_1}) + \sigma_0 D_2(1 - e^{-t/\tau_2}) + ... + \sigma_0 D_i(1 - e^{-t/\tau_{\eta_{pr}}}) \\ &= \sigma_0 D_g + \sigma_0 \sum_{j=1}^{\eta_{pr}} D_j(1 - e^{-t/\tau_j}) \end{aligned} \tag{5.14}$$

Dividing by σ_0 gives

$$D(t) = D_g + \sum_{j=1}^{n_{pr}} D_j(1 - e^{-t/\tau_j}) \tag{5.15}$$

where D_g is instantaneous elastic compliance, D_j are transient retardation strengths, τ_j are

retardation times, and η_{pr} is number of terms in the Prony series. Also, η_{pr} is number of Voigt models in the Kelvin chain. These parameters, including D_g, D_j and τ_j (j = 1, 2, ..., n_{pr}), were determined by minimizing the error between experimental data. MATLAB was used for the curve fitting. The non-linear least-squares fit method was used in the analysis. This method improves the accuracy of parameters by minimizing the sum of squares of the residuals between experimental data and the model. From the experimental results, it was found that the number of Prony terms, η_{pr} = 1, was sufficient to fit the creep data.

However, many users prefer to use Prony series in other format. Park and Schapery converted the creep compliance into other formats with generalized Maxwell model, as shown in Fig. 5.31. In the generalized Maxwell model, the total stress is the sum of stresses in each unit

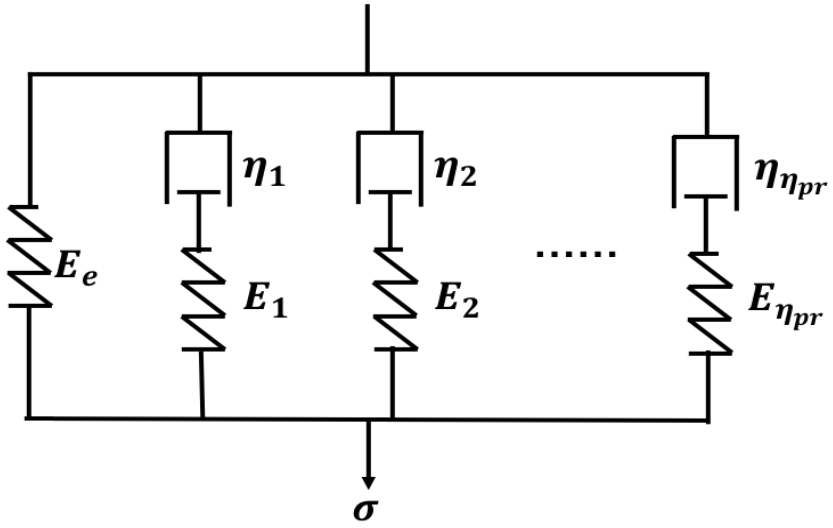

Fig. 5.31 The generalized Maxwell model

and each unit has the same strain, i.e.

$$\sigma = \sigma_e + \sigma_1 + \sigma_2 + ... + \sigma_{\eta_{pr}} \tag{5.16}$$

$$\varepsilon = \varepsilon_e = \varepsilon_1 = \varepsilon_2 = ... = \varepsilon_{\eta_{pr}} \tag{5.17}$$

Therefore, stress at any time t due to the application of a constant strain ε_o is given by

$$\begin{aligned}\sigma(t) &= \sigma_e + \sigma_1 + \sigma_2 + ... + \sigma_{\eta_{pr}} \\ &= \varepsilon_0 E_e + \varepsilon_0 E_1 e^{-t/\rho_1} + \varepsilon_0 E_2 e^{-t/\rho_2} + ... + \varepsilon_0 E_{\eta_{pr}} e^{-t/\rho_{\eta_{pr}}} \\ &= \varepsilon_0 E_e + \varepsilon_0 \sum_{i=1}^{\eta_{pr}} E_i e^{-t/\rho_i}\end{aligned} \tag{5.18}$$

Deviding by ε_0 in Eq. 5.18 gives

$$E(t) = E_e + \sum_{i=1}^{n_{pr}} E_i e^{-t/\rho_i} \tag{5.19}$$

where E_e is the equilibrium moduli, and E_i and ρ_i(i=1, 2, ..., n_{pr}) are the relaxation strengths and relaxation times, respectively.

The relationship between the relaxation modulus E(t) and creep compliance D(t) according to Eq.5.11 is defined as

$$\int_0^t D(t-t')\frac{E(t')}{dt'}dt' = 1 \quad (t > 0) \tag{5.20}$$

The known set D_g, D_j and τ_j (j = 1, 2,..., n_{pr}) in creep compliance function D(t) is used to determine the constants in relaxation modulus by solving the following systems of linear algebraic equations

$$A_{ki}E_i = B_k \tag{5.21}$$

and

$$A_{ki} = \begin{cases} D_g e^{-t_k/\rho_i} + \sum_{j=1}^{n_{pr}} \frac{\rho_i D_i}{\rho_i - \tau_j}(e^{-t_k/\rho_i} - e^{-t_k/\tau_j}), & \rho_i \neq \tau_j \\ D_g e^{-t_k/\rho_i} + \sum_{j=1}^{n_{pr}} \frac{t_k D_j}{\tau_j} e^{-t_k/\rho_i}, & \rho_i = \tau_j \end{cases} \tag{5.22}$$

$$B_k = 1 - E_e(D_g + \sum_{j=1}^{n_{pr}} D_j(1 - e^{-t_k/\tau_j})) \tag{5.23}$$

where k is the number of discrete sampling points and t_k denotes a discrete time points.

As discussed before, the sets of constants, D_g, D_j and τ_j (j = 1, 2,..., n_{pr}) are determined from time-dependent creep curves of experimental data. By solving the system of equations, the equilibrium is determined

$$E_e = \frac{1}{D_g + \sum_{j=1}^{n_{pr}} D_j} \tag{5.24}$$

Park and Schapery proposed a root finding method to determine the relaxation time constants ρ_i. The relaxation strengths E_i are determined by using the least-squares method, solving Eq. 5.21 with MATLAB.

5.6.2 Simulation results based on Prony series

The fitting curve used in MATLAB included the value of initial instantaneous stress-related strain. Each test was repeated once. Theoretically, the instantaneous elastic modulus is independent of the load level in linear viscoelasticity. However, the experimental data of instantaneous elastic modulus was slightly different at each load level. Also, the creep data should be independent on the load level for viscoelastic modelling. To decrease the influence of limited number of experiments, the curve fitting was based on the mean value of creep at each temperature.

Figure 5.32 shows a comparison of time-dependent creep between experimental data and simulation results evaluated by MATLAB. Each time-dependent creep curve was the mean value of experimental data at different load levels after normalisation. The curve fitting was based on 1-term Prony series and 3-term Prony series. As can be seen from Fig. 5.32, the simulation results (the red lines) were similar with different numbers of Prony terms. For this study, the 1-term Prony series describes the creep curve well. However, the number of Prony terms is dependent on specific conditions. More Prony terms may be necessary for longer time. The time-dependent creep simulation was based on 3-term Prony series in this study.

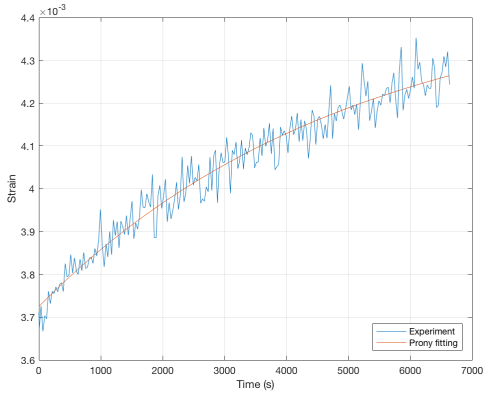

(a) 200 °C, $\eta_{pr} = 1$

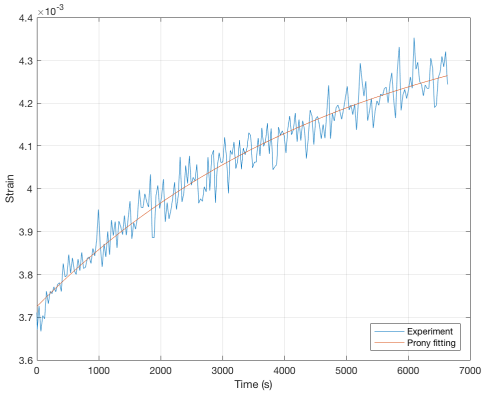

(b) 200 °C, $\eta_{pr} = 3$

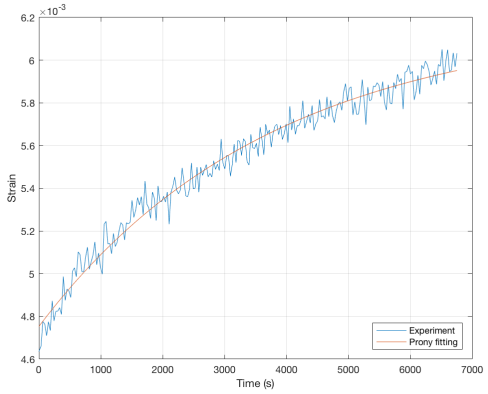

(c) 400 °C, $\eta_{pr} = 1$

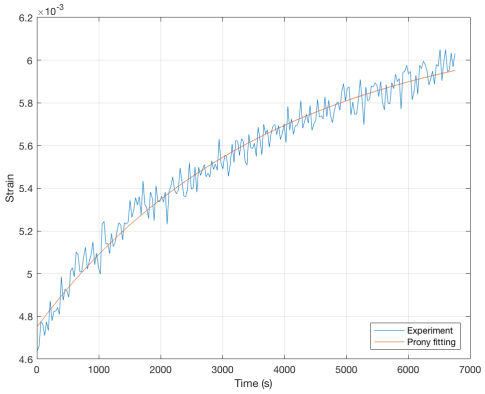

(d) 400 °C, $\eta_{pr} = 3$

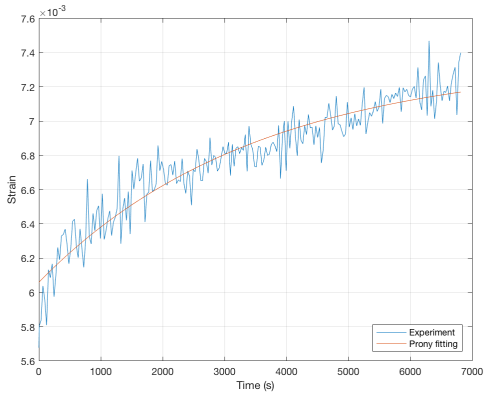

(e) 600 °C, $\eta_{pr} = 1$

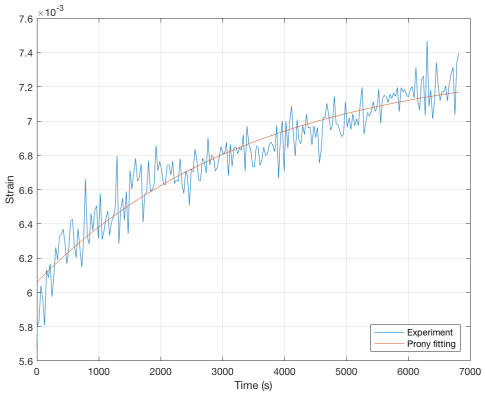

(f) 600 °C, $\eta_{pr} = 3$

Fig. 5.32 Comparison of time-dependent creeps between experimental data and simulation results evaluated by MATLAB

ABAQUS was used to conduct the finite element analysis in this study. To simulate time-dependent creep, the viscoelastic material was used in the model. Without consideration of the recovery, the viscoelastic material is an adequate method to model time-dependent creep. The viscoelastic material model reproduces time-dependent creep behaviour at elevated temperatures using Prony series. It requires the definition of the long-term elastic modulus instead of the instantaneous elastic modulus. The thermal coefficient is not necessary in the simulation as constant temperature is maintained. The unloading process is not considered in this simulation.

In the simulation, the temperature of the model was constant and uniform. The reference temperatures were set to 200 °C, 400 °C and 600 °C, respectively. The load was kept constant for 2 hrs. Figures 5.33 - 5.35 show simulation results of time-dependent creep with the viscoelastic material model.

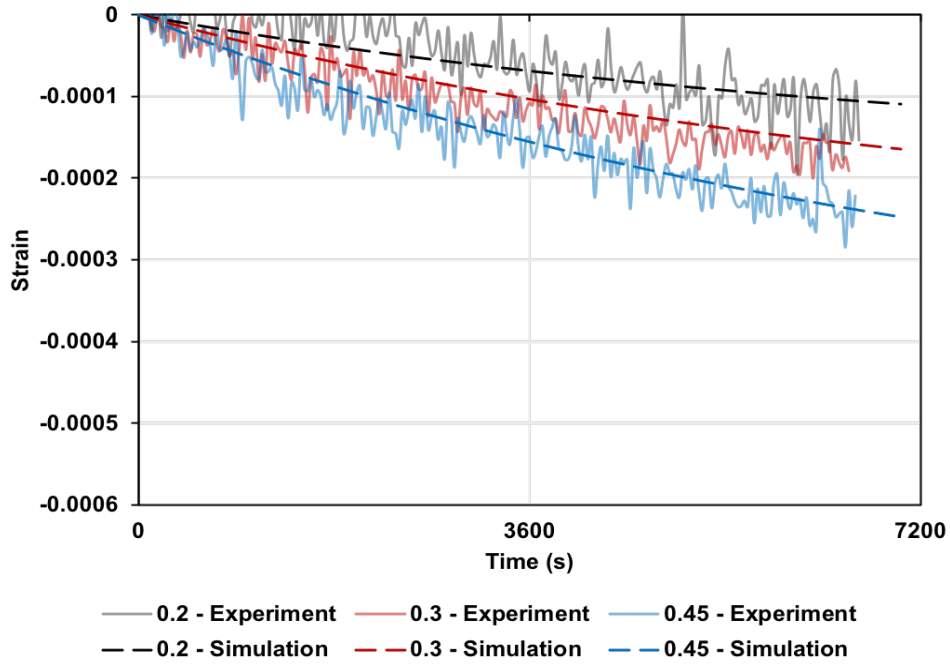

Fig. 5.33 Comparison of time-dependent creeps between experimental data and simulation results at 200 °C and different load levels

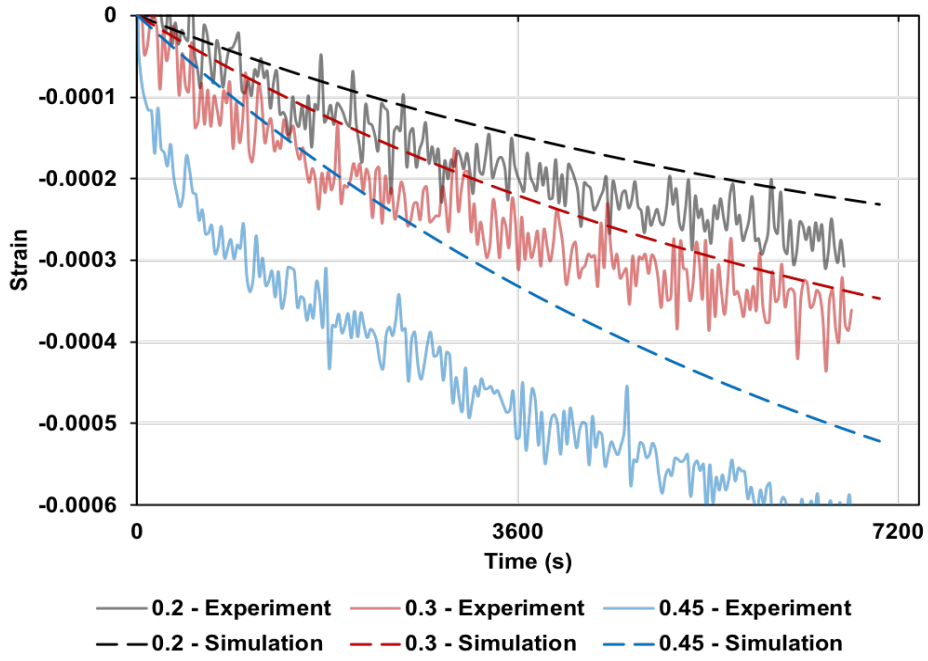

Fig. 5.34 Comparison of time-dependent creeps between experimental data and simulation results at 400 °C and different load levels

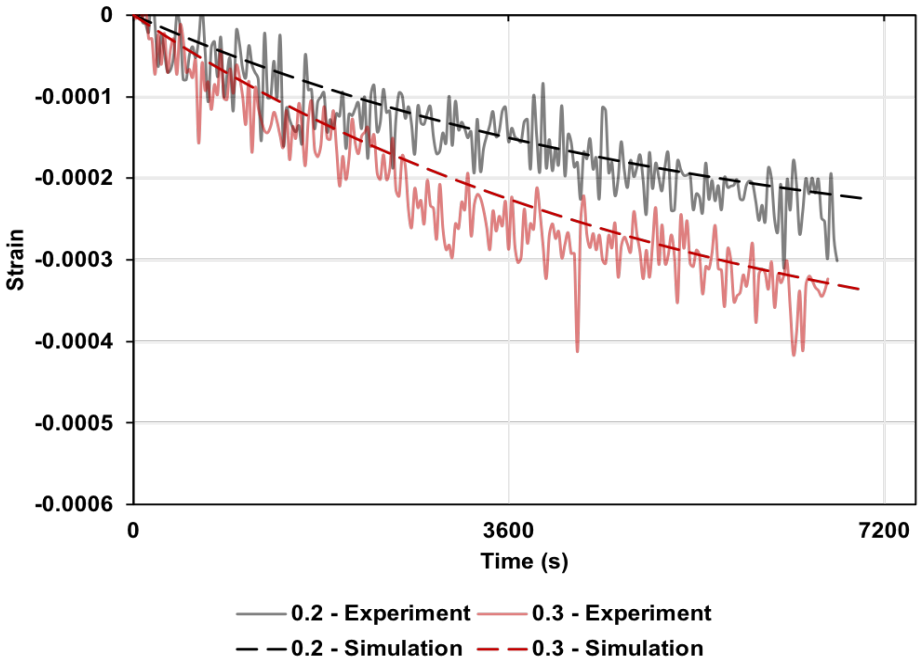

Fig. 5.35 Comparison of time-dependent creeps between experimental data and simulation results at 600 °C and different load levels

Figures 5.33 and 5.35 show that the simulation results give good agreement with the experimental data without consideration of the unloading process at 200 °C and 600 °C. For the simulation results at 400 °C, the simulation results do not match the experimental results, particularly at 45% load level. During the curve fitting, the Prony parameters at 400 °C were based on the mean value of creep under 20% and 30% load levels. For higher load levels, they may contain irrecoverable strains. This is discussed in the following section. The viscoelastic material model provides a simple way to model time-dependent creep.

Prony parameters

The viscoelastic properties are independent of load levels. As can be seen from Fig. 5.19, the 2-hr creep almost increase linearly with increasing load levels. However, the creep at 400 °C has a higher increase than that to be predicted by sealing up the load level. The possible reason is irrecoverable strain developed during loading. Therefore, the curve fitting results at 400 °C were based on experimental data under 20% and 30% load level. To get the mean value of creep strain at each temperature, the creep was divided by the corresponding load level. The time-dependent creep curves at different temperatures are shown in Fig. 5.36.

The viscoelastic material parameters D_g, D_j and τ_j were based on curve fitting results in MATLAB. Then, the creep compliance was converted into the relaxation modulus. The parameters based on 1-term Prony series and 3-term Prony series at elevated temperatures were evaluated using the formulation discussed earlier. The constants for different temperatures with different numbers of terms in the Prony series are shown in Table 5.1. As can be seen from Table 5.1, the main Prony parameters, D_g and E_e, are similar for different numbers of terms in Prony series (η_{pr}). For the parameters based on 3-term Prony series, the value of E_2 and E_3 are negligible. This is similar to the conclusion drawn from Fig. 5.32, the number of terms has little influence on the simulation results in this study.

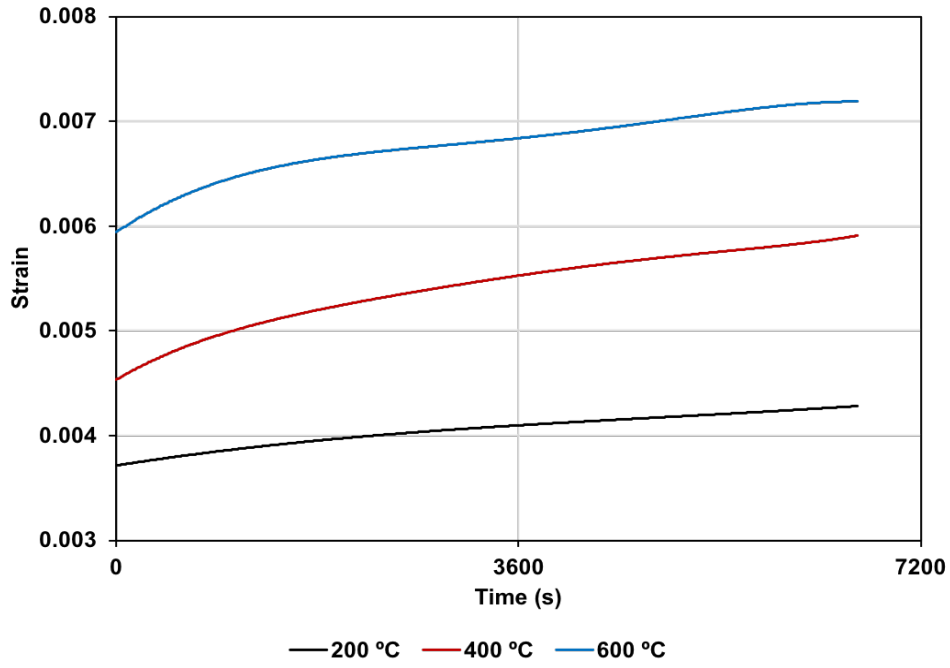

Fig. 5.36 Mean values of time-dependent creep data at different temperatures

Table 5.1 Comparison of Prony parameters with different numbers of terms in the Prony series

θ	η_{pr}	$D_g \times 10^{-5}$	$D_j \times 10^{-5}$			τ_j			$E_e \times 10^3$	$E_i \times 10^3$			ρ_i		
			D_1	D_2	D_3	τ_1	τ_2	τ_3		E_1	E_2	E_3	ρ_1	ρ_2	ρ_3
200	1	8.19	1.61	-	-	5005	-	-	10.2	2.01	-	-	5993	-	-
200	3	8.19	0.54	0.54	0.54	5009	5001	5006	10.2	2.01	$2.56\text{x}10^{-4}$	0.00	5993	5008	5003
400	1	10.44	3.15	-	-	3744	-	-	7.35	2.22	-	-	4874	-	-
400	3	10.44	1.19	0.00	2.02	2928	4742	4506	7.32	1.89	$4.44\text{x}10^{-4}$	0.36	5507	4743	3133
600	1	13.31	2.85	-	-	3499	-	-	6.19	1.32	-	-	4247	-	-
600	3	13.32	1.03	0.89	0.93	3607	3669	3253	6.19	1.26	$3.78\text{x}10^{-3}$	0.06	4305	3639	3335

θ [°C] is the applied temperature. η_{pr} is the number of terms in Prony series. D_g [1/MPa], D_j [1/MPa] and τ_j [s] are the instantaneous elastic compliance, the transient retardation strength, and the retardation time in the Prony series. E_e [MPa], E_i [MPa] and ρ_i [s] are the equilibrium modulus, the relaxation strength, and the relaxation time, respectively.

To use the viscoelastic material in ABAQUS, the set of constants E_e, E_i, and ρ_i in Prony series were used. The long term or the equilibrium modulus is defined as a material property instead of the instantaneous elastic modulus. The moduli ratio is defined by the E_i/E_e.

The glassy or instantaneous compliance (D_g) is found to increase with increasing temperatures. The corresponding creep compliance functions (D(t)) according to Eq. 5.15 are shown in Fig. 5.37.

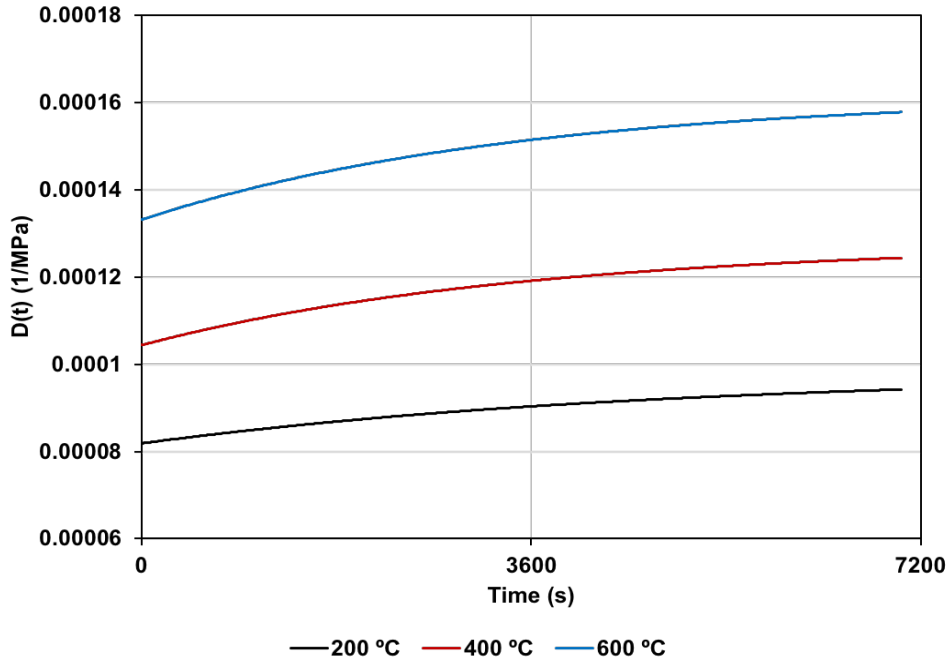

Fig. 5.37 Time-dependent creep compliance functions at different temperatures with 3-term Prony series

The creep compliance increases with time. The time dependent relaxation modulus functions (E(t)) according to Eq. 5.19 are shown in Fig. 5.38. The relaxation modulus decreases with time. Also, it decreases with temperatures as expected.

The instantaneous elastic modulus is achieved when the time is zero in Eq. 5.19. Those values at elevated temperatures are compared with the results from the compressive strength

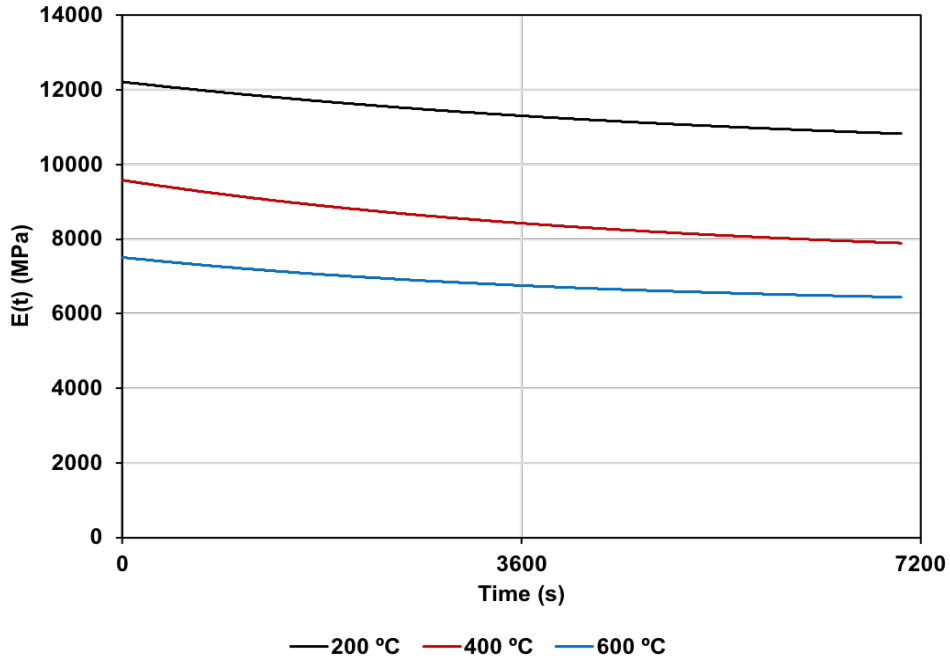

Fig. 5.38 Time-dependent relaxation modulus functions at different temperatures with 3-term Prony series

tests. Figure 5.39 indicates a comparisons of instantaneous elastic modulus at 200 °C, 400 °C and 600 °C. The differences of instantaneous elastic modulus at 200 °C and 600 °C are relatively small. The instantaneous elastic modulus based on Prony series is lower than that obtained from the experiments at 400 °C.

5.6.3 Prony series with different load levels

The viscoelasticity is a simple way to model time-dependent creep. Due to the plastic effects, the instantaneous moduli vary with different load levels. However, if it is assumed that all load levels are independently viscoelastic and curve fitting is undertaken separately for all load levels, the experimental results can be simulated accurately using the Prony series. Figures 5.40 - 5.42 show simulation results of time-dependent creep with the viscoelastic material model. The experimental data are the mean values of strain obtained from HTL tests. The Prony series used in each case is based on the corresponding experimental data.

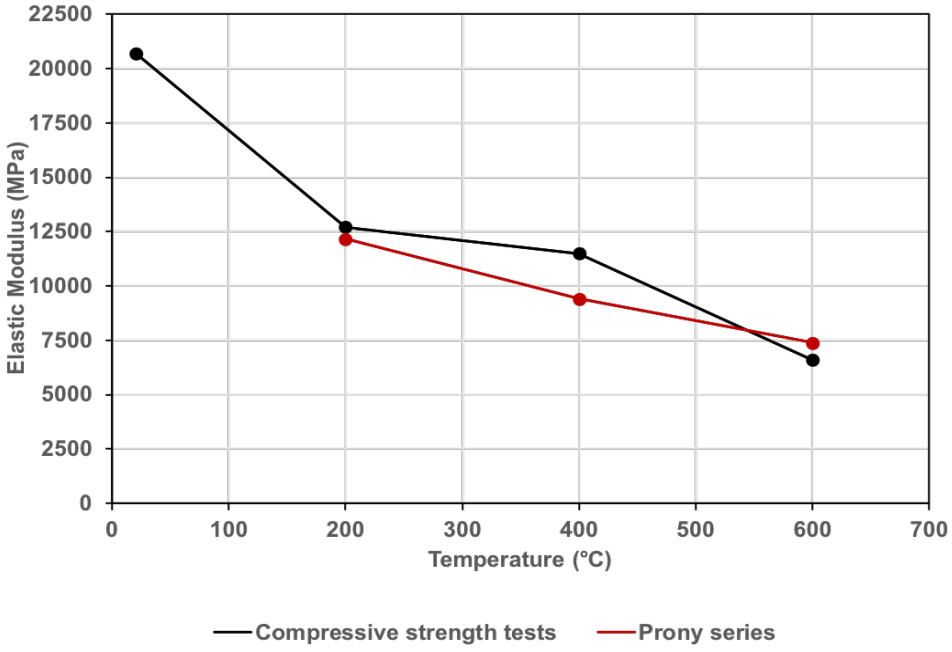

Fig. 5.39 Comparison of instantaneous elastic moduli between compressive strength tests and Prony series

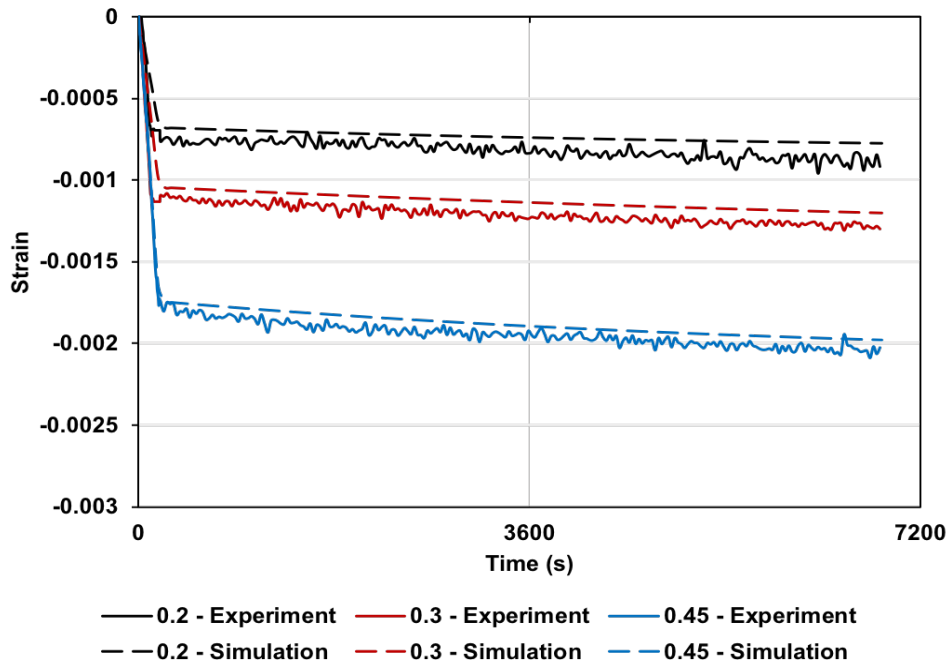

Fig. 5.40 Comparison of time-dependent creeps between experimental data and simulation results at 200 °C, with different load levels

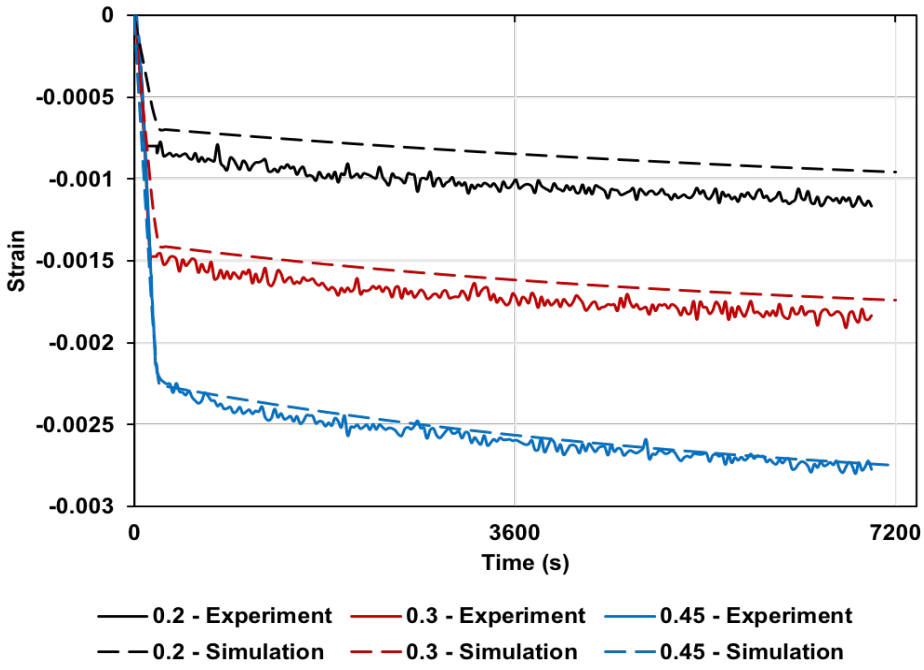

Fig. 5.41 Comparison of time-dependent creeps between experimental data and simulation results at 400 °C, with different load levels

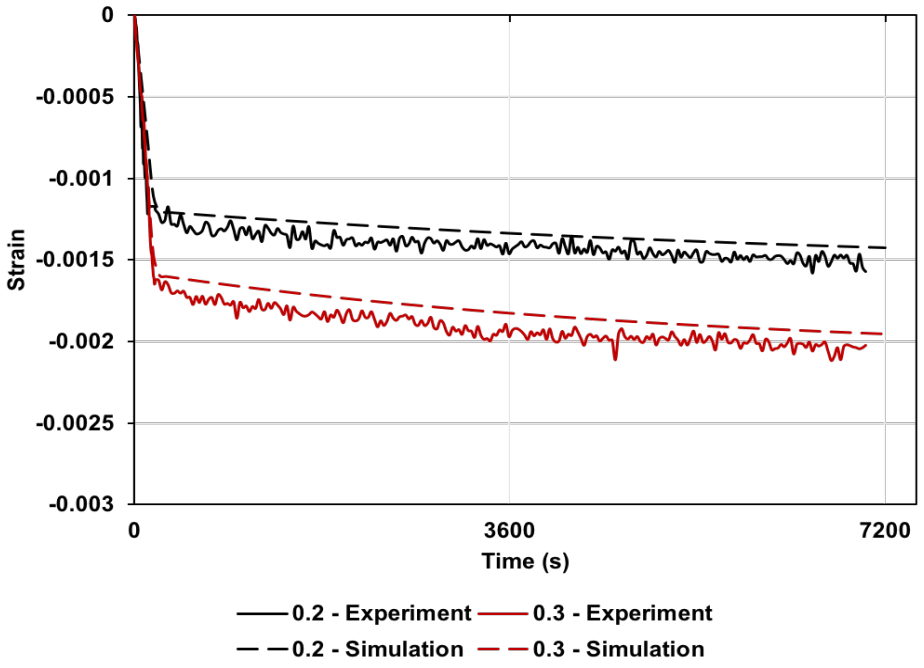

Fig. 5.42 Comparison of time-dependent creeps between experimental data and simulation results at 600 °C, with different load levels

The experimental data includes the initial instantaneous stress-related strain during loading. Figure 5.40 - 5.42 show that the simulation results give good agreement with the experimental data without consideration of the unloading process.

Prony parameters at different load levels

The time dependent creep curves at different temperatures and load levels are shown in Fig. 5.43. The constants for different temperatures and load levels are shown in Table 5.2. The constants are compared with the results in the previous section. The curve fitting is based on 3-term Prony series.

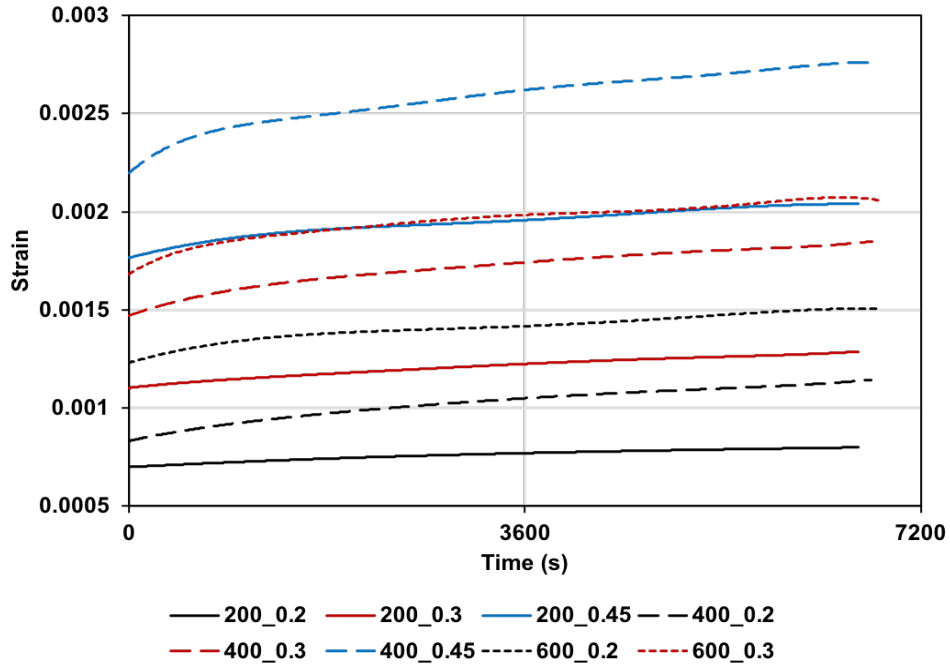

Fig. 5.43 Experimental time-dependent creep data at different temperatures and load levels

Table 5.2 Comparison of Prony parameters with different temperatures and load levels

θ	σ	$D_g \times 10^{-5}$	$D_j \times 10^{-5}$			τ_j			$E_e \times 10^3$	$E_i \times 10^3$			ρ_i		
			D_1	D_2	D_3	τ_1	τ_2	τ_3		E_1	E_2	E_3	ρ_1	ρ_2	ρ_3
200	0.2	7.68	0.39	0.49	0.53	4512	4493	4483	10.99	2.02	$9.64\text{x}10^{-4}$	$1.17\text{x}10^{-35}$	5320	4506	4488
200	0.3	8.11	0.67	0.66	0.65	6282	6294	6315	9.92	2.41	$8.57\text{x}10^{-6}$	$5.21\text{x}10^{-4}$	7826	6307	6288
200	0.45	8.75	0.51	0.51	0.50	4376	4374	4384	9.74	1.69	$2.99\text{x}10^{-4}$	$4.54\text{x}10^{-4}$	5139	4381	4375
200	avg	8.19	0.54	0.54	0.54	5009	5001	5006	10.2	2.01	$2.56\text{x}10^{-4}$	$7.41\text{x}10^{-6}$	5993	5008	5003
400	0.2	9.44	1.7	0.02	2.56	5675	6416	5328	7.29	3.28	$8.04\text{x}10^{-3}$	0.02	7975	7975	5520
400	0.3	10.97	0.94	0.95	0.96	3452	3451	3449	7.24	1.88	$3.56\text{x}10^{-4}$	$1.12\text{x}10^{-5}$	4347	3452	3450
400	0.45	11.10	0.91	0.91	0.92	3661	3658	3652	7.23	1.78	$1.52\text{x}10^{-4}$	$9.57\text{x}10^{-7}$	4558	3660	3655
400	avg	10.44	1.19	0.00	2.02	2928	4742	4506	7.32	1.89	$4.44\text{x}10^{-4}$	0.36	5507	4743	3133
600	0.2	13.94	1.1	1.1	1.1	4629	4360	4628	5.80	1.37	$7.61\text{x}10^{-6}$	$4.53\text{x}10^{-6}$	5724	4630	4629
600	0.3	12.70	0.85	0.87	0.86	2780	2772	2777	6.55	1.33	$5.39\text{x}10^{-4}$	0	3341	2779	2775
600	avg	13.32	1.03	0.89	0.93	3607	3669	3253	6.19	1.26	$3.78*10^{-3}$	0.06	4305	3639	3335

θ [°C] and σ [MPa] are the applied temperature and the applied load, respectively. D_g [1/MPa], D_j [1/MPa] and τ_j [s] are the instantaneous elastic compliance, the transient retardation strength, and the retardation time in the Prony series. E_e [MPa], E_i [MPa] and ρ_i [s] are the equilibrium modulus, the relaxation strength, and the relaxation time, respectively.

The corresponding creep compliance functions (D(t)) are plotted in Fig. 5.44. The relaxation modulus functions (E(t)) are shown in Fig. 5.45.

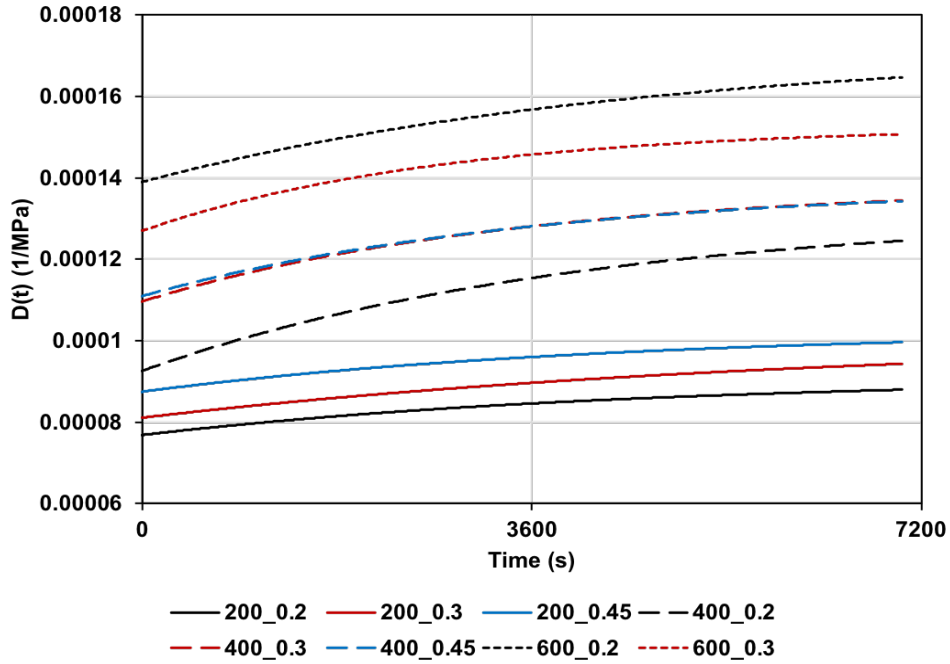

Fig. 5.44 Time-dependent creep compliance functions at different temperatures and load levels

Free thermal strain with Prony series

To model time-dependent creep, the viscoelastic material is used in the finite element analysis. However, the viscoelastic material is not temperature-dependent in ABAQUS. For the time-dependent elastic material, the instantaneous elastic modulus is defined at each temperature and it changes linearly with increasing temperatures. Also, the thermal coefficient at each temperature is defined and it changes linearly with increasing temperatures. For the viscoelastic material, the elastic modulus is temperature independent, i.e. a single value is used for the analysis. In addition, the thermal coefficient is a constant at different temperatures.

As discussed before, the free thermal strain is not sensitive to the thermal coefficient. How-

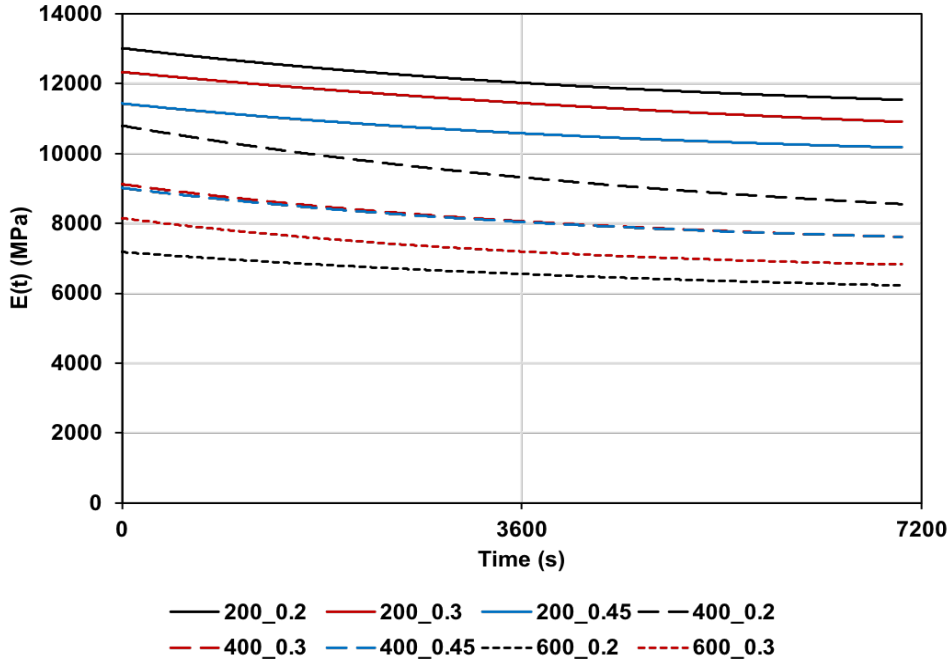

Fig. 5.45 Time-dependent relaxation modulus functions at different temperatures and load levels

ever, the influence of elastic modulus is discussed here. The differences between elastic moduli at different chamber temperatures between elastic material and viscoelastic material are shown in Fig. 5.46. The solid lines show the elastic moduli for the elastic material. These values are measured in the compressive strength tests. The elastic modulus changes linearly between the instantaneous elastic moduli at the ambient temperature and the reference chambergasmperature. The dashed lines show time dependent elastic moduli at the corresponding temperatures predicted by Prony series.

For simulating free thermal strain, the heating rate is set to 2 °C/min. A comparison between performances of the elastic material model and viscoelastic material model is made. The specimen is heated to a reference temperature without restraints. For both models, the thermal coefficient is a constant. In the elastic material model, the instantaneous elastic modulus is defined at each temperature. In the viscoelastic material model, the long term elastic modulus is defined. The instantaneous elastic modulus is dependent on Eq. 5.19 at

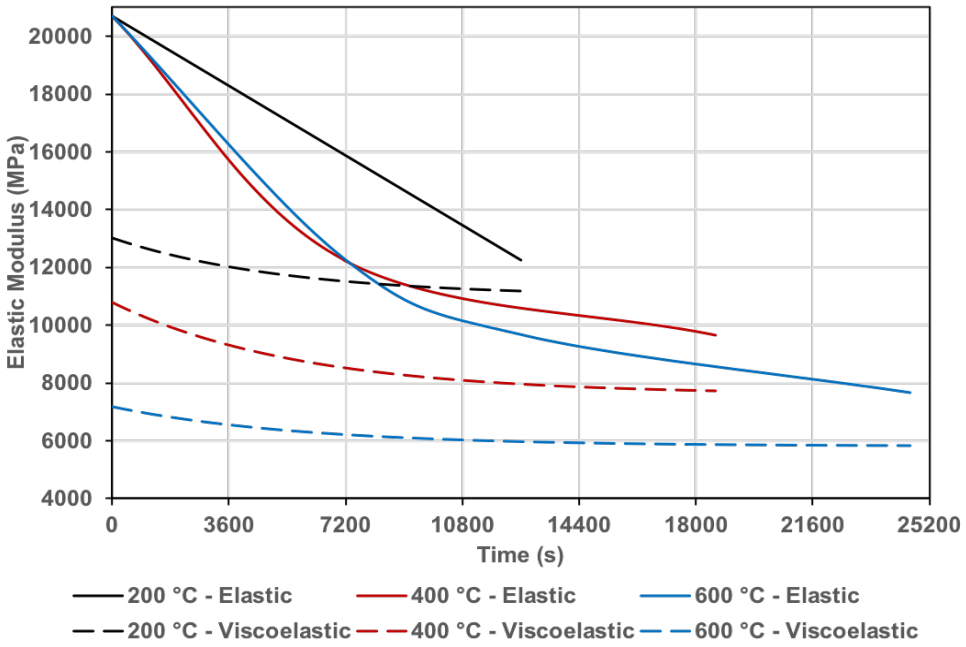

Fig. 5.46 Differences of instantaneous elastic moduli against time between the elastic material and the viscoelastic material, at the heat rate of 2 °C/min

t = 0. The instantaneous elastic modulus used in the elastic material model is same as the viscoelastic material model. Comparison of free thermal strains is shown in Fig. 5.47. Solid lines and dashed lines represent free thermal strains based on the elastic material models and the viscoelastic material model, respectively. Dotted lines represent the experimental results at elevated temperatures. It can be seen that the responses for two models is similar. The differences of elastic moduli between the elastic material model and the viscoelastic model make no influence on free thermal strain simulations.

However, the heating rate is set to 2 °C/min in experiments. For higher heating rate, the influence of elastic modulus is discussed. The free thermal strains are compared between the elastic material model and the viscoelastic material model at the heating rate of 10 °C/min. The differences of instantaneous elastic moduli at each temperature are shown in Fig. 5.48. Figure 5.49 shows the comparison of free thermal strains. The differences of elastic moduli of two material models make no influence on the free thermal strain results with constant

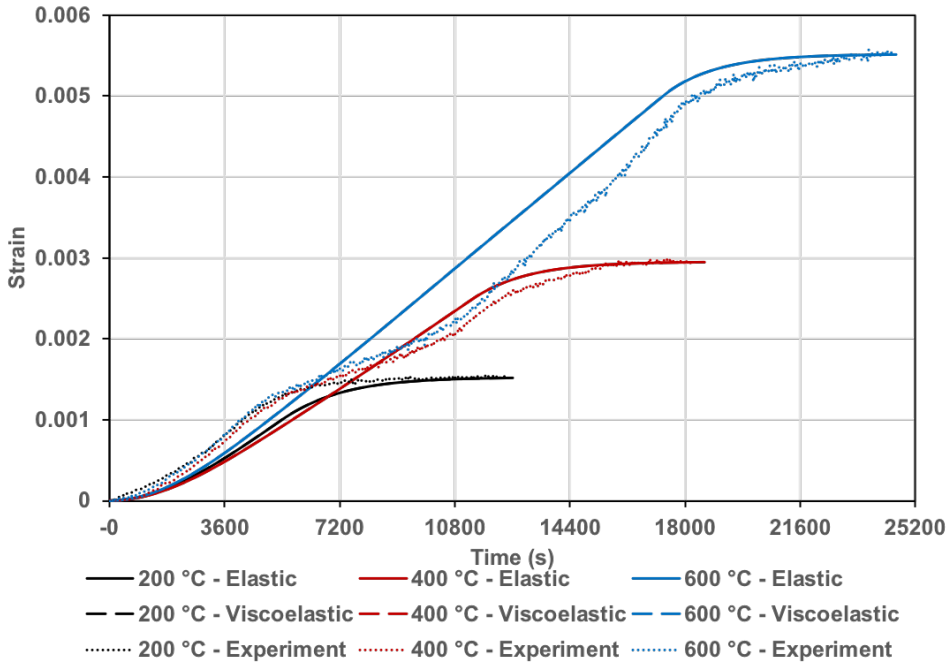

Fig. 5.47 Comparison of free thermal strains between elastic material models and viscoelastic material models at elevated temperatures, at the heat rate of 2 °C/min

thermal coefficient even at the heating rate of 10 °C/min. This is implies that inclusion of viscoelasticity does not alter the free thermal expansion response. The reason perhaps is that differential thermal expansion due to the thermal gradient has a relatively smaller influence on strain.

The difference between elastic material model and the viscoelastic material model is the value of thermal coefficient. For the viscoelastic material model, the thermal coefficient is a constant at different temperatures. On the contrary, thermal coefficients are defined at each temperature and change linearly between each temperature. However, the free thermal strain is not sensitive to the thermal coefficient from the previous analysis. To simplify the simulation, the viscoelastic material model can be used in free thermal strain simulation as well.

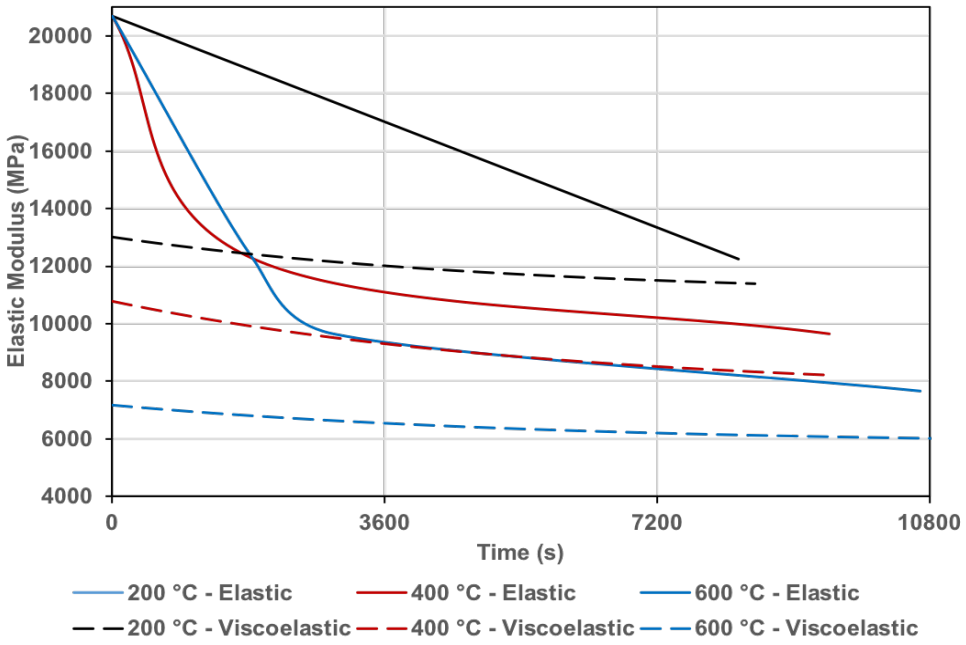

Fig. 5.48 Differences of instantaneous elastic moduli against time between the elastic material and the viscoelastic material, at the heat rate of 2 °C/min

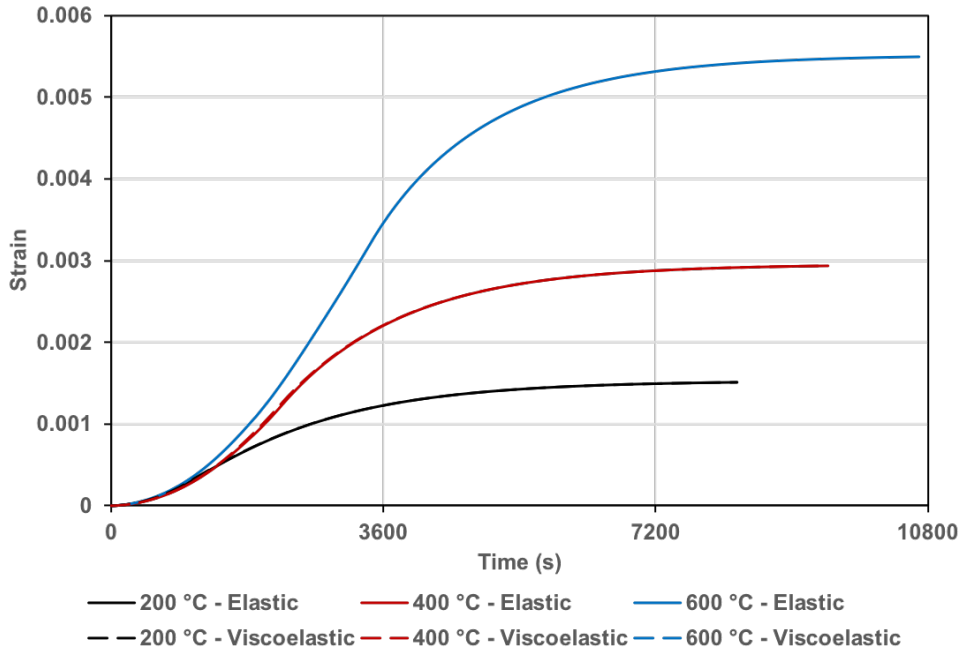

Fig. 5.49 Comparison of free thermal strains between elastic material models and viscoelastic material models at elevated temperatures, at the heat rate of 10 °C/min

5.7 Summary

This chapter discussed the experimental results of the compressive strength tests, stress-strain relations tests, and heating-then-loading tests. Also, simulations were conducted to model free thermal strain and time-dependent creep.

For the heating process, the temperature is not uniform in the oven. The temperature at the higher recording position was found to be higher. It is likely that the use of fire resistant sealant affects the concrete surface temperatures. The temperature data of concrete surface is slightly lower than the real temperature. Although, the oven applies temperatures up to 600 °C. The experimental data shows that the oven only applies temperatures up to 590 °C in real tests. In general, the temperature data is in good agreement with the simulation results of Chapter 3.

For the experimental data of free thermal strain, Eurocode 2 has a higher prediction of thermal expansion. It is hard to say if the free thermal strain suggested by Eurocode 2 is correct or not as thermal expansion is affected by many factors. However, the thermal coefficient is modified with the experimental data and is used in the following simulations.

There is a linear time-dependent creep under stabilized load and temperature. The method of modelling linear creep is via the use of a viscoelastic material. The parameters are based on the experimental data. The method to obtain the parameters was discussed. The simulations show that the simulation results fit the experimental curves well. The viscoelastic material with Prony series provides a simple way to model time-dependent creep.

6

Loading-then-heating (LTH) experiments and analysis

6.1 Introduction

This chapter presents the experimental data of the loading-then-heating (LTH) tests. The temperature data recorded in the LTH tests is discussed. The instantaneous stress related strain at ambient temperature and the total strain during transient heating are measured. Also, the instantaneous stress-related strain at elevated temperatures, the time dependent creep, and the free thermal strain were measured as indicated in Chapter 5. Different strain components during heating under load are compared and discussed in this chapter. LITS comprises of the transient creep, the time-dependent creep and the stress-related strain due to the change of the instantaneous elastic modulus. Different LITS components are compared and discussed in this chapter. Also, the experimental data is compared with different constitutive equations.

6.2 Temperature

For the LTH tests, the specimens were heated to the target temperatures of 200 °C, 400 °C and 600 °C, respectively. Figure 6.1 compares concrete surface temperatures between the

LTH tests and the HTL tests. For evaluating different strain components under different loads and temperatures, the HTL tests chose the same heating rate with the LTH tests. Comparing the temperature data from two series of tests, the temperature curves are similar.Therefore, the free thermal strain achieved in the HTL tests are used for the LITS calculations.

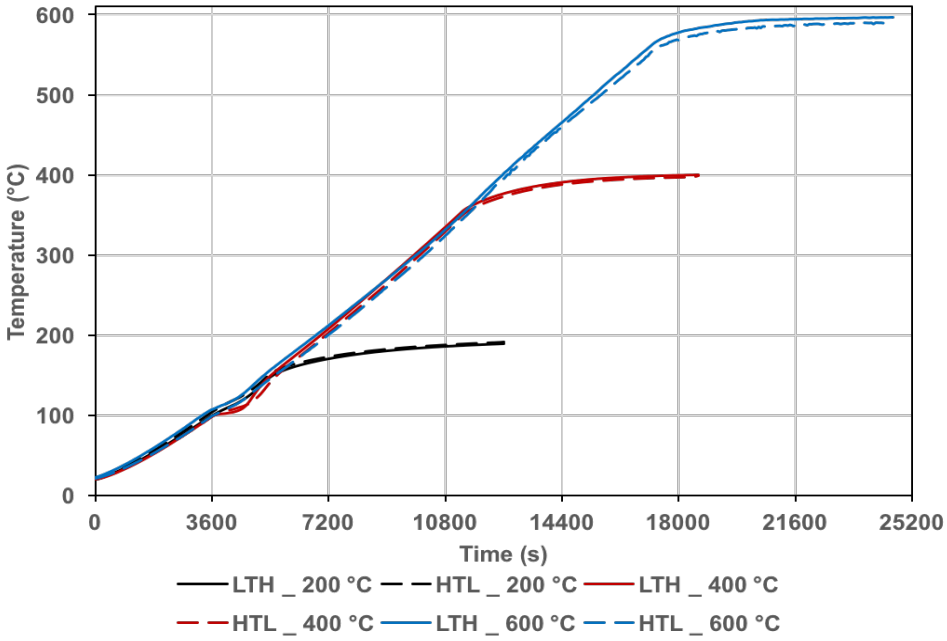

Fig. 6.1 Comparison of concrete surface temperatures between LTH tests and HTL tests

6.3 Loading-then-heating (LTH) tests

The procedure of the LTH tests was described in Chapter 4. A concrete specimen was loaded at the beginning of the test. Then, the specimen was heated to the reference temperature at the heating rate of 2 °C/min. After the chamber temperature reached the test temperature, the temperature and load were maintained constant for 2 hrs. The load was removed at the end of the test. The typical strain against time curve is shown in Fig. 6.2. The strain dropped (becomes compressive) during the application of the compressive load. The instantaneous stress-related strain at ambient temperature was measured immediately. Then, the strain curve rose due to the thermal expansion during heating. However, the expansion was restrained by

the load during heating. This load resulted in the transient strain. The strain again dropped due to the transient strain. The total strain was measured before unloading. The compressive strain decreased with unloading at the end of the test.

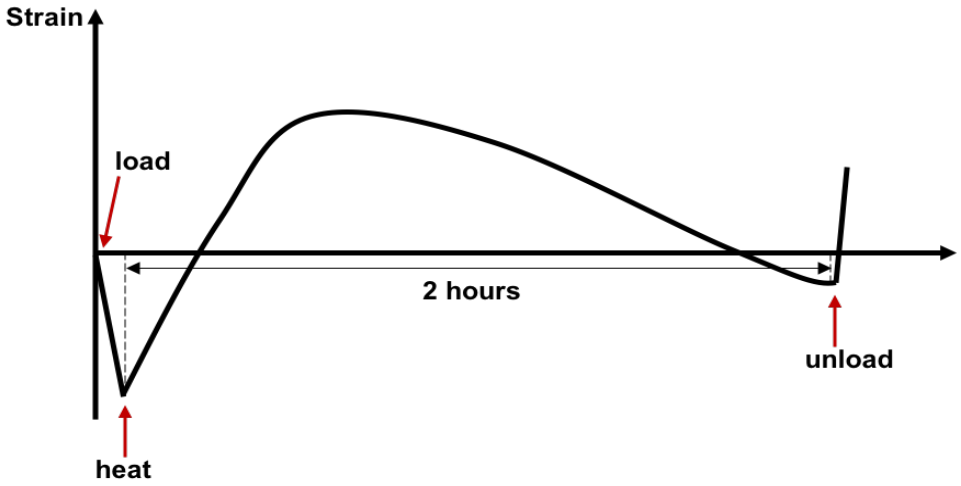

Fig. 6.2 The typical strain against time curve in LTH test

6.3.1 Instantaneous stress-related strain

The specimen was loaded at the beginning of the test. The instantaneous stress-related strain was measured immediately after loading. The instantaneous stress-related strain in LTH tests was measured at ambient temperature.

The mean instantaneous stress-related strains at different load levels are shown in Fig. 6.3. The dashed line was obtained from linear regression. The mean instantaneous stress-related modulus was evaluated as 19000 MPa. Similar instantaneous modulus at ambient temperature was measured in the compressive strength tests.

The measured mean instantaneous stress-related strains for different load levels at ambient temperature are compared with the instantaneous elastic strains at elevated temperatures from the HTL tests and are shown in Fig. 6.4. Moreover, it is apparent that the instantaneous

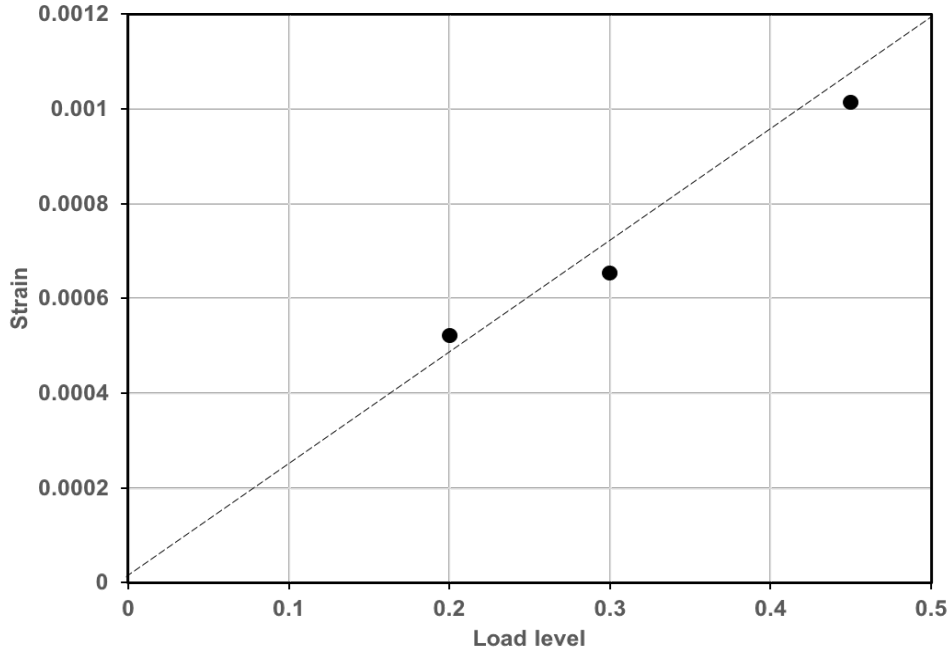

Fig. 6.3 Instantaneous stress-related strain at different load levels measured in the LTH tests

strains increased with temperature due to the decrease in the instantaneous elastic modulus. The load was kept constant during the test. Therefore, considering the results of the last chapter, it is fair to assume that the instantaneous stress-related strains would have increased with temperatures.

Figure 6.5 shows the mean ratio of the instantaneous stress-related strain at ambient temperature to the instantaneous stress-related strain at elevated temperatures. The ratio was in the range of 40% to 60% for temperatures over 400 °C and load levels over 30 %. The instantaneous stress-related strain at elevated temperatures was almost two times greater than the strain at ambient temperature.

6.3.2 Load induced thermal strain

The specimens were heated under constant load during the LTH tests. Figures 6.6 - 6.8 show the mean axial strain response (obtained from two specimens in each case) during the

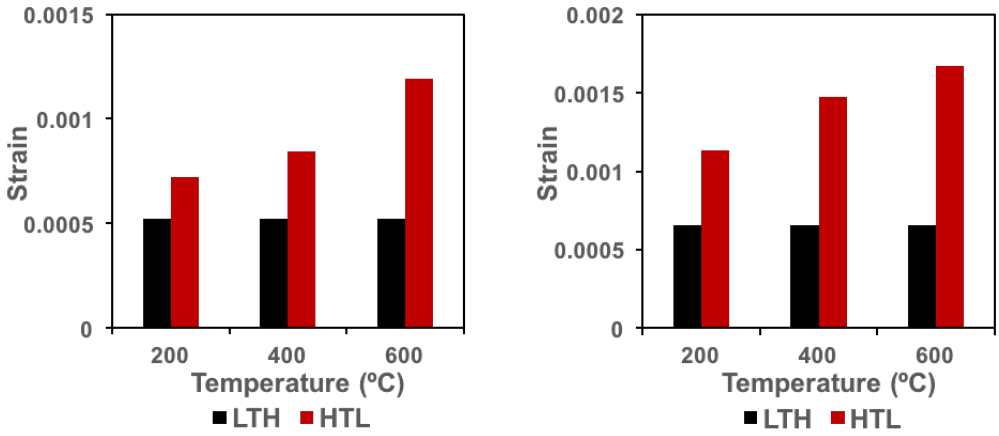

(a) Load level: 0.2

(b) Load level: 0.3

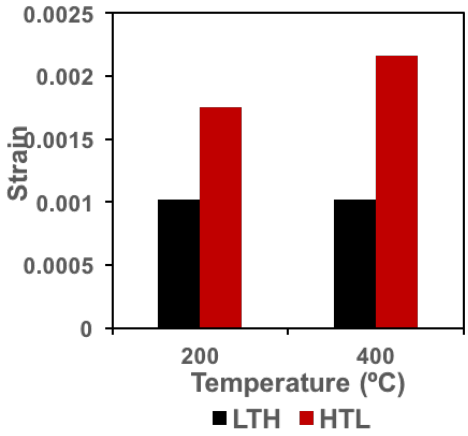

(c) Load level: 0.45

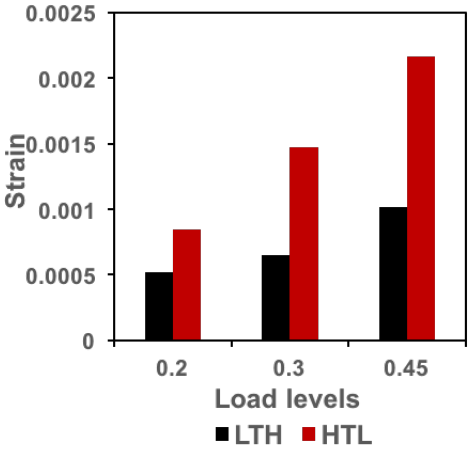

(d) Temperature: 200 °C

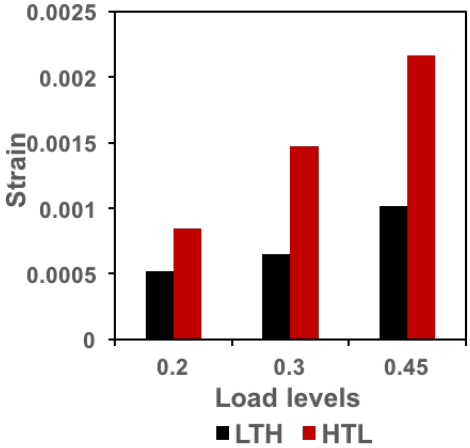

(e) Temperature: 400 °C

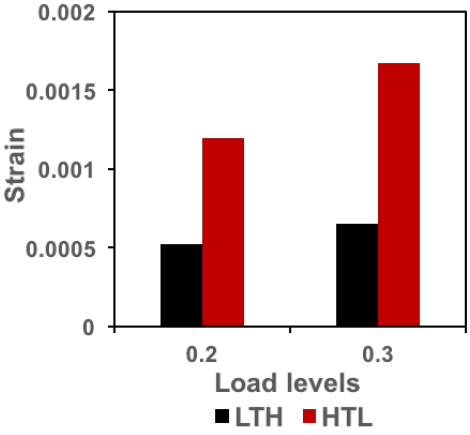

(f) Temperature: 600 °C

Fig. 6.4 Comparison of instantaneous stress-related strain at ambient temperature and instantaneous stress-related strain at elevated temperature for different loading levels and heating temperatures

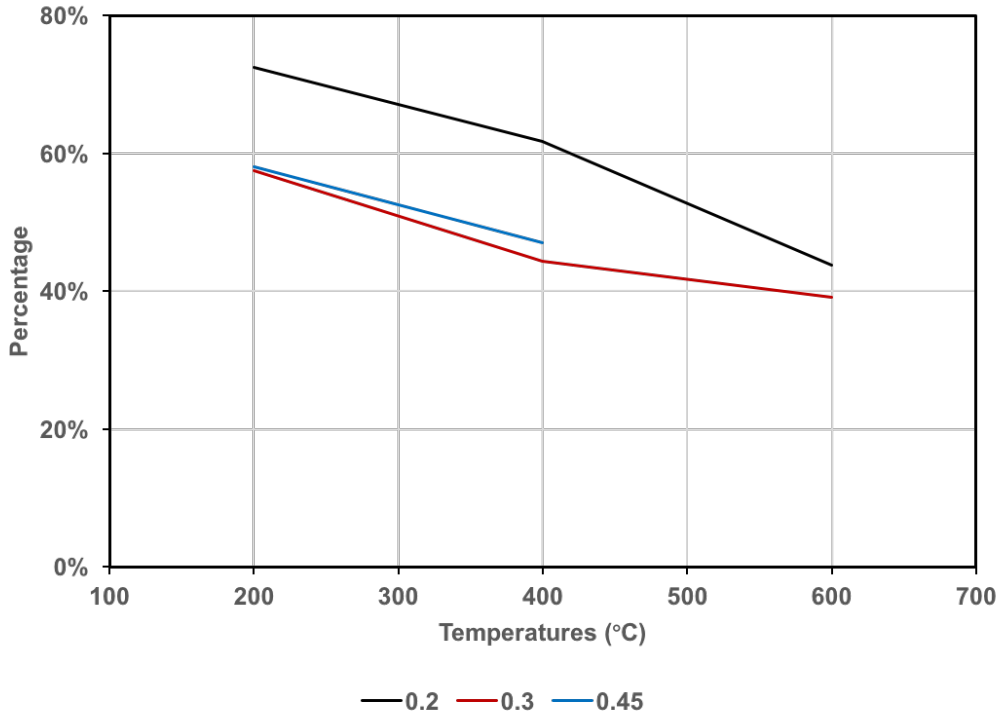

(a)

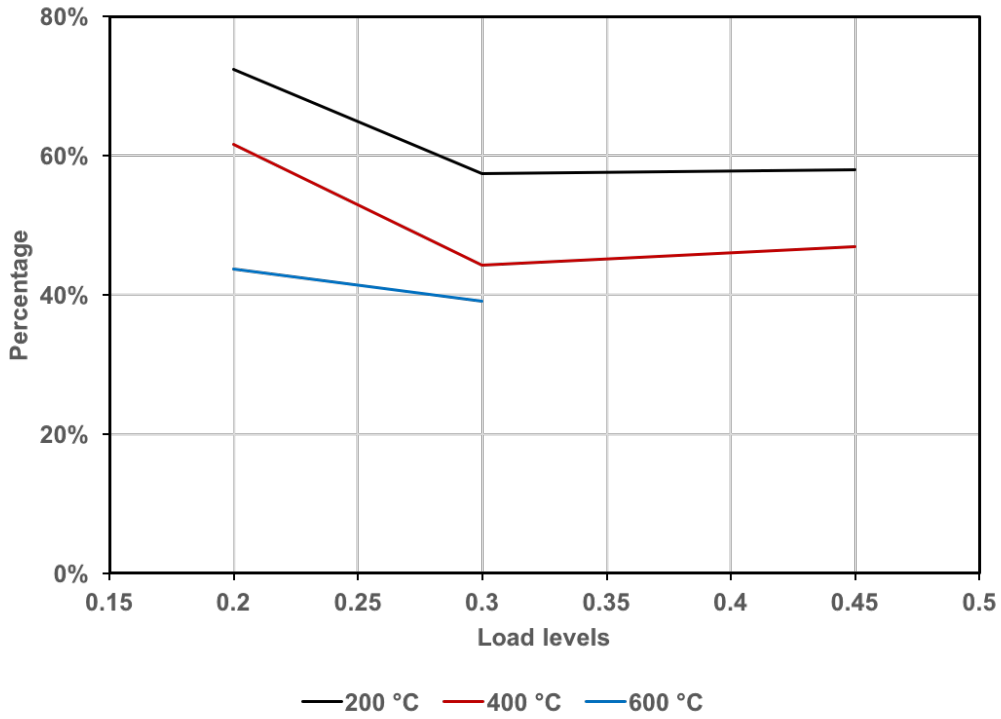

(b)

Fig. 6.5 The mean ratio of the instantaneous stress-related strain at ambient temperature to the instantaneous stress-related strain at elevated temperatures

heating phase on the outer surface of the specimens. The strain response is measured from the initiation of heating, i.e. after the application of the load. It can be seen that the strain increases at the beginning of heating phase due to thermal expansion. Thereafter, the thermal expansion is counteracted by the load. The influence of load causes compressive strains. In the last chapter, it was seen that the instantaneous elastic modulus decreased with increasing temperatures. The difference in elastic moduli results in extra stress-related strain. Also, the time-dependent creep will develop under sustained load. These three factors cause the observed compressive strain response.

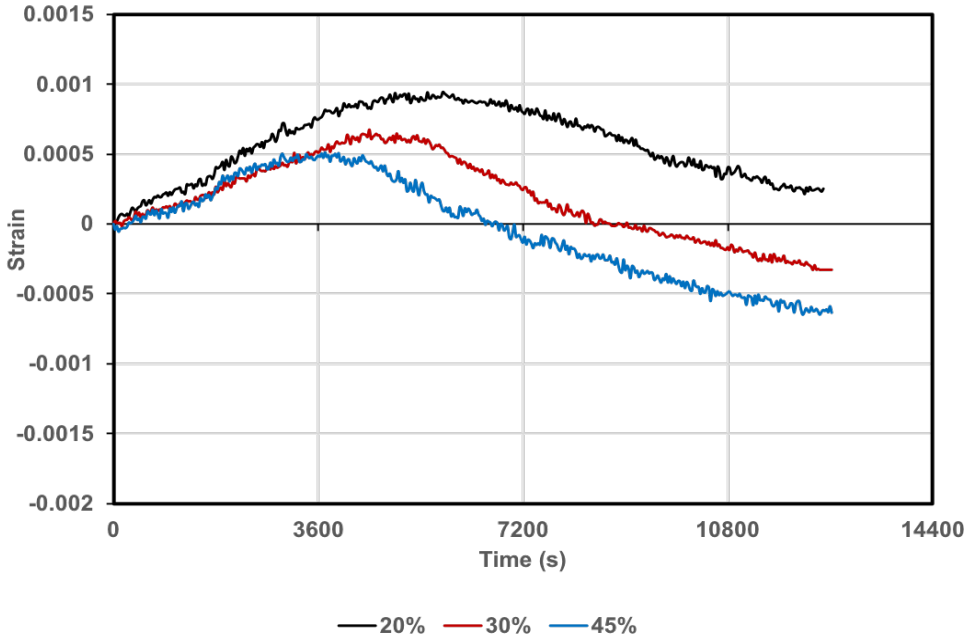

Fig. 6.6 Total strains of LTH tests during heating at 200 °C after initial loading for different loading levels

It is interesting to note that the post-loading strain fluctuates during the heating tests at 600 °C (Fig. 6.8). It can be seen from Fig. 6.8 that the strain increases and then decreases, the same as in Figs. 6.6 and 6.7. Thereafter it starts to increase again at around 11000 seconds. Examining the temperature data of the LTH tests (Fig. 6.1), the temperature of concrete surface reached 400 °C at around 11000 seconds. Experiments conducted in Chapter 5 showed that starting from 400 °C, there is an increase of thermal expansion and reduction

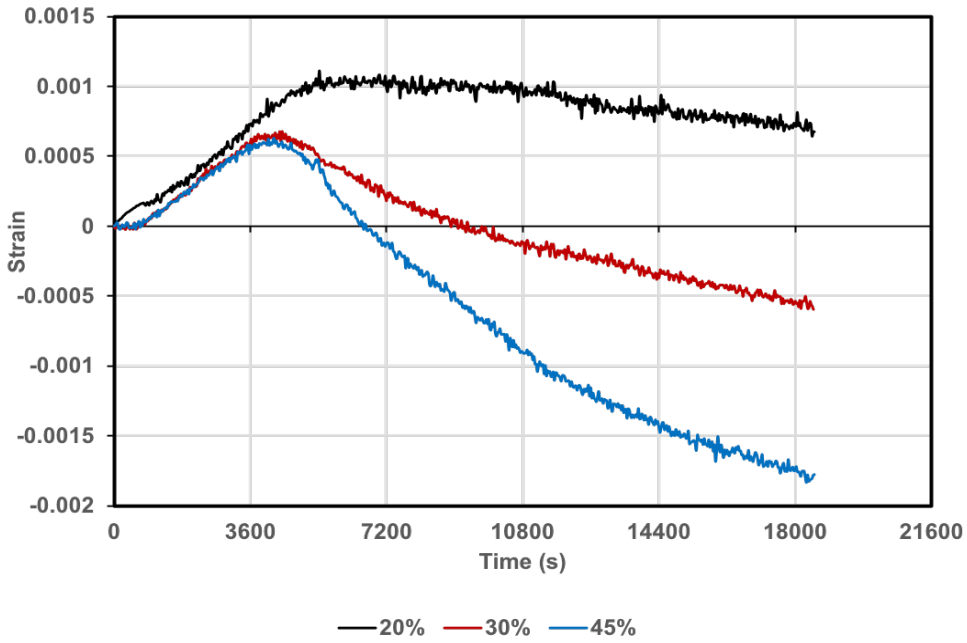

Fig. 6.7 Total strains of LTH tests during heating at 400 °C after initial loading for different loading levels

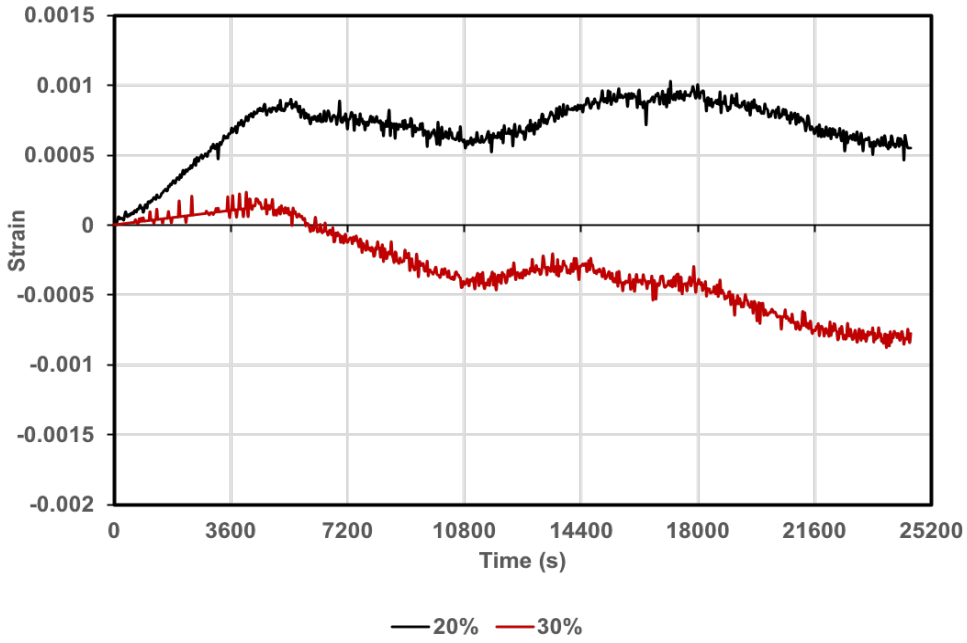

Fig. 6.8 Total strains of LTH tests during heating at 600 °C after initial loading for different loading levels

in the rate of elastic modulus decrease (Fig. 6.9). These reasons explain the second rise in the strain curves. Also, the total strain at around 400 °C in Fig. 6.8 is similar to strain at the end of heating test of 400 °C (Fig. 6.7).

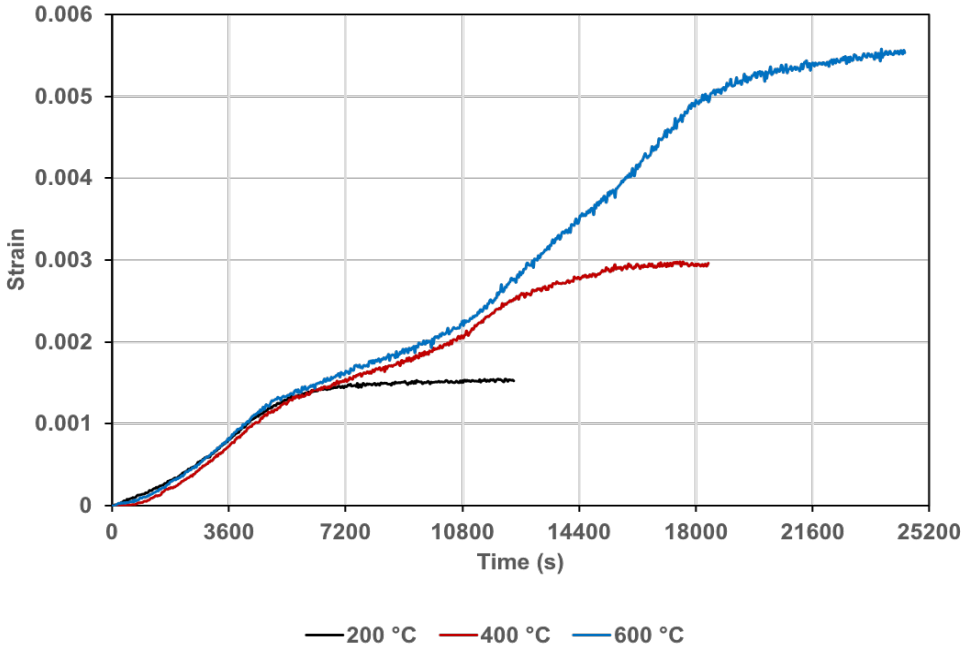

Fig. 6.9 Comparison of free thermal strains at different temperatures

LITS is represented as the difference of between the free thermal strain of an unloaded concrete specimen and the strain measured under load after subtracting the initial elastic strain. LITS is calculated as

$$LITS = \varepsilon_{tot} - \varepsilon_{th} - \varepsilon_{el} \tag{6.1}$$

where ε_{tot} is the total strain measured before unloading, ε_{th} is the free thermal strain (as measured in the HTL tests) and ε_{el} is the instantaneous elastic strain measured at ambient temperature.

Figure 6.10 illustrates the total strains of the LTH tests for different load levels subtracting the initial elastic strains. The total strain at a temperature was measured before unloading.

The total strain at 0% load level is the free thermal strain measured in the HTL tests. The differences between the total strain at 0% load level and the total strains at other load levels where the values of LITS at different load levels.

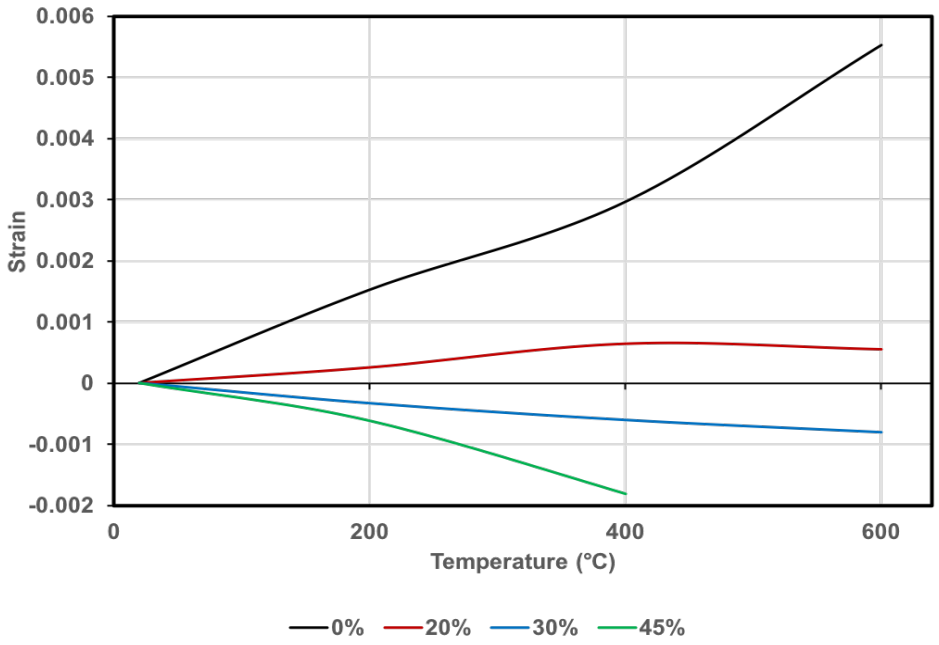

Fig. 6.10 Total strains of LTH tests during heating for different load levels, subtracting initial elastic strains

The values of LITS evaluated from Fig. 6.10 are shown in Fig. 6.11. As can be seen from Fig. 6.11, LITS varies nonlinearly with temperature. It can be observed from Fig. 6.11 that the slopes of LITS between the ambient temperature and 200 °C are larger than the slopes of LITS between 200 °C and 400 °C. Loss of moisture from concrete at around 180 °C is one possible cause for this. For temperatures above 400 °C, the magnitude of LITS had a considerable increase. The values of LITS are compared with other models in the following section.

Figure 6.12 shows LITS as a function of load level. Previously LITS has been linearly related to load levels. It has been shown through the experiments [11] that the LITS curve is more linear when the heating rate is slower and the specimen is pre-dried before the test.

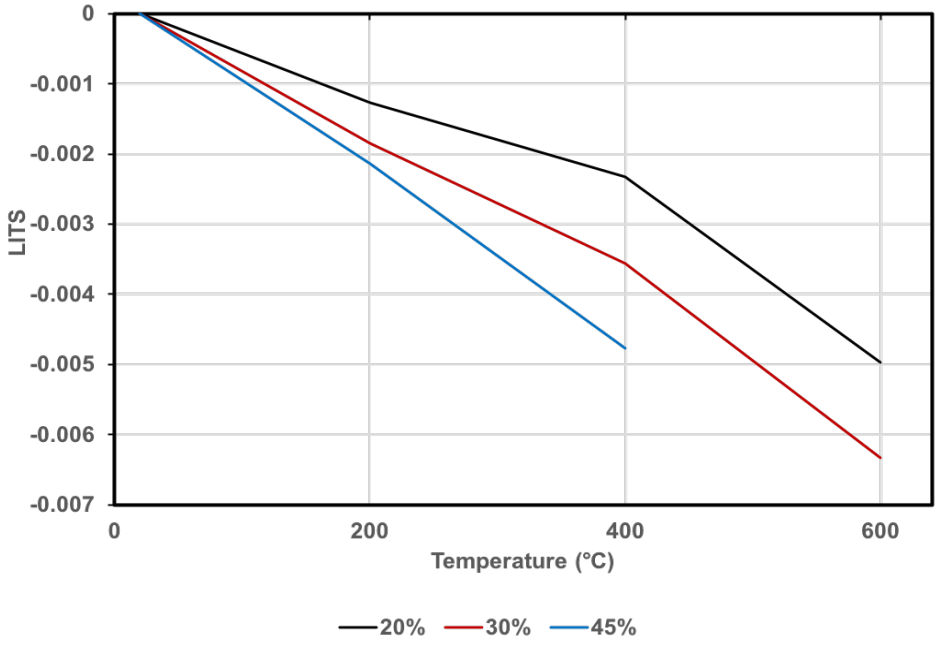

Fig. 6.11 Load induced thermal strain curves for different load levels

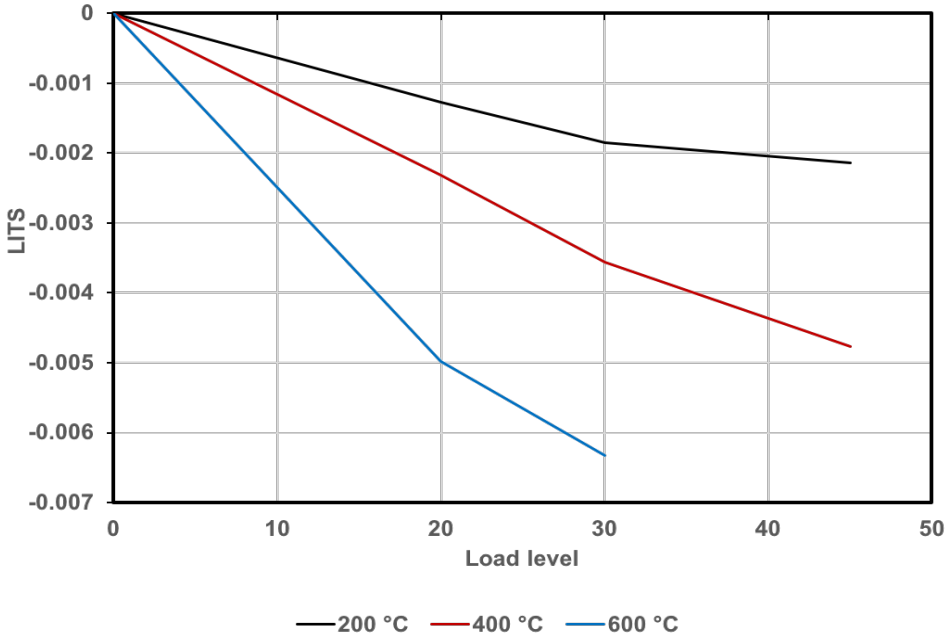

Fig. 6.12 Load induced thermal strain curves against load levels

Figure 6.13 illustrates different strain components at elevated temperatures. The main strain components under sustained load at elevated temperatures were free thermal strain (ε_{th}) and LITS. Comparing free thermal strain and LITS, the proportion of the initial stress-related strain (ε_{el}) is small. The magnitude of LITS is similar to free thermal strain. It is the largest strain component under higher load levels.

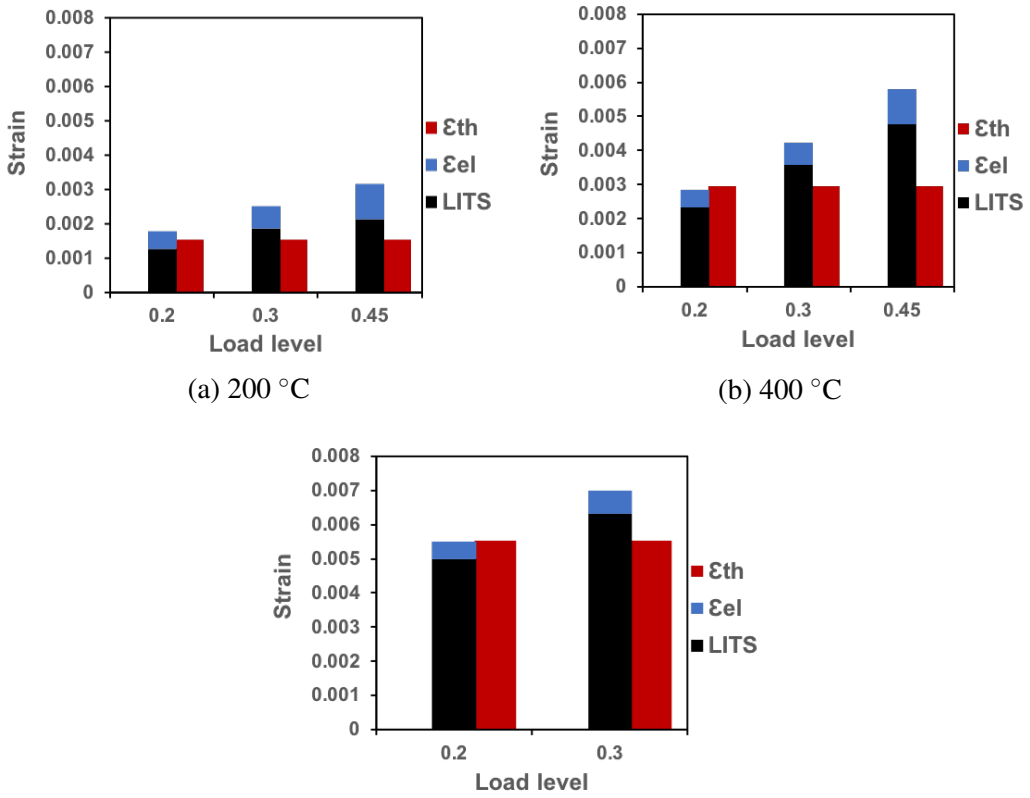

(a) 200 °C

(b) 400 °C

(c) 600 °C

Fig. 6.13 Comparison of different strain components at different temperatures

6.4 LITS components and models

6.4.1 LITS components

As discussed in Chapter 2, LITS includes the variations of the instantaneous stress-related strain due to the reduction of the instantaneous elastic modulus at elevated temperatures, the time-dependent creep, and the transient creep during first heating under load. LITS is given by

$$LITS = \Delta\varepsilon_{el,\theta} + \varepsilon_{cr} + \varepsilon_{tr} \tag{6.2}$$

where $\Delta\varepsilon_{el,\theta}$ represents the variation of the instantaneous stress-related strain, ε_{cr} is the time-dependent creep, and ε_{tr} is the transient creep.

The variations of the instantaneous stress-related strain were discussed in the previous section. The time-dependent creep was discussed in Chapter 5. Figures 6.14 - 6.16 illustrate different components of LITS at different load levels. It can be seen that transient creep is the largest component of LITS. Figure 6.17 compares the values of different LITS components at different temperatures. Time-dependent creep is the smallest component at all load levels and at all temperatures. It is, however, not negligible, particularly at higher load levels. Also, the transient strain developed during the heating phase in these LTH tests, increased with increasing temperatures. The transient creep remained constant when the temperature was constant. There was no extra instantaneous stress-related strain due to the change of the instantaneous elastic modulus. The time-dependent creep developed under the sustained load with time. In this research, the time-dependent creep was measured after 2 hrs. For the tests with longer heating time, the proportion of time-dependent creep increased.

6.4.2 Instantaneous unloading strain

As discussed earlier, LITS is evaluated by excluding the instantaneous stress-related strain at ambient temperature. However, the instantaneous unloading strain measured after unloading

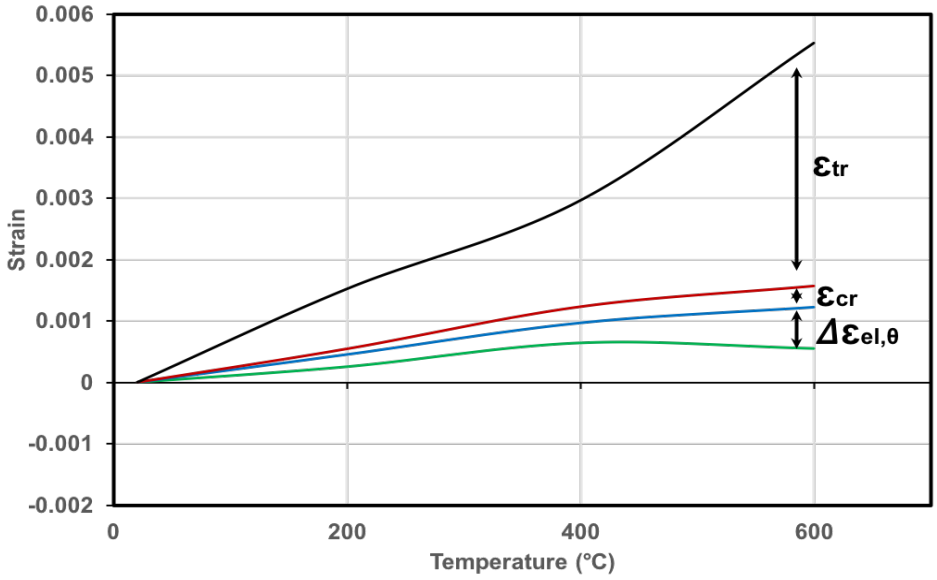

Fig. 6.14 Evaluation of LITS components for 20 % load level

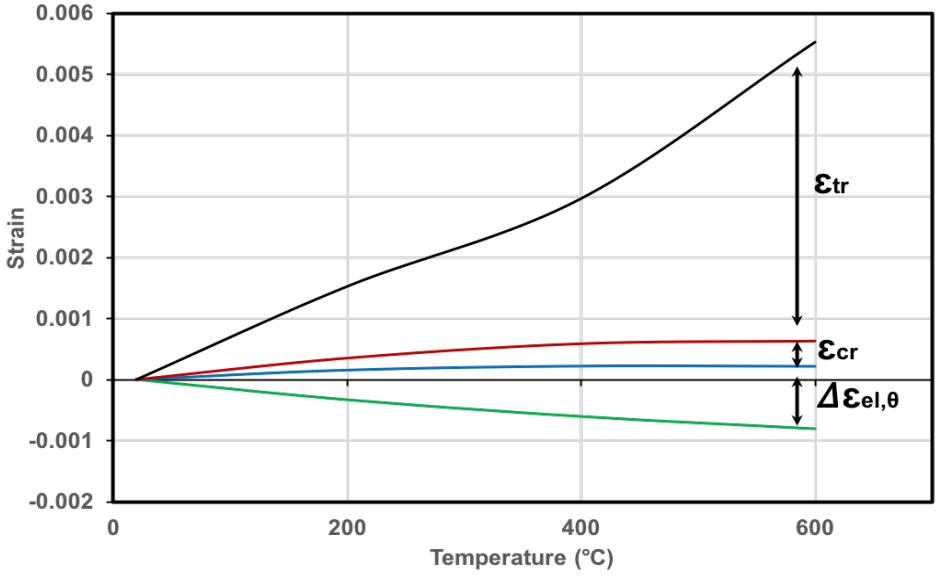

Fig. 6.15 Evaluation of LITS components for 30 % load level

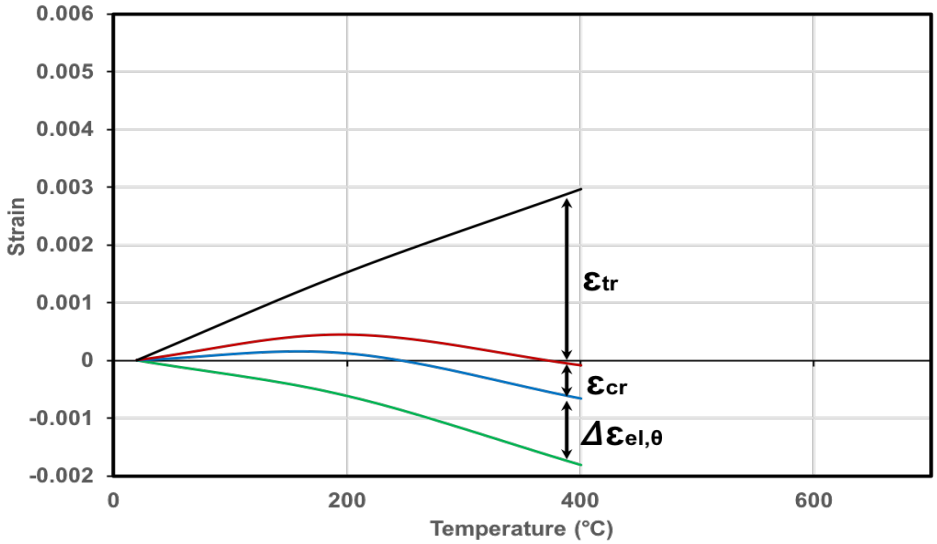

Fig. 6.16 Evaluation of LITS components for 45 % load level

is larger than the excluded value, which means LITS contains recoverable strain. The recoverable strain is calculated as the difference between the instantaneous stress-related strain at ambient temperature and the instantaneous unloading strain at elevated temperatures. The ratios of the recoverable strain to LITS are shown in Fig. 6.18. The ratios are in the range 5% to 15%.

6.4.3 Transient models

The models used to describe transient creep and transient strain were discussed in Chapter 2. The models were based on uniaxial loading. The experimental data were compared with the constitutive models.

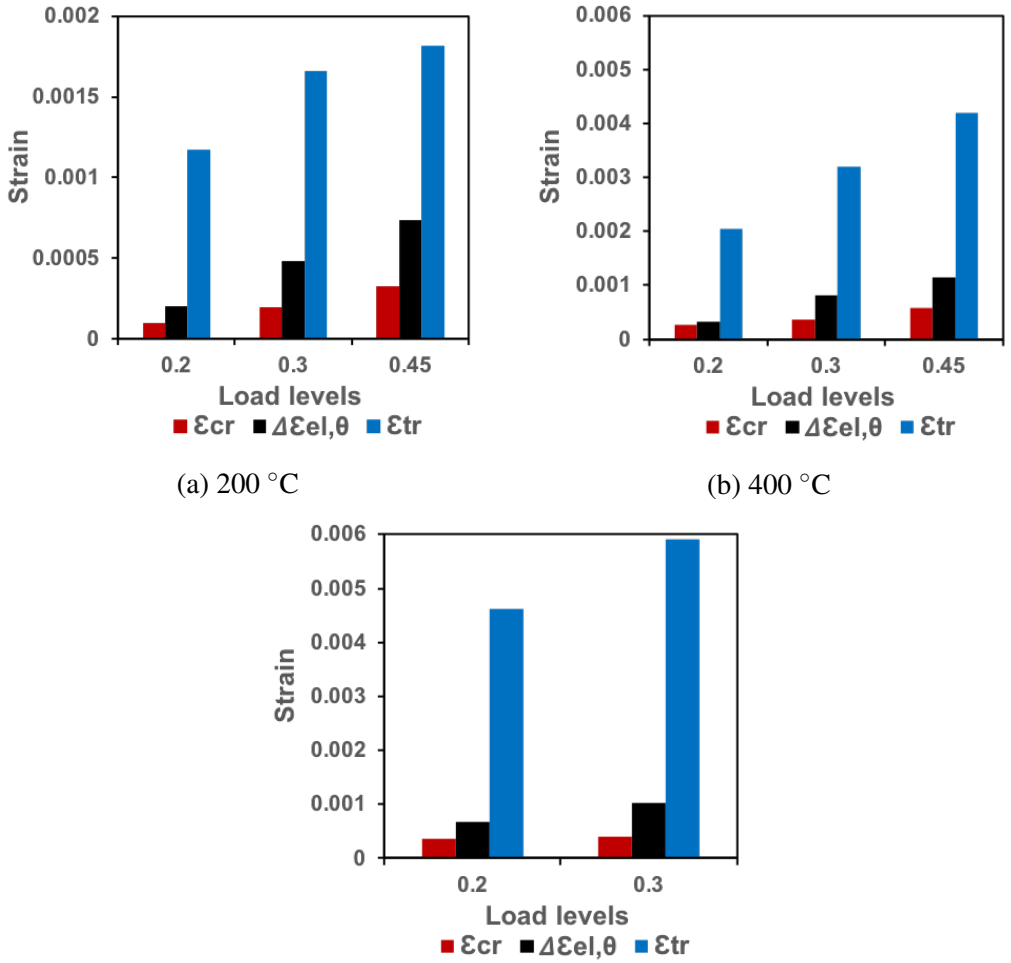

(a) 200 °C

(b) 400 °C

(c) 600 °C

Fig. 6.17 Comparison of different LITS components at different temperatures

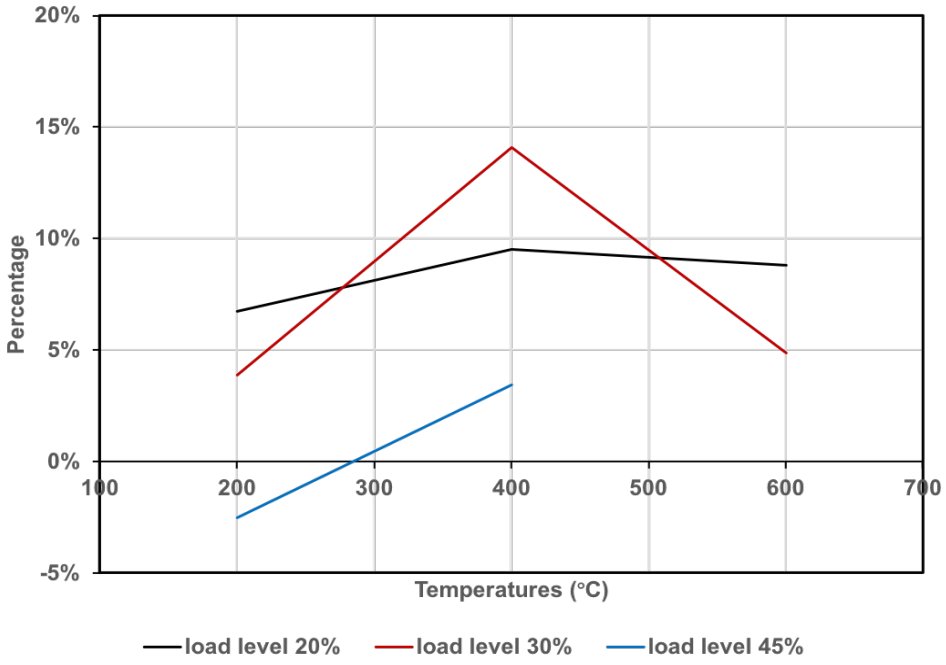

Fig. 6.18 Mean ratios of recoverable strain and LITS

Transient creep

Anderberg [10] generated the equation for the transient creep based on experimental data. The transient creep was calculated as

$$\varepsilon_{tr} = LITS - \Delta\varepsilon_{el,\theta} - \varepsilon_{cr} \tag{6.3}$$

By analyzing the experimental results, the transient creep was found to be approximately proportional to the load level and free thermal strain. The transient creep was represented as

$$\varepsilon_{tr} = k_2 \frac{\sigma}{f_c} \varepsilon_{th} \tag{6.4}$$

where σ/f_c is the load level and k_2 is the constant based on experimental data. Figure 6.19 illustrates the relationship of $\varepsilon_{tr}/(\sigma/f_c)$ and the free thermal strain from this study. The dashed line is the best fit line for the values at 200 °C and 400°C obtained from linear

regression. It can be seen that the relationship expresses by Eq. 6.4 is not entirely valid for higher temperatures. The estimated k_2 value from linear regression was 2.5. It has been agreed by Anderberg that the transient creep equation is not fit for temperatures above 550 °C.

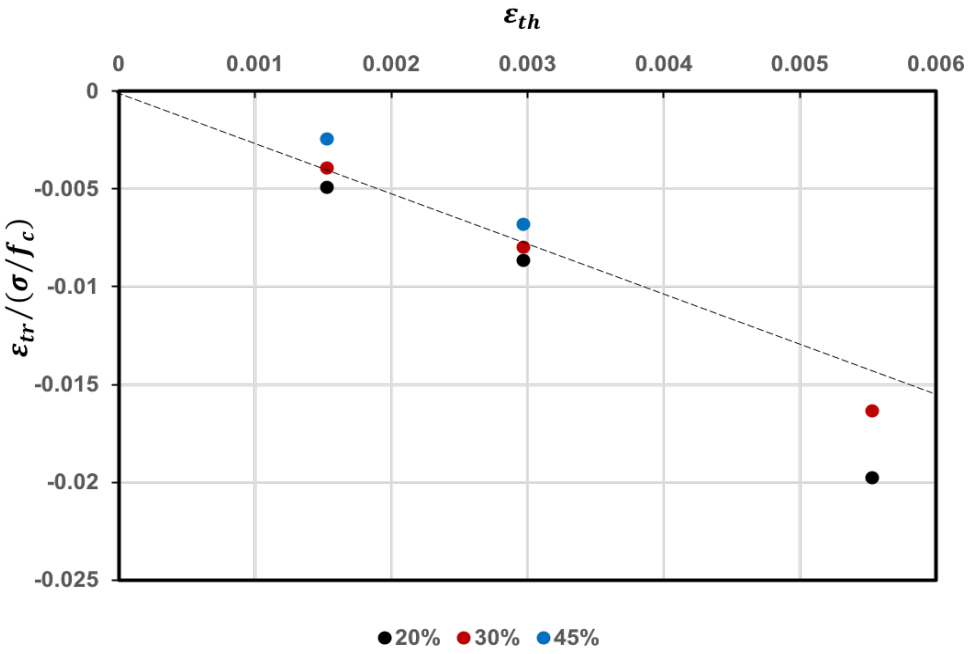

Fig. 6.19 Ratio of transient creep to load level against free thermal strain for different load levels

Nielsen [65] modified Anderberg's equation by assuming a linear relation with the temperature instead of the free thermal strain. The transient creep was represented as

$$\varepsilon_{tr} = \beta \frac{\sigma}{f_c}(\theta - 20) \tag{6.5}$$

where β is a coefficient based on experimental data. Figure 6.20 shows the relationship of $\varepsilon_{tr}/(\sigma/f_c)$ and the temperature. The dashed line was again obtained from linear regression. Similar to Anderberg's equation, β was assumed to be constant for temperatures under 400 °C. For simulating the curve above 400 °C, β varied with temperatures as LITS increased rapidly after 450 °C. It is clearly possible to develop a nonlinear empirical equation based on

the three temperatures considered in this study. However, to be really representative more transient strain data over 400 °C needs to be generated.

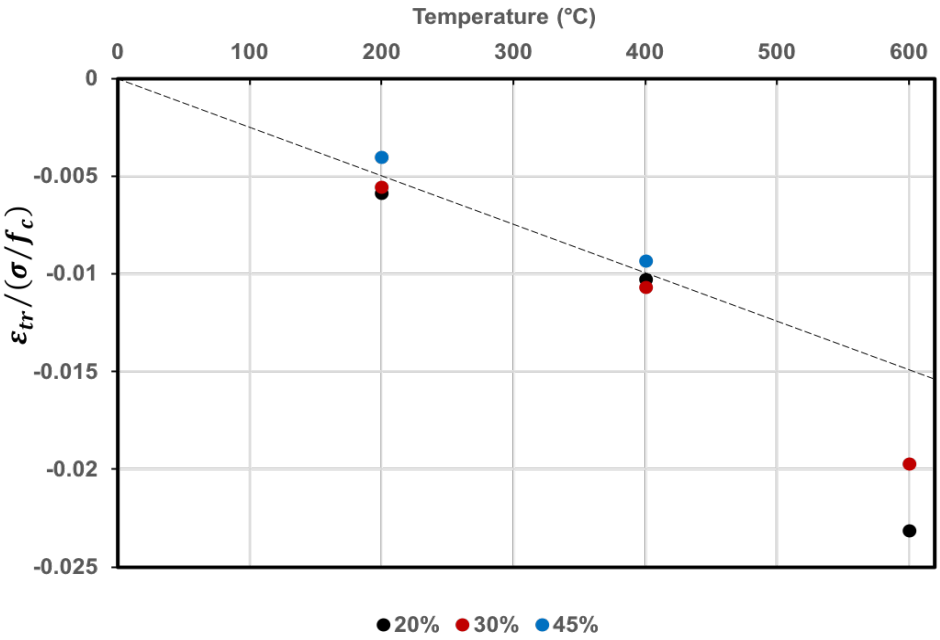

Fig. 6.20 Ratio of transient creep to load level against temperature for different load levels

Load Induced thermal strain

Terro [46] developed the LITS model for concrete with different types of aggregate up to 450 °C. LITS was considered as the linear function of load level. The value of LITS under 30 % load level was expressed as

$$LITS(\theta,0.3) = A_0 + A_1\theta + A_2\theta^2 + A_3\theta^3 + A_4\theta^4 \tag{6.6}$$

where LITS(θ,0.3) is calculated by parameters (A_0, A_1, A_2, A_3, A_4) = (-43.87, 2.73, 6.35x10^{-2}, -2.19x10^{-4}, 2.77x10^{-7}). LITS value at other load levels was evaluated as

$$LITS(\theta,\sigma/f_c) = LITS(\theta,0.3)(0.032 + 3.226\frac{\sigma}{f_c}) \tag{6.7}$$

Figure 6.21 shows a comparison between experimental data from this study and Terro's model. Comparing experimental data with the equation, it can be seen that the transient creep is smaller than that suggested by Terro.

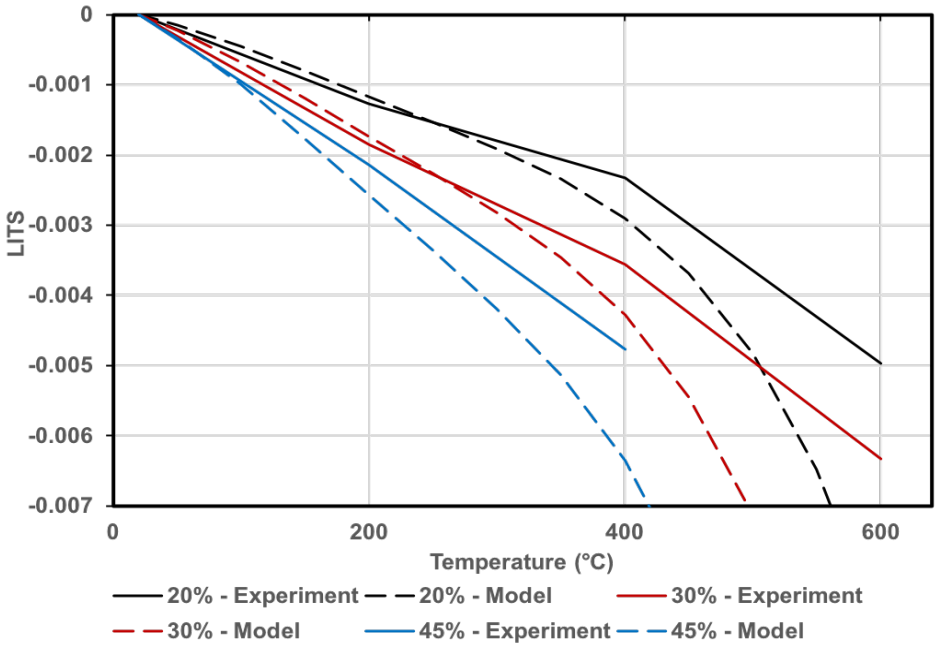

Fig. 6.21 Comparison of LITS between experimental data and Terro's constitutive model

6.5 Summary

The experimental data analyse from the LTH tests were discussed in this chapter. In the LTH tests, the instantaneous stress-related strain was measured at ambient temperature. The total strain during transient heating was also measured. LITS was calculated with the total strain and free thermal strain measured in the HTL tests.

Different LITS components, including the transient creep, the time-dependent creep, and the instantaneous stress-related strain due to the change of instantaneous elastic modulus, were

compared for different temperatures and load levels. As expected, the transient creep was the largest component of LITS. However, the transient creep developed during the transient heating. There was no additional transient creep during constant heating. Although the time-dependent creep only accounted for a small proportion of LITS, it was not negligible. The time-dependent creep increased with longer heating time. The ratio of the recoverable strain to LITS is around 5% to 15%.

The transient strain and transient creep were compared by using available empirical equations. Most equations are applicable to the temperature under 450 °C; there is considerable increase in transient strain after 450 °C. Comparing constitutive models, the transient creep and the transient strain gave a reasonably good agreement with the experimental data under 450 °C. More tests above 450 °C are required to obtain more accurate curves of LITS at high temperatures.

7

Validation of Prony series

7.1 Introduction

In Chapter 5, the method of simulating time-dependent creep was developed. The simulation was based on Prony series. The Prony parameters were based on curve fitting of experimental results. The time-dependent finite element analysis to evaluate time-dependent creep strain was conducted in ABAQUS.

To explore the strengths and limitations of the viscoelastic model using the Prony series, the simulation is compared to previously developed models and experimental data.

7.2 Simulation with the constitutive model

Anderberg [10] explored time-dependent creep through experiments. An empirical constitutive model was developed from the data. The simulation in this section is based on constitutive model.

7.2.1 Constitutive model

The specimens used in the experiment conducted by Anderberg [10] were a concrete cylinders with a diameter of 75 mm and a height of 150 mm. The average compressive strength at ambient temperature was around 50 MPa. During the test, test temperatures varied from 20 °C to 650 °C. Specimens were subjected to different load levels, i.e. 11%, 22.5%, 45%, 67.5% and 90%. The specimens were heated to the test temperature at the beginning. A constant load was applied to the specimen and sustained for 3 hrs.

Anderberg [10] derived the equation for the creep under sustained temperature and stress, which is

$$\varepsilon_{cr} = -0.00053\frac{\sigma}{f_{c,\theta}}(\frac{t}{t_r})^{0.5}e^{0.00304(\theta-20)} \tag{7.1}$$

where ε_{cr} is the time-dependent creep, t is the time, t_r is the sustained time, $\frac{\sigma}{f_{c,\theta}}$ is the load level, and θ is the temperature. As can be seen from the equation, the creep increases linearly with load level at any given temperature. Therefore, the creep is simulated based on the theory of viscoelasticity. Figure 7.1 shows the creep strain curve based on different temperatures at 22.5 % load level.

It is important to note that the creep strain in Fig. 7.1 cannot be used in the curve fitting directly. The creep strain must include initial instantaneous stress-related strain for curve fitting. Figure 7.2 shows the stress-strain relations for different temperatures based on Anderberg's experimental data [10]. As time-dependent creep is independent of the load level, the Prony series employed was based on the creep strain at 22.5 % load level and different temperatures. Figure 7.3 shows the creep strain curves used for curve fitting.

7.2.2 Simulation results

Figure 7.4 shows a comparison of time-dependent creeps from experimental data and simulation results evaluated by MATLAB. Each time-dependent creep curve contained the value of initial instantaneous stress-related strain. The curve fitting was based on 1-term Prony series

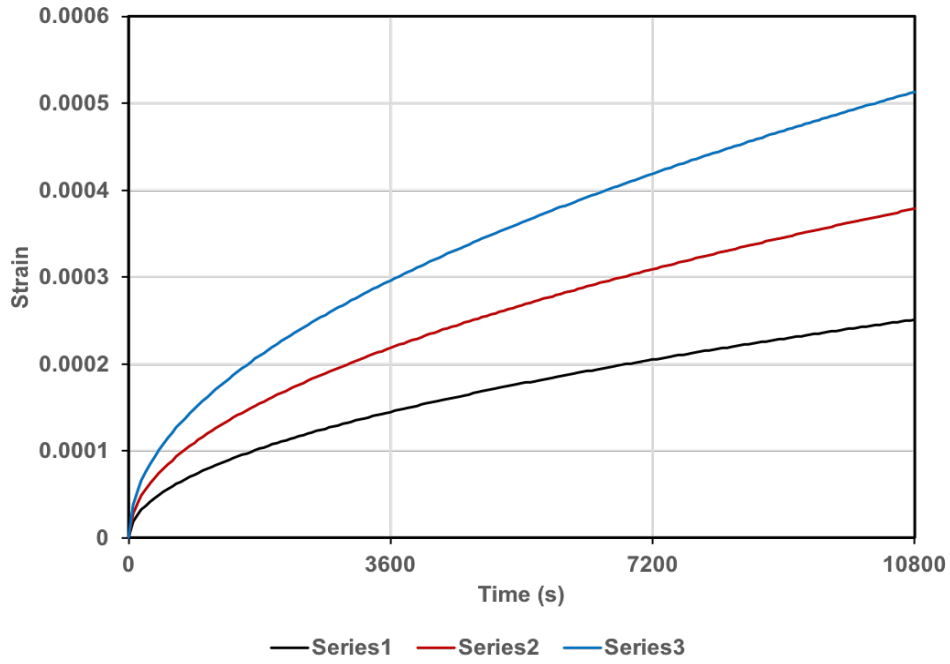

Fig. 7.1 The creep strain curves based on the constitutive model for different temperatures at 22.5% load level

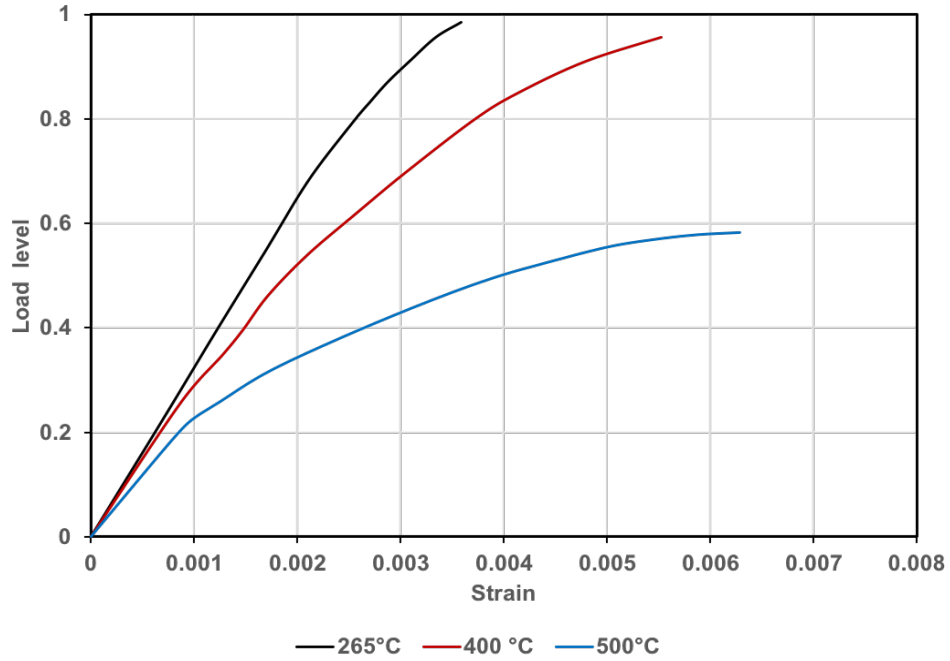

Fig. 7.2 Stress-strain relations at different temperatures based on Anderberg's experiment

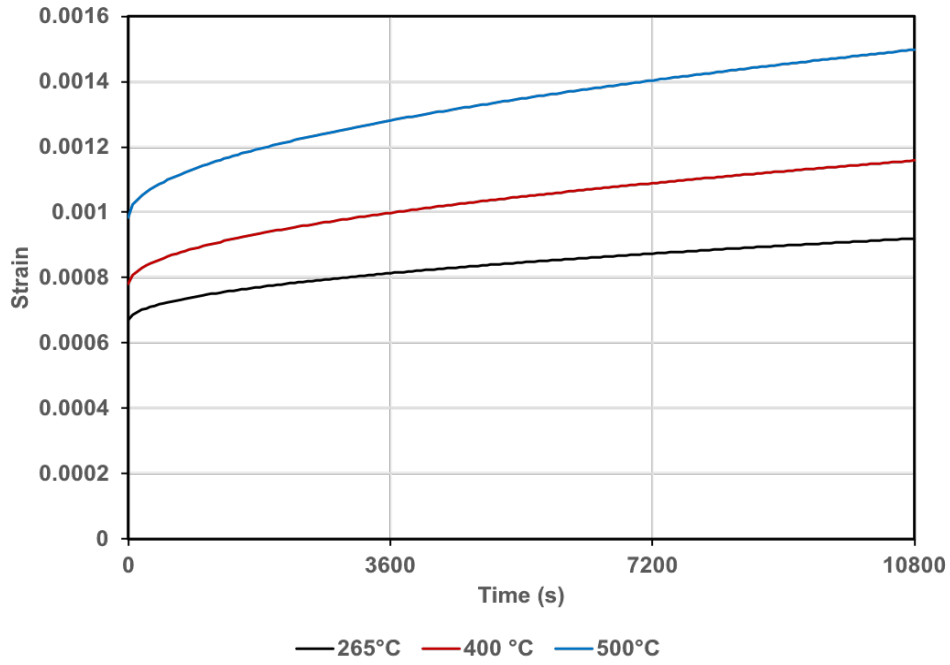

Fig. 7.3 The creep strain curves used for curve fitting, at 22.5% load level and different temperatures

and 3-term Prony series. As can be seen from Fig. 7.4, the simulation results with 3-term Prony series fit the experimental data better than the simulation results with 1-term Prony series. With the increase in the number of Prony terms, the simulation results are more accurate.

The Prony series based on curve fitting was used to conduct time-dependent finite element analysis in ABAQUS. In the simulation, the temperature of the model was constant and uniform. The reference temperatures were set to 265 °C, 400 °C, and 500 °C, respectively. The load was kept constant for two hours. Figures 7.5 and 7.6 show simulation results of time-dependent creep with the viscoelastic material model.

As can be seen from Figs. 7.5 and 7.6, the simulation with more numbers of Prony terms gives more accurate simulation results. The simulations with 3-term Prony series describe the creep strain curves better at the beginning with more accurate initial instantaneous elastic modulus. There is a considerable difference between experimental data and simulation results

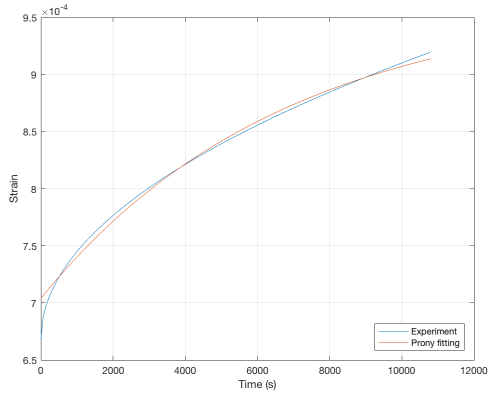

(a) 265 °C, $\eta_{pr} = 1$

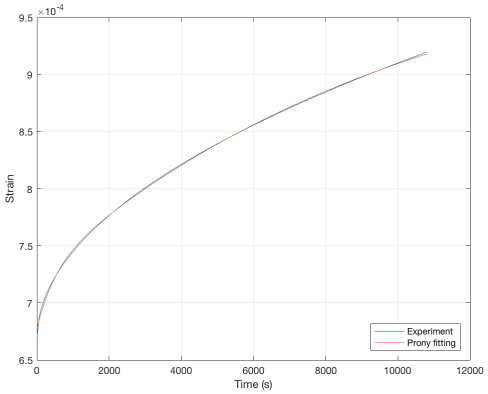

(b) 265 °C, $\eta_{pr} = 3$

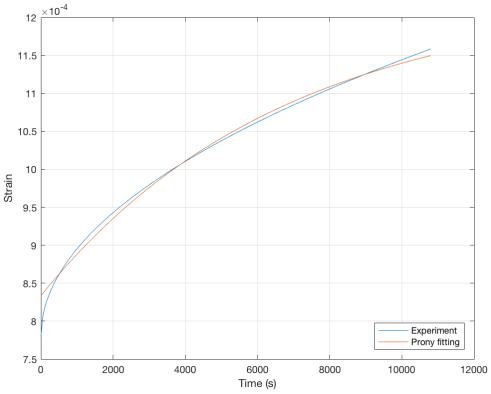

(c) 400 °C, $\eta_{pr} = 1$

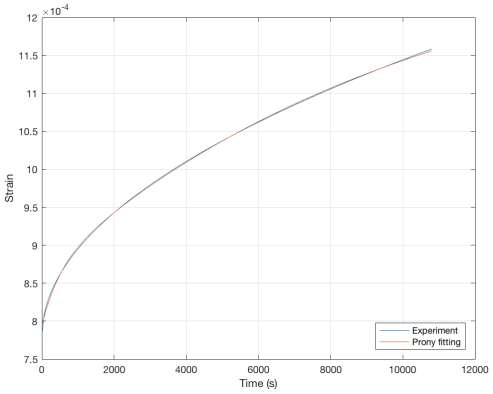

(d) 400 °C, $\eta_{pr} = 3$

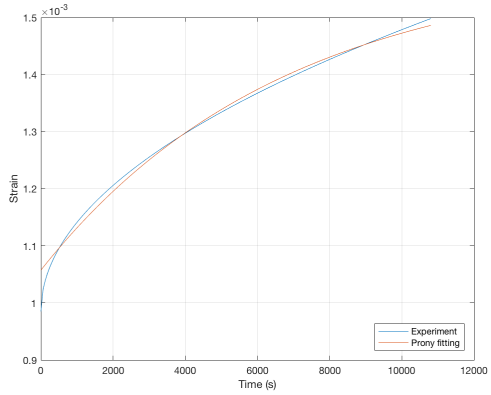

(e) 500 °C, $\eta_{pr} = 1$

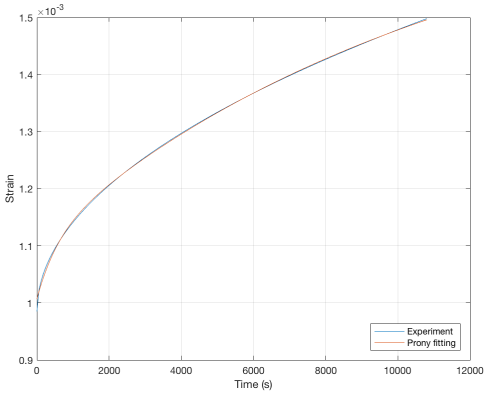

(f) 500 °C, $\eta_{pr} = 3$

Fig. 7.4 Comparison of time-dependent creeps from experimental data and simulation results evaluated by MATLAB for different heating temperatures

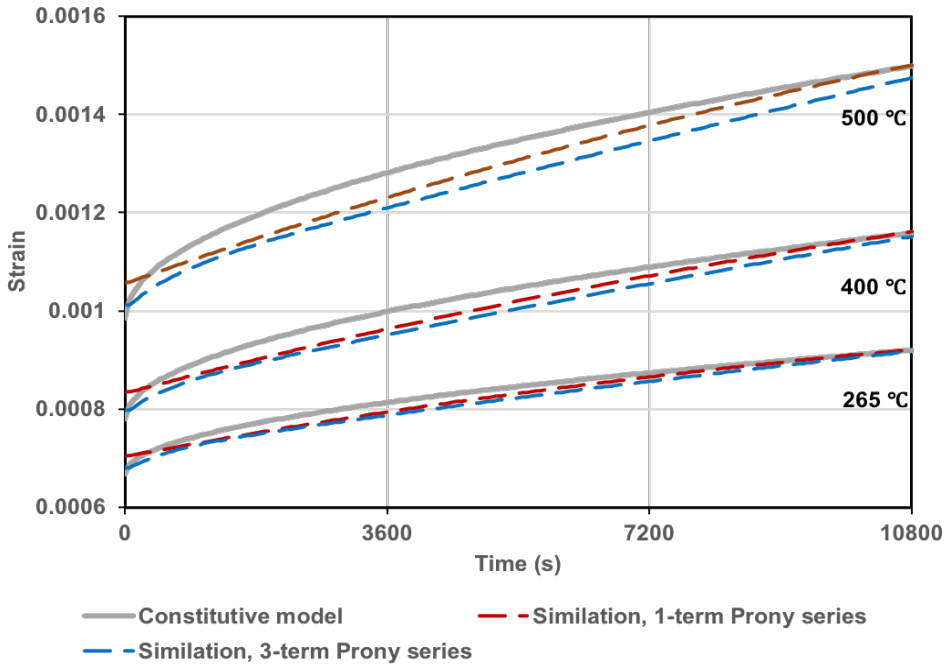

Fig. 7.5 Comparison of time-dependent creeps from experimental data and simulation results at different temperatures, at 22.5% load level

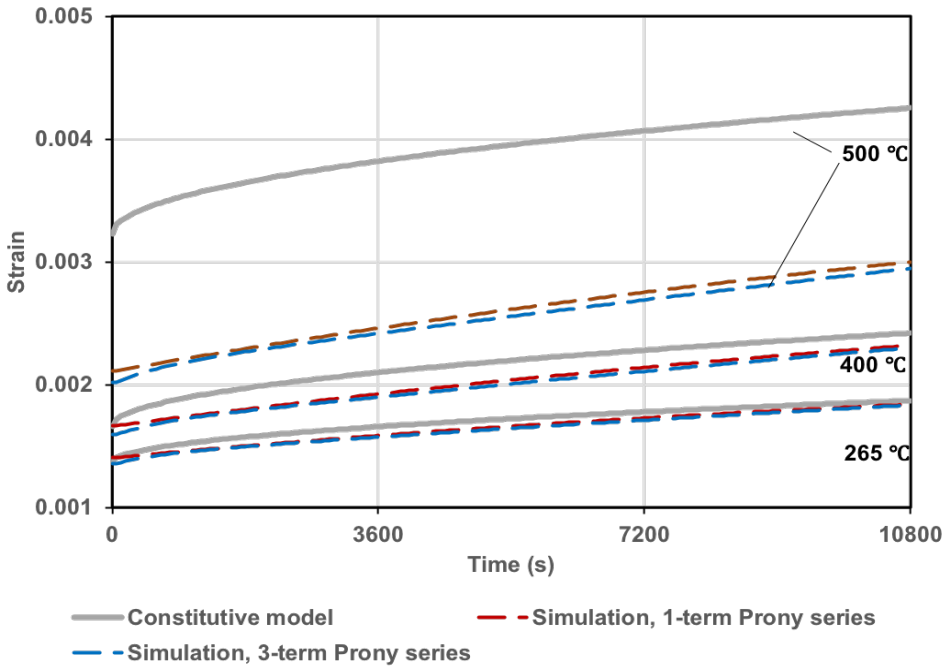

Fig. 7.6 Comparison of time-dependent creeps from experimental data and simulation results at different temperatures, at 45% load level

at 500 °C and 45% load level shown in Fig. 7.6. The main reason is that the plasticity and damage are not included into the simulation. As shown in Fig. 7.2, the plasticity exists from 20% load level at 500 °C.

7.2.3 Prony parameters

As creep strain is independent of load levels as discussed earlier, the curve fitting in MATLAB was based on the creep strain at 22.5% load level and different temperatures. Table 7.1 shows the constants for different temperatures with different numbers of terms in the Prony series.

Table 7.1 Comparison of Prony parameters with different numbers of terms in the Prony series

θ	η_{pr}	$D_g \times 10^{-5}$	$D_j \times 10^{-5}$			τ_j			$E_e \times 10^3$	$E_i \times 10^3$			ρ_i		
			D_1	D_2	D_3	τ_1	τ_2	τ_3		E_1	E_2	E_3	ρ_1	ρ_2	ρ_3
265	1	6.26	2.33	-	-	6723	-	-	11.64	4.34	-	-	9231	-	-
265	3	6.02	1.55	0.42	1.12	11044	491	9808	10.97	4.99	0.11	0.52	15301	10220	515
400	1	7.41	3.52	-	-	6724	-	-	9.15	4.35	-	-	9918	-	-
400	3	7.06	3.56	0.63	0.46	10990	482	7177	8.54	5.02	0.14	0.46	16839	7365	510
500	1	9.4	4.77	-	-	6723	-	-	7.06	3.58	-	-	10135	-	-
500	3	8.95	3.54	0.89	2.08	11887	569	10430	6.47	4.27	0.06	0.38	18598	10865	603

θ [°C] is the applied temperature, η_{pr} is the number of terms in Prony series, D_g [1/MPa], D_j [1/MPa] and τ_j [s] are the instantaneous elastic compliance, the transient retardation strength, and the retardation time in the Prony series, and E_e [MPa], E_i [MPa] ,and ρ_i [s] are the equilibrium modulus, the relaxation strength, and the relaxation time, respectively.

The corresponding creep compliance functions (D(t)) with different numbers of Prony terms are shown in Fig. 7.7. The time-dependent relaxation modulus functions (E(t)) with different numbers of Prony terms are shown in Fig. 7.8. The creep compliances and the time-dependent relaxation moduli with different numbers of Prony terms are slightly different. As can be seen from Fig. 7.7, the initial time-dependent creep compliances are slightly lower with 3-term Prony series. With higher initial instantaneous elastic modulus, the creep curve is simulated more accurately.

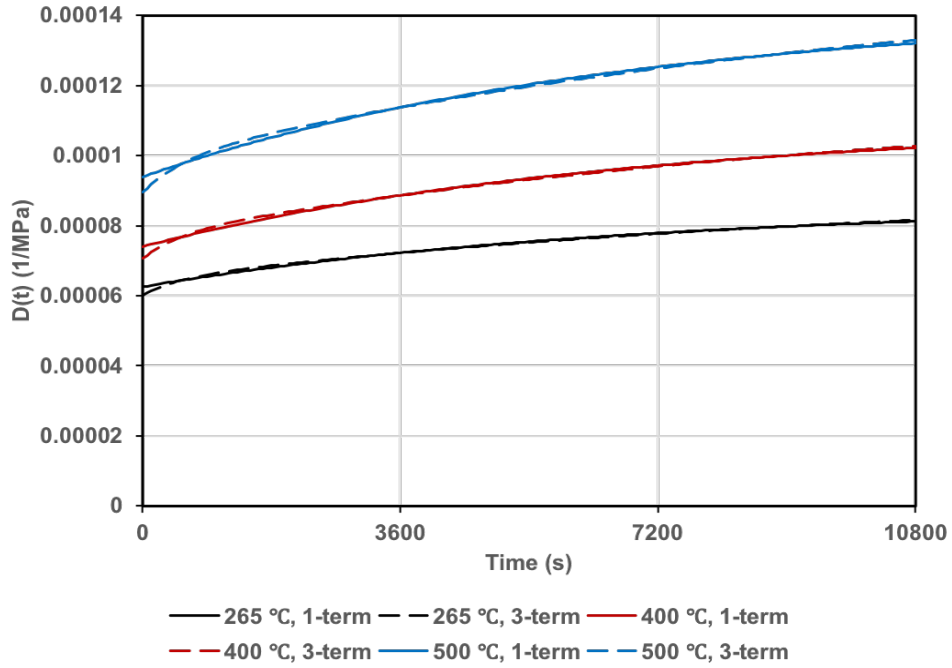

Fig. 7.7 Time-dependent creep compliance functions at different heating temperatures with 1-term Prony series and 3-term Prony series

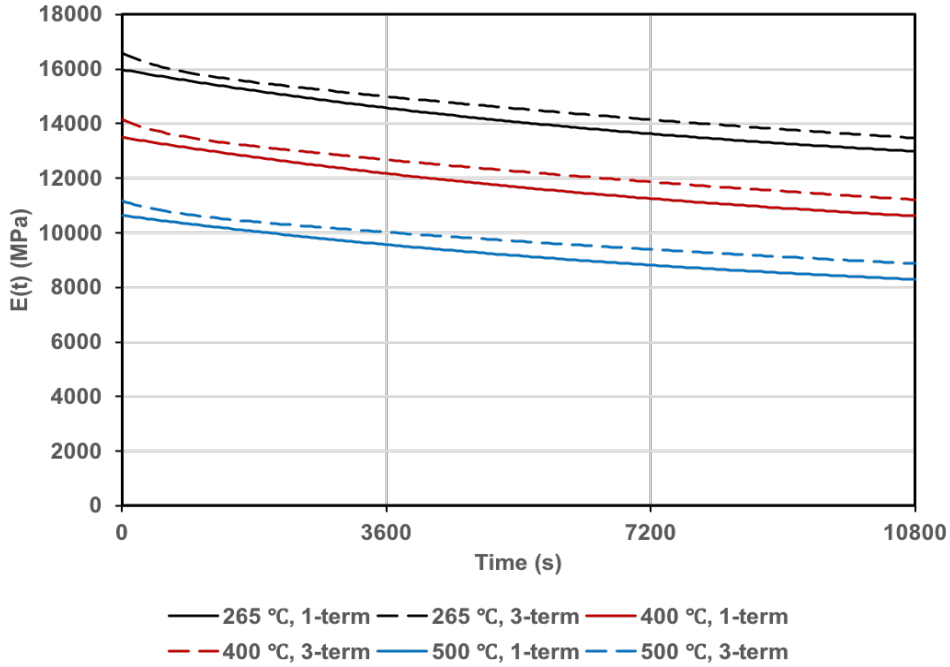

Fig. 7.8 Time-dependent relaxation modulus functions at different heating temperatures with 1-term Prony series and 3-term Prony series

7.3 Simulation with experimental data

Gillen [8] conducted experimental work of short-term creep of calcareous concrete at elevated temperatures. The simulation in this section is based on their experimental data.

7.3.1 Experimental data

The specimens used in the experiment were concrete cylinders with a diameter of 51 mm and a height of 102 mm. The average compressive strength was 23.2 MPa at 28 days. During the tests, test temperatures varied from 22 °C to 649 °C. Specimens were subjected to load levels of 30%, 45% and 60%. At the beginning of the test, specimens were heated to the test temperatures without load. Thereafter, all specimens were subjected to a constant load level and temperature for 5 hrs. Each test was repeated twice for reliability. Figure 7.9 shows the average creep strains of calcareous concrete cylinders under sustained temperatures and load levels for 5 hrs.

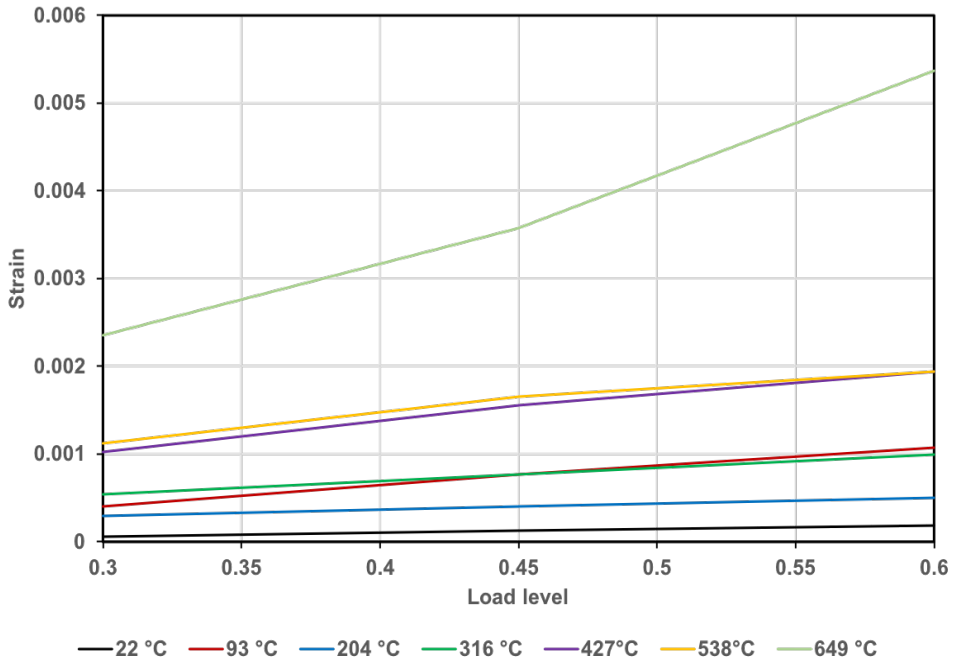

Fig. 7.9 Average creep strains of calcareous aggregate concrete under different sustained temperatures and load levels for 5 hrs

As can be seen from Fig. 7.9, the creep strains increase linearly with load level at 22 °C, 93 °C, 204 °C and 316 °C. At 427 °C and 538 °C, the creep strain at 60% load level is slightly lower than that estimated from linear extrapolation. However, the difference is small. At 649 °C, the creep strain has a considerable increase under 60% load level. The possible reason is post-elastic behaviour under the high temperature and large compressive stress.

For viscoelastic material, the creep strain is independent of load level at same temperature. As discussed before, the creep strain increases linearly with load level, excluding the creep strain under the 60% load level at 649 °C. The simulation was based on experimental data at 204 °C, 316 °C and 538 °C. The curve fitting is based on the creep strain at 30% load level and different temperatures.

There is no specific experimental data of initial instantaneous stress-related strain in the

reference [8]. For simplification, the initial stress-related strain is assumed to increase linearly. Figure 7.10 shows the creep strain curves used in the curve fitting.

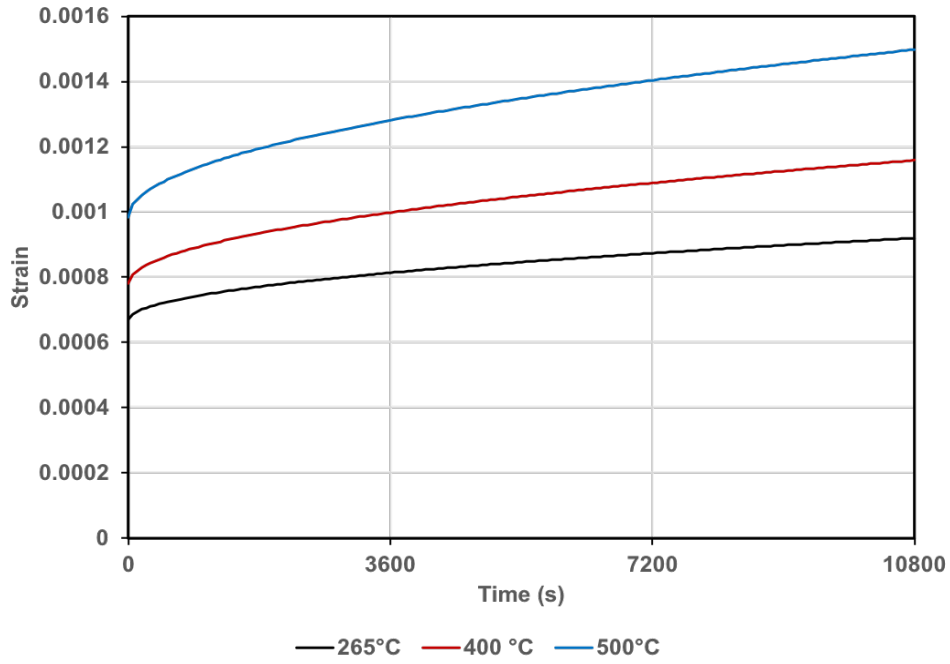

Fig. 7.10 The creep strain curves used for curve fitting, at 30% load level

7.3.2 Simulation results

Figure 7.11 shows a comparison of time-dependent creeps from experimental data and simulation results evaluated by MATLAB. The curve fitting was based on 1-term Prony series and 3-term Prony series. As can be seen from Figs. 7.11 (a) and 7.11 (b), the simulation results with 3-term Prony series fit the experimental data better than the simulation results with 1-term Prony series at 204 °C. For higher temperatures, the simulation results with 1-term Prony series and 3-term Prony series are similar. The creep strain has a considerable increase at the beginning compared to data at 204 °C. By increasing the numbers of Prony terms, the accuracy of simulation can be improved.

The Prony series based on curve fitting was used to conduct time-dependent finite ele-

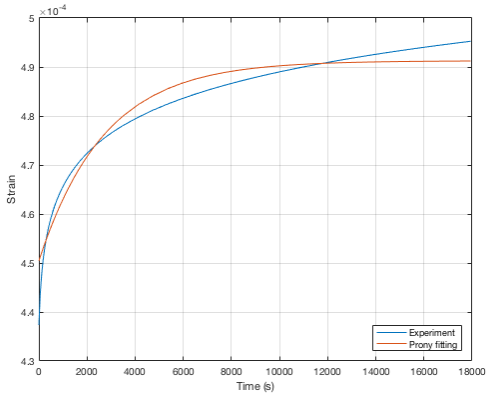

(a) 204 °C, $\eta_{pr} = 1$

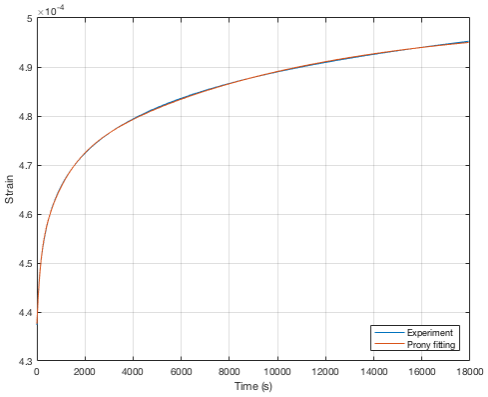

(b) 204 °C, $\eta_{pr} = 3$

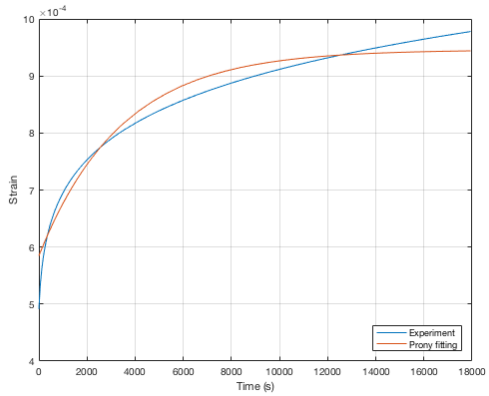

(c) 316 °C, $\eta_{pr} = 1$

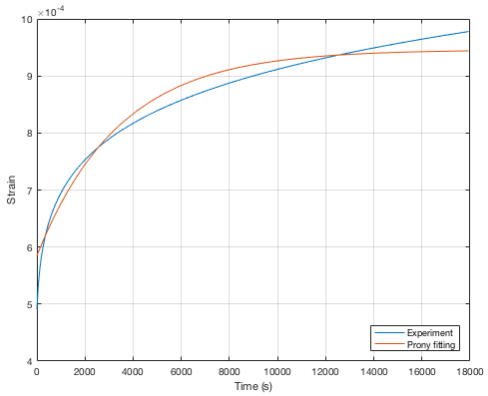

(d) 316 °C, $\eta_{pr} = 3$

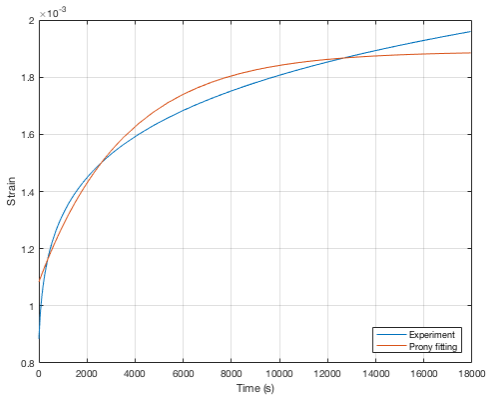

(e) 538 °C, $\eta_{pr} = 1$

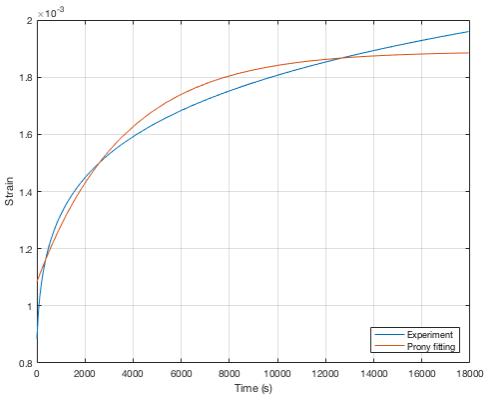

(f) 538 °C, $\eta_{pr} = 3$

Fig. 7.11 Comparison of time-dependent creeps from experimental data and simulation results evaluated by MATLAB for different heating temperatures

ment analysis in ABAQUS. Figure 7.12 shows simulation results of time-dependent creep with the viscoelastic material model. For time-dependent creep strain at 204 °C, the simulation results with different numbers of Prony terms are similar as the creep strain is relatively low at low temperature. For simulation results at 316 °C, the increase in numbers of Prony terms improves the performance of simulation results. With more Prony terms, more accurate initial instantaneous elastic modulus is achieved. For simulation results at 538 °C, there is a significant difference between experimental data and simulation results. As can be seen from Fig. 7.12, the creep strain has a rapid growth at the beginning compared with other strain curves. To achieve more accurate simulation results, more numbers of Prony terms are necessary to describe the curves.

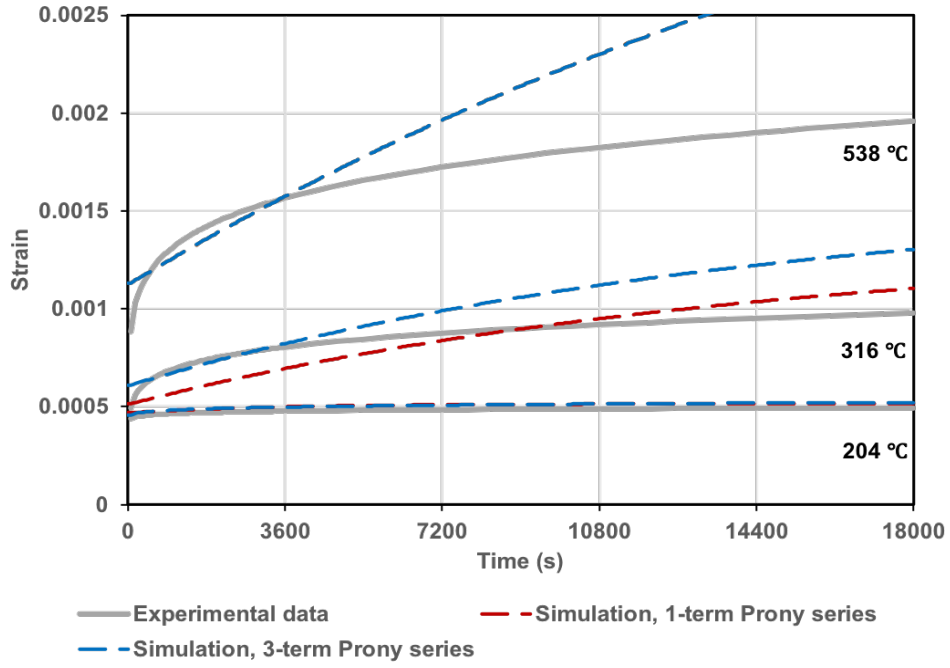

Fig. 7.12 Comparison of time-dependent creeps from experimental data and simulation results at different temperatures, at 30% load level

7.3.3 Prony parameters

As the creep strain is independent of load levels as discussed earlier, the curve fitting in MATLAB is based on the creep strain at 30% load level and different temperatures. Table 7.2

shows the constants for different temperatures with different number of terms in the Prony series terms employed.

Table 7.2 Comparison of Prony parameters with different numbers of terms in the Prony series

θ	η_{pr}	$D_g \times 10^{-5}$	$D_j \times 10^{-5}$			τ_j			$E_e \times 10^3$	$E_i \times 10^3$			ρ_i		
			D_1	D_2	D_3	τ_1	τ_2	τ_3		E_1	E_2	E_3	ρ_1	ρ_2	ρ_3
204	1	6.73	6.11	-	-	2719	-	-	13.62	1.24	-	-	2966	-	-
204	3	6.54	0.46	0.27	0.19	9089	965	136	13.40	1.01	0.53	0.35	9726	1002	139
316	1	8.74	5.40	-	-	3416	-	-	7.07	4.37	-	-	5527	-	-
316	3	8.75	1.80	1.81	1.80	3072	3216	4170	7.06	3.99	0.36	0.01	5835	3647	3134
538	1	16.20	12.06	-	-	3568	-	-	3.54	2.64	-	-	6225	-	-
538	3	16.20	4.09	3.99	3.97	3574	3606	3525	3.54	2.63	$1.19*10^{-4}$	$6.39*10^{-4}$	6226	3592	3544

θ [°C] is the applied temperature, η_{pr} is the number of terms in Prony series, D_g [1/MPa], D_j [1/MPa] and τ_j [s] are the instantaneous elastic compliance, the transient retardation strength, and the retardation time in the Prony series, and E_e [MPa], E_i [MPa] ,and ρ_i [s] are the equilibrium modulus, the relaxation strength, and the relaxation time, respectively.

The corresponding creep compliance functions (D(t)) with different numbers of Prony terms are plotted in Fig. 7.13. The time-dependent relaxation modulus functions (E(t)) with different numbers of Prony terms are shown in Fig. 7.14. The creep compliance and the time-dependent relaxation modulus with different numbers of Prony terms are almost the same. Therefore, the total time-dependent creep strain developed under sustained load and temperature is similar with different numbers of Prony terms.

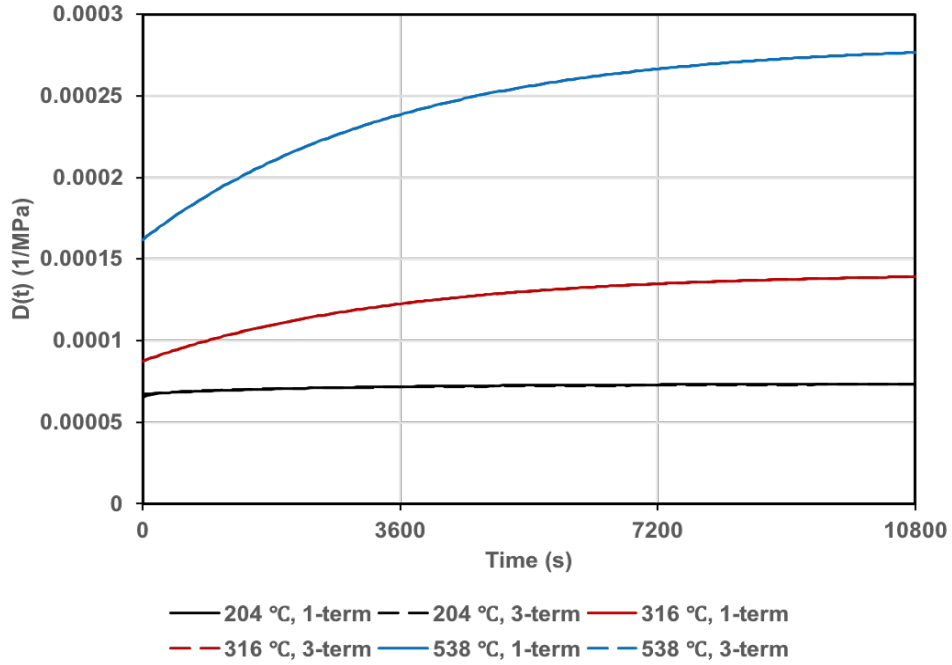

Fig. 7.13 Time-dependent creep compliance functions at different temperatures with 1-term Prony series and 3-term Prony series

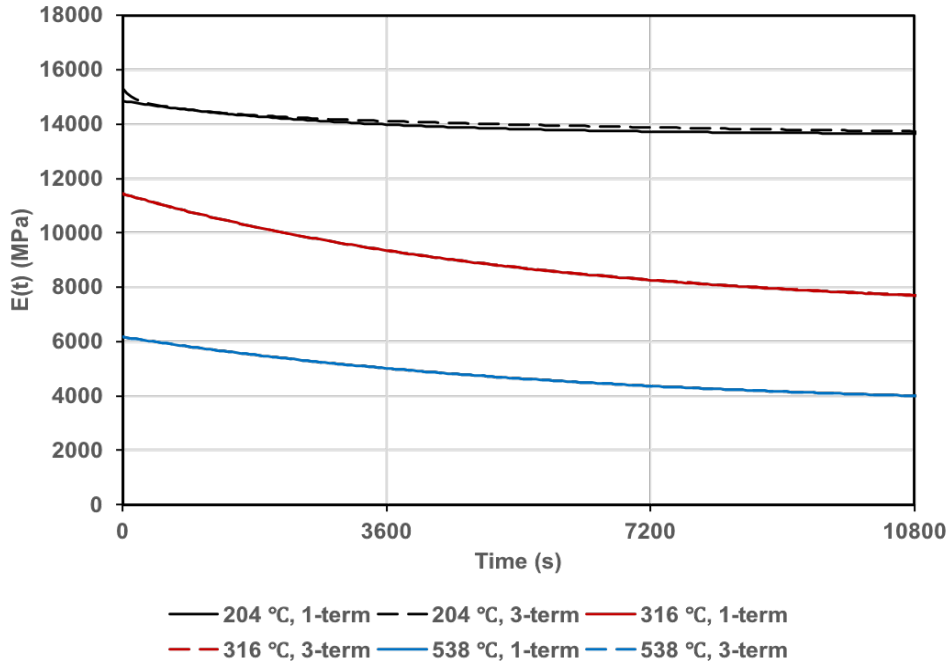

Fig. 7.14 Time-dependent relaxation modulus functions at different temperatures with 1-term Prony series and 3-term Prony series

7.4 Summary

In this chapter, the simulation with Prony series was validated with a previously developed constitutive model and the experimental data.

During the simulation of the constitutive model, the accuracy of the simulation results was improved by increasing numbers of Prony terms. With more numbers of Prony terms, the initial instantaneous elastic modulus was more accurate. The simulation results fit the creep strain curves better than these with 1-term Prony series. Also, the limitation of viscoelasticity was exposed. Plasticity and damage cannot be included in a viscoelastic model. The viscoelastic model is unable to represent post-elastic response at higher load levels.

During the simulation of the experimental data, 3-term Prony series was not sufficient

with a sharp slope of the creep strain curve. More numbers of Prony terms are necessary for describing the time-dependent creep more accurately.

8

Conclusions and suggestions for future work

8.1 Introduction

This thesis has evaluated the behaviour of concrete at elevated temperatures through experiments and numerical simulations. Main conclusions are based on mechanical behaviour of concrete at elevated temperatures, simulations of time-dependent creep, heat transfer analysis, and digital image correlations. Some suggestions for future work are given at the end.

8.2 Mechanical behaviour of concrete at elevated temperatures

Two series of tests were conducted to evaluate different material behaviours of concrete at elevated temperatures: those in which heated samples are subjected to loading, load holding, unloading and recovery; and those in which load samples were subjected to heating, maintenance of constant temperature, unloading and recovery. All tests were conducted under different load levels and temperatures.

The heating-then-loading tests were used to measure free thermal strain, instantaneous stress-related strain, time-dependent creep, and instantaneous unloading strain. It was found that the thermal expansion is lower than the prediction from Eurocode 2. It is difficult to conclude if the free thermal strain suggested by Eurocode is incorrect as thermal expansion is affected by many factors. In this study, the thermal coefficient is modified with experimental data and is used in the simulations.

Comparing the instantaneous stress-related strain with the corresponding instantaneous unloading strain, the recovery of instantaneous stress-related strain after unloading is around 80%. The time-dependent creep strain is evaluated under various sustained temperatures and load levels for 2 hrs. It increases almost linearly with load levels, which indicates that it is independent of load levels.

The loading-then-heating tests were conducted to evaluate instantaneous stress-related strain, load induced thermal strain and instantaneous unloading strain. The difference between free thermal strain and the strain due to heating under sustained load excluding initial stress-related strain at ambient temperature is evaluated as load induced thermal strain. At high temperatures, the LITS is the largest strain component from mechanical response. In some cases, the time-dependent strain is accounted over 10% of load induced thermal strain which is not negligible.

It is found that the increment of instantaneous stress-related strain at elevated temperatures is included in load induced thermal strain. The difference is due to variation of instantaneous elastic strain at elevated temperature. After unloading, around 80% instantaneous stress-related strain at elevated temperature is recovered. Although the instantaneous stress-related strain at ambient temperature is extracted from load induced thermal strain, the load induced thermal strain still contains recoverable strain of around 5% to 15%.

8.3 Modelling time-dependent creep

There is a linear time-dependent creep under sustained temperature and load conducted by work. The method of modelling linear creep is via the use of a viscoelastic material. To meet the requirement of viscoelasticity, the time-dependent creep is independent of load level.

The Prony series introduced and discussed in Chapter 5 are used to simulate time-dependent creep. The parameters are evaluated through curve fitting in MATLAB. Then, the parameters are used in finite element analysis for defining viscoelastic material in ABAQUS. The simulation results fit the experimental data well. The viscoelastic material with Prony series provides a simple way to model time-dependent creep.

Through the validation of Prony series, the simulations are based on a previously developed constitutive model and the experimental data. The accuracy of the simulation results is improved by increasing numbers of Prony terms. It has to be emphasized that the creep strain used in curve fitting includes initial stress-related strain. By improving numbers of Prony terms, the initial instantaneous elastic modulus will be more accurate, which means the simulation results fit the creep strain curves better.

There is a limitation of viscoelasticity, as the concrete plasticity is not considered in the viscoelastic model. The viscoelastic model is unable to represent post-elastic response at higher load levels. In some cases, 3-term Prony series may not be sufficient with sharp slopes for the creep strain curves.

8.4 Heat transfer analysis

The heat transfer analysis is conducted to find the most efficient and reasonable heating rates for the experiment in order to prevent damage due to differential thermal expansions.

For the heating rate of 10 °C/min, the temperature difference between the central line

and the surface exceeds 300 °C when the chamber temperature reaches 600 °C. Also, the heating process with the heating rate of 1 °C/min takes over 10 hrs, which is not efficient.

The concrete has a considerable thermal gradient due to low conductivity. With variable expansion within concrete, stresses arise during transient heating. Thermomechanical analysis is conducted with the heating rates of 2 °C/min and 5 °C/min. In these analyses, stresses caused by temperature gradients during the heating process are evaluated. Through the heat transfer and mechanical analysis, the heating rate is set to 2 °C/min for the experiments. This heating rate can avoid dangerous stresses due to temperature gradient while taking less time in comparison to the rate of 1 °C/min.

The study also shows that the chamber temperature needs to be maintained constant for 2 hrs to achieve uniform temperature in the concrete

8.5 Methodology of strain measurement

The digital image correlation technique is used to measure strain data during the experiment. The camera is set to take photos of unique painted pattern on the concrete surface during the test. By analyzing the movement of pixels with continuous photos by MATLAB, the value of strain is evaluated. The method of post-processing photos is a simple and inexpensive way to evaluate strain data during tests.

8.6 Suggestions for future work

Suggestions for future work are:

- To consider post-elastic behaviour of concrete in the simulation of time-dependent creep, combining the linear time-dependent creep with post-elastic response at higher

load levels should be considered.

- To evaluate accurate thermal gradients during heating, insertion of thermocouples along the radius of the concrete specimen during casting should be undertaken. This will permit measurement of accurate temperature distributions during transient heating and comparison with simulation results.

- To simulate transient strain, which is one of the largest strain components, routines that can incorporate variation of viscoelastic properties with temperatures should be developed.

References

[1] W. Khaliq. Performance Characterization of High Performance Concretes under Fire Conditions. PhD Dissertation, Michigan State University, USA, 2012.

[2] British Standards Institution. BS EN 1992-1-2 Eurocode 2: Design of Concrete Structures. Part 1-2: General Rules – Structural Fire Design. London, UK, 2004.

[3] T.T. Lie. Structural Fire Protection: Structural Fire Protection No 78 (Manuals and Reports on Engineering Practice). American Society of Civil Engineers, 1992.

[4] V.K.R. Kodur and M. Sultan. Thermal properties of high strength concrete at elevated temperatures. ACI Special Publication 179, American Concrete Institute, USA, 467-480, 1998.

[5] T.T. Lie and V.K.R. Kodur. Thermal and mechanical properties of steel-fibre reinforced concrete at elevated temperatures. Canadian Journal of Civil Engineering, 23(2):511–517, 1996.

[6] X.F. Hu, T.T. Lie, G.M. Polomark and J.W. MacLaurin. Thermal Properties of Building Materials at Elevated Temperatures. Internal Report 643, Institute for Research in Construction, National Research Council Canada, 1993.

[7] Z.P. Bažant and J.-C. Chern. Stress-induced thermal and shrinkage strains in concrete. Journal of Engineering Mechanics, 113(10):1493-1511, 1987.

[8] M. Gillen. Short-term creep of concrete at elevated temperatures. Fire and Materials, 5(4):142-148, 1981.

[9] G. Torelli, P. Mandal, M. Gillie and V.X. Tran. Concrete strains under transient thermal conditions: A state-of-the-art review. Engineering Structures, 127:172-188, 2016.

[10] Y. Anderberg and S. Thelandersson. Stress and Deformation Characteristics of Concrete at High Temperatures. 2. Experimental Investigation and Material Behaviour Model. Bulletin 54, Division of Structural Mechanics and Concrete Construction, Lund Institute of Technology, 1976.

[11] G.A. Khoury, B.N. Grainger and P.J.E. Sullivan. Strain of concrete during first heating to 600°C under load. Magazine of Concrete Research, 37(133):195-215, 1985.

[12] U. Schneider. Concrete at high temperatures - A general review. Fire Safety Journal, 13(1):55-68, 1988.

[13] G.A. Khoury. Strain of heated concrete during two thermal cycles. Part 1: Strain over two cycles, during first heating and at subsequent constant temperature. Magazine of Concrete Research, 58(6):367–385, 2006.

[14] H.K.M. Smith. Punching Shear of Flat Reinforced-Concrete Slabs under Fire Conditions. PhD Dissertation, Edinburgh University, UK, 2016.

[15] D. Whiting, A. Litvin and S.E. Goodwin. Specific heat of selected concretes. ACI Journal, 75:299-305, 1978.

[16] D. Campbell-Allen and C.P. Thorne. The thermal conductivity of concrete. Magazine of Concrete Research, 15(43):39–48, 1963.

[17] P.S. Ghoshdastidar. Chapter 1 Introduction. Heat Transfer (2nd Edition), 1–10, Oxford University Press, UK, 2012.

[18] W. Zhang, H. Min, X. Gu, Y. Xi, and Y. Xing. Mesoscale model for thermal conductivity of concrete. Construction and Building Materials, 98:8-16, 2015.

[19] American Society for Testing and Materials. ASTM E1530-06 Standard Test Method for Evaluating the Resistance to Thermal Transmission of Materials by Guarded Heat Flow Meter Technique. ASTM, USA, 2013.

[20] A.S. Gandage, V.R.V. Rao, M.V.N. Sivakumar, A. Vasan, M. Venu and A.B. Yaswanth. Effect of perlite on thermal conductivity of self compacting concrete. Procedia - Social and Behavioral Sciences, 104:188–197, 2013.

[21] P.K. Mehta and P.J.M. Monteiro. Concrete: Microstructure, Properties, and Materials (4th Edition). McGraw-Hill Education, New York, USA, 2013.

[22] K.-H. Kim, S.-E. Jeon, J.-K. Kim and S. Yang. An experimental study on thermal conductivity of concrete. Cement and Concrete Research, 33(3):363-371, 2003.

[23] K.-Y. Shin, S.-B. Kim, J.-H. Kim, M. Chung and P.-S. Jung. Thermo-physical properties and transient heat transfer of concrete at elevated temperatures. Nuclear Engineering and Design, 212(1-3):233–241, 2002.

[24] I. Asadi, P. Shafigh, Z.F.B.A. Hassan and N.B. Mahyuddin. Thermal conductivity of concrete - A review. Journal of Building Engineering, 20:81–93, 2018.

[25] T.Z. Harmathy and L.W. Allen. Thermal properties of selected masonry unit concretes. Journal Proceedings, 70(2):132-142, 1973.

[26] T.Z. Harmathy. Thermal properties of concrete at elevated temperatures. Journal of Materials, 5(1):47-44, 1970.

[27] J. Takeda, T. Harada, S. Yamane and F. Furumura. Strength, elasticity and thermal properties of concrete subjected to elevated temperatures. ACI Special Publication 34, American Concrete Institute, USA, 377-406, 1972.

[28] V.K.R. Kodur, M.M.S. Dwaikat and M.B. Dwaikat. High-temperature properties of concrete for fire resistance modeling of structures. ACI Materials Journal, 105(5):517–527, 2008.

[29] V.K.R. Kodur and T.Z. Harmathy. Properties of building materials. In SFPE Handbook of Fire Protection Engineering (5th Edition), 277–324, 2016.

[30] H.L. Malhotra. The effect of temperature on the compressive strength of concrete. Magazine of Concrete Research, 8(23):85–94, 1956.

[31] M.S. Abrams. Compressive strength of concrete at temperatures to 1600°F. ACI Special Publication SP-25, American Concrete Institute, 33-58, 1971.

[32] K.D. Hertz. Concrete strength for fire safety design. Magazine of Concrete Research, 57(8):445–453, 2005.

[33] M.A. Youssef and M. Moftah. General stress-strain relationship for concrete at elevated temperatures. Engineering Structures, 29(10):2618–2634, 2007.

[34] U. Schneider, U. Diederichs and C. Ehm. Effect of temperature on steel and concrete for PCRV's. Nuclear Engineering and Design, 67(2):245–258, 1982.

[35] U. Schneider. Modelling of concrete behaviour at high temperatures. In International Conference of Design of Structures against Fire, 53–69, 1986.

[36] H. Weigler and R. Fischer. Influence of high temperatures on strength and deformations of concrete. ACI Special Publication SP-34, American Concrete Institute, 481-493, 1972.

[37] D. Naus. The effect of elevated temperature on concrete materials and structures — A literature review. Contract, 6283(1886):184, 2005.

[38] S. Mindess and J.F. Young. Concrete. Prentice-Hall, Englewood Cliffs, NJ, USA, 1981.

[39] V. Kodur. Properties of Concrete at Elevated Temperatures. ISRN Civil Engineering, 2014.

[40] N.K. Raut and V.K.R. Kodur. Response of high-strength concrete columns under design fire exposure. Journal of Structural Engineering, 137(1):69–79, 2011.

[41] Z.P. Bažant. Mathematical model for creep and thermal shrinkage of concrete at high temperature. Nuclear Engineering and Design, 76(2):183–191, 1983.

[42] A.H. Law. The Assessment and Response of Concrete Structures Subjected to Fire. PhD Thesis, Edinburgh University, UK, 2010.

[43] A. Law and M. Gillie. Load induced thermal strain: Implications for structural behaviour. In SiF 2008, Singapore, 2008.

[44] U. Schneider and M. Schneider. An advanced transient concrete model for the determination of restraint in concrete structures subjected to fire. Journal of Advanced Concrete Technology, 7(3):403–413, 2009.

[45] M. Petkovski. Effects of stress during heating on strength and stiffness of concrete at elevated temperature. Cement and Concrete Research, 40(12):1744–1755, 2010.

[46] M.J. Terro. Numerical modeling of the behavior of concrete structures in fire. ACI Structural Journal, 95(2):183–192, 1998.

[47] G. Pickett. The effect of change in moisture-content on the creep of concrete under a sustained load. Journal of the American Concrete Institute, 13(4):333–355, 1942.

[48] G.A. Khoury, B.N. Grainger and P.J.E. Sullivan. Transient thermal strain of concrete: literature review, conditions within specimen and behaviour of individual constituents. Magazine of Concrete Research, 37(132):131–144, 1985.

[49] J.C. Mindeguia, I. Hager, P. Pimienta, H. Carré and C. La Borderie. Parametrical study of transient thermal strain of ordinary and high performance concrete. Cement and Concrete Research, 48:40–52, 2013.

[50] L.J. Parrott. A study of transitional thermal creep in hardened cement paste. Magazine of Concrete Research, 31(107):99-103, 1979.

[51] H. Colina, G. Moreau and D. Cintra. Experimental study of transient thermal creep and other phenomena of concrete at high temperature. Journal of Civil Engineering and Management, 10(4):255-260, 2004.

[52] H. Colina and J. Sercombe. Transient thermal creep of concrete in service conditions at temperatures up to 300°C. Magazine of Concrete Research, 56(10):559–574, 2004.

[53] S. Hassen and H. Colina. Transient thermal creep of concrete in accidental conditions at temperatures up to 400°C. Magazine of Concrete Research, 58(4):201–208, 2006.

[54] J.M. Illston and P.D. Sanders. Characteristics and prediction of creep of a saturated mortar under variable temperature. Magazine of Concrete Research, 26(88):169-179, 1974.

[55] U. Schneider, P. Schweisinger, G. Debicki, U. Diedefichsl, J.M. Franssen, F. Furumura, U.M. Jumppanen, G.A. Khoury, A. Millard and W.A. Morris. RILEM TC 129-MHT: Test methods for mechanical properties of concrete at high temperatures. Part 8: Steady-state creep and creep recovery for service and accident conditions, Materials and Structures, 33:6-13, 2000.

[56] U. Schneider, P. Schwesinger, G. Debicki, U. Diederichs, R. Felicetti, J.M. Franssen, U.M. Jumppanen, G.A. Khoury, A.A. Millard, W.A. Morris and L. Phan. RILEM TC 200-HTC: Mechanical concrete properties at high temperatures-modelling and application. Part 11: Relaxation. Materials and Structures, 40(5):449–458, 2007.

[57] U. Schneider, P. Schweisinger, G. Debicki, U. Diedefichsl, J.M. Franssen, F. Furumura, U.M. Jumppanen, G.A. Khoury, A. Millard and W.A. Morris. RILEM TC 129-MHT: Test methods for mechanical properties of concrete at high temperatures - recommendation. Part 7 Transient creep for service and accident conditions. Materials and Structures, 31:290–295, 1998.

[58] J.E. Dorn. Some fundamental experiments on high temperature creep. Journal of the Mechanics and Physics of Solids, 3:85–116, 1955.

[59] H. Gross. High-temperature creep of concrete. Nuclear Engineering and Design, 32(1):129–147, 1975.

[60] H. Dettling. The thermal expansion of hardened cement paste, aggregates, and concrete, Bulletin No. 164:1-64, Deutscher Ausschus für Stahlbeton, W. Ernst & Sohn, Berlin, Germany, 1964.

[61] J.E. Dorn and J.D. Mote. Physical aspects of creep. In High Temperature Structures and Materials, 95, Pergamon Press, New York, USA, 1963.

[62] Y. Anderberg and N.E. Forsén. Fire Resistance of Concrete Structures, LUTVDG/TVBB-3009-SE, Division of Building Fire Safety and Technology, Lund Institute of Technology, Sweden, 1982.

[63] U. Schneider. Behaviour of concrete under thermal steady state and non-steady state conditions. Fire and Materials, 1(3):103–115, 1976.

[64] U. Schneider. Zur Kinetik festigkeitsmindernder Reaktionen in Normalbetonen bei hohen Temperaturen. Braunschweig, 1973.

[65] C.V. Nielsen, C.J. Pearce and N. Bicanic. Theoretical model of high temperature effects on uniaxial concrete member under elastic restraint. Magazine of Concrete Research, 54(4):239–249, 2002.

[66] M.J. Terro. Numerical Modeling of the Behavior of Concrete Structures in Fire. ACI Structural Journal, 95(2):183-193, 1998.

[67] British Standards Institution. BS EN 12390-1 Testing Hardened Concrete. Part 1: Shape, Dimensions and Other Requirements for Specimens and Moulds, London, UK, 2000.

[68] R.R. Cook, D.S. Malkus, M.E. Pelsha and R.J. Witt. Concepts and Applications of Finite Element Analysis (4th Edition), John Wiley & Sons Inc, 2001.

[69] M.A. Sutton, W.J. Wolters, W.H. Peters, W.F. Ranson and S.R. McNeill. Determination of displacements using an improved digital correlation method. Image and Vision Computing, 1(3):133–139, 1983.

[70] T.C. Chu, W.F. Ranson and M.A. Sutton. Applications of digital-image-correlation techniques to experimental mechanics. Experimental Mechanics, 25(3):232–244, 1985.

[71] S.A. Stanier, J. Blaber, W.A. Take and D.J. White. Improved image-based deformation measurement for geotechnical applications. Canadian Geotechnical Journal, 53(5):727–739, 2016.

[72] L.A. Bisby and W.A. Take. Strain localisations in FRP-confined concrete: New insights. Proceedings of the Institution of Civil Engineers: Structures and Buildings, 162(5):301–309, 2009.

[73] British Standards Institution. BS EN 12390-3 Testing Hardened Concrete. Part 3: Compressive Strength of Test Specimens, London, UK, 2009.